Universiteit
Antwerpen

Faculteit Wetenschappen
Departement Fysica

Quantum Chromodynamics at small Bjorken-x

Kwantumchromodynamica bij kleine Bjorken-x

Pieter Taels

Samenvatting

Door de komst van steeds krachtigere deeltjesversnellers, zoals RHIC en de LHC, wordt het mogelijk om kwantumchromodynamica (QCD) te bestuderen bij een zeer hoge energie, in botsingen die gevoelig zijn aan de gluondichtheid van het proton of van de atoomkern. Vaak wordt deze dichtheid zo groot dat niet-lineaire effecten een rol beginnen te spelen. QCD in dit regime staat bekend als 'small-x QCD', en wordt met grote nauwkeurigheid beschreven door het zogenaamde Color Glass Condensate (CGC): een effectieve theorie voor een proton of atoomkern bij hoge energie. In deze thesis presenteer ik, na een inleiding over small-x QCD en over het CGC, twee projecten waarin het CGC wordt toegepast op twee verschillende problemen.

In het eerste project wordt de voorwaartse productie van twee zware quarks in proton-nucleus botsingen bestudeerd. Gewoonlijk wordt zo'n reactie beschreven binnen een zeker factorisatieschema, waarbij het 'harde deel' van de werkzame doorsnede, d.i. het deel dat we kunnen berekenen in storingstheorie, wordt afgesplitst van de niet-perturbative partondichtheden (PDFs), die de structuur van het hadron in termen van quarks en gluonen beschrijft. Aangezien deze partondichtheden niet perturbatief zijn, kunnen ze niet analytisch verkregen worden vanuit de QCD Lagrangiaan, maar moeten ze gemeten worden in experimenten. Afhankelijk van de precieze configuratie van de impulsschalen in de reactie, kunnen er twee verschillende factorisatieschemas op ons probleem worden toegepast: High-Energy Factorization (HEF) en Transverse Momentum Dependent (TMD) factorisatie. In dit werk wordt de berekening van de voorwaartse zware-quarkproductie in een ander framework uitgevoerd, dat van het CGC, en interessant genoeg zitten de resultaten van zowel het HEF als het TMD schema in deze berekening vervat. Daarnaast kunnen de –normaal gezien niet-perturbatieve– partondichtheden zowel analytisch als numeriek in het CGC gemodelleerd worden, waarvan ik de resultaten presenteer.

Het tweede project kadert in de fysica van zware ionen. In een botsing van twee zware atoomkernen wordt het zogenaamde Quark-Gluon Plasma (QGP) gevormd: een toestand van QCD waarin quarks en gluonen een fractie van een seconde vrij zijn, en dit bij een enorm hoge dichtheid en temperatuur. Energetische 'harde' jets, die gevormd werden tijdens de botsing van de atoomkernen, moeten zich doorheen het QGP voortbewegen alvorens ze de detector bereiken, en zullen beïnvloed worden door hun interactie met het medium. Dit fenomeen, of eerder verzameling van fenomenen, staat bekend als jet quenching, en is een van de voornaamste hulpmiddelen om het QGP te bestuderen. In dit werk wordt één bepaald aspect van jet quenching bestudeerd, namelijk de diffusie in transversale impuls van een energetisch deeltje dat zich door een nucleair medium voortbeweegt. We gebruiken technieken uit small-x QCD en het CGC, om de radiatieve correcties aan deze diffusie, ten gevolge van de straling van zachte gluonen, trachten te hersommeren in de logaritmische benadering, de zogenaamde leading logarithmic approximation (LLA). Het resultaat van deze analyse is een niet-lineaire evolutievergelijking in een medium, die we uiteindelijk enkel kunnen oplossen in de double leading logarithmic approximation (DLA). We presenteren een goed onderbouwd theoretisch kader voor dit probleem, bespreken uitgebreid de verbanden met het CGC, en vergelijken met de literatuur.

Abstract

With the advent of particle accelerators such as RHIC and the LHC, which are more and more powerful, it becomes possible to study quantum chromodynamics (QCD) in very high energy collisions, in which the gluon content of the proton or nucleus is probed and its density becomes often large enough for nonlinear effects to play a role. This so-called small-x regime of QCD is very well described by the Color Glass Condensate (CGC), an effective theory for a proton or nucleus at high energies. In this thesis, after an introduction to small-x QCD and to the CGC, we present two projects in which the CGC is applied to two different problems.

In the first project, we study forward heavy-quark production in proton-nucleus collisions. Such a process is usually studied in a certain factorization scheme, in which the perturbatively calculable 'hard part' of the cross section is separated from the nonperturbative parton distribution functions (PDFs), which encode the hadron structure in terms of quarks and gluons. Being nonperturbative, these PDFs cannot be obtained directly from first principles within QCD, but rather need to be measured experimentally. Moreover, depending on the precise configuration of the transverse momentum scales in the problem, two different factorization schemes are relevant: High-Energy Factorization (HEF) and Transverse Momentum Dependent (TMD) factorization. Interestingly, taking an alternative approach and calculating the cross section within the CGC, we reproduce the results obtained in both the TMD and the HEF scheme in the appropriate limits. Moreover, since the CGC encompasses a well-substantiated model for the nucleus, this matching allows us to make both analytical and numerical predictions for the, in principle, nonperturbative PDFs.

The second project is devoted to an important problem in heavy-ion physics. In the collision of heavy nuclei, a state of matter known as the Quark-Gluon Plasma (QGP) is created, in which quarks and gluons shortly exist freely in a regime characterized by an extremely high density and temperature. Hard jets, produced in the scattering of the two nuclei, have to travel through the QGP before reaching the detector, and will be attenuated as a result of their interaction with this medium. This phenomenon, or rather set of phenomena, is known as jet quenching and is one of the principal probes to investigate the properties of the QGP. To study jet quenching, we focus on the transverse momentum broadening of a hard particle traveling through a nuclear medium, and we employ small-x techniques to attempt to resum the single leading logarithmic corrections, due to soft gluon radiation, to this broadening. Although, ultimately, we can only solve the resulting in-medium evolution equation in the double leading logarithmic approximation, we do present a concise framework for the problem, and draw a detailed comparison with the CGC and with the existing literature.

Contents

I Deep-inelastic scattering at small Bjorken-x

II   Color Glass Condensate

III   Role of gluon polarization in forward heavy quark production in proton-nucleus collisions

IV   Renormalization of the jet quenching parameter

V   Appendices

Introduction

The main topic of this thesis is the study of the structure of hadrons, such as the proton or the neutron. Hadrons are composite particles built from quarks and gluons: the fundamental elementary particles that participate in the strong interaction, which, in the Standard Model, is described by the theory of quantum chromodynamics (QCD).

Quantum chromodynamics is a non-Abelian gauge theory, characterized by two main features. First, the strong coupling constant α_s is not actually a constant, but rather a function of the momentum scale of the process at hand. For large exchanges of momentum, α_s is small and one can apply perturbation theory, while in the opposite regime of small exchanged momenta, α_s is large and therefore perturbation theory fails. Unfortunately, most information on the hadron structure is 'hidden' in this nonperturbative domain of QCD.

A second feature of QCD is confinement: the property that the degrees of freedom of the theory, i.e. quarks and gluons or, collectively, 'partons', cannot be observed separately, but are always grouped into hadrons.

The way to deal with these particular intricacies of QCD is through factorization, which is a consistent framework to separate the perturbative from the nonperturbative part of a cross section. A well-known example is deep-inelastic scattering (DIS), for example in electron-proton collisions. The electron interacts with the proton through the emission of an energetic and highly virtual photon, which doesn't scatter off the proton as a whole, but rather kicks one of the proton's constituents out. The cross section can then be written as the product of the partonic part, which involves the electron-quark or electron-gluon interaction, on the one hand, and the structure function F_2 on the other hand. The virtuality of the photon provides the aforementioned large momentum scale, at which the coupling constant is small enough for the partonic part to be calculable in perturbation theory, up to a certain order in α_s. Therefore, the nonperturbative information on the process is now only contained in the structure function F_2, which can be written as a function of the so-called parton distribution functions (PDFs). Roughly speaking, these PDFs describe the probability to find a quark or gluon with a fraction x of the energy of the proton.

Information on the structure of the proton, and of hadrons in general, in terms of the QCD degrees of freedom, is thus generally encoded inside nonperturbative parton distribution functions. These PDFs are beyond the reach of perturbation theory, but rather need to be extracted from the experiment. They are, however, scale-dependent, and their evolution of one transverse momentum scale to the other can be calculated with great precision in perturbative QCD. The importance of the ensuing 'evolution equations' cannot be overstated, since they allow to plug in the PDFs, measured in a certain experiment and at a certain scale, into any other factorizable cross section.

In this thesis, we will concentrate in particular on hadron collisions at very high energies, in which those constituents are probed that carry a very small energy fraction (Bjorken-x) of their parent. This regime of QCD is mainly dominated by gluons, because the probability of a gluon emission scales with the inverse of the energy, and hence favors arbitrarily low gluon energies. An important consequence is that, at large enough collider energies, a high-density regime of QCD is reached. Moreover, at a certain scale, the gluon density becomes so high that nonlinear effects start

to play a role. In particular, the fast growth of the gluon density towards small energy fractions x is damped due to the rising importance of gluon recombinations, resulting in the so-called 'saturation' of the gluon density function.

Luckily for us, a high-density regime implies large momenta, which in turn corresponds to a small coupling constant. Hence, the applicability of perturbative QCD is extended to the description of the hadron structure in or near the saturation regime. The corresponding effective theory is known as the Color Glass Condensate (CGC), and combines the McLerran-Venugopalan (MV) model: a semi-classical description of a large nucleus or highly energetic proton, with a field theoretical nonlinear evolution equation called BK-JIMWLK, after its authors.

The first project we present in this work, in collaboration with Dr. Cyrille Marquet and Dr. Claude Roiesnel, is related to the forward production of two heavy quarks in proton-nucleus collisions. If the quarks have large transverse momenta and are almost back-to-back in the transverse plane, this process is not characterized by one, but by two momentum scales: the large transverse momentum of a single outgoing quark, and the small imbalance between both momenta. Such a process, with two ordered scales, can be described within 'transverse-momentum dependent' (TMD) factorization, in which one works with so-called TMD PDFs, or simply TMDs, which extend the regular PDFs by including the information on the transverse momentum of the parton inside the proton or, in our case, nucleus. TMD factorization is a framework which contains many intricacies, in particular, the TMDs become dependent on the process under consideration. As a result, not one but six different gluon TMD distribution functions play a role in the cross section for forward heavy diquark production. Interestingly, three of them only couple through the mass of the heavy quarks, and correspond to linearly polarized gluons within the unpolarized nucleus.

In the small-x limit, which –as we will show– applies when the diquark production is forward, we bring in information from the point of view of the Color Glass Condensate. Not only can we calculate the cross section within the CGC, we can also model the gluon TMDs which, again, are in general not perturbatively calculable. Doing so, we obtain analytical expressions for the gluon TMDs in the MV model, as well as numerical results for the evolution of the TMDs with a lattice QCD implementation of JIMWLK.

It was my task to extend the earlier work of Marquet and collaborators (Ref. [1]) on forward dijet production, by including the heavy quark mass. I derived analytically the CGC cross section, Eq. (13.52), as well as the expressions for the gluon TMDs in the MV model at finite-N_c, four of which are new (Eqs. (14.7), (14.8), (14.9) and (14.10)). Furthermore, I implemented them in the numerical code, written by Claude Roiesnel, and analyzed the results of the simulations (Figs. 18, 19).

The second project, in collaboration with Dr. Edmond Iancu, is another application of small-x physics, this time to a problem within heavy-ion physics. A central concept in heavy-ion physics is 'jet quenching': the attenuation of energetic partons when traveling through a nuclear medium, such as the quark-gluon plasma which is created in high-energy collisions of two nuclei. The way these partons are influenced by their interaction with the medium, and the resulting signatures in the detector, are an important probe to the properties of the plasma itself. We focus on one aspect of jet quenching, namely 'transverse momentum broadening': the average transverse momentum obtained by the energetic parton as a result of the scatterings off the medium constituents. Generalizing the JIMWLK equation to be applicable to an extended medium, large logarithmic corrections due to

gluon radiation can be resummed and absorbed into a renormalization of the transverse momentum broadening, or rather, the 'jet quenching parameter' $\hat{q}$ associated with it. It was the aim of the project to extend the currently available calculations (Refs. [2–4]) to a greater precision, i.e. re-summing all the single leading logarithmic corrections rather than the double large logarithms. We were, however, unable to do this, and at present it is not even clear whether such a thing is feasible and/or meaningful. I therefore limit myself to a careful explanation of –my understanding of– the approach of Iancu to the problem (Ref. [4]) supplemented with an outline of, and comparison with, the work in Ref. [2]. Even without reaching our original goal, the project calls for an in-depth analysis of gluon radiation, as well as its interaction with a nuclear medium, and as such it may deepen the understanding of the matters in the preceding parts of the thesis.

Before presenting both projects in Parts III and IV, I introduce the basics of small-x physics through the example of DIS, in Part I, followed by an introduction on the Color Glass Condensate in Part II. For these first parts, I closely follow the very educational review on the CGC in Ref. [5], supplemented with the book by Kovchegov and Levin, Ref. [6], the review by Gelis [7], and of course what I learned during the many discussions with Dr. Iancu and Dr. Marquet. Further references are specified in the main text.

Acknowledgements

which resulted in a nice project together.

I gratefully acknowledge the help of Prof. Al Mueller, explaining me his work on the radiative corrections to transverse momentum broadening, and of Dr. Stéphane Peigné, who explained me with admirable patience the BDMPS formalism. Furthermore, I am very grateful to Dr. Krzysztof Kutak for kindly welcoming me for an internship in his group in Krakow, for involving me in his work, and for the many stimulating discussions. Thanks as well to my fellow PhD student Merijn van de Klundert, for reading parts of my thesis and for the many enlightening conversations that ensued, and to Dr. Hans Van Haevermaet for answering many questions on QCD. Thanks to Prof. Nick Van Remortel for the numerous interesting discussions, and in particular for the very nice trip we made to India, and thanks to Thomas Epelbaum and his wife, Véronique Mariotti, for their friendship and for inviting me in Montréal.

Thanks to the members of the jury that I didn't mention yet: Prof. Francesco Hautmann, Prof. Etienne Goovaerts and the chairman: Prof. Michiel Wouters, for carefully reading the manuscript and giving numerous helpful comments and corrections.

A very special thanks goes to Sarah Van Mierlo, the secretary of our group. For every question that wasn't related to physics, every practical or even emotional problem, every remark or joke, I could go to her. Thanks, Sarah, for all your help and all your kindness, and for making our group such a pleasant place.

Thanks as well to Hilde Evans, the secretary of the physics department, for kindly taking care of all the practical and administrative issues which writing a thesis brings.

Thanks to all my friends in physics, making a day spent at the university a nice day: thanks Ben, Christophe, Mario, Matthias, Maxim, Maya, Merijn, Nikolas, Roeland, Ruben and Sam –I am sure we stay in touch!

During the largest part of my PhD, I lived in Roeach, one of the houses of L'Arche Antwerp: a community in which people with and without an intellectual disability live together[1]. For more than four years, Roeach has been my house, and for much longer L'Arche has been a home. The list of people to acknowledge is endless, so let me just thank my dear housemates and friends of Roeach: Tony, Korneel, Carina, Sonja, Sabien and Greta.

Finally, thanks to my close group of friends from Antwerp (and Leuven and The Netherlands, nowadays), thanks to my loving parents and my dear two sisters, and of course thanks to my beloved Aurélie, whom I love even more than physics!

Krakow, June 26th, 2017

---

[1]See http://www.larche.org (international) or http://www.arkantwerpen.be (Antwerp).

Nomenclature

BDMPS or BDMPS-Z   Baier-Dokshitzer-Mueller-Peigné-Schiff-Zakharov

BFKL   Balitsky-Fadin-Kuraev-Lipatov

BK   Balitsky-Kovchegov

CCFM   Catani-Ciafaloni-Fiorani-Marchesini

CGC   Color Glass Condensate

DGLAP   Dokshitzer-Gribov-Lipatov-Altarelli-Parisi

DIS   Deep-Inelastic Scattering

DLA or DLLA   Double Leading Logarithmic Approximation

GBW   Golec-Biernat and Wüsthoff

HEF   High-Energy Factorization

HERA   Hadron-Electron Ring Accelerator (in DESY, Hamburg)

IMF   Infinite-Momentum Frame

IR   Infrared

JIMWLK   Jalilian-Marian-Iancu-McLerran-Weigert-Leonidov-Kovner

LCPT   Light-Cone Perturbation Theory

LC   Light Cone

LHC   Large Hadron Collider (in CERN, Geneva)

LLA   Leading Logarithmic Approximation

LO   Leading Order

MV   McLerran-Venugopalan

NLO   Next-to-Leading Order

pA   Proton-Nucleus

PDF   Parton Distribution Function

pp   Proton-Proton

QCD   Quantum Chromodynamics

QGP	Quark-Gluon Plasma
RHIC	Relativistic Heavy Ion Collider (in Brookhaven, New York)
TMB	Transverse Momentum Broadening
TMD	Transverse Momentum Dependent parton distribution function
UV	Ultraviolet

Part I

Deep-inelastic scattering at small Bjorken-x

1 Deep-inelastic scattering

We start this work with a quick review of deep-inelastic scattering (DIS) (Refs. [5, 8–10]), in which a nucleon or nucleus is probed by a highly energetic lepton. Not only did DIS play a crucial role in the early development of QCD in the seventies: much later, in the early nineties, the HERA measurements of DIS at high energies sparked a large interest in the phenomenology of small-x physics. In addition, DIS is a particular suited case to introduce the concept of evolution, which will play a central role in this thesis.

For definiteness, let us look at the case of deep-inelastic scattering of an electron off a proton, as is illustrated in Fig. 1. The electron interacts with the proton through the exchange of a highly virtual photon, which kicks out one of the proton's constituents, thus breaking the proton and probing its structure. In pre-QCD language, these constituents are collectively called 'partons', but we know them of course as quarks and gluons.

In the cross section, one can separate the lepton current from the hadronic part of the interaction, and therefore we can just consider the virtual photon-proton part of the scattering process. Furthermore, we work in a so-called infinite momentum frame (IMF), in which the proton has a very large momentum P along the z-axis:

$$P^\mu = \left(\sqrt{P^2 + M^2}, \mathbf{0}_\perp, P \right) \simeq (P, \mathbf{0}_\perp, P),\tag{1.1}$$

and we choose the frame such that the virtual photon has momentum

$$q^\mu = (q_0, \mathbf{q}_\perp, 0).\tag{1.2}$$

The kinematics of the photon-proton scattering is fully determined by two parameters: the virtuality of the photon $Q^2 = -q^2$, and the dimensionless Bjorken-x variable, defined as:

$$x \equiv \frac{Q^2}{2P \cdot q} = \frac{Q^2}{s + Q^2 - M^2} \simeq \frac{Q^2}{s + Q^2} \simeq \frac{Q^2}{s},\tag{1.3}$$

where $s = (P + q)^2$ is the center-of-mass energy, and where the last equality holds in the high-energy regime or 'Regge limit' $s \gg Q^2$. Since in the lab frame $Q^2 = 2EE'(1 - \cos\theta)$, with E and E' the energy of the electron before and after the scattering with an angle θ, Q^2 can be measured experimentally, and so can x, via Eq. (1.3).

In Eq. (1.3), we assumed that the virtuality of the photon is much larger than the proton mass: $Q^2 \gg M^2$. In this case, the scattering will be inelastic and the proton is broken up: the photon interacts not with the proton as a whole, but with one single parton which it kicks out. In comparison with the large virtuality of the photon, the virtualities k^2 and k'^2 of the parton can be neglected, and the parton is assumed to be on shell before and after the interaction. Furthermore, throughout
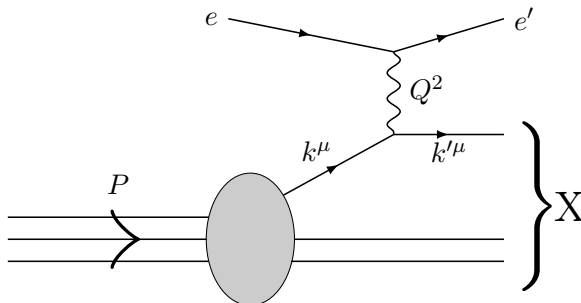
Figure 1: Inclusive deep-inelastic scattering (DIS)

this analysis (and, in fact, the largest part of this thesis) the partons are taken to be massless. Assuming that $k^\mu \simeq \xi P^\mu$, i.e. introducing the fraction ξ of the momentum of the proton that is carried by the parton and neglecting the transverse momentum of the latter, we obtain the following requirement:

$$k'^2 = (\xi P^\mu + q^\mu)^2 \simeq 0, \tag{1.4}$$

from which we easily find that:

$$\xi = x. \tag{1.5}$$

The Bjorken-x variable (1.3), a priori a kinematic parameter which can be controlled in the experiment, therefore turns out to describe the momentum fraction of the proton that is carried by the parton that participates in the scattering.

The time scale over which the photon-parton interaction takes place is estimated as the inverse of the energy of the virtual photon:

$$\Delta t_{\text{coll}} \sim \frac{1}{q^0} = \frac{2xP}{Q^2}. \tag{1.6}$$

Each of the partons, however, have their own characteristic lifetime. In order to compute it, we have to reintroduce the transverse momentum of the parton, which we previously neglected, and which is naturally estimated as being of the same order as Λ_{QCD}, since this is the only scale in the proton at this moment:

$$k^\mu \simeq (\omega \equiv xP, \mathbf{k}_\perp, xP) \quad \text{with} \quad k_\perp \sim \Lambda_{\text{QCD}}. \tag{1.7}$$

The parton lifetime is now, by virtue of Heisenberg's principle, given by the inverse of its virtual mass $m^* = \sqrt{|k_\mu k^\mu|} = k_\perp$, times the Lorentz contraction factor:

$$\Delta t_{\text{fluc}} \simeq \gamma \frac{2}{m^*} = \frac{\omega}{m^*} \frac{2}{m^*} \simeq \frac{2\omega}{k_\perp^2}. \tag{1.8}$$

Since a parton in the proton can only absorb a virtual photon with a shorter lifetime than its own, we require that:

$$\Delta t_{\text{coll}} \lesssim \Delta t_{\text{fluc}}. \tag{1.9}$$

In other words: the parton dynamics is 'frozen' with respect to the interaction with the photon. Comparing expression (1.6) with Eqs. (1.8) and (1.7), we see that the above requirement is tantamount to the statement that the photon interacts with partons with a transverse momentum smaller than its virtuality:

$$k_\perp^2 \lesssim Q^2. \tag{1.10}$$

From Heisenberg's uncertainty relation, these partons are localized over an area $r_\perp^2 \sim 1/Q^2$ in the transverse plane, hence Q^2 can be interpreted as the resolution with which the proton's constituents are probed.

In the high-energy regime $s \gg Q^2$, the virtual photon-proton cross section can be written as follows (see Refs. [8, 11]):

$$\sigma_{\gamma^* p} = \frac{4\pi^2 \alpha_{\text{em}}}{Q^2} F_2\left(x, Q^2\right). \tag{1.11}$$

In the above formula, $F_2\left(x, Q^2\right)$ is the proton structure function, which parametrizes our ignorance about the precise details of its interior. The combined data on the F_2 structure function is shown in Fig. 2. It is extracted from measurements at the H1 and Zeus $e^- p$ and $e^+ p$ deep-inelastic scattering experiments at HERA, as well as some fixed target electron and muon scattering experiments at SLAC, BCDMS & EMC (CERN) and E665 (Fermilab). At fairly large values of x, of the order $x \sim 0.1$, the structure function is approximately constant with varying Q^2. This phenomenon was predicted by Bjorken (Ref. [12]) and is therefore known as Bjorken scaling. Shortly after, Feynman established the so-called parton model (Ref. [13]), in which he interpreted this scaling as a consequence of the fact that the proton is composed of asymptotically free partons, which are point like (hence the scattering is independent of the resolution $1/Q^2$) and which carry an electrical charge. The structure function can then be written as the following function of the quark and antiquark parton distribution functions (PDFs) $q_f\left(x, Q^2\right)$ and $\bar{q}_f\left(x, Q^2\right)$:

$$F_2\left(x, Q^2\right) = \sum_f e_{q_f}^2 \left(x q_f\left(x, Q^2\right) + x \bar{q}_f\left(x, Q^2\right)\right), \tag{1.12}$$

where $e_{q_f}^2$ is the fractional electromagnetic charge carried by the quark with flavor f. It is however clear from the data that Bjorken scaling is violated, which we also suspect from our heuristic argument that increasing Q^2 is tantamount to increasing the phase space for partons to participate in the scattering, see Eq. (1.10). This argument is in fact deeply rooted in QCD: to make this more clear, and to elucidate on the connection with scaling violation, it is worth to do a small calculation.
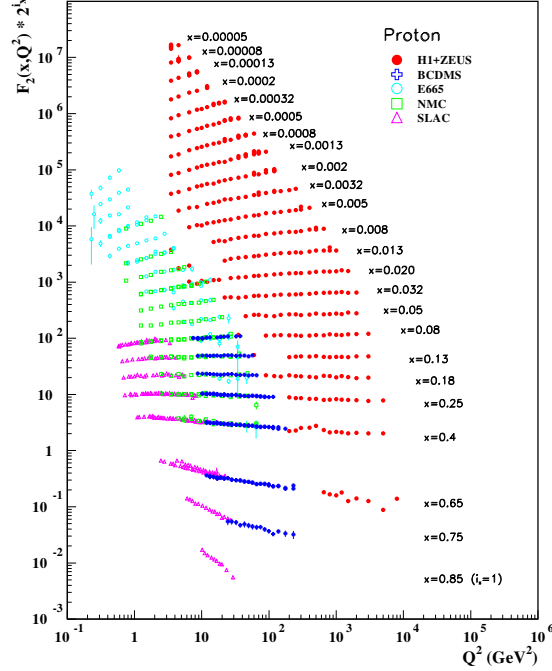
Figure 2: The proton structure function F_2, for clarity multiplied by 2^{i_x}, with i_x the number of the bin in Bjorken-x from $i_x = 1$ (for $x = 0.85$) to $i_x = 24$ (for $x = 5 \cdot 10^{-5}$) [14]

2 The soft Bremsstrahlung law

Let us compute (following Ref. [15]) the probability in QCD for a quark to radiate a gluon in the high-energy limit. This probability can be easily extracted from the cross section of the following process, depicted in Fig. 3, in which a quark, which was created in some hard process $\mathcal{M}_h$, emits a gluon. The amplitude corresponding to this process is:

$$\mathcal{M} = \bar{u}(p) i g_s t^a \not{\epsilon}^\lambda(k) \frac{i\left(\not{p} + \not{k}\right)}{\left(p + k\right)^2 + i\epsilon} \mathcal{M}_h, \tag{2.1}$$

where $\bar{u}(p)$ is the spinor of the outgoing quark, t^a is the generator of the $SU(3)$ group in the fundamental representation, g_s is the strong coupling constant, $\mathcal{M}_h$ is the matrix element of the hard process, $\epsilon^\lambda_\mu(k)$ for $\lambda = 1, 2$ are the polarization vectors of the gluon, and where the Feynman slash denotes multiplication with the gamma matrices: $\not{p} = p_\mu \gamma^\mu$. Since we are interested in the high-energy limit, in which the quark is traveling at almost the speed of light, the process can be best described using light-cone (LC) coordinates, defined as follows:

$$x^+ \equiv \frac{x^0 + x^3}{\sqrt{2}}, \quad x^- \equiv \frac{x^0 - x^3}{\sqrt{2}}, \quad \mathbf{x}_\perp \equiv \left(x^1, x^2\right), \tag{2.2}$$

4
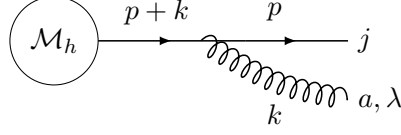
Figure 3: A quark, created in some hard process $\mathcal{M}_h$, loses its virtuality by emitting a gluon. From this process, the Bremsstrahlung law Eq. (2.10) can be extracted.

where the scalar product of two vectors reads:

$$x \cdot y = x^+ y^- + x^- y^+ - \mathbf{x}_\perp \cdot \mathbf{y}_\perp. \tag{2.3}$$

In these coordinates, the momentum of a highly energetic particle which is traveling in the positive z-direction (a 'right-mover') has a large '+' component $q^+ = (E + q_z)/\sqrt{2} \simeq \sqrt{2} q_z$, while its '$-$' component $q^- = (E - q_z)/\sqrt{2} \simeq q_\perp^2/2q^+$ (the last equality holds only when the particle is on shell) is very small:

$$q^\mu \simeq \left(q^+, q^-, \mathbf{q}_\perp\right) \quad \text{with} \quad q^+ > q_\perp > q^-. \tag{2.4}$$

For a right-mover, $x^+ \simeq \sqrt{2} x^0 = \sqrt{2} t$ plays the role of light-cone time, while the particle is sharply located around the longitudinal coordinate $x^- \ll 1$. Likewise, the q^- momentum, conjugate to x^+, can be regarded as the light-cone energy with $x^+ \sim 1/q^-$, while q^+ is the light-cone momentum and is conjugate to x^-, i.e. $x^- \sim 1/q^+$. For a 'left-mover', which travels in the negative z-direction with a large '$-$' momentum component, these roles are reversed.

The momenta of the quark (neglecting its mass and transverse momentum, since it is on shell this implies $p^- = p_\perp^2/2p^+ = 0$) and the gluon in Eq. (2.1) are then given by:

$$p^\mu = \left(p^+, 0, \mathbf{0}_\perp\right), \qquad k^\mu = \left(k^+, k^-, \mathbf{k}_\perp\right). \tag{2.5}$$

The two polarization vectors $\epsilon_\mu^\lambda(k)$ are defined to be transverse with respect to the gluon momentum k^μ:

$$\epsilon_\mu^\lambda(k) = \left(0, \frac{\mathbf{k}_\perp \cdot \boldsymbol{\epsilon}_\perp^\lambda}{k^+}, \boldsymbol{\epsilon}_\perp^\lambda\right) \qquad \lambda = 0, 1,$$
$$\sum_\lambda \epsilon_i^{\lambda\dagger} \epsilon_j^\lambda = \delta^{ij}, \quad \boldsymbol{\epsilon}_\perp^{\lambda\dagger} \cdot \boldsymbol{\epsilon}_\perp^{\lambda'} = \delta^{\lambda\lambda'}, \quad k^\mu \epsilon_\mu^\lambda(k) = 0. \tag{2.6}$$

In order to evaluate the amplitude Eq. (2.1), let us first set $\not{k} \simeq 0$ in the numerator of the propagator, since the momentum p^μ of the highly energetic quark dominates. Next, the gamma matrices can be interchanged according to $\{\gamma^\mu, \gamma^\nu\} = 2g^{\mu\nu}$, after which we apply the Dirac equation $\bar{u}(k)\not{k} = \bar{u}(k)m \simeq 0$:

$$\mathcal{M} \simeq -2g_s t^a \bar{u}(p) p^\mu \epsilon_\mu^\lambda(k) \frac{1}{(p+k)^2 + i\epsilon} \mathcal{M}_h,$$
$$= -2g_s t^a \bar{u}(p) p^+ \frac{\mathbf{k}_\perp \cdot \boldsymbol{\epsilon}_\perp^\lambda}{k^+} \frac{1}{(p+k)^2 + i\epsilon} \mathcal{M}_h. \tag{2.7}$$

5

Furthermore:

$$
\begin{aligned}
\mathcal{M} &= -2g_s t^a \bar{u}(p) p^+ \frac{\mathbf{k}_\perp \cdot \boldsymbol{\epsilon}_\perp^\lambda}{k^+} \frac{1}{2p \cdot k} \mathcal{M}_h, \\
&= -2g_s t^a \bar{u}(p) \frac{\mathbf{k}_\perp \cdot \boldsymbol{\epsilon}_\perp^\lambda}{2k^- k^+} \mathcal{M}_h, \\
&= -2g_s t^a \frac{\mathbf{k}_\perp \cdot \boldsymbol{\epsilon}_\perp^\lambda}{k_\perp^2} \bar{u}(p) \mathcal{M}_h,
\end{aligned}
\tag{2.8}
$$

where, in the last equality, we assumed that the gluon is on shell hence $k^- = k_\perp^2 / 2k^+$. From this amplitude, the cross section is obtained by taking the absolute value squared, averaging over the colors of the quark, summing over the gluon polarization, integrating over the momentum of the gluon, and imposing the mass-shell condition:

$$
\begin{aligned}
\sigma &= \int \frac{\mathrm{d}k^+ \mathrm{d}k^- \mathrm{d}^2\mathbf{k}_\perp}{(2\pi)^4} 2\pi \delta\left(k^2\right) |\mathcal{M}|^2, \\
&= \int \frac{\mathrm{d}k^+ \mathrm{d}^2\mathbf{k}_\perp}{(2\pi)^3 \, 2k^+} 4g_s^2 C_F \frac{1}{k_\perp^2} |\bar{u}(p)\mathcal{M}_h|^2.
\end{aligned}
\tag{2.9}
$$

In the above formula, $C_F = \mathrm{Tr}\left(t^a t^a\right)/N_c = \left(N_c^2 - 1\right)/2N_c$ is the Casimir operator for the fundamental representation. Forgetting about the generic hard part, we can extract from the cross section above the differential probability for a quark to radiate a soft gluon, which we will call the 'soft Bremsstrahlung law':

$$
\frac{\mathrm{d}P_{\text{Brems}}}{\mathrm{d}x \mathrm{d}^2\mathbf{k}_\perp} = \frac{\alpha_s C_F}{\pi} \frac{1}{x} \frac{1}{\pi k_\perp^2},
\tag{2.10}
$$

with $\alpha_s \equiv g_s^2/4\pi$ and where $x \equiv k^+/p^+$. When the emitter is a gluon, rather than a quark, the result is exactly the same, apart from the Casimir operator C_F which should be replaced with the Casimir operator for the adjoint representation: $C_F \to N_c$. Although the above formula is a simple result, from a straightforward calculation, its importance cannot be overstated. First, it should be noted that the Bremsstrahlung law is very general, and holds beyond the process in Fig. 3. In particular, the outgoing particles do not necessarily have to be on shell, but can be further involved in other processes, or emit radiation themselves. Second, Eq. (2.10) is clearly singular both in the limit $x \to 0$, where the energy of the emitted gluon goes to zero, and in the limit $k_\perp^2 \to 0$, in which the gluon's transverse momentum goes to zero. These singularities, called the soft and the collinear divergency, respectively, can be dealt with by including the appropriate infrared cutoffs. However, when integrating over Eq. (2.10), which happens for example in the cross section Eq. (2.9), and when there is a large interval of energy or transverse momentum available, the Bremsstrahlung law gives rise to large logarithms:

$$
\begin{aligned}
P_{\text{Brems}} &= \frac{\alpha_s C_F}{\pi} \int_{\mu^2}^{k_\perp^2} \frac{\mathrm{d}k_\perp'^2}{k_\perp'^2} \int_x^1 \frac{\mathrm{d}x'}{x'}, \\
&= \frac{\alpha_s C_F}{\pi} \ln \frac{k_\perp^2}{\mu^2} \ln \frac{1}{x},
\end{aligned}
\tag{2.11}
$$

where μ is an infrared cutoff for the transverse momentum, and where the upper bound for the energy fraction of the emitted gluon is simply $x_{\max} = 1$. If either one of the above logarithms is large enough to compensate for the small coupling constant:

$$\alpha_s \ln \frac{k_\perp^2}{\mu^2} \sim 1 \quad \text{or} \quad \alpha_s \ln \frac{1}{x} \sim 1, \tag{2.12}$$

then the probability of a single gluon emission becomes of order one or larger, and hence perturbation theory loses its meaning. At this point, it is not correct anymore to regard the probability for two or more emissions as a correction to a Feynman diagram with one single emission. Rather, multiple emissions take place which, to render the theory consistent again, have to be resummed to all orders in α_s. This can be done by dividing the problematic part of the phase space in small intervals, such that $\alpha_s \ln(x_{i+1}/x_i) \lesssim 1$ and $\alpha_s \ln\left(k_{\perp i+1}^2/k_{\perp i}^2\right) \lesssim 1$:

$$x' \in [1, ..., x_i, x_{i+1}, ..., x_{\min}] \quad \text{and} \quad k_\perp^2 \in \left[k_{\perp\min}^2, ..., k_{\perp i}^2, k_{\perp i+1}^2, ..., k_{\perp\max}^2\right]. \tag{2.13}$$

In addition, we impose that consecutive emissions have to be strongly ordered: each emitted gluon has a much larger transverse momentum and much smaller energy than the previous one:

$$k_{\perp i-1}^2 \ll k_{\perp i}^2 \ll k_{\perp i+1}^2 \quad \text{and} \quad x_{i-1} \gg x_i \gg x_{i+1}. \tag{2.14}$$

The result of this condition is that only those emissions are taken into account that are enhanced by a large logarithm both in the transverse momentum and in the energy, and which are therefore the dominant contributions. For example, the probability for two successive strongly-ordered emissions is:

$$\begin{aligned}
P_{\text{Brems}}^{(2)} &= \left(\frac{\alpha_s C_F}{\pi}\right)^2 \int_{k_{\perp\min}^2}^{k_{\perp\max}^2} \frac{\mathrm{d}k_\perp^2}{k_\perp^2} \int_{x_{\min}}^1 \frac{\mathrm{d}x}{x} \int_{k_{\perp\min}^2}^{k_\perp^2} \frac{\mathrm{d}k_\perp'^2}{k_\perp'^2} \int_x^1 \frac{\mathrm{d}x'}{x'}, \\
&= \frac{1}{2!2!} \left(\frac{\alpha_s C_F}{\pi}\right)^2 \ln^2 \frac{k_{\perp\max}^2}{k_{\perp\min}^2} \ln^2 \frac{1}{x_{\min}},
\end{aligned} \tag{2.15}$$

and in general, for n such emissions:

$$P_{\text{Brems}}^{(n)} = \frac{1}{n!n!} \left(\frac{\alpha_s C_F}{\pi} \ln \frac{k_{\perp\max}^2}{k_{\perp\min}^2} \ln \frac{1}{x_{\min}}\right)^n. \tag{2.16}$$

Summing all these probabilities, we obtain a modified Bessel function of the first kind (see Refs. [6, 16]):

$$\begin{aligned}
P_{\text{Brems}} &= \sum_{n=0}^\infty P_{\text{Brems}}^{(n)}, \\
&= I_0 \left(2\sqrt{\frac{\alpha_s C_F}{\pi} \ln \frac{k_{\perp\max}^2}{k_{\perp\min}^2} \ln \frac{1}{x_{\min}}}\right).
\end{aligned} \tag{2.17}$$

In this expression, soft and collinear gluon emissions are resummed to all orders in α_s in what is known as the double leading logarithmic approximation (DLA or DLLA). For the sake of this

discussion, the upper and lower bounds on the phase space were left generic: we will see soon that in practice the appropriate limits are imposed by the physical problem under consideration.

However, computing both the transverse momentum and the energy merely to logarithmic accuracy is a very crude approximation. Often, either integrating over the energies, or integrating over the transverse momenta leads to large logarithms, but not at the same time. In such a case, it is more accurate to work in the so-called leading logarithmic approximation (LLA) in which strong ordering is only imposed on the problematic part of phase space, resumming the ensuing large logarithms, while treating the other part exactly. For instance, when computing radiative corrections to DIS at moderate values of x, there is only a large phase space for the transverse momenta available. Hence, the transverse momenta of emitted partons are required to be strongly ordered, such that logarithms $\alpha_s \ln \left(k_{\perp i}^2/k_{\perp i-1}^2\right)$ can be resummed, but the energy dependence of the emissions is treated exactly, in particular beyond the approximation $\mathrm{d}P_{\mathrm{Brems}} \propto \alpha_s \mathrm{d}x/x$ which only holds for gluons in the limit $x \ll 1$. This is the main idea behind the DGLAP evolution equation, which we will study in the following section, while the BFKL equation, which is the subject of Sec. 5, is applicable in the opposite case of a large phase space for the energy. The DLA approximation to gluon radiation can thus be seen as the common limit of the DGLAP and BFKL evolution equations.

3 DGLAP

We are now ready to compute the various leading-order QCD corrections to the parton model of DIS, Eqs. (1.11) and (1.12), in which, before scattering with the virtual photon, the parton coming from the proton radiates. As announced earlier, the transverse momenta of the splittings will be treated in the leading logarithmic approximation, while we compute the energy-dependence exactly. First, consider the process in which a quark emits a gluon (Fig. 4, a). Unlike the similar calculation that we performed in the previous section, this time we work beyond the high-energy limit, hence the computation becomes a bit more complicated since we explicitly have to keep track of the different helicity configurations. However, instead of performing the computation from scratch (see for instance Ref. [6, 10]), let us take a shortcut. As it happens, we have some results from light-cone perturbation theory (LCPT) at our disposal, which we will use later in this work in order to compute dijet production in proton-nucleus collisions. Without going into the details of LCPT, for which we refer to Ref. [17], let us simply remark that it is a reformulation of perturbation theory, similar to time-ordered or old-fashioned perturbation theory (see for instance Ref. [18]), which is completely equivalent to the more standard covariant approach, but has some useful advantages. In particular, in LCPT the notion of Fock space is reintroduced, hence one can count particle states. The probability for a certain splitting process to occur is then encoded in the corresponding light-cone wave function. In section E of the appendix, the wave function for the $q \to gq$ process is calculated, which turns out to be:

$$\psi_{\alpha\beta}^{\lambda}\left(p, k\right) = \frac{1}{\sqrt{k^+}} \frac{1}{\mathbf{k}_{\perp}^2 + z^2 m^2} \begin{cases} \sqrt{2}\mathbf{k}_{\perp} \cdot \boldsymbol{\epsilon}_{\perp}^1 \left[\delta_{\alpha-}\delta_{\beta-} + (1-z)\,\delta_{\alpha+}\delta_{\beta+}\right] + mz^2\delta_{\alpha+}\delta_{\beta-} & \lambda = 1 \\ \sqrt{2}\mathbf{k}_{\perp} \cdot \boldsymbol{\epsilon}_{\perp}^2 \left[\delta_{\alpha+}\delta_{\beta+} + (1-z)\,\delta_{\alpha-}\delta_{\beta-}\right] - mz^2\delta_{\alpha-}\delta_{\beta+} & \lambda = 2 \end{cases}.$$
(3.1)
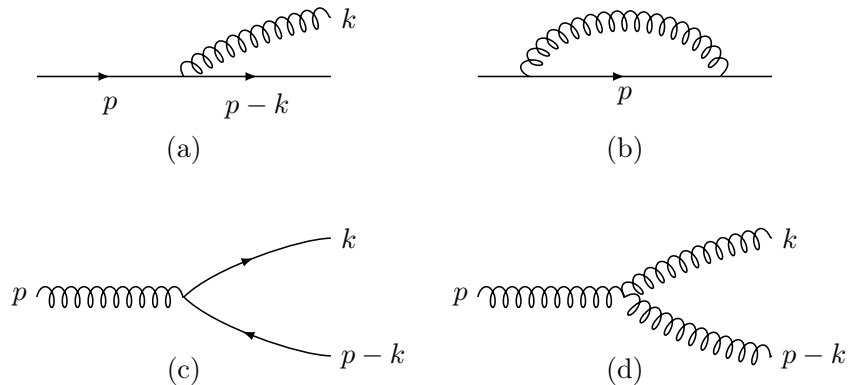
Figure 4: The four DGLAP splitting functions.

In the above expression, p^μ is the four-momentum of the incoming quark, k^μ is the momentum of the outgoing gluon and $z \equiv k^+/p^+$ is the longitudinal momentum fraction carried by the radiated gluon. The helicities of the incoming and outgoing quark are denoted by α and β, respectively, while the gluon has a polarization λ and color c. The full dynamics of the emission process is present in Eq. (3.1), and we can extract it (see for instance [19]) by taking the absolute value squared, Eq. (D.26), from which we obtain the differential probability to find a gluon inside a dressed quark:

$$\frac{\mathrm{d}P_{gq}}{\mathrm{d}k^+\mathrm{d}^2\mathbf{k}_\perp} = \frac{g_s^2}{(2\pi)^3}\frac{1}{N_c}\mathrm{Tr}\left(t^c t^c\right)\left|\psi^{q\to qg}\left(p,k\right)\right|^2. \tag{3.2}$$

In the massless limit, this simplifies to (see Eq. (D.31)):

$$\frac{\mathrm{d}P_{gq}}{\mathrm{d}z\mathrm{d}^2\mathbf{k}_\perp} = \frac{\alpha_s}{2\pi}\frac{1}{\pi k_\perp^2}\mathcal{P}_{gq}\left(z\right), \tag{3.3}$$

where we expressed the probability in terms of z instead of k^+, and where we introduced the Altarelli-Parisi splitting function:

$$\mathcal{P}_{gq}\left(z\right) \equiv C_F\frac{1+\left(1-z\right)^2}{z}. \tag{3.4}$$

Clearly, in the limit in which the gluon is soft with respect to its parent: $z \to 0$, expression (3.3) reduces to the soft Bremsstrahlung law, Eq. (2.10).

Next, we want to compute the probability to find a quark, with a momentum fraction z, within a dressed quark (which is, in leading order, a quark-gluon pair). Naively, one would expect the probability to be simply:

$$\frac{\mathrm{d}P_{qq}}{\mathrm{d}z\mathrm{d}^2\mathbf{k}_\perp} = \frac{\alpha_s}{2\pi}\frac{1}{\pi k_\perp^2}\mathcal{P}_{qq}\left(z\right),$$

$$\mathcal{P}_{qq}\left(z\right) \equiv \mathcal{P}_{gq}\left(1-z\right) = C_F\frac{1+z^2}{1-z}. \tag{3.5}$$

This answer is however only partially true: in contrast to the previous case, in which diagram (a) of Fig. 4 is the only leading-order contribution to the probability to find a gluon in a dressed quark, we now have to include the probability that the quark does not to radiate at all, or that it emits and re-absorbs a virtual gluon (diagram (b) in Fig. 4). One can, however, avoid calculating these contributions explicitly, by looking at the integrated probability:

$$\mathcal{F}_{qq}\left(z,Q^2\right) = \int_{\mu^2}^{Q^2} \mathrm{d}^2 k_\perp \frac{\mathrm{d}P_{qq}}{\mathrm{d}z\mathrm{d}^2\mathbf{k}_\perp}, \tag{3.6}$$

where μ is some infrared cutoff. Indeed, demanding the total probability to find a quark inside a dressed quark to be equal to one:

$$\int_0^1 \mathrm{d}z \mathcal{F}_{qq}\left(z,Q^2\right) = 1, \tag{3.7}$$

Eq. (3.6) can be written as follows:

$$\mathcal{F}_{qq}\left(z,Q^2\right) = \delta\left(1-z\right) + \frac{\alpha_s}{2\pi}\ln\frac{Q^2}{\mu^2}\left(\mathcal{P}_{qq}\left(z\right) - \text{virtual}\right), \tag{3.8}$$

and hence the real and virtual leading-order contributions are required to cancel:

$$\int_0^1 \mathrm{d}z\left(C_F\frac{1+z^2}{1-z} - \text{virtual}\right) = 0. \tag{3.9}$$

Obviously, the first term of this expression, corresponding to the real emission of a gluon, is divergent in the soft limit $z \to 1$. However, this singularity will be cancelled by the virtual correction, as is guaranteed by the Kinoshita-Lee-Nauenberg theorem. Knowing this, we can force the integral over the first term to converge by introducing the so-called plus notation:

$$\int_0^1 \mathrm{d}z\frac{f\left(z\right)}{\left(1-z\right)_+} \equiv \int_0^1 \mathrm{d}z\frac{f\left(z\right) - f\left(1\right)}{1-z}, \tag{3.10}$$

yielding:

$$\int_0^1 \mathrm{d}z\frac{1+z^2}{\left(1-z\right)_+} = \int_0^1 \mathrm{d}z\frac{z^2-1}{1-z} = -\frac{3}{2}. \tag{3.11}$$

The result of this procedure is that we extracted the regular part of the integration over the emission term in Eq. (3.9). We are therefore left with the singular piece (or rather, the piece that will yield a singularity after integration), which, from Eq. (3.9), together with the virtual piece should give:

$$\int_0^1 \mathrm{d}z\left(\text{singular} + \text{virtual}\right) = -\frac{3}{2}C_F. \tag{3.12}$$

Since the cancellation of the problematic terms takes place when $z = 1$, we infer:

$$\text{singular} + \text{virtual} = -\frac{3}{2}C_F\delta\left(1-z\right), \tag{3.13}$$

10

and finally obtain:

$$\frac{\mathrm{d}P_{gq}}{\mathrm{d}z\mathrm{d}^2\mathbf{k}_\perp} = \frac{\alpha_s}{2\pi}\frac{1}{\pi k_\perp^2}\tilde{\mathcal{P}}_{qq}(z),$$

$$\tilde{\mathcal{P}}_{qq}(z) \equiv C_F\frac{1+z^2}{(1-z)_+} + \frac{3}{2}C_F\delta(1-z),$$

(3.14)

where $\tilde{\mathcal{P}}_{qq}(z)$ is the regularized quark-quark splitting function (as opposed to the unregularized splitting function Eq. (3.5) which contains only the real emission).

The next step in our analysis is to include the probability that a gluon splits into a quark-antiquark pair, for which there is at leading order again only one diagram, see (c) in Fig. 4. In analogy with the Eq. (3.2) for the $q \to qg$ case, we can write the probability distribution:

$$\frac{\mathrm{d}P_{qg}}{\mathrm{d}k^+\mathrm{d}^2\mathbf{k}_\perp} = \frac{g_s^2}{(2\pi)^3}n_f\frac{1}{N_c^2-1}\mathrm{Tr}\left(t^c t^c\right)\left|\psi^{g\to q\bar{q}}(p,k)\right|^2,$$

(3.15)

where n_f is the number of quark flavors. With the help of the result for the squared $g \to q\bar{q}$ wave function, Eq. (D.31) from appendix D, we obtain:

$$\frac{\mathrm{d}P_{qg}}{\mathrm{d}z\mathrm{d}^2\mathbf{k}_\perp} = \frac{\alpha_s}{2\pi}\frac{1}{\pi k_\perp^2}\mathcal{P}_{qg}(z),$$

(3.16)

with the splitting function:

$$\mathcal{P}_{qg}(z) = n_f\frac{z^2+(1-z)^2}{2}.$$

(3.17)

Finally, let us take the splitting of a gluon into two other gluons into account, which is depicted in Fig. 4, d. This process corresponds to the following probability:

$$\frac{\mathrm{d}P_{gg}}{\mathrm{d}z\mathrm{d}^2\mathbf{k}_\perp} = \frac{\alpha_s}{2\pi}\frac{1}{\pi k_\perp^2}\tilde{\mathcal{P}}_{gg}(z),$$

(3.18)

with the regularized splitting function given by (see, for instance [6, 19]):

$$\tilde{\mathcal{P}}_{gg}(z) \equiv 2N_c\left[\frac{1-z}{z} + \frac{z}{(1-z)_+} + z(1-z) + \left(\frac{11}{12} - \frac{n_f}{18}\right)\delta(1-z)\right].$$

(3.19)

We now have all the ingredients to resum, in the leading logarithmic approximation, the leading-order radiative contributions to DIS and absorb them into the parton distribution functions. Starting from, for instance, the gluon PDF $x\mathcal{G}(x, Q^2)$, we can calculate the same distribution at a slightly higher resolution $Q^2+\Delta Q^2$, by incorporating the probabilities that the gluon we observe was emitted earlier by another quark or gluon. In formulas:

$$x\mathcal{G}(x, Q^2 + \Delta Q^2) = x\mathcal{G}(x, Q^2) + \int_0^1 \mathrm{d}z \int_0^1 \mathrm{d}z'\delta\left(\frac{x}{z} - z'\right)$$

$$\left[\sum_f \frac{\mathrm{d}P_{gq}}{\mathrm{d}z}\left(z'q_f(z', Q^2) + z'\bar{q}_f(z', Q^2)\right) + \frac{\mathrm{d}P_{gg}}{\mathrm{d}z}z'\mathcal{G}(z', Q^2)\right],$$

(3.20)

11

or, writing the differential:

$$x\mathcal{G}\left(x, Q^2 + \Delta Q^2\right) = x\mathcal{G}\left(x, Q^2\right) + \frac{\alpha_s}{2\pi}\frac{\Delta Q^2}{Q^2}\int_0^1 \mathrm{d}z \int_0^1 \mathrm{d}z' \delta\left(\frac{x}{z} - z'\right)$$
$$\left[\sum_f \tilde{\mathcal{P}}_{gq}\left(z\right)\left(z'q_f\left(z', Q^2\right) + z'\bar{q}_f\left(z', Q^2\right)\right) + \tilde{\mathcal{P}}_{gg}z'\mathcal{G}\left(z', Q^2\right)\right], \tag{3.21}$$

where we used that:

$$\frac{\mathrm{d}P_{pp}}{\mathrm{d}z} = \frac{\alpha_s}{2\pi}\frac{\mathrm{d}Q^2}{Q^2}\tilde{\mathcal{P}}_{pp}\left(z\right). \tag{3.22}$$

By looking at small steps in the virtuality, we effectively cut the problematic transverse-momentum phase space into pieces, as we explained in the previous chapter. From Eq. (3.21), we obtain an integro-differential equation in the logarithm of the virtuality:

$$\frac{\mathrm{d}}{\mathrm{d}\ln Q^2}x\mathcal{G}\left(x, Q^2\right)$$
$$= \frac{\alpha_s}{2\pi}\int_x^1 \mathrm{d}z \left[\sum_f \tilde{\mathcal{P}}_{gq}\left(z\right)\left(\frac{x}{z}q_f\left(\frac{x}{z}, Q^2\right) + \frac{x}{z}\bar{q}_f\left(\frac{x}{z}, Q^2\right)\right) + \tilde{\mathcal{P}}_{gg}\left(z\right)\frac{x}{z}\mathcal{G}\left(\frac{x}{z}, Q^2\right)\right]. \tag{3.23}$$

Analogously, one finds for the quark and antiquark distributions:

$$\frac{\mathrm{d}}{\mathrm{d}\ln Q^2}xq_f\left(x, Q^2\right) = \frac{\alpha_s}{2\pi}\int_x^1 \mathrm{d}z \left[\tilde{\mathcal{P}}_{qq}\left(z\right)\frac{x}{z}q_f\left(\frac{x}{z}, Q^2\right) + \tilde{\mathcal{P}}_{qg}\left(z\right)\frac{x}{z}\mathcal{G}\left(\frac{x}{z}, Q^2\right)\right],$$
$$\frac{\mathrm{d}}{\mathrm{d}\ln Q^2}x\bar{q}_f\left(x, Q^2\right) = \frac{\alpha_s}{2\pi}\int_x^1 \mathrm{d}z \left[\tilde{\mathcal{P}}_{qq}\left(z\right)\frac{x}{z}\bar{q}_f\left(\frac{x}{z}, Q^2\right) + \tilde{\mathcal{P}}_{qg}\left(z\right)\frac{x}{z}\mathcal{G}\left(\frac{x}{z}, Q^2\right)\right]. \tag{3.24}$$

These are the famous Dokshitzer-Gribov-Lipatov-Altarelli-Parisi or DGLAP equations (Refs. [20–22]). They are differential equations which describe to leading-logarithmic accuracy the change in the parton distribution functions when changing Q^2, and are an important example of what one calls evolution equations in quantum field theory. Solving them amounts to the resummation of all the leading-order collinear QCD corrections to DIS into so-called parton ladders, see Figs. 5 and 6. Equivalently, the DGLAP equations can be regarded as renormalization-group equations (see e.g. Ref. [8, 16]) which renormalize the parton densities with respect to the scale Q^2.

The DGLAP equation allows us to finally explain the phenomenon of the scaling violation of the proton structure function F_2 in Fig. 2. Indeed, before scattering with the photon, the parton emits quarks and gluons through DGLAP radiation (see Figs. 5 and 6). The virtuality Q^2 of the photon is the natural upper bound for the transverse momentum of these emitted partons, hence increasing Q^2 amounts to increasing the available transverse phase space for the emissions. The more emissions, the more the parton loses energy, hence when Q^2 increases one observes a shift of the parton distributions, and thus of F_2, towards smaller values of x. Furthermore, according to Eq. (2.10), when x becomes very small, gluons are emitted in abundance. Even though DIS is only sensitive to gluons at next-to-leading order, the growth in the gluon distribution is large enough to magnify the scaling violation dramatically towards smaller values of x.
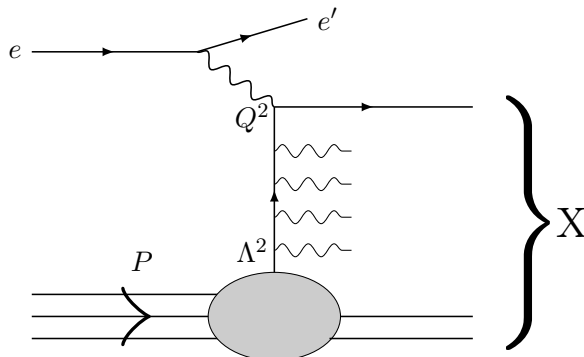
Figure 5: Inclusive deep-inelastic scattering in the QCD-improved parton model. The multiple collinear emissions, resummed by the DGLAP equations and depicted by the wiggly lines, can involve either gluons or (anti)quarks.
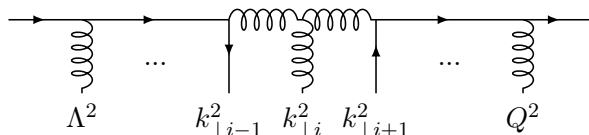
Figure 6: A DGLAP ladder in detail, depicting quark- and gluon emissions with increasing transverse momenta.

To establish the connection with the previous section, let us revert to the double leading logarithmic approximation (DLA), in which we only keep those contributions that are enhanced by an additional large logarithm in the energy. Since

$$\ln \frac{p^+}{k^+} = \ln \frac{1}{x},\tag{3.25}$$

this approximation is valid in the small-x limit of DGLAP. In this regime, as we mentioned already before, the dynamics is dominated by gluons, hence we will solve DGLAP for the gluon distribution, Eq. (3.23), which for $x \ll 1$ reduces to:

$$\begin{aligned}\frac{\mathrm{d}}{\mathrm{d}\ln Q^2} x\mathcal{G}\left(x, Q^2\right) &= \frac{\alpha_s N_c}{\pi} \int_x^1 \frac{\mathrm{d}z}{z} \frac{x}{z} \mathcal{G}\left(\frac{x}{z}, Q^2\right),\\ &= \frac{\alpha_s N_c}{\pi} \int_x^1 \frac{\mathrm{d}z}{z} z\mathcal{G}\left(z, Q^2\right).\end{aligned}\tag{3.26}$$

Rewriting this equation in integral form, we obtain:

$$x\mathcal{G}\left(x, Q^2\right) = x\mathcal{G}\left(x, Q_0^2\right) + \bar{\alpha} \int_{Q_0^2}^{Q^2} \frac{\mathrm{d}k_\perp^2}{k_\perp^2} \int_x^1 \frac{\mathrm{d}z}{z} z\mathcal{G}\left(z, k_\perp^2\right),\tag{3.27}$$

where we introduced the notation $\bar{\alpha} \equiv \alpha_s N_c/\pi$. The second term in the r.h.s. of the above equation is of course nothing else than the convolution of the gluon density with the Bremsstrahlung law,

which we resummed in the previous section. Indeed, solving the above equation iteratively, assuming the initial value to be scale independent:

$$x\mathcal{G}^{(0)}\left(x, Q^2\right) = x\mathcal{G}^{(0)}, \tag{3.28}$$

we obtain, in accordance with Eq. (2.17):

$$x\mathcal{G}\left(x, Q^2\right) = x\mathcal{G}^{(0)} I_0 \left(2\sqrt{\bar{\alpha}\ln\frac{Q^2}{Q_0^2}\ln\frac{1}{x}}\right). \tag{3.29}$$

It should be noted, however, that to obtain the above result we neglected the running of the coupling. This is by no means justified, since the coupling is also enhanced by a large logarithm in the virtuality:

$$\alpha_s\left(Q^2\right) \overset{1-\text{loop}}{=} \frac{1}{b_0 \ln\left(Q^2/\Lambda_{\text{QCD}}^2\right)}, \quad b_0 = \frac{11N_c - 2n_f}{12\pi}. \tag{3.30}$$

A more careful analysis in Mellin space (see e.g. Refs. [6, 23]) shows that including this correction, Eq. (3.29) becomes:

$$x\mathcal{G}\left(x, Q^2\right) \sim x\mathcal{G}^{(0)} \exp\sqrt{\frac{4N_c}{\pi b_0}\ln\frac{\ln\left(Q^2/\Lambda_{\text{QCD}}^2\right)}{\ln\left(Q_0^2/\Lambda_{\text{QCD}}^2\right)}\ln\frac{1}{x}}. \tag{3.31}$$

As expected, the DLA gluon distribution above grows with decreasing x and increasing Q^2. The growth with x is faster than $\ln 1/x$ but slower than any power of $1/x$. We will see shortly that, in the small-x regime, by virtue of the BFKL equation, which resums the logarithms $\ln 1/x$, the gluon distribution turns out to grow even faster, with a power-like behavior in $1/x$:

$$x\mathcal{G}\left(x, Q^2\right) \sim \frac{1}{x^{2.77\times\bar{\alpha}}}. \tag{3.32}$$

With the help of sum rules (see e.g. Ref. [23]) and DGLAP fits at next-to-leading order, the parton distributions have been extracted with great accuracy from DIS experiments, see Fig. 7. Clearly, this approach works very well, except at small values of x, where, as expected, the gluon distribution dominates and large energy logarithms become important.
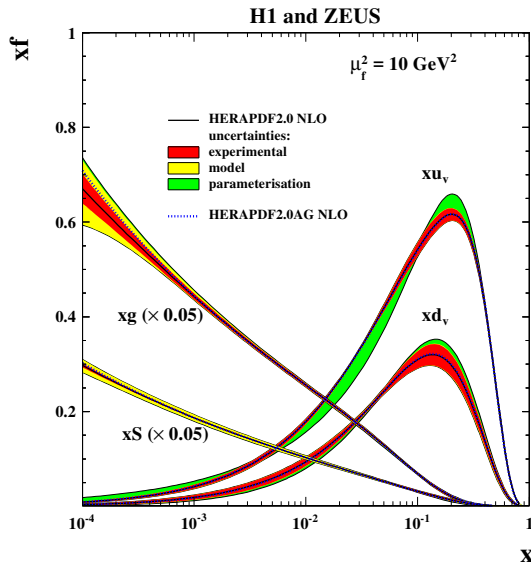
Figure 7: The parton densities at $Q^2 = 10\,\mathrm{GeV}^2$, extracted from H1 and Zeus data with NLO DGLAP fits [24]. The valence quark densities are defined as $xu_v = xu - x\bar{u}$ and $xd_v = xd - x\bar{d}$. For clarity, the sea quark distribution $xS = xu + x\bar{u} + xd + x\bar{d} + xs + x\bar{s}$ and the gluon distribution $xg = x\mathcal{G}$ have been multiplied with a factor 0.05.

4 DIS at small-x: the dipole picture

To describe DIS in the high-energy limit, which, according to Eq. (1.3), corresponds to small values of Bjorken-x, it is very useful to perform a boost from the infinite momentum frame to the so-called dipole frame, in which the photon-quark vertex is pulled out of the hadron (see Refs. [5, 6, 9, 11, 25, 26]). DIS in this 'dipole picture' is then viewed as a two-step process, which is illustrated in Fig. 8: before the interaction, the photon splits up in a color-singlet quark-antiquark pair, called a dipole, which subsequently scatters off the gluon content of the hadron. We will show that in the small-x limit, the lifetime of this dipole is much longer than the interaction time with the proton, and the scattering can be treated as eikonal such that the transverse coordinates of the quark and antiquark do not change.

Let us substantiate these claims with some small calculations. First, we write for the momenta P and q of the proton and the photon, respectively:

$$P^\mu \simeq (P, \mathbf{0}_\perp, P), \quad q^\mu = \left(\sqrt{q^2 - Q^2}, \mathbf{0}_\perp, -q\right). \tag{4.1}$$

Requiring that the photon is highly energetic: $q \gg Q$, the above momenta can be written in light-cone coordinates as follows:

$$P^\mu \simeq \left(P^+, 0, \mathbf{0}_\perp\right), \quad q^\mu = \left(-\frac{Q^2}{2q^-}, q^-, \mathbf{0}_\perp\right), \tag{4.2}$$
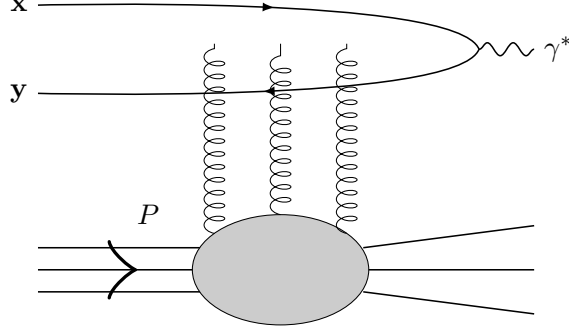
Figure 8: Inclusive deep-inelastic scattering in the dipole picture

where $q^- \simeq q/\sqrt{2}$ and $P^+ = \sqrt{2}P$. Since the photon is a left-mover, its lifetime can be estimated as:

$$\Delta x_{\text{dip}}^- \sim \frac{1}{|q^+|} = \frac{2q^-}{Q^2}. \tag{4.3}$$

The longitudinal extent of the proton is:

$$\Delta x_P^- \sim \frac{2R}{\gamma} = 2R\frac{m}{P} \sim \frac{1}{P}, \tag{4.4}$$

hence, from Eq. (1.3), requiring that the lifetime of the dipole is much larger than the proton size is tantamount to the requirement that x is small:

$$\Delta x_{\text{dip}}^- \gg \Delta x_P^- \quad \leftrightarrow \quad x \ll 1. \tag{4.5}$$

Note that, since in the dipole frame the proton (or nucleus) is squeezed together due to Lorentz dilation, one often speaks of a 'shockwave' in the literature.

One of the big advantages of the dipole frame is that the interaction of the dipole with the proton diagonalizes, in this sense that the interaction becomes eikonal: the transverse positions $\mathbf{x}$ and $\mathbf{y}$ of the quark and antiquark do not change as a result of the scattering. That this is the case is a simple corollary of the above estimates: if the transverse dipole size is approximately equal to $r_\perp^2 \sim 1/Q^2$, and changes by an amount $\Delta r_\perp = \Delta x_P^- k_\perp/q^0$ over the course of the interaction, we have that:

$$\frac{\Delta r_\perp}{r_\perp} \simeq \Delta x_P^- \frac{k_\perp^2}{q^0} \sim x \ll 1. \tag{4.6}$$

One can then show that the photoabsorption cross section can be factorized as follows (see for instance Ref. [27, 28]):

$$\sigma_{\gamma^* p}\left(Y, Q^2\right) = \frac{\alpha_{em} e_q^2}{8\pi^4} p^+ \int_0^1 \mathrm{d}z \int \mathrm{d}^2\mathbf{r} \left|\psi^{\gamma \to q\bar{q}}\left(p^+, z, \mathbf{r}; Q^2\right)\right|^2 \sigma_{\text{dip}}\left(Y, \mathbf{r}\right), \tag{4.7}$$

where the wave function $\psi^{\gamma \to q\bar{q}}$ for the photon with longitudinal momentum p^{+2} and virtuality Q^2 to split in a quark-antiquark pair is convolved with the dipole cross section $\sigma_{\text{dip}}\left(Y, \mathbf{r}\right)$, which encodes

---

[2]The factor p^+ cancels with the $1/p^+$ dependence of the wave function squared.

the eikonal interaction of the dipole with the proton. The $\gamma \to q\bar{q}$ wave function can be calculated in light-cone perturbation theory, and is in fact equal to the $g \to q\bar{q}$ wave function (see Sec. D), up to the coupling constant and a color factor. Note the appearance of the 'rapidity' $Y \equiv \ln 1/x$ in Eq. (4.7), which, as it turns out, is a natural variable to describe small-x processes. It can be viewed as the difference in rapidity between the virtual photon and the proton:

$$
\begin{aligned}
\Delta y &\equiv \frac{1}{2} \ln \frac{q^-}{q^+} - \frac{1}{2} \ln \frac{P^-}{P^+}, \\
&= \frac{1}{2} \ln \frac{4 \left(q^-\right)^2 \left(P^+\right)^2}{Q^2 M^2}, \\
&= \ln \frac{1}{x} + \ln \frac{Q}{M} \sim Y \text{ if } x \ll 1.
\end{aligned}
\tag{4.8}
$$

Obviously, we cannot expect to be able to calculate the dipole cross section $\sigma_{\text{dip}}(Y, \mathbf{r})$ in Eq. (4.7) exactly, since it contains the information on the structure of the proton, which is nonperturbative and hence beyond the reach of perturbative QCD. The expression for $\sigma_{\text{dip}}(Y, \mathbf{r})$ is thus dependent on the way one models the small-x gluon content of the proton. A very well-known phenomenological parametrization is the Golec-Biernat and Wüsthoff (GBW) model (Ref. [29]), in which the dipole cross section is written as follows:

$$
\begin{aligned}
\sigma_{\text{dip}}^{\text{GBW}}(x, \mathbf{r}) &= \sigma_0 \left(1 - e^{-r^2/4R_0^2(x)}\right), \\
R_0^2(x) &= \left(\frac{x}{x_0}\right)^{\lambda} \text{GeV}^{-2}.
\end{aligned}
\tag{4.9}
$$

In the above formulas, R_0 is the so-called correlation length, and its inverse is known as the saturation scale $Q_s = 1/R_0$. The limit in which the dipole size r is very small corresponds to color transparency, in which the legs of the dipole close, upon which the dipole becomes color neutral. In that case, the dipole cannot interact and the cross section vanishes. In the opposite limit, for a very large dipole size r, the dipole is completely absorbed by the target, and the cross section saturates to the maximal possible geometric cross section $\sigma_0 \simeq 2\pi R^2$ known as the black disk limit. Golec-Biernat and Wüsthoff fitted their model to the HERA data (see Fig. 9), and obtained the following parameters (for the light quark flavors u, d and s):

$$
\sigma_0 = 23.03 \, \text{mb}, \quad \lambda = 0.288, \quad x_0 = 3.04 \cdot 10^{-4}.
\tag{4.10}
$$

In order to properly interpret Eq. (4.9), we should elaborate on the saturation scale $Q_s(x) = 1/R_0(x)$, which plays a central role in this thesis. As we argued in the previous section, small-x physics is dominated by gluons, whose distribution grows very fast towards smaller values of x: $x\mathcal{G}(x, Q^2) \sim (1/x)^{2.77\bar{\alpha}}$. However, we saw as well that each gluon has a transverse extent of the order $\sim 1/Q^2$. Introducing the ratio of the total area $x\mathcal{G}(x, Q^2)/Q^2$ occupied by all the gluons, and the transverse hadron size πR^2:

$$
\varphi\left(x, Q^2\right) \simeq \frac{1}{N_c^2 - 1} \frac{1}{\pi R^2} \frac{x\mathcal{G}\left(x, Q^2\right)}{Q^2},
\tag{4.11}
$$
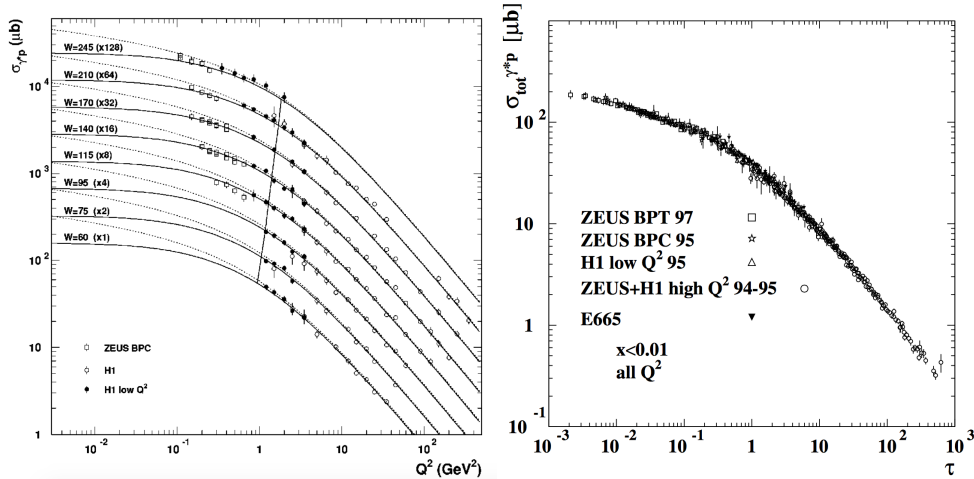
Figure 9: First hints of saturation physics in early HERA data. Left: the Golec-Biernat and Wüsthoff fit [29] to Zeus and H1 data on the photoabsorption cross section. $W = \sqrt{s}$, the center-of-mass energy of the photon-proton scattering (in GeV). The dotted lines are the fits in which the three lightest quarks are massless, and the full lines the ones in which they have a common mass of $m = 140\,\text{MeV}$. Right: the dipole cross section $\sigma_{\gamma *p}$ in the small-x ($x < 10^{-2}$) region, as a function of the scaling variable $\tau = Q^2 R_0^2(x)$ (from Ref. [30]).

the gluons will overlap when the above so-called gluon overlapping factor $\varphi(x, Q^2)$ is of order one. The system is then in a high density regime, in which the gluon occupation factors become so large that one expects the system to reach an equilibrium state. Indeed, although suppressed by powers of α_s, the relative importance of nonlinear gluon merging effects $gg \to g$ increases due to the high density. These recombinations will act against the very fast radiative growth of the gluon distribution, until both effects compensate for each other and the gluon density saturates. There are two ways to reach this highly dense so-called 'saturation' regime of QCD (see Fig. 10): first, fixing Q^2 and increasing the energy, thus decreasing x, the gluon distribution $x\mathcal{G}(x, Q^2)$ rapidly grows, while each gluon has more or less the same transverse extent $\sim 1/Q^2$, and while the hadron area πR^2 grows only logarithmically (see the following section, Eq. (5.37), for a heuristic derivation). At a certain point the gluon overlapping factor becomes of order one, and saturation kicks in. Second, one could keep x fixed and decrease Q^2. Indeed, even though the gluon distribution decreases towards lower values of Q^2 since there is less phase space for radiation available, $\varphi(x, Q^2)$ keeps growing because the transverse area $1/Q^2$ of the gluons increases a lot faster, until the high density regime is reached. The transverse momentum scale that marks the onset of the saturation regime is precisely the saturation scale Q_s:

$$\varphi(x, Q^2) \gtrsim \frac{1}{\alpha_s N_c} \quad \leftrightarrow \quad Q^2 \lesssim Q_s^2. \tag{4.12}$$

The opposite regime, where $Q^2 > Q_s^2$, is known as the dilute regime in which the gluon distribution keeps growing explosively. An approximate expression for Q_s is found by estimating the rate

18
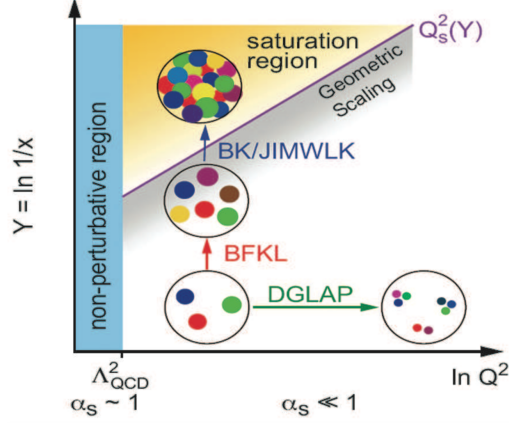
Figure 10: The phase space for DIS, taken from Ref. [31]. The transverse area of the partons are depicted by the colored dots. As we will explain later, BK and JIMWLK are nonlinear evolution equations in $1/x$, which are reduced to BFKL in the dilute limit. Geometric scaling is an effect of the saturation boundary on the evolution in the dilute regime.

$\Gamma\left(x, Q^2\right)$ of gluon recombinations:

$$\Gamma\left(x, Q^2\right) \sim \frac{\alpha_s N_c}{N_c^2 - 1} \frac{1}{\pi R^2} \frac{x\mathcal{G}\left(x, Q^2\right)}{Q^2}, \tag{4.13}$$

which is of order one when $\varphi\left(x, Q^2\right) \sim 1/\alpha_s N_c$. Requiring $\Gamma\left(x, Q^2 = Q_s^2\right) \sim 1$ we then find:

$$Q_s^2\left(x\right) \sim \frac{\alpha_s N_c}{N_c^2 - 1} \frac{1}{\pi R^2} x\mathcal{G}\left(x, Q_s^2\right). \tag{4.14}$$

From the above expression, we expect a power-like growth for the saturation scale, similar to the growth of the gluon density in the dilute regime:

$$Q_s^2\left(x\right) \sim \left(\frac{1}{x}\right)^{\bar{\alpha}c_s}, \tag{4.15}$$

which is encoded as well in the GBW model, Eq. (4.9), and which defines a straight 'saturation line' $\ln Q_s^2\left(x\right)/Q_0^2$ in the kinematical $(\ln Q^2, Y)$ plane for DIS, as is shown in Fig. 10 (see also Refs. [32–34]).

The Golec-Biernat and Wüsthoff fit, as well as later more advanced phenomenological models (see e.g. Refs. [35–38]) are of great historical importance, since their quality made a strong case for saturation physics. However, at present, small-x evolution equations such as BFKL and BK (the subjects of the next section) are known to sufficient theoretical accuracy (including the running coupling [39–42], collinear improvements [43] or even at full NLO accuracy [44–46]) to make such model-dependent fits obsolete. Instead, small-x data can be fitted the same way as in the case of DGLAP: one only models the initial condition (e.g. the MV model, see Part. II) and the impact-parameter dependence (Ref. [38]), after which the evolution is completely fixed by the theory

(see Refs. [47–51]). Despite these theoretical successes, it is however too optimistic to state that saturation has really been observed at HERA: the data points at very small-x lie dangerously close to the nonperturbative region.

There is, however, another striking phenomenon in the DIS data from HERA: geometric scaling (see Ref. [30]). This is the property that, at small-x, the $\gamma^* p$ cross section only depends on x and $Q^2 \sim 1/r^2$ via the dimensionless combination $r^2/R_0^2(x) = Q_s^2(x)/Q^2$. This scaling is explicitly encoded in the GBW-parametrization Eq. (4.9), and indeed seems to hold, at least approximately, for $x < 10^{-2}$ and virtualities $Q^2 \leq 450\,\mathrm{GeV}^2$ (see Fig. 9). In the saturation regime, scaling is a natural consequence of the fact that Q_s is the only relevant scale in this region of phase space. Moreover, theoretical studies (see Ref. [33, 52, 53]) have found that geometric scaling is also consistent with saturation physics in the dilute regime $Q_s^2 \ll Q^2 \ll Q_s^4(x)/\Lambda_{\mathrm{QCD}}^2$, where the linear evolution is influenced by the boundary condition of saturation.

In Part II, we will describe in detail the physics of the hadron structure in the saturation regime. First, however, we should study the small-x evolution equations from the point of view of the projectile. Indeed, the latter will also be sensitive to saturation, via the unitarization of the amplitude for multiple scattering.

5 BFKL and BK evolution equations

We have seen that, when calculating radiative QCD corrections to a certain process, in our case DIS, large logarithms in transverse momentum threaten to jeopardize perturbation theory, and hence have to be resummed in the DGLAP evolution equations. However, as is clear from the Bremsstrahlung law Eq. (2.10), in the small-x regime the logarithms in the energy might become a lot more problematic than the ones in transverse momentum:

$$\ln \frac{1}{x} \gg \ln \frac{Q^2}{Q_0^2}. \tag{5.1}$$

In this case, the situation is opposite to the one we encountered in DGLAP: now, the large logarithms $\alpha_s \ln 1/x$ have to be resummed, while the $k_\perp$-dependence can be computed exactly. The result of such a procedure is the famous Balitsky-Fadin-Kuraev-Lipatov or BFKL equation (Refs. [54–57]), which holds at asymptotic small-x, and hence involves only gluons. Being a LLA equation, the successive gluon emissions are strongly ordered in energy:

$$x_0 \gg ... \gg x_i \gg x_{i+1} \gg ... \gg x_n. \tag{5.2}$$

Building gluon ladders from the proton to the partonic scattering process, like we did for DGLAP (cf. Figs. 6 and 5), turns out to be significantly more involved in the case of BFKL, and involves reshuffling perturbation theory by trading the three-gluon vertices for the so-called Lipatov vertices, which effectively sum different radiative contributions. However, nothing prevents us to go to a Lorentz frame in which the major part of the energy is contained in the dipole, rather than in the proton. In such a frame, one can construct an evolution equation for the dipole (we follow Ref. [7]), which turns out to be much simpler than constructing BFKL from the point of view of the hadron.
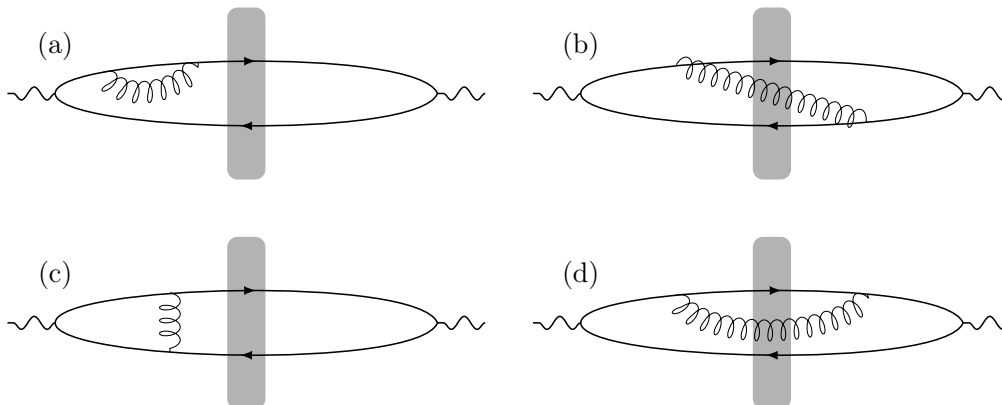
Figure 11: Contributions to the BK equation.

One of the starting points of the calculation is the observation that the multiple scatterings of the dipole off the Lorentz-contracted proton or 'shockwave' are eikonal, as we already argued in the previous chapter. This implies that they can be resummed (see e.g. [10]) into Wilson lines which are directed along each leg of the dipole, and which are defined as:

$$U = \mathcal{P}e^{ig_s \int \mathrm{d}z_\mu A_a^\mu(z)t^a}. \tag{5.3}$$

In the above formula, $\mathcal{P}$ is the path ordering operator, which places the color matrices t^a from left to right in the order of their appearance along the integration path. If the dipole is a left-mover, as in Fig. 8, the Wilson lines are directed along the x^--axis, and hence the quark and antiquark couple only to the A^+ fields of the proton:

$$U(\mathbf{x}) = \mathcal{P}e^{ig_s \int \mathrm{d}z^- A_a^+(z^-,\mathbf{x})t^a}. \tag{5.4}$$

In function of these Wilson lines, the interaction of the dipole with the shockwave can be written as:

$$D_Y(\mathbf{x} - \mathbf{y}) \equiv \langle S(\mathbf{x},\mathbf{y})\rangle_Y, \qquad S(\mathbf{x},\mathbf{y}) \equiv \frac{1}{N_c}\mathrm{Tr}\left(U(\mathbf{x})U^\dagger(\mathbf{y})\right), \tag{5.5}$$

where $D_Y(\mathbf{x} - \mathbf{y})$ is the S-matrix of dipole-shockwave scattering, and where the information on the structure of the proton is now contained in the averages $\langle...\rangle_Y$ over the gluon fields inside the Wilson lines. We will often call $D_Y(\mathbf{x} - \mathbf{y})$ simply a 'dipole'. In the above formula, $U(\mathbf{x})$ corresponds to the quark leg and $U^\dagger(\mathbf{y})$ to the antiquark leg, and we take a trace because the dipole is in a singlet configuration. In addition, we assume translation symmetry in the transverse plane. As an example, the dipole cross section from Eq. (4.7) can be written with the help of the optical theorem as:

$$\sigma_{\mathrm{dip}}(Y,\mathbf{r}) = 2S_\perp \langle T(\mathbf{r},\mathbf{0})\rangle_Y, \qquad T(\mathbf{x},\mathbf{y}) \equiv 1 - S(\mathbf{x},\mathbf{y}), \tag{5.6}$$

where $S_\perp = \pi R^2$ is the transverse area of the proton, and where $T(\mathbf{x},\mathbf{y})$ is the forward scattering amplitude[3].

---

[3]T is defined as the imaginary part of the usual scattering amplitude $\mathcal{A}$, which is in turn defined through the S-matrix as follows: $S = 1 + i\mathcal{A}$.

Let us now compute the leading-order corrections to the dipole, Eq. (5.5), when going to smaller values of x, or equivalently, when increasing the rapidity Y. We already calculated the emission of an eikonal gluon from a quark, and found that it gives an effective vertex (see Eq. (2.8)):

$$-2g_s t^a \frac{\mathbf{k}_\perp \cdot \boldsymbol{\epsilon}_\perp^\lambda}{k_\perp^2}. \tag{5.7}$$

Since such an eikonal emission preserves the transverse position of the quark or antiquark leg, it is more appropriate to work in the mixed Fourier space, in which we only transform the transverse momenta to coordinate space. For the above vertex, this yields:

$$-2g_s t^a \int \frac{\mathrm{d}^2 \mathbf{k}_\perp}{(2\pi)^2} e^{i\mathbf{k}_\perp(\mathbf{x}-\mathbf{z})} \frac{\mathbf{k}_\perp \cdot \boldsymbol{\epsilon}_\perp^\lambda}{k_\perp^2} = -i\frac{g_s}{\pi} t^a \frac{(\mathbf{x}-\mathbf{z}) \cdot \boldsymbol{\epsilon}_\perp^\lambda}{(\mathbf{x}-\mathbf{z})^2}, \tag{5.8}$$

where we made use of formula (B.3). Using $\sum_\lambda \epsilon_i^{\lambda\dagger} \epsilon_j^\lambda = \delta_{ij}$ (from Eq. (2.6)), we obtain the following result for the self-energy corrections from Fig. 11 (a) (compare with Eq. (2.9)):

$$(a) = -2\alpha_s \Delta Y \int \frac{\mathrm{d}^2 \mathbf{z}}{(2\pi)^2} \frac{1}{(\mathbf{x}-\mathbf{z})^2} \mathrm{Tr}\langle t^a t^a U(\mathbf{x}) U^\dagger(\mathbf{y})\rangle_Y. \tag{5.9}$$

The other virtual correction, see Fig. 11 (c), in which the legs of the dipole exchange a gluon before or after the interaction with the target, yields:

$$(c) = 4\alpha_s \Delta Y \int \frac{\mathrm{d}^2 \mathbf{z}}{(2\pi)^2} \frac{(\mathbf{x}-\mathbf{z}) \cdot (\mathbf{y}-\mathbf{z})}{(\mathbf{x}-\mathbf{z})^2 (\mathbf{y}-\mathbf{z})^2} \mathrm{Tr}\langle U(\mathbf{x}) t^a t^a U^\dagger(\mathbf{y})\rangle_Y. \tag{5.10}$$

Combining the four possible self-energy corrections (a), and the two diagrams like (c), we obtain:

$$\begin{aligned}
\text{virtual corrections} &= -4\alpha_s \Delta Y \mathrm{Tr}\langle t^a t^a U(\mathbf{x}) U^\dagger(\mathbf{y})\rangle_Y \\
&\quad \times \int \frac{\mathrm{d}^2 \mathbf{z}}{(2\pi)^2} \left(\frac{1}{(\mathbf{x}-\mathbf{z})^2} + \frac{1}{(\mathbf{y}-\mathbf{z})^2} - 2\frac{(\mathbf{x}-\mathbf{z}) \cdot (\mathbf{y}-\mathbf{z})}{(\mathbf{x}-\mathbf{z})^2 (\mathbf{y}-\mathbf{z})^2} \right), \\
&= -4\alpha_s C_F N_c \Delta Y D_Y(\mathbf{x}-\mathbf{y}) \\
&\quad \times \int \frac{\mathrm{d}^2 \mathbf{z}}{(2\pi)^2} \frac{(\mathbf{x}-\mathbf{y})^2}{(\mathbf{x}-\mathbf{z})^2 (\mathbf{y}-\mathbf{z})^2},
\end{aligned} \tag{5.11}$$

where we made use of definition of the Casimir operator (A.14). Likewise, the real correction in which the emitted gluon crosses the shockwave (Fig. 11, b) yields:

$$(b) = -4\alpha_s \Delta Y \int \frac{\mathrm{d}^2 \mathbf{z}}{(2\pi)^2} \frac{(\mathbf{x}-\mathbf{z}) \cdot (\mathbf{y}-\mathbf{z})}{(\mathbf{x}-\mathbf{z})^2 (\mathbf{y}-\mathbf{z})^2} \mathrm{Tr}\langle t^a U(\mathbf{x}) t^b U^\dagger(\mathbf{y}) W_{ab}(\mathbf{z})\rangle_Y, \tag{5.12}$$

where $W(\mathbf{z})$ is a Wilson line in the adjoint representation:

$$W(\mathbf{z}) = \mathcal{P} e^{ig_s \int \mathrm{d}z^- A_a^+(z^-, \mathbf{z}) T^a}, \tag{5.13}$$

encoding the multiple eikonal scatterings of the soft gluon on the target. Using Eq. (A.10), the expression for (b) can be rewritten as:

$$
\begin{aligned}
\text{(b)} &= -4\alpha_s \Delta Y \int \frac{\mathrm{d}^2\mathbf{z}}{(2\pi)^2} \frac{(\mathbf{x}-\mathbf{z})\cdot(\mathbf{y}-\mathbf{z})}{(\mathbf{x}-\mathbf{z})^2(\mathbf{y}-\mathbf{z})^2} \mathrm{Tr}\langle t^a U(\mathbf{x}) U^\dagger(\mathbf{z}) t^a U(\mathbf{z}) U^\dagger(\mathbf{y})\rangle_Y, \\
&= -4\alpha_s \Delta Y \int \frac{\mathrm{d}^2\mathbf{z}}{(2\pi)^2} \frac{(\mathbf{x}-\mathbf{z})\cdot(\mathbf{y}-\mathbf{z})}{(\mathbf{x}-\mathbf{z})^2(\mathbf{y}-\mathbf{z})^2} \\
&\quad \times \left(\frac{1}{2}\langle \mathrm{Tr}\left(U(\mathbf{x}) U^\dagger(\mathbf{z})\right) \mathrm{Tr}\left(U(\mathbf{z}) U^\dagger(\mathbf{y})\right)\rangle_Y - \frac{1}{2N_c}\mathrm{Tr}\langle U(\mathbf{x}) U^\dagger(\mathbf{y})\rangle_Y \right),
\end{aligned}
\tag{5.14}
$$

where we again made use of Eq. (A.13). Finally, the real correction in Fig. 11 (d) gives:

$$
\begin{aligned}
\text{(d)} &= 2\alpha_s \Delta Y \int \frac{\mathrm{d}^2\mathbf{z}}{(2\pi)^2} \frac{1}{(\mathbf{x}-\mathbf{z})^2} \\
&\quad \times \left(\frac{1}{2}\langle \mathrm{Tr}\left(U(\mathbf{x}) U^\dagger(\mathbf{z})\right) \mathrm{Tr}\left(U(\mathbf{z}) U^\dagger(\mathbf{y})\right)\rangle_Y - \frac{1}{2N_c}\mathrm{Tr}\langle U(\mathbf{x}) U^\dagger(\mathbf{y})\rangle_Y \right).
\end{aligned}
\tag{5.15}
$$

Summing the real emissions, we obtain:

$$
\begin{aligned}
\text{real emissions} &= 2\alpha_s \Delta Y \int \frac{\mathrm{d}^2\mathbf{z}}{(2\pi)^2} \frac{(\mathbf{x}-\mathbf{y})^2}{(\mathbf{x}-\mathbf{z})^2(\mathbf{y}-\mathbf{z})^2} \\
&\quad \times \left(\frac{1}{N_c^2}\langle \mathrm{Tr}\left(U(\mathbf{x}) U^\dagger(\mathbf{z})\right) \mathrm{Tr}\left(U(\mathbf{z}) U^\dagger(\mathbf{y})\right)\rangle_Y - D_Y(\mathbf{x}-\mathbf{y}) \right),
\end{aligned}
\tag{5.16}
$$

and the sum of the real and virtual contributions is:

$$
-2\alpha_s N_c^2 \Delta Y \int \frac{\mathrm{d}^2\mathbf{z}}{(2\pi)^2} \mathcal{M}_{\mathbf{xyz}} \left(D_Y(\mathbf{x}-\mathbf{y}) - \frac{1}{N_c^2}\langle \mathrm{Tr}\left(U(\mathbf{x}) U^\dagger(\mathbf{z})\right) \mathrm{Tr}\left(U(\mathbf{z}) U^\dagger(\mathbf{y})\right)\rangle_Y \right), \tag{5.17}
$$

where $\mathcal{M}_{\mathbf{xyz}}$ is the so-called dipole kernel:

$$
\mathcal{M}_{\mathbf{xyz}} \equiv \frac{(\mathbf{x}-\mathbf{y})^2}{(\mathbf{x}-\mathbf{z})^2(\mathbf{y}-\mathbf{z})^2}. \tag{5.18}
$$

Eq. (5.17) is the sum of the leading-order radiative corrections to the multiple eikonal interactions of a dipole with the shockwave when increasing the phase space in rapidity. Hence, we obtain the following evolution equation:

$$
\frac{\partial}{\partial Y} D_Y(\mathbf{x}-\mathbf{y}) = -\frac{\bar{\alpha}}{2\pi} \int_{\mathbf{z}} \mathcal{M}_{\mathbf{xyz}} \left(D_Y(\mathbf{x}-\mathbf{y}) - \frac{1}{N_c^2}\langle \mathrm{Tr}\left(U(\mathbf{x}) U^\dagger(\mathbf{z})\right) \mathrm{Tr}\left(U(\mathbf{z}) U^\dagger(\mathbf{y})\right)\rangle_Y \right), \tag{5.19}
$$

which a non-closed equation, the first in the so-called Balitsky hierarchy (see Ref. [58]). It should be noted that the dipole kernel is singular for $\mathbf{z} = \mathbf{x}$ and $\mathbf{z} = \mathbf{y}$, causing possible ultraviolet divergences when integrating over $\mathbf{z}$. However, since $U(\mathbf{x}) U^\dagger(\mathbf{x}) = 1$, in these cases both terms in Eq. (5.19) cancel exactly. It was therefore crucial to correctly account for the real and virtual contributions in
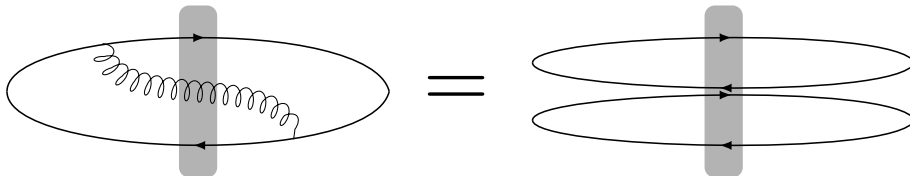
Figure 12: In the large-N_c limit, a dipole emitting a real gluon can be treated as a system of two dipoles.

order to make the equation regular. Equation (5.19) can be closed by going to the large-N_c limit, in which the medium average of two dipoles factorizes :

$$\frac{1}{N_c^2}\langle\text{Tr}\left(U\left(\mathbf{x}\right)U^\dagger\left(\mathbf{z}\right)\right)\text{Tr}\left(U\left(\mathbf{z}\right)U^\dagger\left(\mathbf{y}\right)\right)\rangle_Y = \frac{1}{N_c}\langle\text{Tr}\left(U\left(\mathbf{x}\right)U^\dagger\left(\mathbf{z}\right)\right)\rangle_Y\frac{1}{N_c}\langle\text{Tr}\left(U\left(\mathbf{z}\right)U^\dagger\left(\mathbf{y}\right)\right)\rangle_Y,$$
(5.20)

sacrificing[4] some of the correlations between two dipoles which are built up during the evolution. The result is the Balitsky-Kovchegov (BK) equation (Refs. [60, 61]):

$$\frac{\partial}{\partial Y}D_Y\left(\mathbf{x}-\mathbf{y}\right) = -\frac{\bar{\alpha}}{2\pi}\int_{\mathbf{z}}\mathcal{M}_{\mathbf{xyz}}\Big(D_Y\left(\mathbf{x}-\mathbf{y}\right)-D_Y\left(\mathbf{x}-\mathbf{z}\right)D_Y\left(\mathbf{y}-\mathbf{z}\right)\Big).$$
(5.21)

The interpretation of the BK equation is now very straightforward: opening the phase space, by increasing the rapidity, allows for the emission of a real gluon by one of the legs of the dipole. In the large-N_c limit, this gluon can be seen as a quark-antiquark pair, and effectively a system $D_Y\left(\mathbf{x}-\mathbf{z}\right)D_Y\left(\mathbf{y}-\mathbf{z}\right)$ of two 'child' dipoles scatters off the shockwave (see Fig. 12). The virtual term, in which the gluon is emitted and reabsorbed before or after the scattering, contributes with a term $D_Y\left(\mathbf{x}-\mathbf{y}\right)$ in the r.h.s. of Eq. (5.21), conserving probability and ensuring the cancellation of the ultraviolet divergences.

In the dilute limit $(\mathbf{x}-\mathbf{y})^2 \ll 1/Q_s^2$, the probability for the two child dipoles to simultaneously interact with the shockwave can be neglected. The BK equation Eq. (5.21) can simply be linearized by rewriting it in function of the scattering amplitude $T\left(\mathbf{x},\mathbf{y}\right)$, defined earlier in Eq. (5.6):

$$\frac{\partial}{\partial Y}\left(1-\langle T\left(\mathbf{x},\mathbf{y}\right)\rangle_\tau\right) = -\frac{\bar{\alpha}}{2\pi}\int_{\mathbf{z}}\mathcal{M}_{\mathbf{xyz}}\Big(1-\langle T\left(\mathbf{x},\mathbf{y}\right)\rangle_Y - \left(1-\langle T\left(\mathbf{x},\mathbf{z}\right)\rangle_Y\right)\left(1-\langle T\left(\mathbf{y},\mathbf{z}\right)\rangle_Y\right)\Big),$$
(5.22)

or:

$$\frac{\partial}{\partial Y}\langle T\left(\mathbf{x},\mathbf{y}\right)\rangle_\tau = \frac{\bar{\alpha}}{2\pi}\int_{\mathbf{z}}\mathcal{M}_{\mathbf{xyz}}\left(\langle T\left(\mathbf{x},\mathbf{z}\right)\rangle_Y + \langle T\left(\mathbf{y},\mathbf{z}\right)\rangle_Y - \langle T\left(\mathbf{x},\mathbf{y}\right)\rangle_Y - \langle T\left(\mathbf{x},\mathbf{z}\right)\rangle_Y\langle T\left(\mathbf{y},\mathbf{z}\right)\rangle_Y\right).$$
(5.23)

To linearize the above formulation of the BK equation, one simply neglects the quadratic term:

$$\frac{\partial}{\partial Y}\langle T\left(\mathbf{x},\mathbf{y}\right)\rangle_Y = \frac{\bar{\alpha}}{2\pi}\int_{\mathbf{z}}\mathcal{M}_{\mathbf{xyz}}\left(\langle T\left(\mathbf{x},\mathbf{z}\right)\rangle_Y + \langle T\left(\mathbf{y},\mathbf{z}\right)\rangle_Y - \langle T\left(\mathbf{x},\mathbf{y}\right)\rangle_Y\right).$$
(5.24)

---

[4]Interestingly, it turns out, however, that the differences between the evolution of a dipole with the Balitsky-JIMWLK equation and with BK are remarkably small, of the order of $\sim 0.1\%$, see Ref. [59].

This is the BFKL equation in coordinate space, describing the linear small-x evolution of the projectile (the dipole-hadron scattering amplitude). It was first derived by Mueller (Refs. [62, 63]) for the scattering of two quarkonia.

From Eq. (5.24), one can obtain the more traditional formulation of BFKL as an evolution equation for the gluon distribution in the proton. More specifically, since BFKL treats the $k_\perp$-dependence of the splittings exactly, it pertains to the unintegrated gluon distribution $f(x, k_\perp)$ defined as:

$$f(x, k_\perp) = \pi k_\perp^2 \frac{\mathrm{d}N}{\mathrm{d}Y \mathrm{d}^2\mathbf{k}_\perp},\tag{5.25}$$

which is related to the integrated gluon distribution as follows:

$$x\mathcal{G}(x, Q^2) \equiv \int^{Q^2} \frac{\mathrm{d}^2\mathbf{k}_\perp}{\pi k_\perp^2} f(x, k_\perp) \quad \text{or} \quad f(x, k_\perp) \equiv \frac{\partial x\mathcal{G}(x, k_\perp^2)}{\partial \ln k_\perp^2}.\tag{5.26}$$

In the dilute limit, $f(x, k_\perp)$ is linearly related to the dipole cross section, as we will prove in the following section:

$$\sigma_{\mathrm{dip}}(x, \mathbf{r}) \simeq \frac{4\pi\alpha_s}{N_c} \int \frac{\mathrm{d}^2\mathbf{k}_\perp}{\mathbf{k}_\perp^4} f(x, k_\perp) \left(1 - e^{i\mathbf{k}_\perp \mathbf{r}}\right).\tag{5.27}$$

With the help of the above formula, the BFKL equation (5.24) for the dipole scattering amplitude can be written as an evolution equation for $f(x, k_\perp)$ (this is done by going to Mellin space, see e.g. Ref. [64] and references therein):

$$\frac{\mathrm{d}f(Y, k_\perp)}{\mathrm{d}Y} = \bar{\alpha} \int \frac{\mathrm{d}^2\mathbf{p}_\perp}{\pi} \frac{k_\perp^2}{p_\perp^2 (\mathbf{k}_\perp - \mathbf{p}_\perp)^2} \left(f(Y, p_\perp) - \frac{1}{2} f(Y, k_\perp)\right).\tag{5.28}$$

As one can easily check, the above equation is convergent in the infrared due to the fact that the singularity for $p_\perp = 0$ exactly cancels with the one for $\mathbf{p}_\perp = \mathbf{k}_\perp$. Furthermore, Eq. (5.28) can be solved analytically, with the initial condition inspired by the Bremsstrahlung law:

$$f_0(Y, k_\perp) \simeq \frac{\alpha_s C_F}{\pi},\tag{5.29}$$

yielding (see e.g. Refs. [6, 65]):

$$f(Y, k_\perp) \simeq \sqrt{\frac{k_\perp^2}{\Lambda^2}} \frac{e^{\bar{\alpha}\omega_0 Y}}{\sqrt{2\pi\beta_0\bar{\alpha}Y}} \exp\left(-\frac{\ln^2\left(k_\perp^2/\Lambda^2\right)}{2\beta_0\bar{\alpha}Y}\right),\tag{5.30}$$

where $\omega_0 = 4\ln 2 \simeq 2.77$ and $\beta_0 \simeq 33.7$. The most important feature of the above result is that $f(Y, k_\perp)$ exhibits a very fast asymptotic growth with the rapidity:

$$\begin{aligned} f(Y, k_\perp) &\sim e^{\bar{\alpha}\omega_0 Y}, \\ &= \frac{1}{x^{\bar{\alpha}\omega_0}} \sim s^{\alpha_{I\!P}-1}, \end{aligned}\tag{5.31}$$
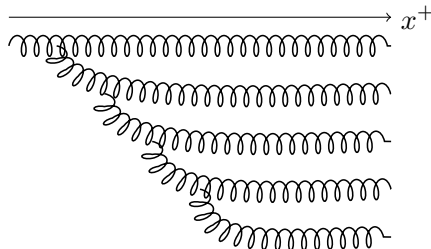
Figure 13: 'Explosive' growth of the gluon distribution in BFKL.

where $\alpha_{I\!P} = 1 + \bar{\alpha}4\ln 2$ is known as the BFKL intercept. In the literature, this solution is often called the hard pomeron, since it is reminiscent of the soft pomeron trajectory in Regge theory, which corresponds to a t-channel exchange with the quantum numbers of the vacuum and exhibits a similar, but much slower, power-like growth of the cross section with s ($\alpha_{I\!P} = 1.081$ in the famous Donnachie-Landshoff fit, Ref. [66]). Note that we could have expected this power-like growth on some simple general grounds. Indeed, since the lifetime of the gluons is given by $\Delta x^+ \sim 2k^+/k_\perp^2$, the strong ordering of the energies implies that:

$$x_0 \gg ... \gg x_i \gg x_{i+1} \gg ... \gg x_n \quad \leftrightarrow \quad \Delta x_0^+ \gg ... \gg \Delta x_i^+ \gg \Delta x_{i+1}^+ \gg ... \gg \Delta x_n^+, \quad (5.32)$$

hence the 'parent' gluons always live to see the subsequent emissions, as is illustrated in Fig. 13. The gluons in a BFKL cascade are thus coherent with each other, and the number of gluons per unit of rapidity is, from the resummation of the Bremsstrahlung law:

$$\begin{aligned} \frac{\mathrm{d}N}{\mathrm{d}Y} &\sim \sum_n \bar{\alpha}^n \int_{x_1}^1 \frac{\mathrm{d}x_0}{x_0} \int_{x_2}^{x_0} \frac{\mathrm{d}x_1}{x_1} ... \int_{x_n}^{x_{n-2}} \frac{\mathrm{d}x_{n-1}}{x_{n-1}}, \\ &= \sum_n \frac{1}{n!} (\bar{\alpha}Y)^n = e^{\omega\bar{\alpha}Y}, \end{aligned} \quad (5.33)$$

where ω is some constant which cannot be determined from this heuristic derivation. The BFKL equation (5.28) and its solution (5.31) raises two important problems. The first problem is that, through the relation (5.27), the power-like growth of the gluon distribution transfers to the dipole-hadron cross section:

$$\sigma_{\mathrm{dip}}(x \ll 1, \mathbf{r}) = 2\pi R^2 \langle T(\mathbf{r}, \mathbf{0}) \rangle_{Y\gg 1} \sim s^{\alpha_{I\!P}-1}. \quad (5.34)$$

Moreover, from the comparison of the black disc limit:

$$\sigma_{\mathrm{tot}} \leq 2\pi R^2, \quad (5.35)$$

with the well-known Froissart bound for total cross sections (Refs. [67, 68]):

$$\sigma_{\mathrm{tot}} \leq \sigma_0 \ln^2 s, \quad (5.36)$$

26

one can deduce that the hadron radius grows as a logarithm of the center-of-mass energy:

$$R \sim \ln s. \tag{5.37}$$

Therefore, we see from Eq. (5.34) that the dipole scattering amplitude grows like a power of s as well:

$$\langle T(\mathbf{r}, \mathbf{0}) \rangle_Y \sim s^{\alpha_{I\!P}-1} \simeq e^{(\alpha_{I\!P}-1)Y}, \tag{5.38}$$

eventually violating the unitarity bound $\langle T(\mathbf{r}, \mathbf{0}) \rangle_Y \leq 1$. This problem is not present in the BK equation (5.23), where $T = 1$ is a fixed point, which turns out to be stable (see Ref. [7]). The nonlinear term in the BK equation therefore provides an unitarization mechanism.

A second problem of BFKL is known as infrared diffusion, and can be explained by comparing with DGLAP. In the latter case, one evolves towards large values of Q^2, and since the coupling constant decreases with increasing Q^2, this implies that DGLAP evolves into more and more perturbative terrain. For BFKL, however, this is not the case: there is no mechanism to prevent deviations into the nonperturbative domain $k_\perp^2 \lesssim \Lambda_{\mathrm{QCD}}^2$. Worse, the more one evolves in rapidity, the more the gluon distribution will receive contributions from the nonperturbative sector (see Refs. [69, 70], and the discussions in Refs. [5, 6]). Once again, saturation physics provides a solution: the dynamically generated saturation scale Q_s, which is hard and thus perturbative, can be regarded as the inverse of the distance $1/Q_s$ over which the gluons arrange themselves to achieve color neutrality (Refs. [52, 71]). The gluon spectrum decreases for transverse momenta below Q_s, and is therefore not sensitive anymore to nonperturbative physics.

For consistency, we should remark that if one approximates the $k_\perp$-dependence in the BFKL equation (5.28) logarithmically, and rewrites it as an equation for $x\mathcal{G}(x, Q^2)$, its solution coincides with the (fixed-coupling) result Eq. (3.29) of DGLAP for the gluon distribution in the DLA. Hence, as we expect from our discussion in Sec. 2, in which we argued that BFKL and DGLAP are in a sense dual, in the double logarithmic approximation the two evolution equations are in fact the same. In particular, the DLA solution Eq. (3.31) also violates the unitarity bound at large energies.

6 Transverse momentum dependent gluon distributions

Before we proceed, a small digression is in place. Indeed, in the preceding section, we introduced the unintegrated gluon distribution $f(x, k_\perp)$, Eq. (5.25). Up to a normalization, $f(x, k_\perp)$ is the same as the so-called Weizsäcker-Williams gluon distribution $\mathcal{F}_{gg}^{(3)}(x, k_\perp)$ (Refs. [72–75]):

$$f(x, k_\perp) = \pi k_\perp^2 \mathcal{F}_{gg}^{(3)}(x, k_\perp), \tag{6.1}$$

which is defined as the number of gluons per unit of rapidity and per unit of area in transverse momentum space:

$$\mathcal{F}_{gg}^{(3)}(x, k_\perp) \equiv \frac{\mathrm{d}N}{\mathrm{d}\ln(1/x)\,\mathrm{d}^2\mathbf{k}_\perp}. \tag{6.2}$$

This definition becomes explicit in the light-cone gauge $A^+ = 0$, in which $\mathcal{F}_{gg}^{(3)}\left(x, k_\perp\right)$ can be written as the number operator in Fock space (Refs. [5, 17, 19, 74]):

$$\mathcal{F}_{gg}^{(3)}\left(x, k_\perp\right) = k^+ \sum_\lambda \left\langle a_a^{\lambda\dagger}\left(x^+, \vec{k}\right) a_a^\lambda\left(x^+, \vec{k}\right)\right\rangle_x, \tag{6.3}$$

where we introduced the notation $\vec{k} = (k^+, \mathbf{k}_\perp)$, and where $a_a^{\lambda\dagger}$ and a_a^λ are the light-cone creation and annihilation operators, with λ the polarization and a the color of the gluon field. They obey the equal-LC-time commutation relation:

$$\left[a_a^\lambda\left(x^+, \vec{k}\right), a_b^{\lambda'}\left(x^+, \vec{p}\right)\right] = 2k^+\delta_{ab}\delta_{\lambda\lambda'}(2\pi)^3 \delta^{(3)}\left(\vec{k} - \vec{p}\right). \tag{6.4}$$

The gluon field can be written as the following decomposition in function of $a_a^{\lambda\dagger}$ and a_a^λ

$$A_c^i\left(x^+, \vec{x}\right) = \sum_\lambda \int \frac{\mathrm{d}^3 k}{(2\pi)^3 2k^+}\theta\left(k^+\right)\left(a_c^\lambda\left(x^+, \vec{k}\right)\epsilon_\lambda^i\left(\vec{k}\right)e^{i\vec{k}\cdot\vec{x}} + a_c^{\lambda\dagger}\left(x^+, \vec{k}\right)\epsilon_\lambda^{i*}\left(\vec{k}\right)e^{-i\vec{k}\cdot\vec{x}}\right), \tag{6.5}$$

with $\vec{x} = (x^-, \mathbf{x})$ and $\vec{k}\cdot\vec{x} = k^+ x^- - \mathbf{k}_\perp\cdot\mathbf{x}$. Still in the LC gauge, the field strength has the following form:

$$F_a^{i+}\left(\vec{k}\right) = ik^+ A_a^i\left(\vec{k}\right), \tag{6.6}$$

hence combining Eqs. (6.5) and (6.3), we find that $\mathcal{F}_{gg}^{(3)}\left(x, k_\perp\right)$ can be written as a correlator of field strengths:

$$\mathcal{F}_{gg}^{(3)}\left(x, k_\perp\right) = \frac{\left\langle F_a^{i+}\left(\vec{k}\right) F_a^{i+}\left(-\vec{k}\right)\right\rangle_x}{4\pi^3}, \tag{6.7}$$

or, in Fourier space:

$$\mathcal{F}_{gg}^{(3)}\left(x, k_\perp\right) = 4 \int \frac{\mathrm{d}^3 v \mathrm{d}^3 w}{(2\pi)^3}e^{i\vec{k}\cdot(\vec{v}-\vec{w})}\mathrm{Tr}\left\langle F^{i+}\left(\vec{v}\right) F^{i+}\left(\vec{w}\right)\right\rangle_x, \tag{6.8}$$

where we used that $\mathrm{Tr}\left(t^a t^b\right) = (1/2)\,\delta^{ab}$. In the small-$x$ limit, the phase $\exp\left(ik^+\left(v^- - w^-\right)\right) = \exp\left(ixp^+\left(v^- - w^-\right)\right) \simeq 1$ can be neglected, and the rapidity-dependence is only left inside the medium averages. Finally, the light-cone Fock states are related to the hadronic states $|A\rangle$ as follows (see Ref. [1, 76]):

$$\langle\mathcal{O}\rangle_x = \frac{\langle A|\mathcal{O}|A\rangle}{\langle A|A\rangle}, \tag{6.9}$$

where the latter are normalized as: $\langle A|A\rangle = (2\pi)^3 2p_A^+\delta^{(3)}\left(\vec{0}\right)$, with p_A the momentum of the hadron. Therefore, we can write

$$\mathcal{F}_{gg}^{(3)}\left(x, k_\perp\right) = 2 \int \frac{\mathrm{d}^3 v \mathrm{d}^3 w}{(2\pi)^3 p_A^+}e^{i\vec{k}\cdot(\vec{v}-\vec{w})}\mathrm{Tr}\left\langle A\left|F^{i+}\left(\vec{v}\right) F^{i+}\left(\vec{w}\right)\right|A\right\rangle, \tag{6.10}$$
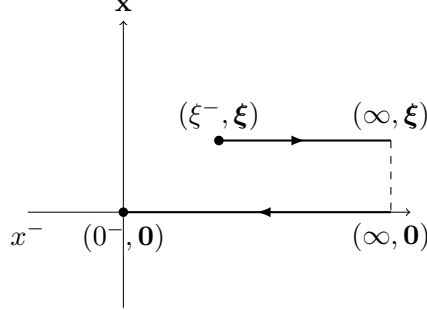
Figure 14: 'Staple' gauge link used in the gauge-invariant definition of the Weizsäcker-Williams gluon TMD.

and finally, using that $k^+ = x p_A^+$ and making use of translational invariance, we obtain the following so-called operator definition of $\mathcal{F}_{gg}^{(3)}(x, k_\perp)$:

$$\mathcal{F}_{gg}^{(3)}(x, k_\perp) \equiv 2 \int \frac{\mathrm{d}^3 \xi}{(2\pi)^3 p_A^+} e^{ixp_A^+\xi^-} e^{-i\mathbf{k}_\perp \cdot \boldsymbol{\xi}} \mathrm{Tr} \Big\langle A \Big| F^{i+}\left(\vec{\xi}\right) F^{i+}\left(\vec{0}\right) \Big| A \Big\rangle. \tag{6.11}$$

This expression, however, only holds in the light-cone gauge. To render it gauge invariant, we can insert Wilson lines that connect the points $\vec{0}$ and $\vec{\xi}$ (see Refs. [10, 77, 78]). In contrast to the integrated gluon distribution, whose gauge-invariant operator definition reads:

$$x\mathcal{G}(x, Q^2) \equiv \int \frac{\mathrm{d}\xi^-}{2\pi p_A^+} e^{ixp_A^+\xi^-} \mathrm{Tr} \Big\langle A \Big| F^{i+}\left(\xi^-\right) U\left(\xi^-, 0^-; \mathbf{0}\right) F^{i+}\left(0^-\right) U\left(0^-, \xi^-; \mathbf{0}\right) \Big| A \Big\rangle, \tag{6.12}$$

with

$$U\left(\xi^-, 0^-; \mathbf{0}\right) \equiv \mathcal{P} e^{ig_s \int_{\xi^-}^{0^-} \mathrm{d}z^- A_a^+(z^-, \mathbf{0}) t^a}, \tag{6.13}$$

in the case of Eq. (6.11), $\vec{0}$ and $\vec{\xi}$ are points in three-dimensional coordinate space, and hence there are different possible paths to connect them. In the case of the Weizsäcker-Williams distribution, one chooses (Ref. [76, 79]):

$$\mathcal{F}_{gg}^{(3)}(x, k_\perp) \equiv 2 \int \frac{\mathrm{d}^3 \xi}{(2\pi)^3 p_A^+} e^{ixp_A^+\xi^-} e^{-i\mathbf{k}_\perp \cdot \boldsymbol{\xi}} \mathrm{Tr} \Big\langle A \Big| F^{i+}\left(\vec{\xi}\right) U^{[+]\dagger} F^{i+}\left(\vec{0}\right) U^{[+]} \Big| A \Big\rangle, \tag{6.14}$$

where $U^{[+]}$, is a so-called staple gauge link (see Fig. 14):

$$\begin{aligned} U^{[+]} &\equiv U\left(0^-, +\infty; \mathbf{0}\right) U\left(+\infty, \xi^-; \boldsymbol{\xi}\right), \\ U^{[+]\dagger} &\equiv U\left(\xi^-, +\infty; \boldsymbol{\xi}\right) U\left(+\infty, 0^-; \mathbf{0}\right). \end{aligned} \tag{6.15}$$

Since these Wilson lines run along the x^--axis and hence only resum A_a^+ gluon fields, the gauge-invariant definition (6.14) is reduced to Eq. (6.11) when choosing the LC gauge.

As we already said, there are different possible Wilson line configurations to render the operator definition (6.11) gauge invariant. Therefore, a multitude of so-called transverse momentum dependent

(TMD) PDFs, TMDs in short, exists, of which the Weizsäcker-Williams distribution $\mathcal{F}_{gg}^{(3)}(x, k_\perp)$ is one example (and, incidentally, the only TMD for which the 'gluon counting' interpretation Eq. (6.3) holds). In general, it is the physical process under consideration which determines which Wilson-line path to chose, and hence which TMD PDF plays a role. In Part III of this thesis we will compute the cross section for forward dijet production in proton-nucleus collisions, and analyze in the small-x limit the various gluon TMDs that play a role. Just like the nonlinear BK equation is reduced to BFKL in the dilute regime, in the limit of large transverse momenta, the Wilson-line structure of the gluon TMDs simplifies, and the latter either disappear or become equal to the Weizsäcker-Williams/unintegrated gluon distribution. That this reduction does indeed take place, can be understood from expression (6.14): for large momenta $k_\perp$, the transverse coordinate $\boldsymbol{\xi}$ becomes small, and the two Wilson lines in Fig. 14 overlap, cancel (since $U(a, b, \mathbf{x}) U^\dagger(a, b, \mathbf{x}) = 1$), upon which the whole path is reduced to the simple one-dimensional path $U(\xi^-, 0^-; \mathbf{0})$ of Eq. (6.12).

We should stress that in principle the TMDs still depend on the hard scale Q^2. However, in the small-x limit this dependence is trivial, which is why we do not include it in the notation. Approaches exist (see e.g. Refs. [80–82]) which do take this hard-scale dependence of TMDs into account in the evolution, allowing one to interpolate between the DGLAP and the BFKL regime. These approaches are usually based on the well-known CCFM (Catani-Ciafaloni-Fiorani-Marchesini, Refs. [83–85]) evolution equation, in which angular ordering is imposed on the parton splittings.

Finally, note that we have all the ingredients to prove Eq. (5.27), i.e. the fact that in the dilute limit the dipole amplitude is linearly related to the unintegrated gluon distribution. Indeed, in the dilute regime, the multiple scatterings of the dipole off the target can be approximated by a single scattering, involving a two-gluon exchange in the forward amplitude $\langle T(\mathbf{x}, \mathbf{y}) \rangle_Y$. This is implemented by expanding the Wilson lines, which resum the gluon fields of the target, to second order:

$$U(\mathbf{x}) \simeq 1 + i g_s \int \mathrm{d}z^- A_a^+(z^-, \mathbf{x}) t^a + \frac{(i g_s)^2}{2!} \mathcal{P} \int \mathrm{d}z_1^- \mathrm{d}z_2^- A_a^+(z_1^-, \mathbf{x}) A_b^+(z_2^-, \mathbf{x}) t^a t^b. \qquad (6.16)$$

To second-order accuracy, the path ordering doesn't play a role, since $\mathrm{Tr}(t^a t^b) = \mathrm{Tr}(t^b t^a) = (1/2) \delta^{ab}$. Consequently, in the dilute regime, governed by the BFKL equation, a strict separation holds between the longitudinal and the transverse dynamics. We can therefore introduce the shorthand notation:

$$\alpha_{\mathbf{x}}^a \equiv \int \mathrm{d}z^- A_a^+(z^-, \mathbf{x}), \qquad (6.17)$$

and the dipole scattering amplitude from definition (5.6) can be written as follows:

$$\langle T(\mathbf{x}, \mathbf{y}) \rangle_Y = 1 - \frac{1}{N_c} \mathrm{Tr} \langle U(\mathbf{x}) U^\dagger(\mathbf{y}) \rangle_Y \simeq \frac{g_s^2}{4 N_c} \left\langle \left(\alpha_{\mathbf{x}}^a - \alpha_{\mathbf{y}}^a \right)^2 \right\rangle_Y. \qquad (6.18)$$

On the other hand, in a covariant gauge, the field strength and the gluon fields obey the relation:

$$F_a^{i+}(\vec{x}) = \partial^i A_a^+(\vec{x}). \qquad (6.19)$$

With the help of this property, we find from Eqs. (6.1) and (6.8) (using partial integration as well as the Casimir property Eq. (A.12), and setting $\exp\left(-ik^+ \cdot (v^- - w^-)\right) = \exp\left(-ixp^+ \cdot (v^- - w^-)\right) = 1$):

$$f(x, k_\perp) = 2\pi \mathbf{k}_\perp^4 \int \frac{\mathrm{d}^3 v \mathrm{d}^3 w}{(2\pi)^3} e^{i\mathbf{k}\cdot(\mathbf{v}-\mathbf{w})} \left\langle A_a\left(v^-, \mathbf{v}\right) A_a\left(w^-, \mathbf{w}\right)\right\rangle_Y. \tag{6.20}$$

Plugging this expression into the r.h.s. of Eq. (5.27), we recover expression (5.27):

$$\begin{aligned}
&\frac{4\pi\alpha_s}{N_c} \int \frac{\mathrm{d}^2 \mathbf{k}_\perp}{k_\perp^4} f(x, k_\perp)\left(1 - e^{i\mathbf{k}_\perp \mathbf{r}}\right) \\
&= \frac{8\pi^2 \alpha_s}{N_c} \int \frac{\mathrm{d}^3 v \mathrm{d}^3 w}{2\pi} \left(\delta^{(2)}(\mathbf{v} - \mathbf{w}) - \delta^{(2)}(\mathbf{r} + \mathbf{v} - \mathbf{w})\right) \left\langle A_a\left(v^-, \mathbf{v}\right) A_a\left(w^-, \mathbf{w}\right)\right\rangle_Y, \\
&= \frac{2\pi\alpha_s}{N_c} \int \mathrm{d}^2 \mathbf{v} \left\langle (\alpha_{\mathbf{r}}^a - \alpha_{\mathbf{0}}^a)^2\right\rangle_Y = \frac{2\pi\alpha_s}{N_c} S_\perp \left\langle (\alpha_{\mathbf{r}}^a - \alpha_{\mathbf{0}}^a)^2\right\rangle_Y \\
&= 2 S_\perp \langle T(\mathbf{r})\rangle_Y = \sigma_{\mathrm{dip}}(x, \mathbf{r}),
\end{aligned} \tag{6.21}$$

making use of the translational invariance of the medium averages in the transverse plane, and restricting the transverse coordinates to the area $S_\perp$ of the target:

$$S_\perp = \int \mathrm{d}^2 \mathbf{v}. \tag{6.22}$$

Combining Eq. (5.27) with the BFKL solution for $f(x, k_\perp)$, Eq. (5.30), and with expression (4.7) for the photon-proton cross section, we obtain the DIS cross section as found in the BFKL approach (see Ref. [65]).

Incidentally, from Eq. (5.27) it is also apparent that the dipole-hadron cross section can be seen as a direct probe of the gluon distribution. Indeed, in the limit of small dipole sizes, which, since $r_\perp^2 \sim 1/Q^2$, is again consistent with the dilute approximation, the exponential can be expanded, yielding:

$$\sigma_{\mathrm{dip}}(x, \mathbf{r}) \simeq r^2 \frac{\alpha_s \pi^2}{N_c} x\mathcal{G}\left(x, 1/r^2\right). \tag{6.23}$$

This implies that, in the dilute regime, the dipole scattering amplitude scales approximately quadratically with the size $\mathbf{r}$ of the dipole:

$$\langle T(\mathbf{r})\rangle_x \propto r^2. \tag{6.24}$$

One can show (see Ref. [5], and references therein) that the high-energy evolution towards the saturation regime (but still in the dilute region $r^2 \ll 1/Q_s^2$, hence inside the window for geometric scaling) introduces a nonperturbative anomalous dimension $\gamma_s \simeq 0.63$, which changes this scaling to:

$$\langle T(\mathbf{r})\rangle_x \propto r^{2\gamma_s}. \tag{6.25}$$

Finally, from Eq. (6.18) we see that there is another way to view the unitarity of the cross section. Indeed, written as a correlator of Wilson lines, the forward scattering amplitude is manifestly unitary, which is broken by expanding the Wilson lines in the single-scattering approximation. It

is therefore multiple scattering that renders the cross section unitary. Multiple scattering becomes important when the exponent of the Wilson lines is of order one, which is equivalent to the statement that the gluon fields are strong:

$$g_s \int \mathrm{d}x^- A^+ \sim 1, \qquad (6.26)$$

and that the gluon distribution in the target saturates. This equivalence is highly nontrivial, but arises naturally in the Color Glass Condensate, which is the subject of the following part of the thesis.

Part II

Color Glass Condensate

7   Introduction

In the previous part, we went through the basics of QCD at small-x, and gave a physical motivation for the saturation of the gluon distribution in the high density regime. We saw that there are not only phenomenological hints for saturation, but also that saturation physics solves in a natural way the problems of unitarity breaking and infrared diffusion in the small-x limit of QCD.

In this part, we discuss the Color Glass Condensate, which is an effective theory for the proton or nucleus in the saturation regime. Its initial condition is the McLerran-Venugopalan (MV) model, a classical theory for the partons in a large nucleus. It is based on the fact that, in the infinite-momentum frame, the valence quarks, which carry a longitudinal momentum fraction $x_{\mathrm{val}} \sim 1$ of their parent nucleon, have a considerably longer lifetime than the so-called wee gluons which carry a momentum fraction $10^{-2} \lesssim x_{\mathrm{wee}} \lesssim 10^{-1}$ (the lower limit guarantees that soft gluon radiation is small enough to be negligible). The resolution Q^2, with which the nucleus is probed, has to be high enough to penetrate the nucleons, but small enough to see a dense collection of color charges, leading to the requirement: $\Lambda_{\mathrm{QCD}}^2 \lesssim Q^2 \lesssim \Lambda_{\mathrm{QCD}}^2 A^{1/3}$, where A is the atomic number of the nucleus. In this region of phase space, the valence quarks are practically frozen with respect to the dynamics of the wee gluons, and act as recoilless color charges ρ_a which generate the gluons through the Yang-Mills equations. Since the scattering of a projectile off the nucleus is described by Wilson lines, which resum the multiple interactions with the soft gluons, scattering in this sense boils down to probing the correlations of the color charges. The latter are distributed according to a Gaussian distribution or weight function $\mathcal{W}_A[\rho]$, over which all observables have to be averaged.

It is to this kinematical separation between frozen valence quarks on the one hand, and short-living wee gluons on the other hand, that the Color Glass Condensate owes its name, since dynamics that takes place over two very different time scales is the hallmark of 'glassy' behavior. In addition, in the saturation regime the gluons behave effectively like a Bose condensate. The typical transverse momentum $k_\perp^2$ of the gluons is of the order of the saturation scale Q_s^2 which, as we will see, scales linearly with μ_A: the density of the color charge squared per color and per unit area. Hence, parametrically we have that $k_\perp^2 \sim Q_s^2 \sim \mu_A$, implying that in the high-density regime, the typical momenta of the hadron constituents are high enough to describe the saturated hadron system within perturbation theory.

To logarithmic accuracy, the MV model can be extended towards smaller values of Bjorken-x, by pushing the scale Λ^+, which separates valence and wee partons, down towards a smaller scale Λ'^+. The so-called semi-fast classical gluons, which have energies in the strip $\Lambda^+ \gg k^+ \gg \Lambda'^+$, are then promoted again to quantum gluons, and subsequently integrated out and absorbed into the new sources which account for the hard partons ($k^+ \gg \Lambda'^+$, so they include the valence partons). After this procedure, which corresponds to one step in the rapidity evolution, one has again a classical theory in which the static color sources generate soft ($\Lambda'^+ \gg k^+$) classical gluon fields by virtue of the Yang-Mills equations. The kinematical 'glassy' structure of the MV model is hence preserved

throughout the evolution. Finally, the nonlinear evolution equation for the weight function $\mathcal{W}_{\Lambda'}[\rho]$ of the color charges, which one obtains through the renormalization group procedure we just described, is the well-known JIMWLK equation.

8 McLerran-Venugopalan model

As already said above, the McLerran-Venugopalan model (Refs. [86–88]) is a classical effective theory for a large nucleus, and is the initial condition of the Color Glass Condensate. Its starting point is the observation that, if one considers a nucleus in the infinite momentum frame, its parton content is kinematically separated in rapidity. Indeed, in light-cone coordinates, taking the nucleus to be a right-mover, the longitudinal extent of a parton with momentum p^+ is given by:

$$\Delta x^- \sim \frac{1}{p^+} = \frac{1}{xP^+}, \tag{8.1}$$

where x is the fraction the parton carries of the momentum P^+ of the parent nucleon. The nucleus itself, with a radius $R_A \simeq R_0 A^{1/3} \simeq \Lambda_{\mathrm{QCD}}^{-1} A^{1/3}$, is squeezed together, due to Lorentz contraction, to a thickness

$$\Delta x_A^- \sim \frac{2R_A}{\gamma} = \frac{2R_A}{P^+} m_N, \tag{8.2}$$

where we used that $\gamma = P_A^+/M_A \simeq P^+/m_N$, with P_A and M_A the momentum and mass of the nucleus, and m_N the mass of an individual nucleon. Comparing with Eq. (8.1), we can label partons according to their energy fraction x and therefore their longitudinal extent. Indeed, valence partons, which carry a large fraction of the nucleus' momentum, are localized on the x^--axis, and appear as a thin sheet in contrast to the 'wee' partons with $x \ll 1$, which are delocalized, well beyond the longitudinal radius of the nucleus. In formulas:

$$\Delta x_{\mathrm{val}}^- \ll \Delta x_A^- \ll \Delta x_{\mathrm{wee}}^-, \tag{8.3}$$

where:

$$x_{\mathrm{val}} \sim 1, \quad x_{\mathrm{wee}} \ll \frac{1}{R_A m_N} \sim A^{-1/3}. \tag{8.4}$$

In addition, for the classical description to remain valid, radiative effects should be negligible. From the Bremsstrahlung law, the probability for partons with x' between x and 1 to radiate is:

$$\int_x^1 \mathrm{d}P_{\mathrm{Bremsstr}} \simeq \frac{\alpha_s N_c}{\pi} \ln\frac{1}{x}, \tag{8.5}$$

hence requiring that this probability is much smaller than one amounts to the lower limit:

$$x_{\mathrm{wee}} \gg e^{-1/\bar{\alpha}}. \tag{8.6}$$

As an example, for lead, with $A = 206$, and a coupling $\bar{\alpha} = 0.3$, we find the following, rather small, phase space for the wee partons: $0.04 \ll x_{\mathrm{wee}} \ll 0.2$.

Of course, the opposite effect is also true: the partons have a lifetime of the order

$$\Delta x^+ \sim \frac{1}{p^-} = \frac{2xP^+}{p_\perp^2}, \tag{8.7}$$

hence the valence partons live considerably longer than the wee partons:

$$\Delta x_{\text{wee}}^+ \ll \Delta x_{\text{val}}^+. \tag{8.8}$$

Thus, with respect to the characteristic time scale of the wee partons, the valence partons appear to be 'frozen' in time. In addition, since their momenta are much larger, they can radiate gluons without experiencing the effects of this radiation, hence without recoil. For these two reasons, the valence partons can be treated to a good approximation as static currents of color charge:

$$J_a^\mu = \delta^{\mu+} \rho_a\left(\vec{x}\right), \tag{8.9}$$

where $\vec{x} = (x^-, \mathbf{x})$, and where the valence parton color charge density ρ_a is random, static (it has no x^+ LC-time dependence), and sharply localized around $x^- \sim 1/p^+$. The wee partons are generated by these currents by virtue of the classical Yang-Mills equation:

$$[D_\nu, F^{\nu\mu}]\left(\vec{x}\right) = \delta^{\mu+} \rho_a\left(\vec{x}\right) T^a,$$
$$\left(\partial_\nu F_a^{\nu\mu} + g_s f^{abc} A_\nu^b F_c^{\nu\mu}\right)\left(\vec{x}\right) = \delta^{\mu+} \rho_a\left(\vec{x}\right). \tag{8.10}$$

with the covariant derivative (in the adjoint representation):

$$D_\mu \equiv \partial_\mu - ig_s A_\mu^a T^a, \tag{8.11}$$

and the field strength:

$$F^{\mu\nu} \equiv \partial^\mu A^\nu - \partial^\nu A^\mu - ig_s\left[A^\mu, A^\nu\right],$$
$$= \left(\partial^\mu A_a^\nu - \partial^\nu A_a^\mu + g_s f^{abc} A_b^\mu A_c^\nu\right) T^a. \tag{8.12}$$

To solve the Yang-Mills equation, Eq. (8.10), we follow the method described in Ref. [89]. First, since the source $\rho(x)$ is static, we expect our solution to be static as well, hence we require $\partial_+ A^\mu = 0$. In addition, we make the ansatz that $A^- = 0$, which ensures that the current is covariantly conserved: $[D^-, J^+] = 0$. With these requirements, the only non-zero components of the field strength are F^{i+} and F^{ij}. However, since we want a solution that vanishes in the absence of a source $\rho(x)$, it follows from the $\mu = i$ component of the Yang-Mills equation:

$$\left[D_\nu, F^{\nu i}\right](x) = \left[D_j, F^{ji}\right](x) = 0, \tag{8.13}$$

that $F^{ij} = 0$. This implies that the gauge fields form a pure gauge in the two transverse dimensions, i.e.:

$$A^i = \frac{i}{g_s} \mathcal{S} \partial^i \mathcal{S}^\dagger, \tag{8.14}$$

with $\mathcal{S} = \mathcal{S}\left(x^-, \mathbf{x}\right) \in SU\left(N_c\right)$.

By fixing the gauge, the remaining degrees of freedom will be further reduced to one, as we will now demonstrate. First, let us choose a gauge in which $\tilde{A}^i = 0$, gauge transforming Eq. (8.14) as follows:

$$
\begin{aligned}
\tilde{A}^i &= \mathcal{S}^\dagger \left(A^i + \frac{i}{g} \partial^i \right) \mathcal{S}, \\
&= \frac{i}{g_s} \mathcal{S}^\dagger \mathcal{S} \left(\partial^i \mathcal{S}^\dagger \right) \mathcal{S} + \frac{i}{g_s} \mathcal{S}^\dagger \partial^i \mathcal{S}, \\
&= 0,
\end{aligned}
\tag{8.15}
$$

where we used the fact that $\left(\partial^i \mathcal{S}^\dagger \right) \mathcal{S} = -\mathcal{S}^\dagger \partial^i \mathcal{S}$. This gauge choice is a covariant gauge since clearly $\partial_\mu \tilde{A}^\mu = 0$. The only field left is now $\alpha_a(\vec{x}) \equiv \tilde{A}^+_a(\vec{x})$, for which the Yang-Mills equation (8.10) yields:

$$
\partial_\mu \partial^\mu \alpha_a(\vec{x}) = -\nabla^2_\perp \alpha_a(\vec{x}) = \rho_a(\vec{x}).
\tag{8.16}
$$

Its solution is easily found by going to Fourier space, and yields:

$$
\begin{aligned}
\alpha_a\left(x^-, \mathbf{x}\right) &= \int \mathrm{d}^2\mathbf{y} \int \frac{\mathrm{d}^2\mathbf{k}_\perp}{(2\pi)^2} \frac{e^{i\mathbf{k}_\perp \cdot (\mathbf{x}-\mathbf{y})}}{k_\perp^2} \rho_a\left(x^-, \mathbf{y}\right), \\
&= \frac{1}{4\pi} \int \mathrm{d}^2\mathbf{y} \ln \frac{1}{(\mathbf{x}-\mathbf{y})^2 \Lambda^2} \rho_a\left(x^-, \mathbf{y}\right),
\end{aligned}
\tag{8.17}
$$

where we made use of Eq. (B.1), and where Λ^2 is some infrared cutoff, such as Λ_{QCD}. The associated field strength is:

$$
\begin{aligned}
F^{i+}_{\mathrm{COV}}\left(x^-, \mathbf{x}\right) &= \partial^i \alpha\left(x^-, \mathbf{x}\right), \\
&= \int \mathrm{d}^2\mathbf{y} \int \frac{\mathrm{d}^2\mathbf{k}_\perp}{(2\pi)^2} \frac{ik_\perp^i}{k_\perp^2} e^{i\mathbf{k}_\perp \cdot (\mathbf{x}-\mathbf{y})} \rho\left(x^-, \mathbf{y}\right), \\
&= -\frac{1}{2\pi} \int \mathrm{d}^2\mathbf{y} \frac{(x-y)^i}{(\mathbf{x}-\mathbf{y})^2} \rho\left(x^-, \mathbf{y}\right).
\end{aligned}
\tag{8.18}
$$

However, the MV model is most naturally formulated in the light-cone gauge $A^+ = 0$. From the solution of the Yang-Mills equation in covariant gauge, one can obtain the classical gluon field $\mathcal{A}^\mu$ in LC gauge with the help of another gauge transformation $\mathcal{V}^\dagger(\vec{x})$:

$$
\mathcal{A}^\mu = \mathcal{V}^\dagger \left(\tilde{A}^\mu + \frac{i}{g_s} \partial^\mu \right) \mathcal{V}.
\tag{8.19}
$$

For the case $\mu = +$, we have:

$$
\mathcal{V}^\dagger \left(\alpha + \frac{i}{g_s} \partial^+ \right) \mathcal{V} = 0,
\tag{8.20}
$$

which is solved by the Wilson line in the adjoint representation:

$$
\mathcal{V}\left(x^-, \mathbf{x}\right) \equiv \mathcal{P} e^{ig_s \int_{-\infty}^{x^-} \mathrm{d}z^- \alpha_a\left(z^-, \mathbf{x}\right) T^a} = W\left(x^-, \mathbf{x}\right).
\tag{8.21}
$$

Hence, from Eq. (8.19) we obtain the gauge field $\mathcal{A}^i$ in the LC gauge, as a pure gauge field with the gauge rotation (8.21):

$$\mathcal{A}^i \left(x^-, \mathbf{x}\right) = \frac{i}{g_s} W^\dagger \left(x^-, \mathbf{x}\right) \partial_- W \left(x^-, \mathbf{x}\right), \tag{8.22}$$

and the associated field strength:

$$F_{\mathrm{LC}}^{i+} \left(\vec{x}\right) = W^\dagger \left(\vec{x}\right) F_{\mathrm{COV}}^{i+} \left(\vec{x}\right) W \left(\vec{x}\right) = W_{ba} \left(\vec{x}\right) \partial^i \alpha_b \left(\vec{x}\right) t^a, \tag{8.23}$$

where we used the property (A.11). In the literature, $\mathcal{A}^i$ is often called the non-Abelian Weizsäcker-Williams field (see e.g. Ref. [90], or Ref. [91] for an instructive comparison with the Abelian case).

Whether they are formulated in the covariant gauge ($\mathcal{A}^+$) or in the LC gauge ($\mathcal{A}^i$), the classical wee gluon fields in the MV model are functions of the color sources $\rho_a \left(x\right)$ which generate them. In order to proceed, we need to study these color sources and their distribution closer. To do so, let us consider deep-inelastic scattering, in which a quark-antiquark dipole probes the nucleus, with a transverse resolution $1/Q^2$. The number of sources seen by the projectile is then given by $\Delta N = n/Q^2$, with $n \equiv N_c A/\pi R_A^2$ the transverse density of valence quarks. Again using that $R_A \simeq \Lambda_{\mathrm{QCD}}^{-1} A^{1/3}$, we find:

$$\Delta N = \frac{\Lambda_{\mathrm{QCD}}^2}{Q^2} \frac{N_c A^{1/3}}{\pi}, \tag{8.24}$$

and therefore, if the virtuality of the photon is small enough: $Q^2 \ll \Lambda_{\mathrm{QCD}}^2 A^{1/3}$ (but still large enough, such that $Q^2 \gg \Lambda_{\mathrm{QCD}}^2$), a large number ΔN of color sources is probed. Since these sources are associated with valence quarks, which belong to different nucleons in the large nucleus, it is safe to assume that they are randomly distributed in the transverse plane, and hence the average of the total color charge $\mathcal{Q}_a$ seen by the probe is zero:

$$\langle \mathcal{Q}_a \rangle_A = 0, \tag{8.25}$$

while the two-point function of the color charges is given by:

$$\langle \mathcal{Q}_a \mathcal{Q}_a \rangle_A = g_s^2 C_F \Delta N, \tag{8.26}$$

and all the higher-point functions are assumed to vanish. Furthermore, note that, in order for boundary effects to be negligible, it is assumed that the transverse extent of the nucleus is infinite. Since Eqs. (8.25) and (8.26) are expected to hold irrespectively of the precise value of the resolution $1/Q^2$, the color charges $\mathcal{Q}_a$ are naturally associated with a continuous distribution of color charge with density ρ_a:

$$\mathcal{Q}_a \equiv \int_{1/Q^2} \mathrm{d}^2\mathbf{x} \int \mathrm{d}x^- \rho_a \left(x^-, \mathbf{x}\right). \tag{8.27}$$

Using $\int_{1/Q^2} \mathrm{d}^2\mathbf{x} = 1/Q^2$, as well as the definition of $C_F \equiv \left(N_c^2 - 1\right)/2N_c$, correlators (8.25) and (8.26) can be written in function of the sources, yielding:

$$\langle \rho_a \left(x^-, \mathbf{x}\right) \rangle_A = 0,$$
$$\langle \rho_a \left(x^-, \mathbf{x}\right) \rho_b \left(y^-, \mathbf{y}\right) \rangle_A = g_s^2 \delta_{ab} \delta \left(x^- - y^-\right) \delta^{(2)} \left(\mathbf{x} - \mathbf{y}\right) \lambda_A \left(x^-\right). \tag{8.28}$$

where

$$\mu_A \equiv g_s^2 \int \mathrm{d}x^- \lambda_A \left(x^- \right) = \frac{g_s^2 A}{2 \pi R_A^2} \tag{8.29}$$

is the density of color charge squared of the valence quarks, per unit area and per color. Finally, the correlators can be generated from the following weight function, which is a Gaussian distribution of the color charges:

$$\mathcal{W}_A \left[\rho \right] = \mathcal{N} \exp \left(-\frac{1}{2} \int \mathrm{d}^3 x \frac{\rho_a \left(\vec{x} \right) \rho_a \left(\vec{x} \right)}{\lambda_A \left(x^- \right)} \right), \tag{8.30}$$

and which can be used to write the averages over observables explicitly:

$$\langle \mathcal{O} \rangle_A = \frac{\int \mathcal{D} \left[\rho \right] \mathcal{W}_A \left[\rho \right] \mathcal{O}}{\int \mathcal{D} \left[\rho \right] \mathcal{W}_A \left[\rho \right]}. \tag{8.31}$$

Note that these averages are purely classical, similar to a Boltzmann average in statistical physics. The correlators Eq. (8.28) can be written in function of the gluon fields $\alpha_a \left(\mathbf{x} \right)$ in the covariant gauge, using Eqs. (8.16) and (8.17):

$$\langle \alpha_a \left(x^-, \mathbf{x} \right) \alpha_b \left(y^-, \mathbf{y} \right) \rangle_A = \frac{1}{g_s^2} \delta_{ab} \delta \left(x^- - y^- \right) \lambda_A \left(x^- \right) L \left(\mathbf{x} - \mathbf{y} \right), \tag{8.32}$$

where:

$$L \left(\mathbf{x} - \mathbf{y} \right) = g_s^4 \int \frac{\mathrm{d}^2 \mathbf{k}_\perp}{\left(2\pi \right)^2} \frac{e^{i \mathbf{k}_\perp \left(\mathbf{x} - \mathbf{y} \right)}}{k_\perp^4}. \tag{8.33}$$

It is a very instructive exercise to evaluate the dipole in the MV model:

$$D \left(\mathbf{x} - \mathbf{y} \right) \equiv \frac{1}{N_c} \mathrm{Tr} \left\langle U \left(\mathbf{x} \right) U^\dagger \left(\mathbf{y} \right) \right\rangle_A, \tag{8.34}$$

which we already encountered earlier in the discussion on deep-inelastic scattering, and which will continue to play an important role in what follows. Note that we do not write an index Y, since the MV model comes with a fixed validity range for x (see Eqs. (8.4) and (8.6)). Let us introduce the following definitions:

$$D \left(L, \mathbf{x} - \mathbf{y} \right) \equiv \frac{1}{N_c} \mathrm{Tr} \left\langle U \left(L, \mathbf{x} \right) U^\dagger \left(L, \mathbf{y} \right) \right\rangle_A,$$
$$U \left(L, \mathbf{x} \right) \equiv \mathcal{P} e^{i g_s \int_{-\infty}^{L} \mathrm{d}z^- \alpha_a \left(z^-, \mathbf{x} \right) t^a}, \tag{8.35}$$

where the dipole and the Wilson lines have support $x^- \in]-\infty, L]$. Increasing L with an infinitesimal

distance ϵ, one obtains:

$$
\begin{aligned}
D\left(L+\epsilon, \mathbf{x}-\mathbf{y}\right) &= \frac{1}{N_c}\text{Tr}\left\langle U\left(L+\epsilon, \mathbf{x}\right)U^\dagger\left(L+\epsilon, \mathbf{y}\right)\right\rangle_A, \\
&\simeq \frac{1}{N_c}\text{Tr}\left\langle U\left(L, \mathbf{x}\right)\left(1+ig_s\epsilon\alpha_a\left(L+\epsilon, \mathbf{x}\right)t^a + \frac{1}{2!}\left(ig_s\right)^2\epsilon^2\left(\alpha_a\left(L+\epsilon, \mathbf{x}\right)t^a\right)^2\right)\right. \\
&\quad \times \left.\left(1-ig_s\epsilon\alpha_a\left(L+\epsilon, \mathbf{y}\right)t^a + \frac{1}{2!}\left(-ig_s\right)^2\epsilon^2\left(\alpha_a\left(L+\epsilon, \mathbf{y}\right)t^a\right)^2\right)U^\dagger\left(L, \mathbf{y}\right)\right\rangle_A, \\
&= D\left(L, \mathbf{x}-\mathbf{y}\right) + D\left(L, \mathbf{x}-\mathbf{y}\right) \\
&\quad \times \frac{-g_s^2}{2N_c}\epsilon^2\text{Tr}\left\langle\left(\alpha_a\left(L, \mathbf{y}\right)t^a\right)^2 + \left(\alpha_a\left(L, \mathbf{x}\right)t^a\right)^2 - 2\alpha_a\left(L, \mathbf{x}\right)t^a\alpha_b\left(L, \mathbf{y}\right)t^b\right\rangle_A,
\end{aligned}
\tag{8.36}
$$

where, in the last line, we factorized $D\left(L, \mathbf{x}-\mathbf{y}\right)$ from the parts that are evaluated at $x^- = L+\epsilon$, since, from Eq. (8.32), the correlator is local in x^-. In addition, we used that $\alpha_a\left(L, \mathbf{x}\right)\simeq \alpha_a\left(L+\epsilon, \mathbf{x}\right)$, and we kept only the quadratic terms in the gluon fields since, from Eq. (8.28), the one-point function disappears. Furthermore, plugging in the discrete version of Eq. (8.32), in which an extra factor $1/\epsilon$ appears (since the delta function becomes upon discretization $\delta\left(x^- - y^-\right) = \delta\left((n-m)\epsilon\right) = \delta_{nm}/\epsilon$), we obtain:

$$
D\left(L+\epsilon, \mathbf{x}-\mathbf{y}\right) - D\left(L, \mathbf{x}-\mathbf{y}\right) = D\left(L, \mathbf{x}-\mathbf{y}\right)\times\frac{-g_s^2 C_F}{2\mu_A}\epsilon\lambda_A\left(L\right)\Gamma\left(\mathbf{x}-\mathbf{y}\right),
\tag{8.37}
$$

where we introduced the dimensionless quantity:

$$
\begin{aligned}
\Gamma\left(\mathbf{x}-\mathbf{y}\right) &\equiv \frac{\mu_A}{g_s^2}\left(L_{\mathbf{xx}} + L_{\mathbf{yy}} - 2L_{\mathbf{xy}}\right) = 2\frac{\mu_A}{g_s^2}\left(L\left(\mathbf{0}\right) - L\left(\mathbf{x}-\mathbf{y}\right)\right), \\
&= 2\mu_A g_s^2\int\frac{\mathrm{d}^2\mathbf{k}_\perp}{(2\pi)^2}\frac{1}{k_\perp^4}\left(1 - e^{i\mathbf{k}_\perp(\mathbf{x}-\mathbf{y})}\right).
\end{aligned}
\tag{8.38}
$$

Eq. (8.37) can be cast in the form of a differential equation:

$$
\frac{\partial}{\partial x^-}D\left(x^-, \mathbf{x}-\mathbf{y}\right) = -\frac{g_s^2}{\mu_A}\frac{C_F}{2}\lambda_A\left(x^-\right)\Gamma\left(\mathbf{x}-\mathbf{y}\right)D\left(x^-, \mathbf{x}-\mathbf{y}\right),
\tag{8.39}
$$

with the solution:

$$
D\left(x^-, \mathbf{x}-\mathbf{y}\right) = \exp\left(-\frac{g_s^2}{\mu_A}\frac{C_F}{2}\int_{-\infty}^{x^-}\mathrm{d}z^-\lambda_A\left(z^-\right)\Gamma\left(\mathbf{x}-\mathbf{y}\right)\right),
\tag{8.40}
$$

or, taking $x^- \to \infty$:

$$
D\left(\mathbf{r}\right) = e^{-\frac{C_F}{2}\Gamma(\mathbf{r})} \simeq e^{-\frac{r^2}{4}Q_s^2(r^2)},
\tag{8.41}
$$

The integral in the expression for $\Gamma\left(\mathbf{x}\right)$ is dominated by small momenta. It can therefore be evaluated, to logarithmic accuracy, by expanding the numerator:

$$
\begin{aligned}
\Gamma\left(\mathbf{r}\right) &\simeq 2\mu_A g_s^2\int_{\Lambda^2}^{1/r^2}\frac{\mathrm{d}^2\mathbf{k}_\perp}{(2\pi)^2}\frac{1}{k_\perp^4}\frac{k_\perp^2 r^2\cos^2\theta}{2!}, \\
&= \frac{r^2}{2}\alpha_s\mu_A\ln\frac{1}{r^2\Lambda^2} = \frac{r^2}{2}\frac{1}{C_F}Q_s^2\left(r^2\right) = \frac{r^2}{2}\frac{1}{N_c}Q_{sg}^2\left(r^2\right),
\end{aligned}
\tag{8.42}
$$

and we recover indeed a large logarithm, assuming that $r \ll 1/\Lambda$, where Λ is an infrared cutoff Λ such as Λ_{QCD}. In the last line of the above expression, we introduced the transverse momentum scales Q_s and Q_{sg}, which are the saturation scales experienced by a quark or a gluon, respectively. In the MV model, they are defined as follows:

$$Q_s^2\left(r^2\right) \equiv \alpha_s C_F \mu_A \ln \frac{1}{r^2\Lambda^2},$$
$$Q_{sg}^2\left(r^2\right) \equiv \alpha_s N_c \mu_A \ln \frac{1}{r^2\Lambda^2}, \tag{8.43}$$

where Λ is the infrared cutoff, most commonly taken to be Λ_{QCD}. From the definition of μ_A, Eq. (8.29), it is clear that the saturation scale rises with the number of nucleons as $Q_s^2 \sim A^{1/3}$. We will show in a few moments how the scales Q_s and Q_{sg} are related to the phenomenon of saturation. First, let us remark that the above results allow us to write the dipole in the MV model as follows:

$$D\left(\mathbf{r}\right) \simeq e^{-\frac{r^2}{4}Q_s^2\left(r^2\right)}. \tag{8.44}$$

Moreover, it is easy to see that, for a dipole in the adjoint representation:

$$D_A\left(\mathbf{x}-\mathbf{y}\right) \equiv \frac{1}{N_c^2-1}\mathrm{Tr}\left\langle W\left(\mathbf{x}\right)W^\dagger\left(\mathbf{y}\right)\right\rangle_A, \tag{8.45}$$

the calculation leading to Eq. (8.40) can be repeated and one obtains exactly the same result, except from the color factor $C_F \to N_c$:

$$D_A\left(\mathbf{r}\right) = e^{-\frac{N_c}{2}\Gamma\left(\mathbf{r}\right)} \simeq e^{-\frac{r^2}{4}Q_{sg}^2\left(r^2\right)}. \tag{8.46}$$

We would now like to evaluate the Weizsäcker-Williams gluon distribution $\mathcal{F}_{gg}^{(3)}\left(x,q_\perp\right)$, introduced in Sec. 6, in the MV model. To do so, we insert the light-cone field strengths, Eq. (8.23), into expression (6.8), which yields:

$$\mathcal{F}_{gg}^{(3)}\left(x,q_\perp\right) = 4\int \frac{\mathrm{d}^3v\mathrm{d}^3w}{(2\pi)^3}e^{-i\mathbf{q}_\perp\cdot(\mathbf{v}-\mathbf{w})}\mathrm{Tr}\left\langle\left(W_{ba}\partial^i\alpha_b t^a\right)\left(\vec{v}\right)\left(W_{cd}\partial^i\alpha_c t^d\right)\left(\vec{w}\right)\right\rangle_A. \tag{8.47}$$

Due to the locality of the correlators in x^-, see Eq. (8.32), the correlator can be factorized as follows:

$$\mathrm{Tr}\left\langle\left(W_{ba}\partial^i\alpha_b t^a\right)\left(\vec{v}\right)\left(W_{cd}\partial^i\alpha_c t^d\right)\left(\vec{w}\right)\right\rangle_A$$
$$= \frac{1}{2}\delta^{ad}\left\langle W_{ba}\left(\vec{v}\right)W_{cd}\left(\vec{w}\right)\right\rangle_A \times \left\langle\partial^i\left(\alpha_b\left(\vec{v}\right)\right)\partial^i\alpha_c\left(\vec{w}\right)\right\rangle_A, \tag{8.48}$$
$$= -\frac{1}{2g_s^2}\delta\left(v^--w^-\right)\lambda_A\left(v^--w^-\right)\mathrm{Tr}\left\langle W\left(\vec{v}\right)W^\dagger\left(\vec{w}\right)\right\rangle_A\partial_\perp^2 L\left(\mathbf{v}-\mathbf{w}\right),$$

where we used the fact that $W_{ab}\left(\vec{x}\right)$ is real. From the definition of $L\left(\mathbf{x}\right)$, see Eq. (8.33), we have that:

$$\partial_\perp^2 L\left(\mathbf{v}-\mathbf{w}\right) = -\frac{g_s^4}{4\pi}\ln\frac{1}{(\mathbf{v}-\mathbf{w})^2\Lambda_{\mathrm{QCD}}^2}. \tag{8.49}$$

Using Eqs. (F.8) (with $C_F \to N_c$, since we now work in the adjoint representation), (8.42) and (8.43), the intermediate result Eq. (8.48) can be written as:

$$
\begin{aligned}
&\mathrm{Tr}\left\langle \left(W_{ba}\partial^i\alpha_b t^a\right)(\vec{v})\left(W_{cd}\partial^i\alpha_c t^d\right)(\vec{w})\right\rangle_A \\
&= \frac{4C_F}{g_s^2}\delta\left(v^- - w^-\right)\frac{1}{(\mathbf{v}-\mathbf{w})^2}\frac{\partial}{\partial v^-}\left(1 - D_A\left(v^-, \mathbf{v}-\mathbf{w}\right)\right),
\end{aligned}
\tag{8.50}
$$

from which we finally obtain:

$$
\begin{aligned}
\mathcal{F}_{gg}^{(3)}(x, q_\perp) &= \frac{2S_\perp C_F}{\alpha_s \pi^2}\int \frac{\mathrm{d}^2\mathbf{r}}{(2\pi)^2}\frac{e^{-i\mathbf{q}_\perp \mathbf{r}}}{r^2}\left(1 - D_A\left(r^2\right)\right), \\
&= \frac{2S_\perp C_F}{\alpha_s \pi^2}\int \frac{\mathrm{d}^2\mathbf{r}}{(2\pi)^2}\left(\frac{e^{-i\mathbf{q}_\perp \mathbf{r}}}{r^2}1 - e^{-\frac{r^2 Q_{sg}^2(r^2)}{4}}\right),
\end{aligned}
\tag{8.51}
$$

where, again, we made use of the fact that the integrals over transverse coordinates are restricted to the transverse surface $S_\perp$ of the nucleus:

$$
S_\perp \equiv \int \mathrm{d}^2\mathbf{x}.
\tag{8.52}
$$

Although the result (8.51) for the Weizsäcker-Williams gluon distribution is purely classical, and holds only in the MV model, we can use it to illustrate many of the properties of the gluon density in the small-x regime, in particular the meaning of the saturation scale Q_s and Q_{sg}. For instance, in the dilute limit, defined as $q_\perp^2 \gg Q_{sg}^2$, the rapidly oscillating exponent will kill most of the integral, except at very small values of r: $r^2 \ll 1/q_\perp^2$. Therefore, the exponential can be expanded in $Q_{sg}^2/q_\perp^2$, yielding to next-to-leading order:

$$
\begin{aligned}
\mathcal{F}_{gg}^{(3)}(x, q_\perp) &\simeq \frac{2S_\perp C_F}{\alpha_s \pi^2}\int \frac{\mathrm{d}^2\mathbf{r}}{(2\pi)^2}\frac{e^{-i\mathbf{q}_\perp \mathbf{r}}}{r^2}\left(\frac{r^2 Q_{sg}^2}{4} - \frac{1}{2}\frac{r^4 Q_{sg}^4}{16} + \mathcal{O}\left(r^6 Q_{sg}^6\right)\right), \\
&\simeq \frac{S_\perp C_F}{2\alpha_s \pi^3}\frac{Q_{sg}^2}{q_\perp^2}\left(1 + \frac{Q_{sg}^2}{q_\perp^2}\left[\ln\frac{q_\perp^2}{\Lambda_{\mathrm{QCD}}^2} + 2\gamma_E - 2\right]\right),
\end{aligned}
\tag{8.53}
$$

where we used the so-called harmonic approximation:

$$
D_A(\mathbf{r}) \simeq e^{-\frac{r^2}{4}Q_{sg}^2},
\tag{8.54}
$$

in which the logarithmic dependence of the saturation scale on the dipole size r^2 is neglected. The result (8.53) becomes more clear once we insert the expression for the saturation scale, Eq. (8.43) (again, without the logarithm), and keep only the leading term:

$$
\mathcal{F}_{gg}^{(3)}(x, q_\perp) \simeq AN_c \times \frac{\alpha_s C_F}{\pi^2 q_\perp^2} = AN_c \times x\frac{\mathrm{d}P_{\mathrm{Brems}}}{\mathrm{d}x\mathrm{d}^2 q_\perp}.
\tag{8.55}
$$

In the dilute limit, we thus recover a simple BFKL-like picture of the gluon density, in which each of the AN_c valence quarks generate the Bremsstrahlung spectrum. It is easy to check that the above

expression is equivalent to the dilute approximation for the dipole-hadron amplitude $\sigma_{\text{dip}} \sim r^2$, Eq. (6.23).

In the opposite limit of small transverse momenta: $q_\perp^2 \ll Q_{sg}^2 \left(\mathbf{r}^2 \right)$, the integral is dominated by large values of r: $r^2 \gg 1/q_\perp^2$, and the exponential can simply be neglected, yielding:

$$
\begin{aligned}
\mathcal{F}_{gg}^{(3)} \left(x, q_\perp \right) &\simeq \frac{2 S_\perp C_F}{\alpha_s \pi^2} \int \frac{\mathrm{d}^2 \mathbf{r}}{(2\pi)^2} \frac{e^{-i \mathbf{q}_\perp \mathbf{r}}}{\mathbf{r}^2} = \frac{S_\perp C_F}{\alpha_s \pi^3} \int_{2/Q_{sg}} \mathrm{d}r \frac{J_0 \left(r q_\perp \right)}{r}, \\
&\simeq \frac{S_\perp C_F}{2 \alpha_s \pi^3} \ln \frac{Q_{sg}^2}{q_\perp^2}.
\end{aligned}
\tag{8.56}
$$

Comparing Eqs. (8.53) and (8.56), which hold in the dilute and the saturation regime, respectively, we see that in the dilute regime $q_\perp^2 \gg Q_{sg}^2$ the gluon spectrum rapidly grows towards smaller transverse momenta, like $Q_{sg}^2/q_\perp^2$. However, around transverse momenta of the order of the saturation scale Q_{sg}^2, the behavior of the spectrum changes, and the growth is damped to a much slower logarithmic growth $\sim \ln Q_{sg}^2/q_\perp^2$. The gluon spectrum thus saturates due to the rising importance of nonlinear effects. In addition, Eq. (8.56) manifests an example of geometric scaling, which is the property that in the saturation regime, x and $q_\perp^2$ only appear in the combination $Q_s^2 \left(x \right)/q_\perp^2$: a consequence of the fact that Q_s^2 is the only meaningful scale in this region of phase space. This is in contrast to the dilute case Eq. (8.53), in which the soft scale Λ_{QCD} appears, acting as an infrared cutoff for the gluon radiation.

9 Evolution of the CGC

In the previous section, we described the classical McLerran-Venugopalan model for a large nucleus, and argued that it is valid for wee gluons with Bjorken-x in the range $x_{\text{wee}} \sim 10^{-2} - 10^{-1}$. These kinematical limits were obtained by requiring, on the one hand, that $x_{\text{wee}} \ll x_{\text{val}} \sim 1$, such that the valence quarks appear to be frozen with respect to the time scale $x^+ \simeq 2 x_{\text{wee}} P^+/p_\perp^2$ of the wee partons. On the other hand, we wanted the radiative effects to be small enough for the wee gluons to be adequately described by classical fields, hence:

$$
\int_{x_0}^{x_{\text{val}}} \mathrm{d} P_{\text{Brems}} = \frac{\alpha_s N_c}{\pi} \ln \frac{x_{\text{val}}}{x_0} \ll 1,
\tag{9.1}
$$

resulting in a lower limit $x_0 \simeq e^{-1/\alpha_s}$ for the wee partons. From the above formula it is clear that, if we want to apply our theory to smaller values of x, lowering the limit x_0, the upper limit of the phase space for the wee partons has to go down as well. If we denote this limit with x', we have that:

$$
x_{\text{val}} \sim 1, \quad x_0 \ll x_{\text{wee}} \ll x_{\text{val}} \overset{x_0 \, \text{smaller}}{\longrightarrow} x' \ll x_{\text{val}} \ll 1, \quad x_0 \ll x_{\text{wee}} \ll x',
\tag{9.2}
$$

hence what we mean with valence or wee partons changes depending on the choice of x': with wee partons we now refer to partons that live in a softer region of phase space, down to x_0, while our definition of valence partons is expanded to include lower-energy partons as well. For our classical description, in which valence partons are treated as sources which generate the wee gluons,

to hold, these 'new' valence partons have to be promoted to color sources as well. This can be done integrating the degrees of freedom in the strip $x' \ll x_{\mathrm{val}}$ out, and including them in the renormalization of the distribution of the sources $\mathcal{W}_{x'}[\rho]$, which becomes now dependent on the scale x'.

In order to describe this renormalization process more precisely, let us revisit the mechanism we mentioned above, but this time we will be a bit more general. If P^+ is the total longitudinal momentum of the hadron we want to describe, one can distinguish between the 'hard' partons with momenta $k^+ > \Lambda^+$, and the 'soft' partons with momenta $k^+ < \Lambda^+$, where we introduced a certain momentum scale $\Lambda^+ \equiv xP^+$. The hard and the soft partons (which are in this context gluons: quarks only play a role of significance as the sources in the MV model) are the generalizations of what we called the valence and the wee partons in the MV model. For each choice of the scale Λ^+, we have an effective classical theory similar to the MV model, in which the hard gluons are described by static color charges, which generate the soft gluons through the Yang-Mills equations. Given this classical theory at a certain scale Λ^+, we can evolve to a smaller scale Λ'^+ by integrating the so-called 'semi-fast' modes in the strip $\Lambda^+ \gg k^+ \gg \Lambda'^+$ out and including them in the new sources $\rho' = \rho + \delta\rho$. The result of this procedure is a renormalization group equation for the distribution function $\mathcal{W}_x[\rho]$.

Since the new color sources are generated through radiation, the evolution of $\mathcal{W}_x[\rho]$ is quantum mechanical. As a consequence, whereas the two-point function for the classical theory at a scale Λ^+ is given by a classical, statistical average:

$$\langle \rho(\vec{x})\, \rho(\vec{y}) \rangle_{\Lambda^+} = \int \mathcal{D}[\rho]\, \mathcal{W}_{\Lambda^+}[\rho]\, \rho(\vec{x})\, \rho(\vec{y}), \tag{9.3}$$

just like in the MV model, this is not the case anymore if we want to evaluate the correlator at a lower scale Λ'^+. Indeed, in order to integrate them out, the semi-fast gluons in the region $\Lambda^+ \gg k^+ \gg \Lambda'^+$ have to be made quantum mechanical again, and the two-point function of the new sources $\rho' = \rho + \delta\rho$ becomes:

$$\langle \rho'(\vec{x})\, \rho'(\vec{y}) \rangle_{\Lambda'^+} = \int \mathcal{D}[\rho]\, \mathcal{W}_{\Lambda^+}[\rho]\, \frac{\int_{\Lambda'^+}^{\Lambda^+} \mathcal{D}[a]\, \rho'(\vec{x})\, \rho'(\vec{y})\, e^{iS[A,\rho]}}{\int_{\Lambda'^+}^{\Lambda^+} \mathcal{D}[a]\, e^{iS[A,\rho]}}. \tag{9.4}$$

In the above formula, we used the following expansion of the gluon field:

$$A^\mu = \mathcal{A}^\mu[\rho] + a^\mu + \delta A^\mu, \tag{9.5}$$

where $\mathcal{A}^\mu[\rho]$ is the classical background field generated through the Yang-Mills equations by the sources ρ, and a^μ is the field corresponding to the quantum fluctuations of the semi-fast modes. The soft ($k^+ \ll \Lambda'^+$) fields, which we denote by δA^μ, do not appear explicitly in the correlator (9.4), but are generated by the sources, as is the case in the MV model. Note that we work in the light-cone gauge, hence it is always understood that $A^+ = 0$. The action $S[A,\rho]$ encodes the dynamics of the gluon fields, in particular of the semi-fast modes a^μ, in the presence of the sources, and quantum correlations between these gluon fields (and by extension the 'new' sources $\rho' = \rho + \delta\rho$ in which the semi-fast modes will be absorbed) are calculated with the help of a path integral. In addition,

everything still needs to be statistically averaged over the 'old' sources ρ at the scale Λ^+. Note that, when $\Lambda'^+ \sim \Lambda^+$, the quantum effects are negligible, and the path integrals can be evaluated in the saddle point approximation: $S[A, \rho] \to S_{\text{classical}}[\mathcal{A}, \rho]$. The correlator of Eq. (9.4), which contains both a quantum mechanical path integration and a classical statistical average, is in this approximation reduced to the purely classical correlator Eq. (9.3).

Once the quantum mechanical evolution to the smaller scale Λ'^+ is carried out, we again have a classical theory in which the sources, distributed according to the renormalized weight function $\mathcal{W}_{\Lambda'^+}[\rho]$ and corresponding to hard gluons with $k^+ \gg \Lambda'^+$, generate classical soft gluon fields with $k^+ \ll \Lambda'^+$. The relevant two-point function is then:

$$\langle \rho'(\vec{x}) \rho'(\vec{y}) \rangle_{\Lambda'^+} = \int \mathcal{D}[\rho'] \, \mathcal{W}_{\Lambda'^+}[\rho'] \, \rho'(\vec{x}) \rho'(\vec{y}). \tag{9.6}$$

Matching this correlator with Eq. (9.4), we will be able to deduce the evolution equation for the distribution function $\mathcal{W}_{\Lambda^+}[\rho]$.

To proceed, let us have a closer look at the action $S[A, \rho]$. It is given by:

$$S[A, \rho] = -\frac{1}{4} \int \mathrm{d}^4 x \, F^a_{\mu\nu} F^{\mu\nu}_a + \frac{i}{g_s N_c} \int \mathrm{d}^3 x \, \mathrm{Tr}\left(\rho(\vec{x}) W_T(\vec{y})\right), \tag{9.7}$$

where $W_T(\vec{x})$ is a temporal Wilson line, running along the time direction x^+:

$$W_T(\vec{x}) = \mathrm{T} \exp\left(ig_s \int \mathrm{d}x^+ A^-\left(x^+, \vec{x}\right)\right), \tag{9.8}$$

with T the time-ordering operator. Applying the Euler-Lagrange equations $\partial_\mu \delta S / \delta \partial_\mu A^\nu = \delta S / \delta A^\nu$, one recovers the Yang-Mills equations:

$$[D_\nu, F^{\nu\mu}](x) = J^\mu, \tag{9.9}$$

with the current:

$$J^\mu \equiv \delta^{\mu+} W_T\left(x^+, \vec{x}\right) \rho(\vec{x}) W_T^\dagger\left(x^+, \vec{x}\right),$$
$$W_T\left(x^+, \vec{x}\right) \equiv \mathrm{T} \exp\left(ig_s \int^{x^+} \mathrm{d}z^+ A^-\left(z^+, \vec{x}\right)\right). \tag{9.10}$$

We mentioned already that, in the classical case, one can always find a solution with $A^- = 0$, for which one recovers the current in Eq. (8.10). In contrast to the MV model, however, the action $S[A, \rho]$ pertains to quantum gluons, which is why we need the gauge-invariant expression Eq. (9.7). We can expand the action to second order in the weak field a^μ, around the background $\mathcal{A}^\mu$, as follows:

$$S[A, \rho] \simeq S[\mathcal{A}, \rho] + \int \mathrm{d}^4 x \left.\frac{\delta S}{\delta A^\mu_a}\right|_{\mathcal{A}} a^\mu_a(x) + \frac{1}{2} \int \mathrm{d}^4 x \mathrm{d}^4 y \left.\frac{\delta^2 S}{\delta A^\mu_a \delta A^\nu_b}\right|_{\mathcal{A}} a^\mu_a(x) a^\nu_b(y). \tag{9.11}$$
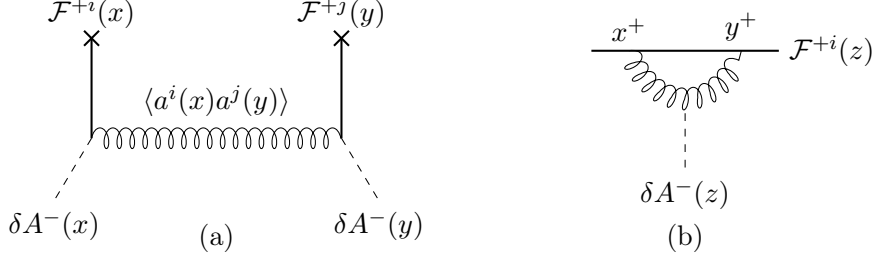
Figure 15: Contributions to the charge-charge correlator χ_{bc}^{ij}, (a), and to the induced color charge density σ_a, (b).

From this expression, one obtains the following propagator for the semi-fast gluon fields in the presence of the background field $\mathcal{A}^\mu$ and the sources ρ:

$$\langle a_a^\mu (x) \, a_b^\nu (y) \rangle_\rho = \frac{1}{2} \left. \frac{\delta^2 S}{\delta A_a^\mu \delta A_b^\nu} \right|_\mathcal{A}^{-1}. \tag{9.12}$$

Finally, we need to calculate the new contributions $\delta\rho$ to the sources, due to the semi-fast gluons a^μ. These sources couple linearly, as $\delta\rho_a \delta A_a^-$, to the soft gluon fields δA_a^-, hence, from the expansion (9.5), one finds:

$$\delta\rho_a (x) = \left. \frac{\delta S}{\delta A_a^- (x)} \right|_{\mathcal{A}+a}. \tag{9.13}$$

We thus have an effective quantum field theory, describing the dynamics of semi-fast gluon fields a^μ in the presence of a background $\mathcal{A}^\mu$. Explicit expressions for the propagator (9.12) and the effective sources (9.13) can be found in Ref. [92], for example.

Let us simply state the results of the analysis of the effective theory (see e.g. Ref. [92]). It turns out that, to logarithmic accuracy, only the one-point function and the two-point function play a role of importance:

$$\langle \delta\rho_a (\vec{x}) \rangle_\rho \propto \sigma_a (\vec{x}), \quad \langle \delta\rho_a (\vec{x}) \, \delta\rho_b (\vec{y}) \rangle_\rho \propto \chi_{ab} (\vec{x}, \vec{y}). \tag{9.14}$$

The two-point function $\langle \delta\rho_a (\vec{x}) \, \delta\rho_b (\vec{y}) \rangle_\rho$ is known as the induced charge-charge correlator, and describes the 'real' emission of semi-fast gluons by the color charges (see Fig. 15, a). The one-point function $\langle \delta\rho_a (\vec{x}) \rangle_\rho$ is the color charge density induced by the semi-fast fields, and provides virtual corrections to the gluon cascades in the semi-fast region. These virtual corrections can be both one-loop corrections to the emission vertices (see Fig. 15, b) and self-energy corrections. Both σ_a and χ_{ab} and nonlinear in ρ, and thus contain diagrams such as gluon mergings, as we expect in the saturation regime. Furthermore, they are x^+-independent. We will give their explicit expressions later.

First, we should scrutinize the longitudinal structure of our theory, which is an important aspect which we previously glossed over. Whereas in the MV model the valence partons were localized in a very sharp peak around $x^- = 0$, the longitudinal extent of the sources becomes larger for each step

in the evolution. Indeed, each strip of semi-fast gluons with $\Lambda'^+ = b\Lambda^+ \ll k^+ \ll \Lambda^+$, included in the renormalized sources $\rho' = \rho + \delta\rho$, is delocalized over a region $1/\Lambda^+ \lesssim x^- \lesssim 1/\Lambda'^+$, which becomes bigger as the momentum scales become smaller. When integrating these semi-fast gluons out, one has to keep track of their multiple scatterings with the background field $\mathcal{A}^\mu$, which are encoded in Wilson lines along the x^--axis. Due to the color structure of QCD, these scatterings are non-commutative, and hence the longitudinal structure of ρ cannot simply be neglected. In particular, when calculating the induced color charge density for a given configuration of the background sources ρ, the result turns out to be:

$$\langle \delta\rho_a \left(x^-, \mathbf{x} \right) \rangle_\rho = F_\Lambda \left(x^- \right) \sigma_a \left(\mathbf{x} \right), \tag{9.15}$$

with

$$F_\Lambda \left(x^- \right) = \theta \left(x^- \right) \frac{e^{-i\Lambda'^+ x^-} - e^{-i\Lambda^+ x^-}}{x^-}, \quad \int \mathrm{d}x^- F_\Lambda \left(x^- \right) = \ln \frac{\Lambda^+}{\Lambda'^+} = \ln \frac{1}{b} \equiv \mathrm{d}Y. \tag{9.16}$$

The above equations illustrate how, integrating the semi-fast modes out in layers of $\Lambda^+ \gg k^+ \gg b\Lambda^+$, layers of an extent $\mathrm{d}Y \equiv \ln 1/b$ along the x^--axis are added. The natural way to describe the evolution is therefore in discrete rapidity steps $\mathrm{d}\tau$ of the order $1/\alpha_s$, since due to the Bremsstrahlung law:

$$\int_{b\Lambda'^+}^{\Lambda^+} \mathrm{d}P_{\text{Brems}} = \alpha_s \int_{b\Lambda'^+}^{\Lambda^+} \frac{\mathrm{d}k^+}{k^+} = \alpha_s \mathrm{d}Y, \tag{9.17}$$

resummation becomes necessary when $P \sim 1$. Defining the evolution 'time' $Y \equiv \ln P^+/\Lambda^+$, we can write

$$\delta\rho_Y^a \left(\mathbf{x} \right) \mathrm{d}Y \equiv \int \mathrm{d}x^- \delta\rho^a \left(x^-, \mathbf{x} \right), \tag{9.18}$$

with $\delta\rho_Y^a \left(\mathbf{x} \right)$ the induced color charge by integrating out the interval $\Lambda^+ \gg k^+ \gg b\Lambda^+$ or equivalently the rapidity bin $Y \ll \ln 1/x \ll Y + \mathrm{d}Y$. To the desired logarithmic accuracy, the longitudinal structure of each layer $\mathrm{d}Y$ is thus not important, only the relative ordering of the different rapidity layers. We then have that:

$$\langle \delta\rho_Y^a \left(\mathbf{x} \right) \rangle_\rho \equiv \sigma_Y^a \left(\mathbf{x} \right). \tag{9.19}$$

Similarly, for the induced charge-charge correlator:

$$\langle \delta\rho_Y^a \left(\mathbf{x} \right) \delta\rho_Y^b \left(\mathbf{y} \right) \rangle_\rho = \frac{1}{\mathrm{d}Y} \chi_Y^{ab} \left(\mathbf{x}, \mathbf{y} \right), \quad \chi_Y^{ab} \left(\mathbf{x}, \mathbf{y} \right) \mathrm{d}Y \equiv \int \mathrm{d}x^- \mathrm{d}y^- \langle \delta\rho_Y^a \left(x^-, \mathbf{x} \right) \delta\rho_Y^b \left(y^-, \mathbf{y} \right) \rangle. \tag{9.20}$$

We are now finally ready to perform the matching procedure between Eqs. (9.4) and (9.6) that we alluded to earlier. Indeed, given a source $\rho_Y^a \left(\mathbf{x} \right)$, the induced source in the next rapidity bin $Y + \mathrm{d}Y$ is a variable distributed according to a Gaussian distribution $\mathcal{W}_{\mathrm{d}Y} [\delta\rho|\rho]$. Since we integrated the semi-fast modes out and incorporated them in the new distribution function, the correlator Eq. (9.4) becomes:

$$\langle \rho \left(\mathbf{x} \right) \rho \left(\mathbf{y} \right) \rangle_{Y + \mathrm{d}Y} = \int \mathcal{D} [\rho] \, \mathcal{W}_Y [\rho] \int \mathcal{D} [\delta\rho] \, \mathcal{W}_{\mathrm{d}Y} [\delta\rho|\rho] \left(\rho + \delta\rho \right) \left(\mathbf{x} \right) \left(\rho + \delta\rho \right) \left(\mathbf{y} \right), \tag{9.21}$$

which has to be equal to the two-point function of the classical theory at rapidity $Y + \mathrm{d}Y$ (cf.. Eq. (9.6)):

$$\langle \rho\left(\mathbf{x}\right)\rho\left(\mathbf{y}\right)\rangle_{Y+\mathrm{d}Y} = \int \mathcal{D}\left[\rho'\right]\mathcal{W}_{Y+\mathrm{d}Y}\left[\rho'\right]\rho'\left(\mathbf{x}\right)\rho'\left(\mathbf{y}\right). \tag{9.22}$$

One important subtlety is the fact that the support on the x^--axis for the sources in Eqs. (9.21) and (9.22) is not the same: in the first correlator, ρ is defined for $\ln\left(1/x\right) < Y$, while the renormalized ρ' in the second correlator involves the additional bin $\mathrm{d}Y$ and hence has support $\ln\left(1/x\right) < Y + \mathrm{d}Y$. In what follows, it is therefore understood that ρ is defined for arbitrary values of y, but that instead the weight functions $\mathcal{W}_Y\left[\rho\right]$ take care of the correct support:

$$\mathcal{W}_Y\left[\rho\right] = \mathcal{W}_Y\left[\rho\left(\ln\frac{1}{x} < Y\right)\right]\delta\left[\rho\left(\ln\frac{1}{x} > Y\right)\right]. \tag{9.23}$$

With this redefinition, we can make a change of variables $\rho \to \rho - \delta\rho$ in Eq. (9.21):

$$\langle \rho\left(\mathbf{x}\right)\rho\left(\mathbf{y}\right)\rangle_{Y+\mathrm{d}Y} = \int \mathcal{D}\left[\rho\right]\int \mathcal{D}\left[\delta\rho\right]\mathcal{W}_Y\left[\rho - \delta\rho\right]\mathcal{W}_{\mathrm{d}Y}\left[\delta\rho|\rho - \delta\rho\right]\rho\left(\mathbf{x}\right)\rho\left(\mathbf{y}\right), \tag{9.24}$$

and comparing with Eq. (9.22), we find that:

$$\mathcal{W}_{Y+\mathrm{d}Y}\left[\rho\right] = \int \mathcal{D}\left[\delta\rho\right]\mathcal{W}_Y\left[\rho - \delta\rho\right]\mathcal{W}_{\mathrm{d}Y}\left[\delta\rho|\rho - \delta\rho\right]. \tag{9.25}$$

Expanding the integrand:

$$\mathcal{W}_Y\left[\rho - \delta\rho\right]\mathcal{W}_{\mathrm{d}Y}\left[\delta\rho|\rho - \delta\rho\right] \simeq \left(1 - \mathrm{d}Y\int_{\mathbf{x}}\delta\rho_Y^a\left(\mathbf{x}\right)\frac{\delta}{\delta\rho_Y^a\left(\mathbf{x}\right)}\right.$$
$$\left. + \frac{\left(\mathrm{d}Y\right)^2}{2}\int_{\mathbf{xy}}\delta\rho_Y^a\left(\mathbf{x}\right)\delta\rho_Y^b\left(\mathbf{y}\right)\frac{\delta^2}{\delta\rho_Y^a\left(\mathbf{x}\right)\delta\rho_Y^b\left(\mathbf{y}\right)}\right)\mathcal{W}_Y\left[\rho\right]\mathcal{W}_{\mathrm{d}Y}\left[\delta\rho|\rho\right], \tag{9.26}$$

we have:

$$\mathcal{W}_{Y+\mathrm{d}Y}\left[\rho\right] - \mathcal{W}_Y\left[\rho\right] = -\mathrm{d}Y\int_{\mathbf{x}}\frac{\delta}{\delta\rho_Y^a\left(\mathbf{x}\right)}\mathcal{W}_Y\left[\rho\right]\sigma_Y^a\left(\mathbf{x}\right) + \frac{\mathrm{d}Y}{2}\int_{\mathbf{xy}}\frac{\delta^2}{\delta\rho_Y^a\left(\mathbf{x}\right)\delta\rho_Y^b\left(\mathbf{y}\right)}\mathcal{W}_Y\left[\rho\right]\chi_Y^{ab}\left(\mathbf{x},\mathbf{y}\right), \tag{9.27}$$

where we used that:

$$\int \mathcal{D}\left[\delta\rho\right]\mathcal{W}_{\mathrm{d}Y}\left[\delta\rho|\rho\right] = 1,$$

$$\int \mathcal{D}\left[\delta\rho\right]\delta\rho_Y^a\left(\mathbf{x}\right)\mathcal{W}_{\mathrm{d}Y}\left[\delta\rho|\rho\right] = \sigma_Y^a\left(\mathbf{x}\right), \tag{9.28}$$

$$\int \mathcal{D}\left[\delta\rho\right]\delta\rho_Y^a\left(\mathbf{x}\right)\delta\rho_Y^b\left(\mathbf{y}\right)\mathcal{W}_{\mathrm{d}Y}\left[\delta\rho|\rho\right] = \frac{1}{\mathrm{d}Y}\chi_Y^{ab}\left(\mathbf{x},\mathbf{y}\right).$$

Hence, we finally obtain a renormalization group equation for $\mathcal{W}_Y\left[\rho\right]$:

$$\frac{\partial \mathcal{W}_Y\left[\rho\right]}{\partial Y} = \frac{1}{2}\int_{\mathbf{xy}}\frac{\delta^2}{\delta\rho_Y^a\left(\mathbf{x}\right)\delta\rho_Y^b\left(\mathbf{y}\right)}\mathcal{W}_Y\left[\rho\right]\chi_Y^{ab}\left(\mathbf{x},\mathbf{y}\right) - \int_{\mathbf{x}}\frac{\delta}{\delta\rho_Y^a\left(\mathbf{x}\right)}\mathcal{W}_Y\left[\rho\right]\sigma_Y^a\left(\mathbf{x}\right). \tag{9.29}$$

It turns out to be simpler to express the above equation in terms of the solutions $\alpha_a \equiv \tilde{A}_a^+$ of the Yang-Mills equations in the covariant gauge, Eq. (8.16) (where Φ, σ and χ are now understood to be functionals of α):

$$\frac{\partial \mathcal{W}_Y[\alpha]}{\partial Y} = \frac{1}{2} \int_{\mathbf{xy}} \frac{\delta^2}{\delta \alpha_Y^a(\mathbf{x}) \, \delta \alpha_Y^b(\mathbf{y})} \mathcal{W}_Y[\alpha] \, \chi^{ab}(\mathbf{x}, \mathbf{y}) - \int_{\mathbf{x}} \frac{\delta}{\delta \alpha_Y^a(\mathbf{x})} \mathcal{W}_Y[\alpha] \, \sigma^a(\mathbf{x}). \tag{9.30}$$

The induced color charge $\sigma^a(\mathbf{x})$ and charge-charge correlator $\chi^{ab}(\mathbf{x}, \mathbf{y})$ (we can omit the index Y, since the information on the longitudinal support is carried by the charge distribution $\mathcal{W}_Y[\alpha]$) are, after explicit evaluation of all the diagrams in the effective theory, found to be (Refs. [89, 93]):

$$\sigma^a(\mathbf{x}) = i \frac{g_s}{2\pi} \int \frac{\mathrm{d}^2\mathbf{z}}{(2\pi)^2} \frac{1}{(\mathbf{x} - \mathbf{z})^2} \mathrm{Tr} \left(T^a W^\dagger(\mathbf{x}) W(\mathbf{z}) \right),$$

$$\chi^{ab}(\mathbf{x}, \mathbf{y}) = \frac{1}{\pi} \int \frac{\mathrm{d}^2\mathbf{z}}{(2\pi)^2} \mathcal{K}_{\mathbf{xyz}} \left(1 + W^\dagger(\mathbf{x}) W(\mathbf{y}) - W^\dagger(\mathbf{x}) W(\mathbf{z}) - W^\dagger(\mathbf{z}) W(\mathbf{y}) \right)^{ab}, \tag{9.31}$$

with the transverse kernel:

$$\mathcal{K}_{\mathbf{xyz}} \equiv \frac{(x - z)^i (y - z)^i}{(\mathbf{x} - \mathbf{z})^2 (\mathbf{y} - \mathbf{z})^2}, \tag{9.32}$$

and the Wilson lines $W(\mathbf{x})$:

$$W(\mathbf{x}) = \mathcal{P} e^{i g_s \int \mathrm{d}z^- \alpha_a(z^-, \mathbf{x}) T^a}. \tag{9.33}$$

Note that, due to the fact that the longitudinal support of the sources, and therefore of the fields α_y, is encoded in the weight function Eq. (9.23), the integration path of the Wilson line is effectively cut of at rapidity $\ln(1/x) = Y$:

$$W(\mathbf{x}) = \mathcal{P} e^{i g_s \int^Y \mathrm{d}x \, \alpha_x^a(\mathbf{x}) T^a}. \tag{9.34}$$

The renormalization group equation (9.30) is known as the JIMWLK evolution equation, named after its authors Jalilian-Marian, Iancu, McLerran, Weigert, Leonidov and Kovner (see Refs. [89, 92–98]).

10 Properties of the JIMWLK equation

The properties presented in this section are not commonly found in the literature, I mainly relied on Refs. [5, 99].

The JIMWLK equation, Eq. (9.30), can be written in a more convenient Hamiltonian form, using the following relation between χ^{ab} and σ^a:

$$\frac{1}{2} \int_{\mathbf{y}} \frac{\delta \chi^{ab}(\mathbf{x}, \mathbf{y})}{\delta \alpha_Y^b(\mathbf{y})} = \sigma^a(\mathbf{x}). \tag{10.1}$$

To prove the above formula, note that we have:

$$\frac{\delta W^\dagger (\mathbf{x})}{\delta \alpha_Y^a (\mathbf{y})} = \frac{\delta}{\delta \alpha_Y^a (\mathbf{y})} \bar{\mathcal{P}} e^{-ig_s \int^Y \mathrm{d}x\, \alpha_x^a (\mathbf{x}) T^a} = -ig_s \delta_{\mathbf{xy}}^{(2)} T^a W^\dagger (\mathbf{x}),$$

$$\frac{\delta W (\mathbf{x})}{\delta \alpha_Y^a (\mathbf{y})} = ig_s \delta_{\mathbf{xy}}^{(2)} W (\mathbf{x}) T^a. \tag{10.2}$$

Using these properties, we find that

$$\frac{\delta W_{ac}^\dagger (\mathbf{x}) W_{cb} (\mathbf{y})}{\delta \alpha_Y^b (\mathbf{y})} = -ig_s \delta_{\mathbf{xy}}^{(2)} T_{ad}^b W_{dc}^\dagger (\mathbf{x}) W_{cb} (\mathbf{y}) + W_{ac}^\dagger (\mathbf{x}) ig_s \delta_{\mathbf{yy}}^{(2)} W_{cd} (\mathbf{x}) T_{db}^a,$$

$$= -ig_s \delta_{\mathbf{xy}}^{(2)} T_{ad}^b \delta_{db} + ig_s \delta_{\mathbf{yy}}^{(2)} \delta_{ad} T_{db}^a = 0, \tag{10.3}$$

where we made use of the property that $W_{ac}^\dagger (\mathbf{x}) W_{cb} (\mathbf{x}) = \delta_{ab}$, and where both terms vanish due to the antisymmetry of the color matrices. Similarly, one obtains:

$$\frac{\delta W_{ac}^\dagger (\mathbf{x}) W_{cb} (\mathbf{z})}{\delta \alpha_Y^b (\mathbf{y})} = -ig_s \delta_{\mathbf{xy}}^{(2)} T_{ad}^b W_{dc}^\dagger (\mathbf{x}) W_{cb} (\mathbf{z}) + W_{ac}^\dagger (\mathbf{x}) ig_s \delta_{\mathbf{yz}}^{(2)} W_{cd} (\mathbf{z}) T_{db}^b,$$

$$= ig_s \delta_{\mathbf{xy}}^{(2)} T_{bd}^a W_{dc}^\dagger (\mathbf{x}) W_{cb} (\mathbf{z}) = ig_s \delta_{\mathbf{xy}}^{(2)} \mathrm{Tr} \left(T^a W^\dagger (\mathbf{x}) W (\mathbf{z}) \right). \tag{10.4}$$

Therefore, we find:

$$\frac{1}{2} \int_{\mathbf{y}} \frac{\delta \chi^{ab} (\mathbf{x}, \mathbf{y})}{\delta \alpha_Y^b (\mathbf{y})} = \frac{ig_s}{2\pi} \int \mathrm{d}^2 \mathbf{y} \int \frac{\mathrm{d}^2 \mathbf{z}}{(2\pi)^2} \mathcal{K}_{\mathbf{xyz}} \delta_{\mathbf{xy}}^{(2)} \mathrm{Tr} \left(T^a W^\dagger (\mathbf{x}) W (\mathbf{z}) \right) = \sigma^a (\mathbf{x}), \tag{10.5}$$

proving Eq. (10.1). Plugging this relation into the JIMWLK equation, Eq.(9.30), yields:

$$\frac{\partial \mathcal{W}_Y [\alpha]}{\partial Y} = -H_{\mathrm{JIMWLK}} \mathcal{W}_Y [\alpha],$$

$$H_{\mathrm{JIMWLK}} \equiv -\frac{1}{2} \int_{\mathbf{xy}} \frac{\delta}{\delta \alpha_Y^a (\mathbf{x})} \chi^{ab} (\mathbf{x}, \mathbf{y}) \frac{\delta}{\delta \alpha_Y^b (\mathbf{y})}, \tag{10.6}$$

where we defined the JIMWLK Hamiltonian H_{JIMWLK}.

We can apply the JIMWLK equation Eq. (10.6) for the weight function $\Phi_Y [\alpha]$, to obtain an evolution equation for a generic observable $\mathcal{O}$. Indeed, at every value of rapidity Y, the CGC provides a classical theory, in which the expectation value for a certain observable can be obtained as follows:

$$\langle \mathcal{O} \rangle_Y = \int \mathcal{D} [\alpha] \mathcal{W}_Y [\alpha] \mathcal{O} [\alpha]. \tag{10.7}$$

In the above formula, the rapidity dependence is completely encoded in the weight function, and can therefore easily be turned into an evolution equation for $\mathcal{O}$ by taking the derivative with respect

to Y:

$$\frac{\partial}{\partial Y}\langle\mathcal{O}\rangle_Y = \int \mathcal{D}\left[\alpha\right]\frac{\partial \mathcal{W}_Y\left[\alpha\right]}{\partial Y}\mathcal{O}\left[\alpha\right],$$

$$= \int \mathcal{D}\left[\alpha\right]\frac{1}{2}\int_{\mathbf{xy}}\frac{\delta}{\delta\alpha_Y^a\left(\mathbf{x}\right)}\left(\chi^{ab}\left(\mathbf{x},\mathbf{y}\right)\frac{\delta}{\delta\alpha_Y^b\left(\mathbf{y}\right)}\mathcal{W}_Y\left[\alpha\right]\right)\mathcal{O}\left[\alpha\right],$$

$$= -\int \mathcal{D}\left[\alpha\right]\frac{1}{2}\int_{\mathbf{xy}}\chi^{ab}\left(\mathbf{x},\mathbf{y}\right)\left(\frac{\delta}{\delta\alpha_Y^b\left(\mathbf{y}\right)}\mathcal{W}_Y\left[\alpha\right]\right)\frac{\delta}{\delta\alpha_Y^a\left(\mathbf{x}\right)}\mathcal{O}\left[\alpha\right], \qquad (10.8)$$

$$= \int \mathcal{D}\left[\alpha\right]\frac{1}{2}\int_{\mathbf{xy}}\mathcal{W}_Y\left[\alpha\right]\frac{\delta}{\delta\alpha_Y^b\left(\mathbf{y}\right)}\chi^{ab}\left(\mathbf{x},\mathbf{y}\right)\frac{\delta}{\delta\alpha_Y^a\left(\mathbf{x}\right)}\mathcal{O}\left[\alpha\right],$$

$$= -\langle H_{\mathrm{JIMWLK}}\mathcal{O}\rangle_Y.$$

In the last equality, we made use of the fact that:

$$\chi^{ab}\left(\mathbf{x},\mathbf{y}\right) = \chi^{ba}\left(\mathbf{y},\mathbf{x}\right), \qquad (10.9)$$

which follows immediately from expression (9.31) for χ^{ab}:

$$\chi^{ab}\left(\mathbf{x},\mathbf{y}\right) = \frac{1}{\pi}\int\frac{\mathrm{d}^2\mathbf{z}}{\left(2\pi\right)^2}\mathcal{K}_{\mathbf{xyz}}\left(1 + W^\dagger\left(\mathbf{y}\right)W\left(\mathbf{x}\right) - W^\dagger\left(\mathbf{z}\right)W\left(\mathbf{x}\right) - W^\dagger\left(\mathbf{y}\right)W\left(\mathbf{z}\right)\right)^{ab},$$

$$= \frac{1}{\pi}\int\frac{\mathrm{d}^2\mathbf{z}}{\left(2\pi\right)^2}\mathcal{K}_{\mathbf{xyz}}\left(\left(1 + W^\dagger\left(\mathbf{y}\right)W\left(\mathbf{x}\right) - W^\dagger\left(\mathbf{z}\right)W\left(\mathbf{x}\right) - W^\dagger\left(\mathbf{y}\right)W\left(\mathbf{z}\right)\right)^\dagger\right)^{ba},$$

$$= \frac{1}{\pi}\int\frac{\mathrm{d}^2\mathbf{z}}{\left(2\pi\right)^2}\mathcal{K}_{\mathbf{xyz}}\left(1 + W^\dagger\left(\mathbf{x}\right)W\left(\mathbf{y}\right) - W^\dagger\left(\mathbf{x}\right)W\left(\mathbf{z}\right) - W^\dagger\left(\mathbf{z}\right)W\left(\mathbf{y}\right)\right)^{ba}, \qquad (10.10)$$

$$= \chi^{ba}\left(\mathbf{y},\mathbf{x}\right),$$

where, in the second equality, we made use of the fact that Wilson lines in the adjoint representation are real. The property (10.9) is even more apparent if one casts $\chi^{ab}\left(\mathbf{x},\mathbf{y}\right)$ in the following form:

$$\chi^{ab}\left(\mathbf{x},\mathbf{y}\right) = \frac{1}{\pi}\int\frac{\mathrm{d}^2\mathbf{z}}{\left(2\pi\right)^2}\mathcal{K}_{\mathbf{xyz}}\left(1 - W^\dagger\left(\mathbf{x}\right)W\left(\mathbf{z}\right)\right)^{ac}\left(1 - W^\dagger\left(\mathbf{z}\right)W\left(\mathbf{y}\right)\right)^{cb}. \qquad (10.11)$$

Before moving to applications of the JIMWLK equation, we should scrutinize the kernel $\mathcal{K}_{\mathbf{xyz}}$, Eq. (9.32), which has two poles at $\mathbf{z} = \mathbf{x}$ and $\mathbf{z} = \mathbf{y}$ which could give rise to short-distance singularities when integrating over $\mathbf{z}$. However, as one can see from the above expression for $\chi_{\mathbf{xy}}^{ab}$, the residues of these poles are zero. The JIMWLK Hamiltonian is thus free of ultraviolet divergences, but it is not immediately clear that this is also the case for soft divergences. Indeed, in the limit $z \to \infty$ the kernel behaves as $\mathcal{K}_{\mathbf{xyz}} \to 1/z^2$, which after integration could lead to a logarithmic singularity. It turns out that these soft divergences do in fact cancel, but only in the case of gauge-invariant observables $\mathcal{O}$, as we will now demonstrate. First, let us illustrate this cancellation in an example, considering the dilute limit of the JIMWLK equation, which will turn out to be the BFKL equation, which is explicitly infrared safe. To compute $\chi^{ab}\left(\mathbf{x},\mathbf{y}\right)$ in the dilute regime, starting from Eq. (10.11), it is sufficient to expand the Wilson lines to leading order (this is a simplification due to the factorized

form of Eq. (10.11). If we were to start from Eq. (9.31), we should expand quadratically like usual, see e.g. the discussion around Eq. (6.16)) :

$$W\left(\mathbf{x}\right) \simeq 1 + ig_s\alpha_{\mathbf{x}}^a T^a, \tag{10.12}$$

where we introduced the short-hand notation:

$$\alpha_{\mathbf{x}}^a \equiv \int \mathrm{d}z^- \alpha_a\left(z^-, \mathbf{x}\right). \tag{10.13}$$

The induced charge-charge correlator then becomes:

$$\chi^{ab}\left(\mathbf{x}, \mathbf{y}\right) \simeq -\frac{g_s^2}{\pi} \int \frac{\mathrm{d}^2\mathbf{z}}{(2\pi)^2} \mathcal{K}_{\mathbf{xyz}} \left(\alpha_{\mathbf{x}}^d - \alpha_{\mathbf{z}}^d\right)\left(\alpha_{\mathbf{z}}^e - \alpha_{\mathbf{y}}^e\right) T_{ac}^d T_{cb}^e, \tag{10.14}$$

from which we find the following Hamiltonian

$$H_{BFKL} \equiv -\frac{\alpha_s}{2\pi^2} \int_{\mathbf{xyz}} \mathcal{K}_{\mathbf{xyz}} T_{ac}^d T_{cb}^e \left(\alpha_{\mathbf{x}}^d - \alpha_{\mathbf{z}}^d\right) \frac{\delta}{\delta\alpha_{\mathbf{x}}^a} \left(\alpha_{\mathbf{z}}^e - \alpha_{\mathbf{y}}^e\right) \frac{\delta}{\delta\alpha_{\mathbf{y}}^b}. \tag{10.15}$$

It is very important to note that, writing (10.13) and making the changes $\delta\alpha_Y^a\left(\mathbf{x}\right) \to \delta\alpha_{\mathbf{x}}^a$, we threw away the longitudinal structure about the theory, which we carefully constructed in the previous paragraph. This is tantamount to the statement that in the dilute regime, also called the BFKL approximation or the regime of $k_\perp$-factorization, multiple scattering can be neglected and a complete factorization holds between the longitudinal and the transverse dynamics. To show that Eq. (10.15) is indeed the BFKL Hamiltonian, let us apply it to a gauge invariant quantity, say the elastic scattering amplitude of a color dipole off the CGC, Eq. (5.6):

$$\sigma_{\mathrm{dip}}\left(x, \mathbf{r}\right) = 2\pi R_A^2 T\left(r\right), \tag{10.16}$$

with:

$$\langle T\left(\mathbf{x}, \mathbf{y}\right)\rangle_Y = 1 - D\left(\mathbf{x}, \mathbf{y}\right) = 1 - \frac{1}{N_c}\mathrm{Tr}\langle U\left(\mathbf{x}\right) U^\dagger\left(\mathbf{y}\right)\rangle_Y. \tag{10.17}$$

In the weak-field approximation, the scattering amplitude is given by:

$$\begin{aligned}
\langle T\left(\mathbf{x}, \mathbf{y}\right)\rangle_Y &\simeq \frac{g_s^2}{4N_c}\langle\left(\alpha_{\mathbf{x}}^a - \alpha_{\mathbf{y}}^a\right)^2\rangle_Y, \\
&= \frac{g_s^2}{4N_c}\langle\alpha_{\mathbf{x}}^a\alpha_{\mathbf{x}}^a + \alpha_{\mathbf{y}}^a\alpha_{\mathbf{y}}^a - 2\alpha_{\mathbf{x}}^a\alpha_{\mathbf{y}}^a\rangle_Y,
\end{aligned} \tag{10.18}$$

Applying the BFKL Hamiltonian, Eq. (10.15), on the substructure $\langle\alpha_{\mathbf{x}}^a\alpha_{\mathbf{y}}^a\rangle_Y$ yields (we frequently

made use of Eq. (A.15)):

$$
\begin{aligned}
\frac{\partial}{\partial Y}\langle \alpha_\mathbf{x}^a \alpha_\mathbf{y}^a \rangle_Y &= -\langle H_{BFKL}\alpha_\mathbf{x}^a \alpha_\mathbf{y}^a \rangle_Y \\
&= -\frac{\alpha_s}{2\pi^2}\int_\mathbf{vwz}\mathcal{K}_\mathbf{vwz}T^d_{a'c}T^e_{cb}\Big\langle \Big(\alpha_\mathbf{v}^d - \alpha_\mathbf{z}^d\Big)\frac{\delta}{\delta\alpha_\mathbf{v}^{a'}}\Big(\alpha_\mathbf{z}^e - \alpha_\mathbf{w}^e\Big)\frac{\delta}{\delta\alpha_\mathbf{w}^b}\alpha_\mathbf{x}^a\alpha_\mathbf{y}^a\Big\rangle_Y \\
&= -\frac{\alpha_s N_c}{2\pi^2}\int_\mathbf{z}\Big\langle \mathcal{K}_\mathbf{xxz}\left(\alpha_\mathbf{x}^a - \alpha_\mathbf{z}^a\right)\alpha_\mathbf{y}^a + \mathcal{K}_\mathbf{yyz}\left(\alpha_\mathbf{y}^a - \alpha_\mathbf{z}^a\right)\alpha_\mathbf{x}^a \\
&\quad + 2\mathcal{K}_\mathbf{xyz}\left(\alpha_\mathbf{z}^a - \alpha_\mathbf{x}^a\right)\left(\alpha_\mathbf{y}^a - \alpha_\mathbf{z}^a\right)\Big\rangle_Y \\
&= -\frac{\alpha_s N_c}{2\pi^2}\int_\mathbf{z}\Big\langle \mathcal{M}_\mathbf{xyz}\alpha_\mathbf{x}^a\alpha_\mathbf{y}^a - \mathcal{K}_\mathbf{xxz}\alpha_\mathbf{z}^a\alpha_\mathbf{y}^a \\
&\quad - \mathcal{K}_\mathbf{yyz}\alpha_\mathbf{x}^a\alpha_\mathbf{z}^a + 2\mathcal{K}_\mathbf{xyz}\left(\alpha_\mathbf{y}^a\alpha_\mathbf{z}^a - \alpha_\mathbf{z}^a\alpha_\mathbf{z}^a + \alpha_\mathbf{z}^a\alpha_\mathbf{x}^a\right)\Big\rangle_Y
\end{aligned}
\tag{10.19}
$$

In the first term of the last line in the above expression, the kernels combined in the familiar dipole kernel:

$$
\begin{aligned}
\mathcal{M}_\mathbf{xyz} &\equiv \frac{(\mathbf{x}-\mathbf{y})^2}{(\mathbf{x}-\mathbf{z})^2(\mathbf{y}-\mathbf{z})^2}, \\
&= \mathcal{K}_\mathbf{xxz} + \mathcal{K}_\mathbf{yyz} - 2\mathcal{K}_\mathbf{xyz}.
\end{aligned}
\tag{10.20}
$$

In the soft limit $z \to \infty$, this kernel behaves as $\mathcal{M}_\mathbf{xyz} \to 1/z^4$ and therefore goes to zero fast enough for the integral over z to converge. The other terms in Eq. (10.18) are still problematic, though. As we predicted, however, they cancel when looking at the evolution of the full gauge invariant object $T(\mathbf{x},\mathbf{y})$

$$
\begin{aligned}
\frac{\partial}{\partial\tau}\Big\langle \left(\alpha_\mathbf{x}^a - \alpha_\mathbf{y}^a\right)^2 \Big\rangle_Y &= -\frac{\alpha_s N_c}{2\pi^2}\int_\mathbf{z}\Big\langle 2\mathcal{M}_\mathbf{xyz}\left(\alpha_\mathbf{y}^a\alpha_\mathbf{z}^a - \alpha_\mathbf{z}^a\alpha_\mathbf{z}^a + \alpha_\mathbf{z}^a\alpha_\mathbf{x}^a - \alpha_\mathbf{x}^a\alpha_\mathbf{y}^a\right)\Big\rangle_Y, \\
&= \frac{\alpha_s N_c}{2\pi^2}\int_\mathbf{z}\Big\langle \mathcal{M}_\mathbf{xyz}\left(-\left(\alpha_\mathbf{x}^a - \alpha_\mathbf{y}^a\right)^2 + \left(\alpha_\mathbf{x}^a - \alpha_\mathbf{z}^a\right)^2 + \left(\alpha_\mathbf{y}^a - \alpha_\mathbf{z}^a\right)^2\right)\Big\rangle_Y,
\end{aligned}
\tag{10.21}
$$

yielding the familiar BFKL evolution equation for the dipole cross section (10.16) which is explicitly infrared finite:

$$
\frac{\partial}{\partial Y}T_Y(\mathbf{x}-\mathbf{y}) = \frac{\bar{\alpha}}{2\pi}\int_\mathbf{z}\mathcal{M}_\mathbf{xyz}\left(T_Y(\mathbf{x}-\mathbf{z}) + T_Y(\mathbf{y}-\mathbf{z}) - T_Y(\mathbf{x}-\mathbf{y})\right).
\tag{10.22}
$$

With the BFKL equation as an example, we showed that gauge invariance is essential if we want the evolution equation to be free of infrared divergences.

To extend this claim beyond the dilute limit, we should specify a bit what we mean with a gauge invariant operator in the context of the CGC. Since the CGC is formulated in the light-cone gauge, with the help of the classical field solutions in the covariant gauge, an operator is gauge invariant if it can be written as a function of Wilson loops in the covariant gauge, i.e.:

$$
\begin{aligned}
\mathcal{O}[\alpha] &= \mathrm{Tr}\left(U_\mathbf{x}^\dagger U_\mathbf{y} W_\mathbf{v}^\dagger W_\mathbf{w}...\right), \\
U(\mathbf{x}) &\equiv \mathcal{P}e^{ig\int dz^- \alpha_a\left(z^-,\mathbf{x}\right)t^a}, \\
W(\mathbf{x}) &\equiv \mathcal{P}e^{ig\int dz^- \alpha_a\left(z^-,\mathbf{x}\right)T^a},
\end{aligned}
\tag{10.23}
$$

where the classical gauge fields thus have the structure: $A_a^\mu(x) = \delta^{\mu+}\alpha_a(x)$. To quantify this requirement on a generic operator $\mathcal{O}[\alpha]$, one can make use of the observation that this specific structure of the gauge fields is preserved under residual gauge transformations $\Omega(x^-) = \exp(ig_s\omega^a(x^-)t^a)$:

$$\alpha_a(x^-, \mathbf{x}) \to \Omega(x^-)\left(\alpha_a(x^-, \mathbf{x}) + \frac{i}{g_s}\partial^+\right)\Omega^\dagger(x^-). \tag{10.24}$$

An operator $\mathcal{O}[\alpha]$ is therefore gauge invariant if it does not change under the above gauge transformation, which for a Wilson line amounts to:

$$U^\dagger(\mathbf{x}) \to \Omega(x^- = +\infty)U^\dagger(\mathbf{x})\Omega^\dagger(x^- = -\infty), \tag{10.25}$$

or

$$U^\dagger(\mathbf{x}) \to \Omega_L U^\dagger(\mathbf{x})\Omega_R^\dagger. \tag{10.26}$$

It is easy to show that these independent and global (since they take place beyond the longitudinal support of the nucleus) color rotations, are generated by the following operators:

$$\mathcal{G}_L \equiv \int \mathrm{d}^2\mathbf{x}\frac{\delta}{\delta\alpha_Y^a(\mathbf{x})}, \quad \mathcal{G}_R \equiv -\int \mathrm{d}^2\mathbf{x}W_\mathbf{x}^{ab}\frac{\delta}{\delta\alpha_Y^b(\mathbf{x})}. \tag{10.27}$$

As an example, let us show that an adjoint dipole is gauge invariant, according to the above criteria. Indeed, we have:

$$\begin{aligned}
\mathcal{G}_L D_A(\mathbf{x} - \mathbf{y}) &= \frac{1}{N_c^2 - 1}\int \mathrm{d}^2\mathbf{z}\frac{\delta}{\delta\alpha_Y^a(\mathbf{z})}\mathrm{Tr}\left\langle W(\mathbf{x})W^\dagger(\mathbf{y})\right\rangle_Y, \\
&= \frac{1}{N_c^2 - 1}\int \mathrm{d}^2\mathbf{z}\,\mathrm{Tr}\left\langle ig_s\delta_{\mathbf{xz}}W(\mathbf{x})T^aW^\dagger(\mathbf{y}) - ig_s\delta_{\mathbf{yz}}W(\mathbf{x})T^aW^\dagger(\mathbf{y})\right\rangle_Y, \\
&= 0,
\end{aligned} \tag{10.28}$$

and

$$\begin{aligned}
\mathcal{G}_R D_A(\mathbf{x} - \mathbf{y}) &= \frac{-1}{N_c^2 - 1}\int \mathrm{d}^2\mathbf{z}W_\mathbf{z}^{ab}\frac{\delta}{\delta\alpha_Y^b(\mathbf{z})}\mathrm{Tr}\left\langle W(\mathbf{x})W^\dagger(\mathbf{y})\right\rangle_Y, \\
&= \frac{-1}{N_c^2 - 1}\int \mathrm{d}^2\mathbf{z}\,\mathrm{Tr}\left\langle ig_s\delta_{\mathbf{xz}}W(\mathbf{x})W_\mathbf{z}^{ab}T^bW^\dagger(\mathbf{y}) - ig_s\delta_{\mathbf{yz}}W(\mathbf{x})W_\mathbf{z}^{ab}T^bW^\dagger(\mathbf{y})\right\rangle_Y, \\
&= \frac{-ig_s}{N_c^2 - 1}\int \mathrm{d}^2\mathbf{z}\,\mathrm{Tr}\left\langle \delta_{\mathbf{xz}}W(\mathbf{x})W^\dagger(\mathbf{z})T^aW(\mathbf{z})W^\dagger(\mathbf{y})\right. \\
&\quad \left. - \delta_{\mathbf{yz}}W(\mathbf{x})W^\dagger(\mathbf{z})T^aW(\mathbf{z})W^\dagger(\mathbf{y})\right\rangle_Y, \\
&= \frac{-ig_s}{N_c^2 - 1}\mathrm{Tr}\left\langle T^aW(\mathbf{x})W^\dagger(\mathbf{y}) - W(\mathbf{x})W^\dagger(\mathbf{y})T^a\right\rangle_Y = 0.
\end{aligned} \tag{10.29}$$

We can use this to rewrite the JIMWLK equation in a simpler dipole form, which is explicitly infrared safe. To do this, observe that the relation between the transverse kernel and the dipole

kernel, Eq. (10.20), can be inverted:

$$\mathcal{K}_{\mathbf{xyz}} = \frac{1}{2}\left(\frac{1}{(\mathbf{x}-\mathbf{z})^2} + \frac{1}{(\mathbf{y}-\mathbf{z})^2} - \frac{(\mathbf{x}-\mathbf{y})^2}{(\mathbf{x}-\mathbf{z})^2(\mathbf{y}-\mathbf{z})^2}\right). \tag{10.30}$$

Furthermore, one can show (see Ref. [99]) that for gauge invariant observables, the contributions of the first two terms in the above equation, which are potentially divergent, disappear. One thus obtains:

$$H_{\text{JIMWLK}} \equiv \frac{1}{16\pi^3}\int_{\mathbf{xyz}}\mathcal{M}_{\mathbf{xyz}}\left(1 + W_{\mathbf{x}}^\dagger W_{\mathbf{y}} - W_{\mathbf{x}}^\dagger W_{\mathbf{z}} - W_{\mathbf{z}}^\dagger W_{\mathbf{y}}\right)^{ab}\frac{\delta}{\delta\alpha_Y^a(\mathbf{x})}\frac{\delta}{\delta\alpha_Y^b(\mathbf{y})}. \tag{10.31}$$

Note that in the above dipole form, one can freely change around the functional derivative with respect to $\alpha_Y^a(\mathbf{x})$, since:

$$\frac{\delta}{\delta\alpha_Y^a(\mathbf{x})}\left(1 + W_{\mathbf{x}}^\dagger W_{\mathbf{y}} - W_{\mathbf{x}}^\dagger W_{\mathbf{z}} - W_{\mathbf{z}}^\dagger W_{\mathbf{y}}\right)^{ab}$$
$$= ig_s\left(\delta_{\mathbf{xy}}W_{\mathbf{x}}^\dagger W_{\mathbf{y}}T^a - \delta_{\mathbf{zx}}W_{\mathbf{x}}^\dagger W_{\mathbf{z}}T^a - \delta_{\mathbf{xy}}W_{\mathbf{z}}^\dagger W_{\mathbf{y}}T^a\right)^{ab}, \tag{10.32}$$
$$= -ig_s\delta_{\mathbf{xy}}\left(W_{\mathbf{z}}^\dagger W_{\mathbf{y}}T^a\right)^{ab},$$

which disappears in combination with the dipole kernel $\mathcal{M}_{\mathbf{xyz}}$.

To conclude this chapter, let us show that the JIMWLK equation is equal to the Balitsky hierarchy of equations, when one choses to evolve a dipole in the fundamental representation. We have that:

$$\frac{\delta}{\delta\alpha_Y^a(\mathbf{x})}\frac{\delta}{\delta\alpha_Y^b(\mathbf{y})}D(\mathbf{v}-\mathbf{w}) = \frac{1}{N_c}\frac{\delta}{\delta\alpha_Y^a(\mathbf{x})}\frac{\delta}{\delta\alpha_Y^b(\mathbf{y})}\text{Tr}\left\langle U^\dagger(\mathbf{v})U(\mathbf{w})\right\rangle_Y$$
$$= \frac{ig_s}{N_c}\frac{\delta}{\delta\alpha_Y^a(\mathbf{x})}\text{Tr}\left\langle -t^b\delta_{\mathbf{vy}}U^\dagger(\mathbf{v})U(\mathbf{w}) + \delta_{\mathbf{wy}}t^bU^\dagger(\mathbf{v})U(\mathbf{w})\right\rangle_{Y},$$
$$= \frac{(ig_s)^2}{N_c}\text{Tr}\left\langle\left(\delta_{\mathbf{vy}}\delta_{\mathbf{vx}}t^bt^a - \delta_{\mathbf{xw}}\delta_{\mathbf{vy}}t^at^b - \delta_{\mathbf{vx}}\delta_{\mathbf{wy}}t^bt^a + \delta_{\mathbf{wx}}\delta_{\mathbf{wy}}t^at^b\right)U^\dagger(\mathbf{v})U(\mathbf{w})\right\rangle_{Y}, \tag{10.33}$$
$$= -\frac{g_s^2}{N_c}(\delta_{\mathbf{vy}} - \delta_{\mathbf{wy}})\left(\delta_{\mathbf{vx}}\text{Tr}\left\langle t^bt^aU_{\mathbf{v}}^\dagger U_{\mathbf{w}}\right\rangle_Y - \delta_{\mathbf{xw}}\text{Tr}\left\langle t^at^bU_{\mathbf{v}}^\dagger U_{\mathbf{w}}\right\rangle_Y\right).$$

Together with the dipole kernel, the contributions $\delta_{\mathbf{vy}}\delta_{\mathbf{vx}}$ and $\delta_{\mathbf{wy}}\delta_{\mathbf{wx}}$ disappear. The other two terms both yield the same kernel $\mathcal{M}_{\mathbf{vwz}}$, and their combination with the Wilson line structure can be calculated as follows:

$$\left(1 + W_{\mathbf{x}}^\dagger W_{\mathbf{y}} - W_{\mathbf{x}}^\dagger W_{\mathbf{z}} - W_{\mathbf{z}}^\dagger W_{\mathbf{y}}\right)^{ab}\delta_{\mathbf{wy}}\delta_{\mathbf{vx}}\text{Tr}\left\langle t^bt^aU_{\mathbf{v}}^\dagger U_{\mathbf{w}}\right\rangle_Y$$
$$= \left(1 + W_{\mathbf{v}}^\dagger W_{\mathbf{w}} - W_{\mathbf{v}}^\dagger W_{\mathbf{z}} - W_{\mathbf{z}}^\dagger W_{\mathbf{w}}\right)^{ab}\text{Tr}\left\langle t^bt^aU_{\mathbf{v}}^\dagger U_{\mathbf{w}}\right\rangle_{Y},$$
$$= \left(\text{Tr}\left\langle t^at^aU_{\mathbf{v}}^\dagger U_{\mathbf{w}}\right\rangle_Y + \text{Tr}\left\langle W_{\mathbf{w}}^{cb}t^bW_{\mathbf{v}}^{ca}t^aU_{\mathbf{v}}^\dagger U_{\mathbf{w}}\right\rangle_Y\right. \tag{10.34}$$
$$\left. - \text{Tr}\left\langle W_{\mathbf{z}}^{cb}t^bW_{\mathbf{v}}^{ca}t^aU_{\mathbf{v}}^\dagger U_{\mathbf{w}}\right\rangle_Y - \text{Tr}\left\langle W_{\mathbf{w}}^{cb}t^bW_{\mathbf{z}}^{ca}t^aU_{\mathbf{v}}^\dagger U_{\mathbf{w}}\right\rangle_Y\right).$$

With the help of the Lie algebra identities Eqs. (A.10) and (A.13), we find that:

$$\begin{aligned}
\text{Tr}\left\langle t^a t^a U_{\mathbf{v}}^\dagger U_{\mathbf{w}}\right\rangle_Y &= \left\langle t_{ij}^a t_{jk}^a U_{\mathbf{v}}^{\dagger kl} U_{\mathbf{w}}^{li}\right\rangle_Y, \\
&= \frac{1}{2}\delta_{jj}\left\langle U_{\mathbf{v}}^{\dagger il} U_{\mathbf{w}}^{li}\right\rangle_Y - \frac{1}{2N_c}\left\langle U_{\mathbf{v}}^{\dagger jl} U_{\mathbf{w}}^{lj}\right\rangle_Y, \\
&= C_F \text{Tr}\left\langle U_{\mathbf{v}}^\dagger U_{\mathbf{w}}\right\rangle_Y,
\end{aligned} \tag{10.35}$$

and:

$$\begin{aligned}
\text{Tr}\left\langle W_{\mathbf{z}}^{cb} t^b W_{\mathbf{v}}^{ca} t^a U_{\mathbf{v}}^\dagger U_{\mathbf{w}}\right\rangle_Y &= \text{Tr}\left\langle U_{\mathbf{z}}^\dagger t^c U_{\mathbf{z}} U_{\mathbf{v}}^\dagger t^c U_{\mathbf{w}}\right\rangle_Y, \\
&= \frac{1}{2}\text{Tr}\left\langle U_{\mathbf{z}}^\dagger U_{\mathbf{w}}\right\rangle_Y \text{Tr}\left\langle U_{\mathbf{v}} U_{\mathbf{z}}^\dagger\right\rangle_Y - \frac{1}{2N_c}\text{Tr}\left\langle U_{\mathbf{v}}^\dagger U_{\mathbf{w}}\right\rangle_Y.
\end{aligned} \tag{10.36}$$

Similarly, one obtains:

$$\text{Tr}\left\langle W_{\mathbf{w}}^{cb} t^b W_{\mathbf{v}}^{ca} t^a U_{\mathbf{v}}^\dagger U_{\mathbf{w}}\right\rangle_Y = C_F \text{Tr}\left\langle U_{\mathbf{v}}^\dagger U_{\mathbf{w}}\right\rangle_Y, \tag{10.37}$$

and

$$\text{Tr}\left\langle W_{\mathbf{w}}^{cb} t^b W_{\mathbf{z}}^{ca} t^a U_{\mathbf{v}}^\dagger U_{\mathbf{w}}\right\rangle_Y = \frac{1}{2}\text{Tr}\left\langle U_{\mathbf{v}}^\dagger U_{\mathbf{z}}\right\rangle_Y \text{Tr}\left\langle U_{\mathbf{w}} U_{\mathbf{z}}^\dagger\right\rangle_Y - \frac{1}{2N_c}\text{Tr}\left\langle U_{\mathbf{v}}^\dagger U_{\mathbf{w}}\right\rangle_Y, \tag{10.38}$$

such that Eq. (10.34) becomes:

$$\begin{aligned}
&\left(1 + W_{\mathbf{x}}^\dagger W_{\mathbf{y}} - W_{\mathbf{x}}^\dagger W_{\mathbf{z}} - W_{\mathbf{z}}^\dagger W_{\mathbf{y}}\right)^{ab} \delta_{\mathbf{wy}} \delta_{\mathbf{vx}} \text{Tr}\left\langle t^b t^a U_{\mathbf{v}}^\dagger U_{\mathbf{w}}\right\rangle_Y \\
&= N_c^2 \left(D\left(\mathbf{v}-\mathbf{w}\right) - \frac{1}{N_c^2}\left\langle \text{Tr}\left(U_{\mathbf{z}}^\dagger U_{\mathbf{w}}\right) \text{Tr}\left(U_{\mathbf{v}} U_{\mathbf{z}}^\dagger\right)\right\rangle_Y\right).
\end{aligned} \tag{10.39}$$

The calculation for the $\delta_{\mathbf{xw}}\delta_{\mathbf{vy}}$ term in Eq. (10.33) is completely analogous, and yields exactly the same result as above. Since the dipole kernel $\mathcal{M}_{\mathbf{xyz}}$ is symmetric in $\mathbf{x}$ and $\mathbf{y}$, we end up with:

$$\frac{\partial}{\partial Y} D_Y\left(\mathbf{x}-\mathbf{y}\right) = -\frac{\bar{\alpha}}{2\pi^2}\mathcal{M}_{\mathbf{xyz}} \int_{\mathbf{z}} \left(D_Y\left(\mathbf{x}-\mathbf{y}\right) - \frac{1}{N_c^2}\left\langle \text{Tr}\left(U_{\mathbf{x}} U_{\mathbf{z}}^\dagger\right) \text{Tr}\left(U_{\mathbf{z}}^\dagger U_{\mathbf{y}}\right)\right\rangle_Y\right), \tag{10.40}$$

which we recognize as the first equation of the Balitsky hierarchy, Eq. (5.19). From the CGC theory for the saturated target, we thus reproduced the Balitsky-Kovchegov and BFKL equations which we derived in Sec. 5 from the point of view of the projectile.

Part III

Role of gluon polarization in forward heavy quark production in proton-nucleus collisions

11   Introduction

One of the most important concepts in QCD is factorization (see [77, 100, 101] for some standard references). Due to the fact that the running coupling $\alpha_s\left(Q^2\right)$ is large for small momentum transfers Q^2, many of the ingredients of a QCD cross section cannot be calculated in perturbation theory. Factorization provides a consistent framework to separate the perturbatively calculable 'hard part' of the cross section, from the nonperturbative or 'soft part'. In particular, most of the information on the hadron structure is part of this nonperturbative domain.

A famous example is deep-inelastic scattering, which we already studied in detail in Part I. The leading-order cross section is given by (see Eqs. (1.11), (1.12)):

$$\sigma_{\gamma^* p} = \underbrace{\frac{4\pi^2 \alpha_{\text{em}}}{Q^2} \sum_f e_{q_f}^2 \underbrace{\left(x q_f\left(x, Q^2\right) + x\bar{q}_f\left(x, Q^2\right) \right)}_{\text{DGLAP}(\mu^2 \to Q^2) \otimes q_f(x, \mu^2)}}_{\sigma_{\text{hard}}(x, Q^2)}, \tag{11.1}$$

in which the perturbatively calculable partonic cross section $\sigma_{\text{hard}}\left(x, Q^2\right)$ is separated from the nonperturbative PDFs. The DGLAP evolution equations, also perturbative, can be viewed as the connection between both, bringing the PDFs, measured at a certain (perturbative) scale μ^2, up to the 'hard scale' Q^2, which has to be large enough for the coupling $\alpha_s\left(Q^2\right)$ to be small. Schematically:

$$\sigma_{\text{coll}}\left(x, Q^2\right) = \sigma_{\text{hard}}\left(x, Q^2\right) \otimes \text{DGLAP}\left(\mu^2 \to Q^2\right) \otimes \text{PDFs}\left(x, \mu^2\right). \tag{11.2}$$

This is an example of what is known as collinear factorization (Ref. [102]). A central feature of this framework is the property that the PDFs are universal. This means that, once they are measured in a certain experiment, the PDFs can be plugged into any other cross section in collinear factorization, and evolved with DGLAP to the desired hard scale Q^2.

It is well known that, for less inclusive processes characterized by a second transverse scale, collinear factorization breaks down. An important example is the differential cross section of the Drell-Yan process $pp \to \gamma^* \to ll$, in which both the invariant mass Q^2 of the lepton pair, and its total transverse momentum $q_\perp^2$ play a role. As long as $q_\perp^2 \sim Q^2$, a collinear factorization formula reminiscent of Eq. (11.2) holds (Ref. [103, 104]):

$$\frac{\mathrm{d}\sigma_{\text{DY}}}{\mathrm{d}^4 q} = \sum_f \int \mathrm{d}x_A \int \mathrm{d}x_B\, q_{f/A}\left(x_A, Q^2\right) \bar{q}_{\bar{f}/B}\left(x_B, Q^2\right) \hat{\sigma}_0, \tag{11.3}$$

where $q_{f/A}\left(x_A, Q^2\right)$ and $\bar{q}_{\bar{f}/B}\left(x_B, Q^2\right)$ are the (anti)quark PDFs of the two protons, and where $\hat{\sigma}_0$ is the partonic cross section for the process $q\bar{q} \to \gamma^*$. However, when $q_\perp^2 \ll Q^2$, large corrections

from initial-state radiation become important and the above expression diverges as $q_\perp \to 0$. It should be replaced by (Ref. [103, 104]):

$$\frac{\mathrm{d}\sigma_{\mathrm{DY}}}{\mathrm{d}^4 q} = \sum_f \int \mathrm{d}^2 \mathbf{k}_{\perp A} \mathrm{d}^2 \mathbf{k}_{\perp B} \delta^{(2)} \left(\mathbf{k}_{\perp A} + \mathbf{k}_{\perp B} - \mathbf{q}_\perp \right)$$
$$\times \mathcal{F}_{f/A} \left(x_A, k_{\perp A} \right) \mathcal{F}_{\bar{f}/B} \left(x_B, k_{\perp B} \right) \hat{\sigma}_0. \tag{11.4}$$

The above formula is an example of transverse-momentum dependent (TMD) factorization, in which one works with transverse-momentum dependent PDFs $\mathcal{F}_{f/A} \left(x_A, k_{\perp A} \right)$ (TMDs for short) which, just like the unintegrated PDFs, contain a three-dimensional picture of the hadron by including the $k_\perp$-dependence of the parton (for some contemporary reviews, see Refs. [77, 105–108]). For example, TMDs can provide detailed information on the correlation between transverse momentum and spin, thus explaining many phenomena in which the spin degree of freedom is taken into account.

Though widely used, and successful in describing many data, TMD factorization suffers from several difficulties. First, it is very hard to establish formal factorization theorems that are valid to all orders. Such theorems nowadays only exist for the Drell-Yan process we mentioned above (Refs. [103, 109, 110]), for semi-inclusive deep-inelastic scattering (Ref. [111]), and for $e^+ e^-$ annihilation into two hadrons (see Ref. [77]). For many other processes, one assumes TMD factorization and works within this framework, even when a formal proof is not available.

Moreover, TMD parton distributions are more complicated than the usual, collinear PDFs, in that they are process dependent rather than universal (Refs. [112–117]). Indeed, in Sec. 6 we studied the example of the unintegrated gluon distribution, and argued that many different gluon TMDs arise, depending on the precise Wilson-line configuration that is used to render the operator structure gauge invariant. In general, the physical process to which the TMD factorization is applied determines the appropriate Wilson-line structure. A well-known example is the Sivers function (Ref. [118]), which is the TMD that describes the azimuthal distribution of unpolarized partons inside a nucleon that is transversely polarized with respect to its direction of motion. The Sivers function can be probed in the study of single spin asymmetries (SSAs, see e.g. Ref. [119, 120]) in polarized $p^\uparrow p$ collisions, defined as the ratio:

$$A_N \equiv \frac{\mathrm{d}\sigma^\uparrow - \mathrm{d}\sigma^\downarrow}{\mathrm{d}\sigma^\uparrow + \mathrm{d}\sigma^\downarrow}, \tag{11.5}$$

where the arrow indicates the polarization of the proton, which is transverse w.r.t. the beam line. It is widely predicted (see e.g. Refs. [79, 116, 117, 121, 122]) that the quark Sivers function probed in the SSA in the Drell-Yan process has the opposite sign of the one probed in SIDIS. This sign difference, and hence process-dependence, can be explained as the difference between the Wilson-line configuration that takes the effect of the initial-state interactions in the Drell-Yan process into account, and the one that encodes the final-state interactions in SIDIS, resulting in two different quark Sivers TMDs.

Processes that are sensitive to TMDs are in general difficult to measure, and as a consequence there are relatively few data on TMDs available (see Ref. [123] for a recent extraction of unpolarized quark TMDs.) Data on gluon TMDs are even more scarce due to the high energies needed to access them.

In the small-x limit and at large enough transverse momentum ($Q^2 \gg Q_s^2$), there is yet another factorization scheme known as $k_\perp$-factorization or high-energy factorization (HEF) (Ref. [65, 72, 124–126]). The unintegrated PDF $f(x, k_\perp)$ can, with the help of BFKL, be evolved in rapidity to match the hard parts of the cross section, which are commonly called impact factors. Since the gluons from the unintegrated PDF carry transverse momentum and are in general off shell, these impact factors are calculated with off-shell incoming partons. This is in contrast to TMD factorization, in which the incoming virtualities in the matrix elements are neglected and all the information on the transverse kinematics is solely encoded in the Wilson lines (Ref. [77]).

In this part of the thesis, we study forward dijet production in proton-nucleus collisions (Ref. [127]), a process which is sensitive to the large-x content of the proton, and to the small-x content of the nucleus. This process is characterized by three momentum scales: $\tilde{P}_\perp$, the typical transverse momentum of one of the jets and always the largest scale; $q_\perp$, the transverse-momentum imbalance between both jets, which is a measure of the $k_\perp$ of the gluons coming from the target; and the saturation scale Q_s of the nucleus which is always the softest scale. The value of $q_\perp$ with respect to Q_s and $\tilde{P}_\perp$ governs which factorization scheme is valid. Indeed, when $q_\perp \sim Q_s \ll \tilde{P}_\perp$, there are effectively two strongly ordered scales $q_\perp$ and $\tilde{P}_\perp$ in the problem and TMD factorization applies (Refs. [79, 113, 117, 128–132]). In the other regime: $Q_s \ll q_\perp \sim \tilde{P}_\perp$, $q_\perp$ and $\tilde{P}_\perp$ are of the same order and far above the saturation scale, hence high-energy factorization is applicable (Refs. [49, 133–136]). In both cases, the large-x parton coming from the proton is described by an integrated PDF, just like in collinear factorization.

However, since forward dijet production in pA collisions is sensitive to small-x dynamics, it can also be computed in the CGC formalism (Refs. [1, 127, 136–138]), again using a hybrid approach (see Refs. [139–141]) in which the parton from the proton is described by an integrated PDF. Since the CGC provides a weakly-coupled and hence perturbatively calculable theory for a proton or nucleus in the high-energy limit, one can match the result with the one from the TMD point of view, such that one obtains analytical or numerical expressions for the –in principle– nonperturbative TMDs from the nucleus. One can then exploit the full CGC machinery to compute these small-x TMDs explicitly within the McLerran-Venugopalan model, and evolve them in rapidity with the help of the JIMWLK equation. This research program was developed in recent years, and indeed, both the TMD and the HEF (taking the limit $Q_s \ll q_\perp \sim \tilde{P}_\perp$) results can be reproduced from the CGC calculation, see for instance Refs. [1, 76, 127, 137, 138, 142–146]. We should mention that it is also possible to generalize the TMD factorization formula for dijet production by keeping the small-x gluon in the matrix elements off shell. This approach, dubbed the 'Improved TMD factorization' (Refs. [127, 138]), allows one to interpolate between the HEF and the TMD frameworks without resorting to the CGC, and has the advantage that it is more applicable to phenomenology.

Specifically, in this part we build further on the work done in Ref. [1] by studying the forward production of two heavy quarks, performing the CGC calculation while keeping track of the masses. As already observed earlier for the case of $ep \to q\bar{q}$ (see for instance Ref. [114, 144, 145, 147]), by adding masses the cross section becomes sensitive to additional TMDs which describe the linearly polarized gluon content of the unpolarized proton, or in our case, nucleus. In our calculation, this means that the three gluon TMDs that describe the gluon channel $gA \to q\bar{q}$ will be accompanied by three 'polarized' partners. We compute the gluon TMDs analytically in both the MV and the

GBW model, after which they are numerically evaluated and evolved in rapidity with the help of a lattice implementation of the JIMWLK equation. Finally, we compare our results with the existing literature.

Before starting with the calculation, let us discuss the relevant kinematics. As already explained, we study forward dijet or heavy quark production in pA collisions. We choose the forward case because this implies that the partons from the proton have a generic Bjorken-x of the order $x_p \sim 1$, while on the nucleus side mainly gluons with $x \ll 1$ are involved. We therefore expect the transverse momentum of the parton coming from the proton to be of the order of Λ_{QCD}, which is much smaller than the average transverse momentum of the gluons in the target, which should be around the saturation scale Q_s. Furthermore, the requirement that the two outgoing particles are almost back-to-back, provides us with the two strongly ordered scales required by TMD factorization. Indeed, while the momenta $k_{1\perp} \sim k_{2\perp} \sim \tilde{P}_\perp$ of the individual jets can be fairly large, the total transverse momentum $\mathbf{q}_\perp = \mathbf{k}_{1\perp} + \mathbf{k}_{2\perp}$ of the dijet system is small. Moreover, since the imbalance between the jets is caused by the interaction with the nucleus, we expect the total transverse momentum to be of the order of the saturation scale: $q_\perp \sim Q_s$. To summarize, we have parametrically:

$$
\begin{aligned}
\Lambda_{\mathrm{QCD}}^2 \ll Q_s^2 \ll \tilde{P}_\perp^2 \ll \hat{s}, \\
0.04\,\mathrm{GeV}^2 \ll 4\,\mathrm{GeV}^2 \ll 400\,\mathrm{GeV}^2 \ll 40\,\mathrm{TeV}^2,
\end{aligned}
\tag{11.6}
$$

and we reach values of Bjorken-x (of the nucleus) down to approximately:

$$
x \simeq \frac{\tilde{P}_\perp^2}{\hat{s}} \sim 10^{-5}.
\tag{11.7}
$$

12 Kinematics

Let us study the kinematics of our process in some more detail, and confirm the claims that we made above. Although we will compute the $pA \to q\bar{q}X$ cross section in the CGC, it is arguably more illuminating to study the kinematics from the TMD point of view. At leading order, the reaction is depicted in Fig. 16. In light-cone coordinates, the momenta of the proton and the nucleus are:

$$
p_p = \sqrt{\frac{s}{2}}\,(1, 0, \mathbf{0})\,, \qquad p_A = \sqrt{\frac{s}{2}}\,(0, 1, \mathbf{0})\,,
\tag{12.1}
$$

where $s = (p_p + p_A)^2$ is the center of mass energy squared. On the level of the partons, we have $g(p) + g(k) \to q(k_1) + \bar{q}(k_2)$, where p is the momentum of the gluon coming from the proton, k the momentum of the gluon from the target, and where k_1 and k_2 are the momenta of the outgoing quark and antiquark. As already stated in the introduction, we assume that the transverse momentum $p_\perp \sim \Lambda_{\mathrm{QCD}}$ of the gluon from the proton can be neglected with respect to the transverse momentum
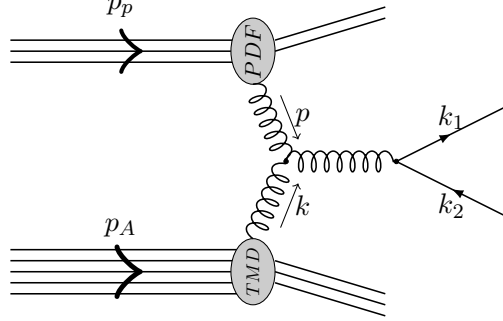
Figure 16: One of the leading order diagrams for inclusive heavy dijet production in pA collisions.

$k_\perp \sim Q_s$ of the gluon from the target. We have, in the eikonal approximation:

$$
\begin{aligned}
p &= \left(p^+, 0^-, \mathbf{0}_\perp\right), \\
k &= \left(0^+, k_1^- + k_2^-, \mathbf{k}_{1\perp} + \mathbf{k}_{2\perp}\right), \\
k_1 &= \left(k_1^+, k_1^-, \mathbf{k}_{1\perp}\right) = \left(k_1^+, \frac{m^2 + k_{1\perp}^2}{2k_1^+}, \mathbf{k}_{1\perp}\right), \\
k_2 &= \left(k_2^+, k_2^-, \mathbf{k}_{2\perp}\right) = \left(k_2^+, \frac{m^2 + k_{2\perp}^2}{2k_2^+}, \mathbf{k}_{2\perp}\right).
\end{aligned}
\tag{12.2}
$$

The Bjorken-x of the gluon from the target is given by:

$$
x \equiv \frac{k^-}{p_A^-} = \sqrt{\frac{2}{s}}\left(k_1^- + k_2^-\right) = \frac{1}{\sqrt{s}}\left(k_{1\perp}e^{-y_1} + k_{2\perp}e^{-y_2}\right),
\tag{12.3}
$$

which confirms our claim in the introduction, namely that in forward dijet production, and therefore at large rapidities y_1 and y_2, the small-x gluon content of the nucleus is probed. The energy fraction carried by the gluon from the proton is:

$$
x_p \equiv \frac{p^+}{p_p^+} = \frac{1}{\sqrt{s}}\left(k_{1\perp}e^{y_1} + k_{2\perp}e^{y_2}\right),
\tag{12.4}
$$

hence we expect $x_p \sim 1$.

For later reference, it is useful to compare with the three main parameters that will turn up in the CGC cross section, namely: z, the fraction of the energy of the gluon from the proton carried by the outgoing jet or heavy quark, $\tilde{\mathbf{P}}_\perp$, which is approximately equal to the transverse momentum of both of the jets, and $\mathbf{q}_\perp$, the vector sum of the transverse momenta of the two jets. In formulas:

$$
z = \frac{k_1^+}{p^+}, \qquad \tilde{\mathbf{P}}_\perp = (1-z)\,\mathbf{k}_{1\perp} - z\mathbf{k}_{2\perp}, \qquad \mathbf{q}_\perp = \mathbf{k}_{1\perp} + \mathbf{k}_{2\perp}.
\tag{12.5}
$$

It is straightforward to show that in terms of the variables above, the Mandelstam variables on the

parton level:

$$\hat{s} = (p + k)^2 = (k_1 + k_2)^2 \,,$$
$$\hat{t} = (p - k_1)^2 = (k - k_2)^2 \,,$$
$$\hat{u} = (p - k_2)^2 = (k - k_1)^2 \,,$$

(12.6)

can be written as follows:

$$\hat{s} = \frac{m^2 + \tilde{P}_\perp^2}{z\,(1-z)}, \quad \hat{t} = -\frac{(1-z)\,m^2 + k_{1\perp}^2}{z}, \quad \hat{u} = -\frac{zm^2 + k_{2\perp}^2}{1-z},$$

(12.7)

with:

$$\hat{s} + \hat{t} + \hat{u} = 2m^2 - q_\perp^2.$$

(12.8)

13 Color Glass Condensate approach

13.1 CGC calculation of the $gA \to q\bar{q}X$ cross section

After these preliminaries, let us now derive the cross section for massive quark production in pA collisions, within the framework of the Color Glass Condensate. We will closely follow Ref. [148], in which dijet production in the $qA \to qg$ channel is studied. Although, since we study a different channel, the details of our calculation will be different, the line of reasoning and the structure of the calculation in this reference equally applies to our case.

The main idea of the CGC calculation is that the outgoing quark-antiquark pair is a fluctuation stemming from the gluon coming from the projectile. This $g \to q\bar{q}$ splitting takes place either before or after the interaction with the target, as illustrated in Fig. 17. Since the target is a heavily contracted shockwave, the case in which the splitting takes place during the interaction can be neglected. An essential assumption is that the gluon or the quark pair scatters off the nucleus through multiple eikonal interactions with the soft gluon fields from the target. These interactions are resummed into Wilson lines, through which the final cross section will depend on the target. To be more specific: the gauge links are sensitive to the two-point correlators of the classical gluon fields in the target, which subsequently can be computed in models such as the McLerran-Venugopalan or Golec-Biernat-Wüsthoff model, and evolved in rapidity using the JIMWLK equation.

Let us start with examining the gluon coming from the proton, for which we can write the following first order Fock-space decomposition:

$$|\vec{p}, c, \lambda\rangle = Z|\vec{p}, c, \lambda\rangle_0 + \sum_{\alpha\beta ij} \int \mathrm{d}^3k \, g_s t_{ji}^c \psi_{\alpha\beta}^{T\lambda}\left(\vec{p}, \vec{k}, Q_p^2\right) |\left(\vec{k}, i, \beta\right); \left(\vec{p} - \vec{k}, j, \alpha\right)\rangle_0.$$

(13.1)

In the above expression, $\vec{p}$ is the three-momentum, c the color, λ the polarization, and $Q_p^2 = p_\mu p^\mu$ the virtuality of the gluon. The dressed gluon state, in the left hand side of the equation, is decomposed into a bare state, with corresponding renormalization factor Z, and a the second term which describes the gluon being split into a quark and an antiquark, with spins β and α, colors i
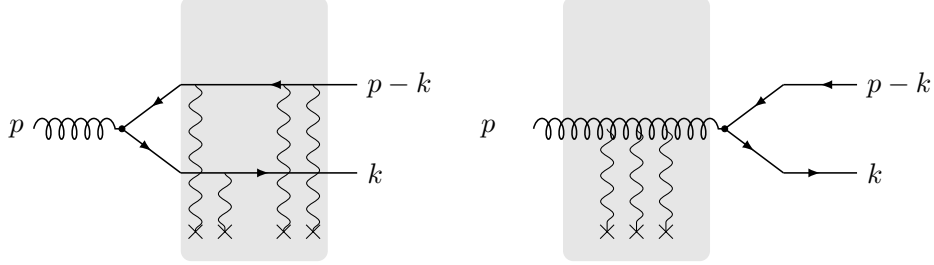
Figure 17: The two amplitudes in which the gluon interacts with the nucleus before (right) or after (left) it has fluctuated in a quark-antiquark pair.

and j, and momenta $\vec{k}$ and $\vec{p} - \vec{k}$. The wave function $\psi_{\alpha\beta}^{T\lambda}\left(\vec{p}, \vec{k}, Q_p^2\right)$ encodes the probability for a transversely polarized gluon to split up and is given by (the explicit calculation is performed in the appendix, Sec. D):

$$\psi_{\alpha\beta}^{T\lambda}\left(\vec{p}, \vec{k}, Q_p^2\right) = \sqrt{\frac{2}{p^+}} \frac{1}{\left(\mathbf{k}_\perp - z\mathbf{p}_\perp\right)^2 + m^2}$$
$$\times \begin{cases} \left(z\delta_{\alpha+}\delta_{\beta+} - (1-z)\,\delta_{\alpha-}\delta_{\beta-}\right)\left(\mathbf{k}_\perp - z\mathbf{p}_\perp\right) \cdot \boldsymbol{\epsilon}_\perp^1 + \frac{m}{\sqrt{2}}\delta_{\alpha+}\delta_{\beta-} & \lambda = 1 \\ \left(z\delta_{\alpha-}\delta_{\beta-} - (1-z)\,\delta_{\alpha+}\delta_{\beta+}\right)\left(\mathbf{k}_\perp - z\mathbf{p}_\perp\right) \cdot \boldsymbol{\epsilon}_\perp^2 - \frac{m}{\sqrt{2}}\delta_{\alpha-}\delta_{\beta+} & \lambda = 2 \end{cases}. \tag{13.2}$$

As already mentioned earlier, the transverse momentum $p_\perp$ and hence the virtuality Q_p of the incoming gluon is expected to be of the order Λ_{QCD}, which is negligible with respect to the virtualities $\sim Q_s$ of the gluons in the target. We can therefore neglect the case in which the incoming gluon is longitudinally polarized, and in what follows we suppress the index T and the dependence on Q_p^2, and simply write $\psi_{\alpha\beta}^{\lambda}\left(\vec{p}, \vec{k}\right)$.

Let us now transform Eq. (13.1) to 'mixed Fourier space', in which only the transverse momenta are Fourier transformed. Using the conventions

$$|\vec{p}, c, \lambda\rangle = \int \frac{\mathrm{d}^2\mathbf{b}}{(2\pi)^2} e^{i\mathbf{P}_\perp \cdot \mathbf{b}}|p^+, \mathbf{b}, c, \lambda\rangle,$$
$$\psi_{\alpha\beta}^{\lambda}\left(\vec{p}, \vec{k}\right) = \int \frac{\mathrm{d}^2\mathbf{x}}{(2\pi)^2} e^{-i\mathbf{k}_\perp \cdot \mathbf{x}} \phi_{\alpha\beta}^{\lambda}\left(p^+, z, \mathbf{x}\right), \tag{13.3}$$

where $\phi_{\alpha\beta}^{\lambda}\left(p^+, z, \mathbf{r}\right)$ is the $g \to q\bar{q}$ wave function in mixed Fourier space (we use the notation $r = |\mathbf{r}|$):

$$\phi_{\alpha\beta}^{\lambda}\left(p^+, z, \mathbf{r}\right) = 2\pi \sqrt{\frac{2}{p^+}} e^{iz\mathbf{p}_\perp \cdot \mathbf{r}}$$
$$\times \begin{cases} imK_1\left(mr\right)\frac{\mathbf{r}\cdot\boldsymbol{\epsilon}_\perp^1}{r}\left(z\delta_{\alpha-}\delta_{\beta-} - (1-z)\,\delta_{\alpha+}\delta_{\beta+}\right) + \frac{m}{\sqrt{2}}K_0\left(mr\right)\delta_{\alpha+}\delta_{\beta-} & \lambda = 1 \\ imK_1\left(mr\right)\frac{\mathbf{r}\cdot\boldsymbol{\epsilon}_\perp^2}{r}\left(z\delta_{\alpha+}\delta_{\beta+} - (1-z)\,\delta_{\alpha-}\delta_{\beta-}\right) - \frac{m}{\sqrt{2}}K_0\left(mr\right)\delta_{\alpha-}\delta_{\beta+} & \lambda = 2 \end{cases}, \tag{13.4}$$

we obtain:

$$
\begin{aligned}
|p^+, \mathbf{b}, c, \lambda\rangle &= Z|p^+, \mathbf{b}, c, \lambda\rangle_0 \\
&\quad + g_s \int \mathrm{d}^2 \mathbf{p}_\perp e^{-i\mathbf{p}_\perp \cdot \mathbf{b}} \sum_{\alpha\beta ij} t_{ji}^c \int \mathrm{d}^3 k \, \psi_{\alpha\beta}^\lambda \left(\vec{p}, \vec{k}\right) | \left(\vec{k}, i, \beta\right); \left(\vec{p} - \vec{k}, j, \alpha\right)\rangle_0, \\
&= Z|p^+, \mathbf{b}, c, \lambda\rangle_0 + g_s \sum_{\alpha\beta ij} t_{ji}^c \int \mathrm{d}^3 k \int \mathrm{d}^2 \mathbf{p}_\perp \int \frac{\mathrm{d}^2 \mathbf{y}}{(2\pi)^2} \frac{\mathrm{d}^2 \mathbf{x}}{(2\pi)^2} \frac{\mathrm{d}^2 \mathbf{b}'}{(2\pi)^2} e^{-i\mathbf{p}_\perp \cdot \mathbf{b}} \\
&\quad \times e^{-i\mathbf{k}_\perp \cdot \mathbf{y}} e^{i\mathbf{k}_\perp \cdot \mathbf{x}} e^{i(\mathbf{p}_\perp - \mathbf{k}_\perp) \cdot \mathbf{b}'} \phi_{\alpha\beta}^\lambda \left(\vec{p}, z, \mathbf{y}\right) | \left(k^+, \mathbf{x}, i, \beta\right); \left(p^+ - k^+, \mathbf{b}'j, \alpha\right)\rangle_0, \\
&= Z|p^+, \mathbf{b}, c, \lambda\rangle_0 + g_s \sum_{\alpha\beta ij} t_{ji}^c \int \mathrm{d} k^+ \frac{\mathrm{d}^2 \mathbf{x}}{(2\pi)^2} \frac{\mathrm{d}^2 \mathbf{b}'}{(2\pi)^2} (2\pi)^2 \delta^{(2)} \left(\mathbf{b} - z\mathbf{x} - (1-z)\mathbf{b}'\right) \\
&\quad \times \tilde{\phi}_{\alpha\beta}^\lambda \left(p^+, z, \mathbf{x} - \mathbf{b}'\right) | \left(k^+, \mathbf{x}, i, \beta\right); \left(p^+ - k^+, \mathbf{b}'j, \alpha\right)\rangle_0.
\end{aligned}
\tag{13.5}
$$

A few remarks are in order: the particular delta function comes from integrating over $\mathbf{p}_\perp$, over, amongst others, the factor $\exp(iz\mathbf{p}_\perp \cdot \mathbf{y})$ inside the wave function. The last line of the above expression is hence not dependent on $\mathbf{p}_\perp$ anymore, and we introduced the $\mathbf{p}_\perp$-independent wave function:

$$
\tilde{\phi}_{\alpha\beta}^\lambda \left(p^+, z, \mathbf{x} - \mathbf{b}'\right) \equiv e^{-iz\mathbf{p}_\perp \cdot (\mathbf{x} - \mathbf{b}')} \phi_{\alpha\beta}^\lambda \left(p, z, \mathbf{x} - \mathbf{b}'\right).
\tag{13.6}
$$

As usual, the interaction of the gluon or the quark-antiquark pair with the target, is quantified in the action of the S-matrix on the ingoing states. One of the powers of the present formalism is that, in mixed Fourier space, this action diagonalizes, as will become apparent shortly. First, we need the in- and outgoing states of the dressed gluon, which are given by:

$$
|\Psi_{\text{in}}\rangle = |\vec{p}, c, \lambda\rangle \otimes |\mathcal{T}\rangle, \qquad |\Psi_{\text{out}}\rangle = S|\Psi_{\text{in}}\rangle.
\tag{13.7}
$$

In the above formula, the dressed gluon state is convolved with the state ket of the target $|\mathcal{T}\rangle$, which in the CGC consists of many classical color gauge fields, distributed according to the CGC wave function $\Phi_x[\mathcal{A}]$:

$$
|\mathcal{T}\rangle = \int \mathcal{D}[\mathcal{A}] \, \Phi_x[\mathcal{A}] \, |\mathcal{A}\rangle.
\tag{13.8}
$$

We should stress that the quantum mechanical wave function $\Phi_x[\mathcal{A}]$ of the target is not known, and that we use it in a purely symbolic fashion. However, in our calculation, we will only need to evaluate its absolute value squared $|\Phi_x[\mathcal{A}]|^2$, and this is naturally associated with the Gaussian distribution $\mathcal{W}_x[\mathcal{A}]$ which we known from the CGC.

As already alluded to above, acting with the S-matrix on the dressed gluon state in mixed Fourier space is simple: it merely amounts to multiplying the bare gluon state with an eikonal Wilson line $W(\mathbf{x})$ in the adjoint representation, while the quark and the antiquark have to be multiplied with an eikonal Wilson line $U(\mathbf{x})$ or $U^\dagger(\mathbf{x})$ in the fundamental representation.[5] The outgoing state thus

---

[5]Note that care should be taken with the conventions. In contrast to Part II, the target here is a left-mover. Choosing a covariant gauge with $A^+ = 0$, its multiple interactions with a right-moving quark are resummed as $U(\mathbf{x}) = \mathcal{P} \exp\left(ig_s \int \mathrm{d}x^+ A(x^+, \mathbf{x})\right)$.

becomes:

$$|\Psi_{\text{out}}\rangle = \int \mathcal{D}\left[\mathcal{A}\right] \Phi_x\left[\mathcal{A}\right] \int \frac{\mathrm{d}^2\mathbf{b}}{(2\pi)^2} e^{i\mathbf{p}_\perp \cdot \mathbf{b}} \Bigg(Z\, W\left(\mathbf{b}\right) |p^+, \mathbf{b}, c, \lambda\rangle_0 \otimes |\mathcal{A}\rangle + g_s \sum_{\alpha\beta ij} \int \mathrm{d}k^+ \int \frac{\mathrm{d}^2\mathbf{x}}{(2\pi)^2}$$
$$\times \tilde{\phi}_{\alpha\beta}^\lambda\left(p^+, k^+, \mathbf{x} - \mathbf{b}\right) U_{jk}^\dagger\left(\mathbf{b}\right) t_{kl}^c U_{li}\left(\mathbf{x}\right) | \left(k^+, \mathbf{x}, i, \beta\right); \left(p^+ - k^+, \mathbf{b}, j, \alpha\right)\rangle_0 \otimes |\mathcal{A}\rangle \Bigg). \tag{13.9}$$

It becomes now clear what the definitions (13.7) and (13.8) mean: the gluon and the quark-antiquark pair are created from the QCD vacuum $|0\rangle$, while the target state $|\mathcal{T}\rangle$ only pertains to the classical gluon fields of the CGC. The latter are resummed in the Wilson lines, which therefore effectively contain all the information on the structure of the nucleus. According to the CGC, one has to take the statistical average over all possible classical gauge field configurations, and hence we expect the cross section to take the following form:

$$\sigma = \sigma_0 \int \mathcal{D}\left[\mathcal{A}\right] |\Phi_x\left[\mathcal{A}\right]|^2 \langle\mathcal{A}|\text{Wilson lines}|\mathcal{A}\rangle, \tag{13.10}$$

with, as explained earlier, $|\Phi_x\left[\mathcal{A}\right]|^2 = \mathcal{W}_x\left[\mathcal{A}\right]$.

We mentioned earlier that the scattering of the projectile off the target is described by two amplitudes: the one in which the gluon interacts with the nucleus and then splits in the quark pair, and the amplitude in which the splitting takes place earlier and therefore the quark-antiquark pair interacts. In the expression for the outgoing state, Eq. (13.9), only the latter case is apparent, as the first term in the formula describes a bare gluon. However, the next step in our calculation comes from the observation that the former case is in fact contained in this bare gluon term, which becomes apparent if we invert Eq. (13.1):

$$Z|\vec{p}, c, \lambda\rangle_0 = |\vec{p}, c, \lambda\rangle - \sum_{\alpha\beta ij} \int \mathrm{d}^3k\, g_s t_{ji}^c \psi_{\alpha\beta}^\lambda\left(\vec{p}, \vec{k}\right) | \left(\vec{k}, i, \beta\right); \left(\vec{p} - \vec{k}, j, \alpha\right)\rangle_0. \tag{13.11}$$

Plugging the Fourier transform, Eq. (13.5), of this formula in Eq. (13.9), and throw away the term containing $|\vec{p}, c, \lambda\rangle$ since the dressed gluon does not contribute to the production of the dijet, we find:

$$|\Psi_{\text{out}}\rangle = g_s \int \mathcal{D}\left[\mathcal{A}\right] \Phi_x\left[\mathcal{A}\right] \sum_{\alpha\beta ij} \int \mathrm{d}k^+ \frac{\mathrm{d}^2\mathbf{x}}{(2\pi)^2} \frac{\mathrm{d}^2\mathbf{b}}{(2\pi)^2} e^{i\mathbf{p}_\perp \cdot \mathbf{b}}$$
$$\times \Phi_{\alpha\beta ij}^\lambda\left(p^+, k^+, \mathbf{x} - \mathbf{b}\right) | \left(k^+, \mathbf{x}, i, \beta\right); \left(p^+ - k^+, \mathbf{b}, j, \alpha\right)\rangle_0 \otimes |\mathcal{A}\rangle, \tag{13.12}$$

where we defined:

$$\Phi_{\alpha\beta ij}^\lambda\left(p^+, k^+, \mathbf{x} - \mathbf{b}\right)$$
$$\equiv \left(U_{jk}^\dagger\left(\mathbf{b}\right) t_{kl}^c U_{li}\left(\mathbf{x}\right) - W_{cd}\left(z\mathbf{x} + (1-z)\,\mathbf{b}\right) t_{ji}^d \right) \tilde{\phi}_{\alpha\beta}^\lambda\left(p^+, k^+, \mathbf{x} - \mathbf{b}\right). \tag{13.13}$$

Indeed, in the above expression, both amplitudes of Fig. 17: the one in which the gluon fluctuates in a quark-antiquark pair that subsequently interacts with the nucleus, and the other one in which this fluctuation takes place after the interaction of the gluon with the medium, are now explicit.

64

We have finally gathered all the ingredients to compute the $gA \to q\bar{q}X$ cross section, which is given formally by the following expression:

$$\frac{\mathrm{d}\sigma^{gA \to q\bar{q}X}}{\mathrm{d}^3 k_1 \mathrm{d}^3 k_2} = \frac{1}{2} \frac{1}{N_c^2 - 1} \sum_{\lambda c} \langle \Psi_{\text{out}} | N_q \left(\vec{k}_1 \right) N_{\bar{q}} \left(\vec{k}_2 \right) | \Psi_{\text{out}} \rangle, \tag{13.14}$$

where N_q and $N_{\bar{q}}$ are counting operators defined as:

$$\begin{aligned} N_q \left(\vec{k} \right) &\equiv \sum_{is} b_{i,s}^{\dagger} \left(\vec{k} \right) b_{i,s} \left(\vec{k} \right), \\ N_{\bar{q}} \left(\vec{k} \right) &\equiv \sum_{js'} d_{j,s'}^{\dagger} \left(\vec{k} \right) d_{j,s'} \left(\vec{k} \right). \end{aligned} \tag{13.15}$$

In the above definitions, $b_{i,s}^{\dagger} \left(\vec{k} \right)$, $b_{i,s} \left(\vec{k} \right)$ and $d_{j,s'}^{\dagger} \left(\vec{k} \right)$, $d_{j,s'} \left(\vec{k} \right)$ are the creation and annihilation operators for quarks and antiquarks, respectively, satisfying the following relations in the mixed Fourier space:

$$\begin{aligned} b_{i,s}^{\dagger} \left(k^+, \mathbf{x} \right) |0\rangle &= |k^+, \mathbf{x}, i, s\rangle_0, \\ b_{i,s} \left(k^+, \mathbf{x} \right) |0\rangle &= 0, \\ \left\{ b_{i,s} \left(k^+, \mathbf{x} \right), b_{j,s'}^{\dagger} \left(p^+, \mathbf{y} \right) \right\} &= (2\pi)^2 \delta_{ij} \delta_{ss'} \delta \left(k^+ - p^+ \right) \delta^{(2)} \left(\mathbf{x} - \mathbf{y} \right), \end{aligned} \tag{13.16}$$

where the same relations hold for the antiquark operators. Plugging in our results for the $|\Psi_{\text{out}}\rangle$ state, Eq. (13.12), into the expression for the cross section, Eq. (13.14), we obtain:

$$\begin{aligned} \frac{\mathrm{d}\sigma^{gA \to q\bar{q}X}}{\mathrm{d}^3 k_1 \mathrm{d}^3 k_2} = &\frac{1}{2} \frac{1}{N_c^2 - 1} \int \frac{\mathrm{d}^2 \mathbf{v}}{(2\pi)^2} \frac{\mathrm{d}^2 \mathbf{v}'}{(2\pi)^2} \frac{\mathrm{d}^2 \mathbf{u}}{(2\pi)^2} \frac{\mathrm{d}^2 \mathbf{u}'}{(2\pi)^2} e^{i\mathbf{k}_{1\perp} \cdot (\mathbf{v} - \mathbf{v}')} e^{i\mathbf{k}_{2\perp} \cdot (\mathbf{u} - \mathbf{u}')} \\ &\sum_{\lambda c} \sum_{ijss'} \langle \Psi_{\text{out}} | b_{k,s}^{\dagger} \left(k_1^+, \mathbf{v} \right) d_{l,s'}^{\dagger} \left(k_2^+, \mathbf{u} \right) d_{l,s'} \left(k_2^+, \mathbf{u}' \right) b_{k,s} \left(k_1^+, \mathbf{v}' \right) | \Psi_{\text{out}} \rangle. \end{aligned} \tag{13.17}$$

The action of the annihilation operators on the $|\psi_{\text{out}}\rangle$ state yields:

$$\begin{aligned} &d_{l,s'} \left(k_2^+, \mathbf{u}' \right) b_{k,s} \left(k_1^+, \mathbf{v}' \right) | \Psi_{\text{out}} \rangle \\ &= g_s \int \mathcal{D}\left[\mathcal{A}\right] \Phi_x \left[\mathcal{A}\right] \sum_{\alpha\beta ij} \int \mathrm{d}k^+ \frac{\mathrm{d}^2 \mathbf{x}}{(2\pi)^2} \frac{\mathrm{d}^2 \mathbf{b}}{(2\pi)^2} e^{i\mathbf{p}_\perp \cdot \mathbf{b}} \Phi_{\alpha\beta ij}^{\lambda} \left(p^+, l^+, \mathbf{x} - \mathbf{b} \right) \\ &\times d_{l,s'} \left(k_2^+, \mathbf{u}' \right) b_{k,s} \left(k_1^+, \mathbf{v}' \right) b_{i,\beta}^{\dagger} \left(k^+, \mathbf{x} \right) d_{j,\alpha}^{\dagger} \left(p^+ - k^+, \mathbf{b} \right) |0\rangle \otimes |\mathcal{A}\rangle, \\ &= g_s \int \mathcal{D}\left[\mathcal{A}\right] \Phi_x \left[\mathcal{A}\right] \int \mathrm{d}k^+ \frac{\mathrm{d}^2 \mathbf{x}}{(2\pi)^2} \frac{\mathrm{d}^2 \mathbf{b}}{(2\pi)^2} e^{i\mathbf{p}_\perp \cdot \mathbf{b}} \Phi_{s'slk}^{\lambda} \left(p^+, k^+, \mathbf{x} - \mathbf{b} \right) \\ &\times (2\pi)^4 \delta \left(k_2^+ + k^+ - p^+ \right) \delta \left(k_1^+ - k^+ \right) \delta^{(2)} \left(\mathbf{u}' - \mathbf{b} \right) \delta^{(2)} \left(\mathbf{v}' - \mathbf{x} \right) |0\rangle \otimes |\mathcal{A}\rangle, \\ &= g_s \delta \left(k_2^+ + k_1^+ - p^+ \right) \int \mathcal{D}\left[\mathcal{A}\right] \Phi_x \left[\mathcal{A}\right] e^{i\mathbf{p}_\perp \cdot \mathbf{u}'} \Phi_{s'slk}^{\lambda} \left(p^+, k_1^+, \mathbf{u}' - \mathbf{v}' \right) |0\rangle \otimes |\mathcal{A}\rangle, \end{aligned} \tag{13.18}$$

while we find for the action of the creation operators on the $\langle \Psi_{\text{out}}|$ state:

$$
\langle \Psi_{\text{out}}| b^\dagger_{k,s} \left(k_1^+, \mathbf{v} \right) d^\dagger_{l,s'} \left(k_2^+, \mathbf{u} \right) = g_s \delta \left(p^+ - k_2^+ - k_1^+ \right)
$$
$$
\times \int \mathcal{D} \left[\mathcal{A} \right] \Phi^\dagger_x \left[\mathcal{A} \right] \langle \mathcal{A}| \otimes \langle 0| e^{-i \mathbf{p}_\perp \cdot \mathbf{u}} \Phi^{\lambda \dagger}_{s'slk} \left(p^+, k_1^+, \mathbf{u} - \mathbf{v} \right).
$$

(13.19)

We finally obtain the following result for the $gA \to q\bar{q}X$ cross section:

$$
\frac{\mathrm{d}\sigma^{gA \to q\bar{q}X}}{\mathrm{d}^3 k_1 \mathrm{d}^3 k_2}
$$
$$
= \frac{\alpha_s}{N_c^2 - 1} \delta \left(k_1^+ + k_2^+ - p^+ \right) \sum_{ijss'} \int \frac{\mathrm{d}^2 \mathbf{v}}{(2\pi)^2} \frac{\mathrm{d}^2 \mathbf{v}'}{(2\pi)^2} \frac{\mathrm{d}^2 \mathbf{u}}{(2\pi)^2} \frac{\mathrm{d}^2 \mathbf{u}'}{(2\pi)^2} e^{i\mathbf{k}_{1\perp} \cdot (\mathbf{v} - \mathbf{v}')} e^{i(\mathbf{k}_{2\perp} - \mathbf{p}_\perp) \cdot (\mathbf{u} - \mathbf{u}')}
$$

(13.20)

$$
\times \int \mathcal{D} \left[\mathcal{A} \right] |\Phi_x \left[\mathcal{A} \right]|^2 \langle \mathcal{A}| \Phi^{\lambda \dagger}_{s'sij} \left(p^+, k_1^+, \mathbf{u} - \mathbf{v} \right) \Phi^\lambda_{s'sij} \left(p^+, k_1^+, \mathbf{u}' - \mathbf{v}' \right) |\mathcal{A}\rangle,
$$

where we divided by a factor $2\pi \delta \left(k_1^+ + k_2^+ - p^+ \right)$ to remove the spurious divergency related to the use of plane waves instead of wave packets (see Ref. [148]). The interaction part becomes:

$$
\int \mathcal{D} \left[\mathcal{A} \right] |\Phi_x \left[\mathcal{A} \right]|^2 \langle \mathcal{A}| \left(U^\dagger \left(\mathbf{u} \right) t^c U \left(\mathbf{v} \right) - W_{cd} \left(z\mathbf{u} + (1-z) \mathbf{v} \right) t^d \right)^\dagger \tilde{\phi}^{\lambda *}_{ss'} \left(p^+, k_1^+, \mathbf{u} - \mathbf{v} \right)
$$
$$
\times \left(U^\dagger \left(\mathbf{u}' \right) t^c U \left(\mathbf{v}' \right) - W_{ce} \left(z\mathbf{u}' + (1-z) \mathbf{v}' \right) t^e \right) \tilde{\phi}^\lambda_{ss'} \left(p^+, k_1^+, \mathbf{u}' - \mathbf{v}' \right) |\mathcal{A}\rangle
$$
$$
= \tilde{\phi}^{\lambda *}_{ss'} \left(p^+, k_1^+, \mathbf{u} - \mathbf{v} \right) \tilde{\phi}^\lambda_{ss'} \left(p^+, k_1^+, \mathbf{u}' - \mathbf{v}' \right)
$$
$$
\times \left(\mathrm{Tr} \left\langle U^\dagger \left(\mathbf{v} \right) t^c U \left(\mathbf{u} \right) U^\dagger \left(\mathbf{u}' \right) t^c U \left(\mathbf{v}' \right) \right\rangle_x + \mathrm{Tr} \left\langle W_{dc} \left(z\mathbf{u} + (1-z) \mathbf{v} \right) t^d W_{ce} \left(z\mathbf{u}' + (1-z) \mathbf{v}' \right) t^e \right\rangle_x \right.
$$
$$
\left. - \mathrm{Tr} \left\langle U^\dagger \left(\mathbf{v} \right) t^c U \left(\mathbf{u} \right) W_{ce} \left(z\mathbf{u}' + (1-z) \mathbf{v}' \right) t^e \right\rangle_x - \mathrm{Tr} \left\langle W_{cd} \left(z\mathbf{u} + (1-z) \mathbf{v} \right) t^d U^\dagger \left(\mathbf{u}' \right) t^c U \left(\mathbf{v}' \right) \right\rangle_x \right),
$$

(13.21)

where we introduced the notation:

$$
\langle \mathcal{O} \rangle_x = \int \mathcal{D} \left[\mathcal{A} \right] \mathcal{W}_x \left[\mathcal{A} \right] \langle \mathcal{A}| \mathcal{O} |\mathcal{A}\rangle
$$

(13.22)

to indicate an operator being evaluated in the Color Glass Condensate at a certain Bjorken-x. Using the Lie algebra and Wilson line identities Eq. (A.9) and Eq. (A.12), we finally obtain the following result for the cross section: (for future convenience, we changed the notation for the transverse coordinates $\mathbf{x} \leftrightarrow \mathbf{u}$ and $\mathbf{y} \leftrightarrow \mathbf{v}$)

$$
\frac{\mathrm{d}\sigma^{gA\to q\bar{q}X}}{\mathrm{d}^3 k_1 \mathrm{d}^3 k_2} = \frac{\alpha_s}{2} \frac{\delta\left(\left(k_1^+ + k_2^+\right)/p^+ - 1\right)}{p^+}
$$
$$
\times \int \frac{\mathrm{d}^2\mathbf{x}}{(2\pi)^2} \frac{\mathrm{d}^2\mathbf{y}}{(2\pi)^2} \frac{\mathrm{d}^2\mathbf{x}'}{(2\pi)^2} \frac{\mathrm{d}^2\mathbf{y}'}{(2\pi)^2} e^{i\mathbf{k}_{1\perp}\cdot(\mathbf{y}-\mathbf{y}')} e^{i(\mathbf{k}_{2\perp}-\mathbf{p}_\perp)\cdot(\mathbf{x}-\mathbf{x}')}
$$
$$
\times \sum_{\lambda ss'} \tilde{\phi}_{s's}^{\lambda *}\left(p^+, k_1^+, \mathbf{x}-\mathbf{y}\right) \tilde{\phi}_{s's}^{\lambda}\left(p^+, k_1^+, \mathbf{x}'-\mathbf{y}'\right) \tag{13.23}
$$
$$
\times \Bigg(C\left(\mathbf{x},\mathbf{y},\mathbf{x}',\mathbf{y}'\right) + D_A\left(z\mathbf{x}+(1-z)\mathbf{y}, z\mathbf{x}'+(1-z)\mathbf{y}'\right)
$$
$$
- S^{(3)}\left(\mathbf{x}, z\mathbf{x}'+(1-z)\mathbf{y}', \mathbf{y}\right) - S^{(3)}\left(\mathbf{y}', z\mathbf{x}+(1-z)\mathbf{y}, \mathbf{x}'\right) \Bigg),
$$

where we defined the following CGC averages over Wilson lines:

$$
C\left(\mathbf{x},\mathbf{y},\mathbf{x}',\mathbf{y}'\right) \equiv \frac{1}{C_F N_c}\mathrm{Tr}\Big\langle U^\dagger\left(\mathbf{y}\right) t^c U\left(\mathbf{x}\right) U^\dagger\left(\mathbf{x}'\right) t^c U\left(\mathbf{y}'\right)\Big\rangle_x,
$$
$$
D_A\left(\mathbf{x},\mathbf{y}\right) \equiv \frac{1}{N_c^2-1}\mathrm{Tr}\Big\langle W\left(\mathbf{x}\right) W^\dagger\left(\mathbf{y}\right)\Big\rangle_x, \tag{13.24}
$$
$$
S^{(3)}\left(\mathbf{y},\mathbf{z},\mathbf{x}\right) \equiv \frac{1}{C_F N_c}\Big\langle \mathrm{Tr}\left(U^\dagger\left(\mathbf{x}\right) t^c U\left(\mathbf{y}\right) t^a\right) W_{ca}\left(\mathbf{z}\right)\Big\rangle_x.
$$

This result is the same as the one quoted in, for example, Refs. [1, 76].

13.2 Correlation limit

According to the hybrid dilute-dense factorization formalism, described in Refs. [127, 138], the full pA cross section is obtained as the convolution of our result for $gA \to q\bar{q}X$, Eq. (13.23), with the gluon PDF $x_p\mathcal{G}\left(x_p, \mu^2\right)$. Furthermore, in order to make contact with the TMD approach, we have to take the so-called correlation limit, in which the two jets are almost back-to-back. This way, we recover the two strongly ordered transverse momentum scales, necessary to be able to use the TMD formalism.

We first introduce the following transverse coordinates, which will facilitate taking the correlation limit later:

$$
\begin{aligned}
\mathbf{u} &\equiv \mathbf{x}-\mathbf{y}, & \mathbf{u}' &\equiv \mathbf{x}'-\mathbf{y}', \\
\mathbf{v} &\equiv z\mathbf{x}+(1-z)\mathbf{y}, & \mathbf{v}' &\equiv z\mathbf{x}'+(1-z)\mathbf{y}',
\end{aligned} \tag{13.25}
$$

or:

$$
\begin{aligned}
\mathbf{x} &= \mathbf{v}+(1-z)\mathbf{u}, & \mathbf{x}' &= \mathbf{v}'+(1-z)\mathbf{u}', \\
\mathbf{y} &= \mathbf{v}-z\mathbf{u}, & \mathbf{y}' &= \mathbf{v}'-z\mathbf{u}',
\end{aligned} \tag{13.26}
$$

as well as their conjugate momenta:

$$
\begin{aligned}
\tilde{\mathbf{P}}_\perp &\equiv z\mathbf{k}_{1\perp}-(1-z)\mathbf{k}_{2\perp}, \\
\mathbf{q}_\perp &\equiv \mathbf{k}_{1\perp}+\mathbf{k}_{2\perp}.
\end{aligned} \tag{13.27}
$$

Furthermore we make use of the notation:

$$
\begin{aligned}
\mathrm{d}\mathcal{P}.\mathcal{S}. &\equiv \mathrm{d}y_1 \mathrm{d}y_2 \mathrm{d}^2\mathbf{q}_\perp \mathrm{d}^2\tilde{\mathbf{P}}_\perp, \\
&= \frac{1}{k_1^+ k_2^+} \mathrm{d}^3 k_1 \mathrm{d}^3 k_2,
\end{aligned}
\tag{13.28}
$$

and from Eq. (13.23) (neglecting $\mathbf{p}_\perp$, since $p_\perp \ll k_\perp$, as we already mentioned earlier) we obtain the $pA \to q\bar{q}X$ cross section:

$$
\begin{aligned}
\frac{\mathrm{d}\sigma^{pA\to q\bar{q}X}}{\mathrm{d}\mathcal{P}.\mathcal{S}.} &= \frac{\alpha_s}{2} \frac{k_1^+ k_2^+}{p^+} x_p \mathcal{G}\left(x_p, \mu^2\right) \int \frac{\mathrm{d}^2\mathbf{v}}{(2\pi)^2} \frac{\mathrm{d}^2\mathbf{u}}{(2\pi)^2} \frac{\mathrm{d}^2\mathbf{v}'}{(2\pi)^2} \frac{\mathrm{d}^2\mathbf{u}'}{(2\pi)^2} e^{i\mathbf{q}_\perp\cdot(\mathbf{v}-\mathbf{v}')} e^{-i\tilde{\mathbf{P}}_\perp\cdot(\mathbf{u}-\mathbf{u}')} \\
&\times \sum_{\lambda ss'} \tilde{\phi}_{s's}^{\lambda*}\left(p^+, k_1^+, \mathbf{u}\right) \tilde{\phi}_{s's}^{\lambda}\left(p^+, k_1^+, \mathbf{u}'\right) \\
&\times \Big(C\left(\mathbf{x},\mathbf{y},\mathbf{x}',\mathbf{y}'\right) + D_A\left(\mathbf{v},\mathbf{v}'\right) - S^{(3)}\left(\mathbf{v}+(1-z)\mathbf{u},\mathbf{v}',\mathbf{v}-z\mathbf{u}\right) \\
&\quad - S^{(3)}\left(\mathbf{v}'-z\mathbf{u}',\mathbf{v},\mathbf{v}'+(1-z)\mathbf{u}'\right) \Big).
\end{aligned}
\tag{13.29}
$$

A last manipulation before we take the correlation limit, is to take a closer look at Wilson line correlators in the above cross section. In order to compare with the TMD formalism, they have to be rewritten in terms of only the fundamental representations. From the definitions Eq. (13.24), we have:

$$
\begin{aligned}
D_A\left(\mathbf{v},\mathbf{v}'\right) &= \frac{1}{N_c^2-1} \left\langle W_{ab}\left(\mathbf{v}\right) \delta^{bc} W_{ca}^\dagger\left(\mathbf{v}'\right) \right\rangle_x = \frac{2}{N_c^2-1} \left\langle W_{ab}\left(\mathbf{v}\right) t_{ij}^b t_{ji}^c W_{ca}^\dagger\left(\mathbf{v}'\right) \right\rangle_x, \\
&= \frac{2}{N_c^2-1} \mathrm{Tr}\left\langle U\left(\mathbf{v}\right) t^a U^\dagger\left(\mathbf{v}\right) U\left(\mathbf{v}'\right) t^a U^\dagger\left(\mathbf{v}'\right) \right\rangle_x, \\
&= \frac{1}{N_c^2-1} \left(\left\langle \mathrm{Tr}\left(U\left(\mathbf{v}\right)U^\dagger\left(\mathbf{v}'\right)\right) \mathrm{Tr}\left(U\left(\mathbf{v}'\right)U^\dagger\left(\mathbf{v}\right)\right) \right\rangle_x - 1 \right).
\end{aligned}
\tag{13.30}
$$

In the second equality of the calculation above, we used the trace of two generators of the fundamental representation $SU\left(N_c\right)$, Eq. (A.12), after which, in the third equality, we made use of Eq. (A.10) to transform the Wilson lines in the adjoint representation to the fundamental representation. Writing the color indices explicitly, we used the Fierz identity, Eq. (A.13), in the fourth equality, after which the second term in the result could be simplified, since two Wilson lines on the same transverse position, but in the opposite direction, cancel:

$$
\left(U\left(\mathbf{v}\right) U^\dagger\left(\mathbf{v}\right) \right)_{ij} = \delta_{ij}.
\tag{13.31}
$$

Using the same manipulations, it is easy to show that

$$
S^{(3)}\left(\mathbf{x},\mathbf{z},\mathbf{y}\right) = \frac{1}{2C_F N_c} \left\langle \mathrm{Tr}\left(U\left(\mathbf{x}\right)U^\dagger\left(\mathbf{z}\right)\right) \mathrm{Tr}\left(U\left(\mathbf{z}\right)U^\dagger\left(\mathbf{y}\right)\right) - \frac{1}{N_c}\mathrm{Tr}\left(U\left(\mathbf{x}\right)U^\dagger\left(\mathbf{y}\right)\right) \right\rangle_x,
\tag{13.32}
$$

and finally, for the quadrupole operator

$$C\left(\mathbf{x},\mathbf{y},\mathbf{x}',\mathbf{y}'\right) = \frac{1}{2C_F N_c}\Big\langle \mathrm{Tr}\left(U\left(\mathbf{x}\right)U^\dagger\left(\mathbf{x}'\right)\right)\mathrm{Tr}\left(U\left(\mathbf{y}'\right)U^\dagger\left(\mathbf{y}\right)\right)$$
$$-\frac{1}{N_c}\mathrm{Tr}\left(U\left(\mathbf{x}\right)U^\dagger\left(\mathbf{x}'\right)U\left(\mathbf{y}'\right)U^\dagger\left(\mathbf{y}\right)\right)\Big\rangle_x. \tag{13.33}$$

From the above expressions, making use of Eq. (13.31), it is very straightforward to derive the following relations between the Wilson line structures:

$$C\left(\mathbf{v},\mathbf{v},\mathbf{w},\mathbf{w}\right) = D_A\left(\mathbf{x},\mathbf{y}\right),$$
$$C\left(\mathbf{x},\mathbf{y},\mathbf{w},\mathbf{w}\right) = S^{(3)}\left(\mathbf{x},\mathbf{w},\mathbf{y}\right),$$
$$C\left(\mathbf{w},\mathbf{w},\mathbf{x},\mathbf{y}\right) = S^{(3)}\left(\mathbf{y},\mathbf{w},\mathbf{x}\right),$$
$$S^{(3)}\left(\mathbf{x},\mathbf{y},\mathbf{x}\right) = D_A\left(\mathbf{x},\mathbf{y}\right). \tag{13.34}$$

With these preliminaries, we are finally ready to take the correlation limit of Eq. (13.29), which amounts to the requirement that:

$$\tilde{P}_\perp^2 \gg q_\perp^2, \tag{13.35}$$

implying that the outgoing jets or heavy quarks are almost back-to-back. Indeed, $\tilde{P}_\perp \sim k_{1\perp} \sim k_{2\perp}$ is of the order of the transverse momenta of the individual jets, while $\mathbf{q}_\perp = \mathbf{k}_{1\perp} + \mathbf{k}_{2\perp}$ is the vector sum of their transverse momenta. The latter therefore quantifies the transverse momentum imbalance of the dijet, and since this imbalance is caused by the multiple scatterings off the target, we have that $q_\perp \sim Q_s$, since the saturation scale Q_s is approximately equal to the average transverse momentum of the gluons in the nucleus. Thus, in the correlation limit, we obtain two strongly ordered scales, necessary for the TMD approach to be valid. Note also that, as stated earlier, the transverse momentum $\mathbf{p}_\perp$ of the incoming gluon is in the ballpark of Λ_{QCD}, and therefore very small in comparison with $\mathbf{q}_\perp$ and $\tilde{\mathbf{P}}_\perp$. We can therefore set $\mathbf{p}_\perp \simeq 0$.

The correlation limit, Eq. (13.35), is tantamount to the requirement

$$\mathbf{u},\,\mathbf{u}' \ll \mathbf{v},\,\mathbf{v}'. \tag{13.36}$$

In particular, the Wilson line correlators in the cross section Eq. (13.29) can be Taylor expanded in $\mathbf{u}$ and $\mathbf{u}'$, yielding, with the help of the relations in Eq. (13.34):

$$C\left(\mathbf{x},\mathbf{y},\mathbf{x}',\mathbf{y}'\right) + D_A\left(\mathbf{v},\mathbf{v}'\right) - S^{(3)}\left(\mathbf{x},\mathbf{v}',\mathbf{y}\right) - S^{(3)}\left(\mathbf{y}',\mathbf{v},\mathbf{x}'\right)$$
$$\simeq -z\left(1-z\right)u_i u_j' \frac{\partial^2}{\partial x_i \partial y_j'}C\left(\mathbf{x},\mathbf{v},\mathbf{v}',\mathbf{y}'\right) - z\left(1-z\right)u_i u_j' \frac{\partial^2}{\partial y_i \partial x_j'}C\left(\mathbf{v},\mathbf{y},\mathbf{x}',\mathbf{v}'\right)$$
$$+ z^2 u_i u_j' \frac{\partial^2}{\partial y_i \partial y_j'}C\left(\mathbf{v},\mathbf{y},\mathbf{v}',\mathbf{y}'\right) + \left(1-z\right)^2 u_i u_j' \frac{\partial^2}{\partial x_i \partial x_j'}C\left(\mathbf{x},\mathbf{v},\mathbf{x}',\mathbf{v}'\right). \tag{13.37}$$

Using the expression for the quadrupole in terms of Wilson lines in the fundamental representation, Eq. (13.33), as well as the fact that we can change derivatives around as follows:

$$\left[\partial_i U^\dagger\left(\mathbf{w}\right)\right]U\left(\mathbf{w}\right) = -U^\dagger\left(\mathbf{w}\right)\left[\partial_i U\left(\mathbf{w}\right)\right], \tag{13.38}$$

it is straightforward to see that the four terms in (13.37) combine to give

$$
\begin{aligned}
& C\left(\mathbf{x}, \mathbf{y}, \mathbf{x}', \mathbf{y}'\right) + D_A\left(\mathbf{v}, \mathbf{v}'\right) - S^{(3)}\left(\mathbf{x}, \mathbf{v}', \mathbf{y}\right) - S^{(3)}\left(\mathbf{y}', \mathbf{v}, \mathbf{x}'\right) \\
& \simeq u_i u_j' \frac{1}{N_c^2 - 1} \mathcal{WL}_{ij}\left(\mathbf{v}, \mathbf{v}'\right),
\end{aligned}
\tag{13.39}
$$

where we defined:

$$
\begin{aligned}
\mathcal{WL}_{ij}\left(\mathbf{v}, \mathbf{v}'\right) \equiv & \left[-2z\left(1-z\right)\operatorname{Re}\Big\langle \operatorname{Tr}\left(\left[\partial_i U\left(\mathbf{v}\right)\right] U^\dagger\left(\mathbf{v}'\right)\right) \operatorname{Tr}\left(\left[\partial_j U\left(\mathbf{v}'\right)\right] U^\dagger\left(\mathbf{v}\right)\right)\Big\rangle_x \right. \\
& + z^2 \Big\langle \operatorname{Tr}\left(\left[\partial_i U\left(\mathbf{v}\right)\right]\left[\partial_j U^\dagger\left(\mathbf{v}'\right)\right]\right) \operatorname{Tr}\left(U\left(\mathbf{v}'\right) U^\dagger\left(\mathbf{v}\right)\right)\Big\rangle_x^* \\
& + \left(1-z\right)^2 \Big\langle \operatorname{Tr}\left(\left[\partial_i U\left(\mathbf{v}\right)\right]\left[\partial_j U^\dagger\left(\mathbf{v}'\right)\right]\right) \operatorname{Tr}\left(U\left(\mathbf{v}'\right) U^\dagger\left(\mathbf{v}\right)\right)\Big\rangle_x \\
& \left. + \Big\langle \frac{1}{N_c}\operatorname{Tr}\left(\left[\partial_i U\left(\mathbf{v}\right)\right] U^\dagger\left(\mathbf{v}'\right)\left[\partial_j U\left(\mathbf{v}'\right)\right] U^\dagger\left(\mathbf{v}\right)\right)\Big\rangle_x \right].
\end{aligned}
\tag{13.40}
$$

In the correlation limit, the cross section, Eq. (13.29), therefore becomes:

$$
\begin{aligned}
\frac{\mathrm{d}\sigma^{pA \to q\bar{q}X}}{\mathrm{d}\mathcal{P}.\mathcal{S}.} = & \frac{\alpha_s}{2\left(N_c^2 - 1\right)} \frac{k_1^+ k_2^+}{p^+} x_p \mathcal{G}\left(x_p, \mu^2\right) \int \frac{\mathrm{d}^2\mathbf{u}}{(2\pi)^2} \frac{\mathrm{d}^2\mathbf{u}'}{(2\pi)^2} e^{-i\tilde{\mathbf{P}}_\perp \cdot (\mathbf{u} - \mathbf{u}')} u_i u_j' \\
& \times \sum_{\lambda s s'} \tilde{\phi}_{s's}^{\lambda *}\left(p^+, k_1^+, \mathbf{u}\right) \tilde{\phi}_{s's}^{\lambda}\left(p^+, k_1^+, \mathbf{u}'\right) \int \frac{\mathrm{d}^2\mathbf{v}}{(2\pi)^2} \frac{\mathrm{d}^2\mathbf{v}'}{(2\pi)^2} e^{i\mathbf{q}_\perp \cdot (\mathbf{v} - \mathbf{v}')} \mathcal{WL}_{ij}\left(\mathbf{v}, \mathbf{v}'\right).
\end{aligned}
\tag{13.41}
$$

This expression can be simplified further by performing the $\mathbf{u}$ and $\mathbf{u}'$ integrations explicitly. The absolute value squared of the wave functions, summed (and not averaged) over the two different polarizations of the gluon as well as over the quark spins, is given by:

$$
\begin{aligned}
& \left|\tilde{\phi}^{g \to q\bar{q}}\left(p^+, z, \mathbf{u}, \mathbf{u}'\right)\right|^2 \\
& = \frac{8\pi^2}{p^+}\left(2m^2 K_1\left(mu\right) K_1\left(mu'\right) \frac{\mathbf{u} \cdot \mathbf{u}'}{uu'} P_{qg}\left(z\right) + m^2 K_0\left(mu\right) K_0\left(mu'\right)\right),
\end{aligned}
\tag{13.42}
$$

where

$$
P_{qg}\left(z\right) = \frac{z^2 + \left(1-z\right)^2}{2}.
\tag{13.43}
$$

Using the identity:

$$
\frac{\partial}{\partial u_i} K_0\left(mu\right) = -m\frac{u_i}{u} K_1\left(mu\right),
\tag{13.44}
$$

the integrals over $\mathbf{u}$ and $\mathbf{u}'$ in Eq. (13.41) can be performed:

$$
\begin{aligned}
& \int \frac{\mathrm{d}^2\mathbf{u}}{(2\pi)^2} \frac{\mathrm{d}^2\mathbf{u}'}{(2\pi)^2} e^{-i\tilde{\mathbf{P}}_\perp \cdot (\mathbf{u} - \mathbf{u}')} u_i u_j' \left|\tilde{\phi}^{g \to q\bar{q}}\left(p^+, z, \mathbf{u}, \mathbf{u}'\right)\right|^2 \\
& = \frac{2}{p^+}\left[2\Big(\frac{\delta_{ij}}{(\tilde{P}_\perp^2 + m^2)^2} - \frac{4m^2 \tilde{P}_i \tilde{P}_j}{(\tilde{P}_\perp^2 + m^2)^4}\Big) P_{qg}\left(z\right) + \frac{4m^2 \tilde{P}_i \tilde{P}_j}{(\tilde{P}_\perp^2 + m^2)^4}\right].
\end{aligned}
\tag{13.45}
$$

We finally arrive at the following CGC result for the $pA \to q\bar{q}X$ cross section in the correlation limit:

$$
\begin{aligned}
\frac{\mathrm{d}\sigma^{pA \to q\bar{q}X}}{\mathrm{d}\mathcal{P}.\mathcal{S}.} &= \frac{2\alpha_s}{(N_c^2 - 1)} z \left(1 - z\right) x_p \mathcal{G}\left(x_p, \mu^2\right) \\
&\times \left[\left(\frac{\delta_{ij}}{(\tilde{P}_\perp^2 + m^2)^2} - \frac{4m^2 \tilde{P}_i \tilde{P}_j}{(\tilde{P}_\perp^2 + m^2)^4} \right) P_{qg}\left(z\right) + \frac{2m^2 \tilde{P}_i \tilde{P}_j}{(\tilde{P}_\perp^2 + m^2)^4} \right] \\
&\times \int \frac{\mathrm{d}^2\mathbf{v}}{(2\pi)^2} \frac{\mathrm{d}^2\mathbf{v}'}{(2\pi)^2} e^{i\mathbf{q}_\perp \cdot (\mathbf{v} - \mathbf{v}')} \mathcal{WL}_{ij}\left(\mathbf{v}, \mathbf{v}'\right).
\end{aligned}
\tag{13.46}
$$

13.3 Identifying the gluon TMDs

We will now demonstrate that the Wilson line correlators, Eq. (13.40), that appear in the CGC cross section, can in fact be identified as the small-x limit of gluon TMDs. Indeed, when Fourier transforming the correlators, each of them can be decomposed into two parts by projecting the transverse Lorentz indices: a part that is linear in δ^{ij}, and another one that is traceless. For example:

$$
\begin{aligned}
&\frac{4}{g_s^2} \frac{1}{N_c} \int \frac{\mathrm{d}^2\mathbf{v}\mathrm{d}^2\mathbf{v}'}{(2\pi)^3} e^{-i\mathbf{q}_\perp \cdot (\mathbf{v} - \mathbf{v}')} \left\langle \mathrm{Tr}\left(\left[\partial_i U\left(\mathbf{v}\right)\right] \left[\partial_j U^\dagger\left(\mathbf{v}'\right)\right] \right) \mathrm{Tr}\left(U\left(\mathbf{v}'\right) U^\dagger\left(\mathbf{v}\right) \right) \right\rangle_x \\
&= \frac{1}{2} \delta^{ij} \mathcal{F}_{gg}^{(1)}\left(x, q_\perp\right) + \frac{1}{2} \left(\frac{2q_\perp^i q_\perp^j}{q_\perp^2} - \delta^{ij} \right) \mathcal{H}_{gg}^{(1)}\left(x, q_\perp\right).
\end{aligned}
\tag{13.47}
$$

Both parts of the projection turn out to be gluon TMDs, as we will demonstrate in this subsection. Interestingly, the traceless parts –in the above formula $\mathcal{H}_{gg}^{(1)}$– are the TMDs that correspond to the linearly polarized gluons inside the unpolarized nucleus (Refs. [114, 144, 145, 147]). Gluon polarization hence does play a role in forward heavy quark production in dilute-dense collisions, even when the proton and the nucleus themselves are not polarized.

Indeed, performing the decomposition for the whole Wilson-line structure $\mathcal{WL}_{ij}$, Eq. (13.40), we find:

$$\int \frac{\mathrm{d}^2 \mathbf{v}}{(2\pi)^2} \frac{\mathrm{d}^2 \mathbf{v}'}{(2\pi)^2} e^{-i\mathbf{q}_\perp \cdot (\mathbf{v}-\mathbf{v}')} \mathcal{WL}_{ij}(\mathbf{v}, \mathbf{v}') =$$

$$\frac{\alpha_s N_c}{2} \left[2z(1-z) \left(\frac{1}{2}\delta^{ij}\mathcal{F}_{gg}^{(2)}(x, q_\perp) + \frac{1}{2}\left(\frac{2q_\perp^i q_\perp^j}{q_\perp^2} - \delta^{ij} \right) \mathcal{H}_{gg}^{(2)}(x, q_\perp) \right) \right.$$

$$+ z^2 \left(\frac{1}{2}\delta^{ij}\mathcal{F}_{gg}^{(1)}(x, q_\perp) + \frac{1}{2}\left(\frac{2q_\perp^i q_\perp^j}{q_\perp^2} - \delta^{ij} \right) \mathcal{H}_{gg}^{(1)}(x, q_\perp) \right) \qquad (13.48)$$

$$+ (1-z)^2 \left(\frac{1}{2}\delta^{ij}\mathcal{F}_{gg}^{(1)}(x, q_\perp) + \frac{1}{2}\left(\frac{2q_\perp^i q_\perp^j}{q_\perp^2} - \delta^{ij} \right) \mathcal{H}_{gg}^{(1)}(x, q_\perp) \right)$$

$$\left. - \frac{1}{N_c^2} \left(\frac{1}{2}\delta^{ij}\mathcal{F}_{gg}^{(3)}(x, q_\perp) + \frac{1}{2}\left(\frac{2q_\perp^i q_\perp^j}{q_\perp^2} - \delta^{ij} \right) \mathcal{H}_{gg}^{(3)}(x, q_\perp) \right) \right],$$

in which we identify six different gluon TMDs: $\mathcal{F}_{gg}^{(1)}$, $\mathcal{F}_{gg}^{(2)}$, and $\mathcal{F}_{gg}^{(3)}$, defined as:

$$\mathcal{F}_{gg}^{(1)}(x, q_\perp) \equiv \frac{4}{g_s^2} \frac{1}{N_c} \int \frac{\mathrm{d}^2 \mathbf{v}\mathrm{d}^2 \mathbf{v}'}{(2\pi)^3} e^{-i\mathbf{q}_\perp \cdot (\mathbf{v}-\mathbf{v}')} \left\langle \mathrm{Tr}\left([\partial_i U(\mathbf{v})]\left[\partial_i U^\dagger(\mathbf{v}')\right]\right) \mathrm{Tr}\left(U(\mathbf{v}') U^\dagger(\mathbf{v}) \right) \right\rangle_x,$$

$$\mathcal{F}_{gg}^{(2)}(x, q_\perp) \equiv -\frac{4}{g_s^2} \frac{1}{N_c} \int \frac{\mathrm{d}^2 \mathbf{v}\mathrm{d}^2 \mathbf{v}'}{(2\pi)^3} e^{-i\mathbf{q}_\perp \cdot (\mathbf{v}-\mathbf{v}')} \mathrm{Re}\left\langle \mathrm{Tr}\left([\partial_i U(\mathbf{v})] U^\dagger(\mathbf{v}')\right) \mathrm{Tr}\left([\partial_i U(\mathbf{v}')] U^\dagger(\mathbf{v}) \right) \right\rangle_x,$$

$$\mathcal{F}_{gg}^{(3)}(x, q_\perp) \equiv -\frac{4}{g_s^2} \int \frac{\mathrm{d}^2 \mathbf{v}\mathrm{d}^2 \mathbf{v}'}{(2\pi)^3} e^{-i\mathbf{q}_\perp \cdot (\mathbf{v}-\mathbf{v}')} \mathrm{Tr}\left\langle [\partial_i U(\mathbf{v})] U^\dagger(\mathbf{v}') [\partial_i U(\mathbf{v}')] U^\dagger(\mathbf{v}) \right\rangle_x,$$

$$\qquad (13.49)$$

as well as their 'polarized partners' $\mathcal{H}_{gg}^{(1)}$, $\mathcal{H}_{gg}^{(2)}$, and $\mathcal{H}_{gg}^{(3)}$, given by

$$\mathcal{H}_{gg}^{(1)}(x, q_\perp) \equiv \left(\frac{2q_\perp^i q_\perp^j}{q_\perp^2} - \delta^{ij} \right) \frac{4}{g_s^2} \frac{1}{N_c} \int \frac{\mathrm{d}^2 \mathbf{v}\mathrm{d}^2 \mathbf{v}'}{(2\pi)^3} e^{-i\mathbf{q}_\perp \cdot (\mathbf{v}-\mathbf{v}')}$$

$$\left\langle \mathrm{Tr}\left([\partial_i U(\mathbf{v})]\left[\partial_j U^\dagger(\mathbf{v}')\right]\right) \mathrm{Tr}\left(U(\mathbf{v}') U^\dagger(\mathbf{v}) \right) \right\rangle_x,$$

$$\mathcal{H}_{gg}^{(2)}(x, q_\perp) \equiv \left(\frac{2q_\perp^i q_\perp^j}{q_\perp^2} - \delta^{ij} \right) \left(-\frac{4}{g_s^2} \right) \frac{1}{N_c} \int \frac{\mathrm{d}^2 \mathbf{v}\mathrm{d}^2 \mathbf{v}'}{(2\pi)^3} e^{-i\mathbf{q}_\perp \cdot (\mathbf{v}-\mathbf{v}')} \qquad (13.50)$$

$$\mathrm{Re}\left\langle \mathrm{Tr}\left([\partial_i U(\mathbf{v})] U^\dagger(\mathbf{v}')\right) \mathrm{Tr}\left([\partial_j U(\mathbf{v}')] U^\dagger(\mathbf{v}) \right) \right\rangle_x,$$

$$\mathcal{H}_{gg}^{(3)}(x, q_\perp) \equiv \left(\frac{2q_\perp^i q_\perp^j}{q_\perp^2} - \delta^{ij} \right) \left(-\frac{4}{g_s^2} \right) \int \frac{\mathrm{d}^2 \mathbf{v}\mathrm{d}^2 \mathbf{v}'}{(2\pi)^3} e^{-i\mathbf{q}_\perp \cdot (\mathbf{v}-\mathbf{v}')}$$

$$\mathrm{Tr}\left\langle [\partial_i U(\mathbf{v})] U^\dagger(\mathbf{v}') [\partial_j U(\mathbf{v}')] U^\dagger(\mathbf{v}) \right\rangle_x.$$

On a technical note: in Eq. (13.40), the Wilson line correlator for $\mathcal{F}_{gg}^{(1)}$ and $\mathcal{H}_{gg}^{(1)}$ that is multiplied by z^2, is complex conjugated with respect to Eq. (13.47). However, since $\mathcal{F}_{gg}^{(1)}$ and $\mathcal{H}_{gg}^{(1)}$ (and the

other TMDs) are a function of $q_\perp = |\mathbf{q}_\perp|$ and are real, it is easy to show that the result is the same as the one in definitions (13.49) and (13.50).

Introducing the angle ϕ between $\tilde{\mathbf{P}}_\perp$ and $\mathbf{q}_\perp$:

$$\frac{1}{2}\left(\frac{2\tilde{P}_i q_\perp^i \tilde{P}_j q_\perp^j}{q_\perp^2} - \tilde{P}_\perp^2\right) = \frac{1}{2}\tilde{P}_\perp^2 \cos(2\phi), \tag{13.51}$$

we obtain the following result for the cross section:

$$
\begin{aligned}
\frac{\mathrm{d}\sigma^{pA \to q\bar{q}X}}{\mathrm{d}\mathcal{P}.\mathcal{S}.} = {}& \frac{\alpha_s^2}{2C_F}\frac{z(1-z)}{(\tilde{P}_\perp^2 + m^2)^2} x_p \mathcal{G}(x_p, \mu^2)\left\{\left(P_{qg}(z) + z(1-z)\frac{2m^2\tilde{P}_\perp^2}{(\tilde{P}_\perp^2 + m^2)^2}\right)\right. \\
& \times \left(\left(z^2 + (1-z)^2\right)\mathcal{F}_{gg}^{(1)}(x, q_\perp) + 2z(1-z)\mathcal{F}_{gg}^{(2)}(x, q_\perp) - \frac{1}{N_c^2}\mathcal{F}_{gg}^{(3)}(x, q_\perp)\right) \\
& + z(1-z)\frac{2m^2\tilde{P}_\perp^2}{(\tilde{P}_\perp^2 + m^2)^2}\cos(2\phi) \\
& \left.\times \left(\left(z^2 + (1-z)^2\right)\mathcal{H}_{gg}^{(1)}(x, q_\perp) + 2z(1-z)\mathcal{H}_{gg}^{(2)}(x, q_\perp) - \frac{1}{N_c^2}\mathcal{H}_{gg}^{(3)}(x, q_\perp)\right)\right\}.
\end{aligned}
\tag{13.52}
$$

As is clear from the above formula, the information on the gluon polarization, encoded in $\mathcal{H}_{gg}^{(1,2,3)}$, couples to the mass m of the heavy quarks, and exhibits an angular dependence $\cos(2\phi)$, where ϕ is the angle between the transverse momentum of one of the jets, and the transverse-momentum imbalance of the two jets.

We will now show that the cross section Eq. (13.52) is the same as the one obtained from the TMD factorization approach. This involves, as announced, identifying the structures $\mathcal{F}_{gg}^{(1,2,3)}$ and $\mathcal{H}_{gg}^{(1,2,3)}$ as being the small-x limits of gluon TMDs. A well-known reference work which provides a 'library' of the different TMDs and their operator definitions is Ref. [79]. In order to compare with this work, let us introduce the following notation for a Wilson line with generic integration limits:

$$U(a^+, b^+; \mathbf{x}) \equiv \mathcal{P}\exp\left(ig\int_{a^+}^{b^+}\mathrm{d}x^+ A_c^-(x^+, \mathbf{x})t^c\right). \tag{13.53}$$

Note that in our conventions, the path ordering operator sets the color matrices from left to right in the order they appear along the path: the further towards the integration limit b^+, the more to the right. With this convention, we can easily prove the following identity:

$$
\begin{aligned}
\partial_i U(\mathbf{x}) &= \partial_i \mathcal{P}\exp\left(ig\int_{-\infty}^{\infty}\mathrm{d}x^+ A_c^-(x^+, \mathbf{x})t^c\right), \\
&= ig\int_{-\infty}^{\infty}\mathrm{d}z^+ U(-\infty, z^+; \mathbf{x})\left[\partial_i A_c^-(z^+, \mathbf{x})t^c\right]U(z^+, +\infty; \mathbf{x}), \\
&= ig\int_{-\infty}^{\infty}\mathrm{d}z^+ U(-\infty, z^+; \mathbf{x})F^{i-}(z^+, \mathbf{x})U(z^+, +\infty; \mathbf{x}).
\end{aligned}
\tag{13.54}
$$

In the last line of the above expression, we used the fact that, choosing a covariant gauge with $A^i, A^+ = 0$, the field strength takes the following form:

$$F^{i-}\left(x^+, \mathbf{x}\right) = \partial_i A_c^-\left(x^+, \mathbf{x}\right) t^c. \tag{13.55}$$

As an example, let us rewrite $\mathcal{F}_{gg}^{(3)}\left(x, q_\perp\right)$:

$$\mathcal{F}_{gg}^{(3)}\left(x, q_\perp\right) \equiv -\frac{4}{g_s^2} \int \frac{\mathrm{d}^2\mathbf{v}\mathrm{d}^2\mathbf{v}'}{(2\pi)^3} e^{-i\mathbf{q}_\perp\cdot(\mathbf{v}-\mathbf{v}')} \mathrm{Tr}\Big\langle \left[\partial_i U\left(\mathbf{v}\right)\right] U^\dagger\left(\mathbf{v}'\right) \left[\partial_i U\left(\mathbf{v}'\right)\right] U^\dagger\left(\mathbf{v}\right)\Big\rangle_x,$$

$$= -\frac{4}{g_s^2}\left(ig_s\right)^2 \int \frac{\mathrm{d}^3 v \mathrm{d}^3 v'}{(2\pi)^3} e^{-i\mathbf{q}_\perp\cdot(\mathbf{v}-\mathbf{v}')} \mathrm{Tr}\Big\langle U\left(-\infty, v^+; \mathbf{v}\right) F^{i-}\left(v^+, \mathbf{v}\right) \tag{13.56}$$

$$\times U\left(v^+, +\infty; \mathbf{v}\right) U^\dagger\left(\mathbf{v}'\right) U\left(-\infty, v'^+; \mathbf{v}'\right) F^{i-}\left(v'^+, \mathbf{v}'\right) U\left(v'^+, +\infty; \mathbf{v}'\right) U^\dagger\left(\mathbf{v}\right)\Big\rangle_x.$$

Using the fact that overlapping Wilson lines that are oriented in the opposite direction cancel:

$$U^\dagger\left(\mathbf{x}\right) U\left(-\infty, x^+; \mathbf{x}\right) = U\left(+\infty, x^+; \mathbf{x}\right) U\left(x^+, -\infty; \mathbf{x}\right) U\left(-\infty, x^+; \mathbf{x}\right),$$
$$= U\left(+\infty, x^+; \mathbf{x}\right), \tag{13.57}$$

expression (13.56) becomes:

$$\mathcal{F}_{gg}^{(3)}\left(x, q_\perp\right) = 4 \int \frac{\mathrm{d}^3 v \mathrm{d}^3 v'}{(2\pi)^3} e^{-i\mathbf{q}_\perp\cdot(\mathbf{v}-\mathbf{v}')} \mathrm{Tr}\Big\langle F^{i-}\left(v^+, \mathbf{v}\right) U\left(v^+, +\infty; \mathbf{v}\right) U\left(+\infty, v'^+; \mathbf{v}'\right) \tag{13.58}$$

$$\times F^{i-}\left(v'^+, \mathbf{v}'\right) U\left(v'^+, +\infty; \mathbf{v}'\right) U\left(+\infty, v^+; \mathbf{v}\right)\Big\rangle_x.$$

With the techniques explained in Sec. 6 (invariance of the CGC under translations in the transverse plane, writing the CGC average in terms of the hadron states, Eq. (6.9)), we recover the Weizsäcker-Williams gluon distribution, which we introduced in Sec. 6 and calculated in the MV model in Sec. 8:

$$\mathcal{F}_{gg}^{(3)}\left(x, q_\perp\right) = 2 \int \frac{\mathrm{d}^3\xi}{(2\pi)^3 p_A^-} e^{ixp_A^-\xi^+} e^{-i\mathbf{q}_\perp\cdot\boldsymbol{\xi}} \mathrm{Tr}\Big\langle A\Big| F^{i-}\left(\vec{\xi}\right) U^{[+]\dagger} F^{i-}\left(\vec{0}\right) U^{[+]}\Big| A\Big\rangle. \tag{13.59}$$

In the above expression, we introduced the Bjorken-x-dependent exponential $e^{ixp_A^-\xi^+}$, which in the small-x limit was set equal to one. Note this exponential is the only way in which the TMDs depend on x in the TMD factorization approach, while in the CGC-description of the TMDs: Eqs. (13.49) and (13.50), the x-dependence is hidden within the CGC averages $\langle\hat{\mathcal{O}}\rangle_x$.

Expression (13.59) proves our claim that $\mathcal{F}_{gg}^{(3)}\left(x, q_\perp\right)$, introduced as the Wilson line correlator in the decomposition Eq. (13.48), is indeed a gluon TMD in the small-x limit. Using the same techniques,

we can do the same for the other structures defined in Eqs. (13.49) and (13.50):

$$
\mathcal{F}_{gg}^{(1)}\left(x, q_\perp\right) = \frac{2}{N_c} \int \frac{\mathrm{d}^3\xi}{(2\pi)^3 p_A^-} e^{ixp_A^-\xi^+} e^{-i\mathbf{q}_\perp\cdot\boldsymbol{\xi}}
$$
$$
\left\langle A\Big|\mathrm{Tr}\left(F^{i-}\left(\vec{\xi}\right)U^{[-]\dagger}F^{i-}\left(\vec{0}\right)U^{[+]}\right)\mathrm{Tr}\left(U^{[-]}U^{[+]\dagger}\right)\Big|A\right\rangle,
$$
$$
\mathcal{F}_{gg}^{(2)}\left(x, q_\perp\right) = \frac{2}{N_c} \int \frac{\mathrm{d}^3\xi}{(2\pi)^3 p_A^-} e^{ixp_A^-\xi^+} e^{-i\mathbf{q}_\perp\cdot\boldsymbol{\xi}}
$$
$$
\mathrm{Re}\left\langle A\Big|\mathrm{Tr}\left(F^{i-}\left(\vec{\xi}\right)U^{[+]\dagger}U^{[-]}\right)\mathrm{Tr}\left(F^{i-}\left(\vec{0}\right)U^{[+]}U^{[-]\dagger}\right)\Big|A\right\rangle. \tag{13.60}
$$

As we already mentioned, the TMDs are required to be real, as well as symmetric in $\mathbf{q}_\perp$, and hence one can write equivalently:

$$
\mathcal{F}_{gg}^{(1)}\left(x, q_\perp\right) = \frac{2}{N_c} \int \frac{\mathrm{d}^3\xi}{(2\pi)^3 p_A^-} e^{-ixp_A^-\xi^+} e^{-i\mathbf{q}_\perp\cdot\boldsymbol{\xi}}
$$
$$
\left\langle A\Big|\mathrm{Tr}\left(F^{i-}\left(\vec{\xi}\right)U^{[+]\dagger}F^{i-}\left(\vec{0}\right)U^{[-]}\right)\mathrm{Tr}\left(U^{[+]}U^{[-]\dagger}\right)\Big|A\right\rangle,
$$
$$
\mathcal{F}_{gg}^{(2)}\left(x, q_\perp\right) = \frac{2}{N_c} \int \frac{\mathrm{d}^3\xi}{(2\pi)^3 p_A^-} e^{-ixp_A^-\xi^+} e^{-i\mathbf{q}_\perp\cdot\boldsymbol{\xi}}
$$
$$
\mathrm{Re}\left\langle A\Big|\mathrm{Tr}\left(F^{i-}\left(\vec{\xi}\right)U^{[-]\dagger}U^{[+]}\right)\mathrm{Tr}\left(F^{i-}\left(\vec{0}\right)U^{[-]}U^{[+]\dagger}\right)\Big|A\right\rangle. \tag{13.61}
$$

Likewise, we find the following expressions for the 'polarized' gluon TMDs $\mathcal{H}_{gg}^{(1)}$, $\mathcal{H}_{gg}^{(2)}$ and $\mathcal{H}_{gg}^{(3)}$:

$$
\mathcal{H}_{gg}^{(1)}\left(x, q_\perp\right) \equiv \left(\frac{2q_\perp^i q_\perp^j}{q_\perp^2} - \delta^{ij}\right)\frac{2}{N_c}\int\frac{\mathrm{d}^3\xi}{(2\pi)^3 p_A^-}e^{ixp_A^-\xi^+}e^{-i\mathbf{q}_\perp\cdot\boldsymbol{\xi}}
$$
$$
\left\langle A\Big|\mathrm{Tr}\left(F^{i-}\left(\vec{\xi}\right)U^{[-]\dagger}F^{j-}\left(\vec{0}\right)U^{[+]}\right)\mathrm{Tr}\left(U^{[-]}U^{[+]\dagger}\right)\Big|A\right\rangle,
$$
$$
\mathcal{H}_{gg}^{(2)}\left(x, q_\perp\right) \equiv \left(\frac{2q_\perp^i q_\perp^j}{q_\perp^2} - \delta^{ij}\right)\frac{2}{N_c}\int\frac{\mathrm{d}^3\xi}{(2\pi)^3 p_A^-}e^{ixp_A^-\xi^+}e^{-i\mathbf{q}_\perp\cdot\boldsymbol{\xi}}
$$
$$
\mathrm{Re}\left\langle A\Big|\mathrm{Tr}\left(F^{i-}\left(\vec{\xi}\right)U^{[+]\dagger}U^{[-]}\right)\mathrm{Tr}\left(F^{i-}\left(\vec{0}\right)U^{[+]}U^{[-]\dagger}\right)\Big|A\right\rangle, \tag{13.62}
$$
$$
\mathcal{H}_{gg}^{(3)}\left(x, q_\perp\right) \equiv \left(\frac{2q_\perp^i q_\perp^j}{q_\perp^2} - \delta^{ij}\right)
$$
$$
\times 2\int\frac{\mathrm{d}^3\xi}{(2\pi)^3 p_A^-}e^{ixp_A^-\xi^+}e^{-i\mathbf{q}_\perp\cdot\boldsymbol{\xi}}\mathrm{Tr}\left\langle A\Big|F^{i-}\left(\vec{\xi}\right)U^{[+]\dagger}F^{i-}\left(\vec{0}\right)U^{[+]}\Big|A\right\rangle.
$$

It is worth noting that $\mathcal{F}_{gg}^{(1)}$, $\mathcal{F}_{gg}^{(2)}$, $\mathcal{H}_{gg}^{(1)}$, and $\mathcal{H}_{gg}^{(2)}$ are not independent but can be related to each other with the help of the dipole distribution in the adjoint representation, $xG_A^{(2)}\left(x, q_\perp\right)$, defined as:

$$
xG_A^{(2)}\left(x, q_\perp\right) \equiv 4\frac{C_F}{g_s^2}\int\frac{\mathrm{d}^2\mathbf{v}\mathrm{d}^2\mathbf{v}'}{(2\pi)^3}e^{-i\mathbf{q}_\perp(\mathbf{v}-\mathbf{v}')}\frac{\partial^2}{\partial x^i\partial y^i}D_A\left(\mathbf{x}-\mathbf{y}\right)\Bigg|_{\mathbf{x}=\mathbf{v},\,\mathbf{y}=\mathbf{v}'}, \tag{13.63}
$$

where:

$$D_A\left(\mathbf{x}-\mathbf{y}\right) \equiv \frac{1}{N_c^2-1}\mathrm{Tr}\left\langle W\left(\mathbf{x}\right)W^\dagger\left(\mathbf{y}\right)\right\rangle_x. \tag{13.64}$$

We already showed in Eq. (13.30) that:

$$D_A\left(\mathbf{x}-\mathbf{y}\right) = \frac{1}{N_c^2-1}\left(\left\langle\mathrm{Tr}\left(U\left(\mathbf{x}\right)U^\dagger\left(\mathbf{y}\right)\right)\mathrm{Tr}\left(U\left(\mathbf{y}\right)U^\dagger\left(\mathbf{x}\right)\right)\right\rangle_x - 1\right). \tag{13.65}$$

Taking the derivatives, one then obtains:

$$
\begin{aligned}
&\left.\frac{\partial^2}{\partial x^i \partial y^j}D_A\left(\mathbf{x}-\mathbf{y}\right)\right|_{\mathbf{x}=\mathbf{v},\,\mathbf{y}=\mathbf{v}'} \\
&= \frac{1}{N_c^2-1}\left\{\left\langle\mathrm{Tr}\left(U\left(\mathbf{v}\right)U^\dagger\left(\mathbf{v}'\right)\right)\mathrm{Tr}\left(\left[\partial_j U\left(\mathbf{v}'\right)\right]\left[\partial_i U^\dagger\left(\mathbf{v}\right)\right]\right)\right\rangle_x\right. \\
&\quad + \left\langle\mathrm{Tr}\left(U\left(\mathbf{v}'\right)U^\dagger\left(\mathbf{v}\right)\right)\mathrm{Tr}\left(\left[\partial_i U\left(\mathbf{v}\right)\right]\left[\partial_j U^\dagger\left(\mathbf{v}'\right)\right]\right)\right\rangle_x \\
&\quad \left. + 2\mathrm{Re}\left\langle\mathrm{Tr}\left(\left[\partial_i U\left(\mathbf{v}\right)\right]U^\dagger\left(\mathbf{v}'\right)\right)\mathrm{Tr}\left(\left[\partial_j U\left(\mathbf{v}'\right)\right]U^\dagger\left(\mathbf{v}\right)\right)\right\rangle_x\right\}.
\end{aligned}
\tag{13.66}
$$

In the definitions (13.49) and (13.50) of the gluon TMDs, $\mathbf{v}$ and $\mathbf{v}'$ can be interchanged, owing to the fact that the gluon TMDs are functions of $|q_\perp|$ only. Therefore, if we multiply Eq. (13.66) with δ_{ij} and plug it into the definition of $xG_A^{(2)}\left(x,q_\perp\right)$, Eq. (13.63), the last term of the above equation becomes equal to $-\mathcal{F}_{gg}^{(2)}\left(x,q_\perp\right)$, whereas both the first and the second correlator contribute to $\mathcal{F}_{gg}^{(1)}\left(x,q_\perp\right)$, yielding the following sum rule:

$$\mathcal{F}_{gg}^{(1)}\left(x,q_\perp\right) - \mathcal{F}_{gg}^{(2)}\left(x,q_\perp\right) = xG_A^{(2)}\left(x,q_\perp\right). \tag{13.67}$$

Using the same argument, in combination with the fact that:

$$
\begin{aligned}
&xG_A^{(2)}\left(x,q_\perp\right) \\
&= 4\frac{C_F}{g_s^2}\int\frac{\mathrm{d}^2\mathbf{v}\mathrm{d}^2\mathbf{v}'}{(2\pi)^3}q_\perp^2 e^{-i\mathbf{q}_\perp(\mathbf{v}-\mathbf{v}')}D_A\left(\mathbf{v}-\mathbf{v}'\right), \\
&= 4\frac{C_F}{g_s^2}\int\frac{\mathrm{d}^2\mathbf{v}\mathrm{d}^2\mathbf{v}'}{(2\pi)^3}e^{-i\mathbf{q}_\perp(\mathbf{v}-\mathbf{v}')}\left(\frac{2q_i q_j}{q_\perp^2}-\delta_{ij}\right)\frac{\partial^2}{\partial v^i \partial v'^j}D_A\left(\mathbf{v}-\mathbf{v}'\right),
\end{aligned}
\tag{13.68}
$$

we immediately obtain as well:

$$\mathcal{H}_{gg}^{(1)}\left(x,q_\perp\right) - \mathcal{H}_{gg}^{(2)}\left(x,q_\perp\right) = xG_A^{(2)}\left(x,q_\perp\right). \tag{13.69}$$

The TMD $\mathcal{F}_{gg}^{(3)}\left(x,q_\perp\right)$ is the very well-known Weizsäcker-Williams distribution, which we introduced already in Sec. 6. It is the only gluon TMD that allows, in the light-cone gauge, for an interpretation as the number density of gluons.

14 Matching the CGC approach with the TMD calculations

In the previous section, we identified the individual TMDs that appear in the CGC cross section, Eq. (13.52). The next step is now to compare the CGC cross section itself with the results that are obtained from the calculation in the TMD approach. In order to do this, we have to rewrite our cross section in function of the Mandelstam variables Eq. (12.7). In the correlation limit, we have $k_{1\perp}^2 \simeq k_{2\perp}^2 \simeq \tilde{P}_\perp^2$, and we can easily express z and $\tilde{P}_\perp^2$ as functions of $\hat{s}$, $\hat{t}$ and $\hat{u}$:

$$z = \frac{m^2 - \hat{u}}{\hat{s}}, \quad 1 - z = \frac{m^2 - \hat{t}}{\hat{s}}, \quad \tilde{P}_\perp^2 = \frac{\hat{u}\hat{t} - m^4}{\hat{s}}. \tag{14.1}$$

With the help of the above relations, the CGC cross section, Eq. (13.52), becomes:

$$\frac{\mathrm{d}\sigma^{pA \to q\bar{q}X}}{\mathrm{d}\mathcal{P}.\mathcal{S}.} = \frac{\alpha_s^2}{2C_F} \frac{\left(m^2 - \hat{t}\right)\left(m^2 - \hat{u}\right)}{\left(\hat{u}\hat{t} + m^2\hat{s} - m^4\right)^2} x_p \mathcal{G}\left(x_p, \mu^2\right)$$

$$\left\{ \left(\frac{\left(m^2 - \hat{t}\right)^2 + \left(m^2 - \hat{u}\right)^2}{2\hat{s}^2} + 2m^2 \frac{\hat{u}\hat{t} - m^4}{\hat{s}} \frac{\left(m^2 - \hat{t}\right)\left(m^2 - \hat{u}\right)}{\left(\hat{u}\hat{t} + m^2\hat{s} - m^4\right)^2} \right) \right.$$

$$\times \left(\frac{\left(m^2 - \hat{t}\right)^2 + \left(m^2 - \hat{u}\right)^2}{\hat{s}^2} \mathcal{F}_{gg}^{(1)}\left(x, q_\perp\right) + 2\frac{\left(m^2 - \hat{t}\right)\left(m^2 - \hat{u}\right)}{\hat{s}^2} \mathcal{F}_{gg}^{(2)}\left(x, q_\perp\right) - \frac{1}{N_c^2} \mathcal{F}_{gg}^{(3)}\left(x, q_\perp\right) \right)$$

$$+ 2m^2 \frac{\hat{u}\hat{t} - m^4}{\hat{s}} \frac{\left(m^2 - \hat{t}\right)\left(m^2 - \hat{u}\right)}{\left(\hat{u}\hat{t} + m^2\hat{s} - m^4\right)^2} \cos\left(2\phi\right)$$

$$\left. \times \left(\frac{\left(m^2 - \hat{t}\right)^2 + \left(m^2 - \hat{u}\right)^2}{\hat{s}^2} \mathcal{H}_{gg}^{(1)}\left(x, q_\perp\right) + 2\frac{\left(m^2 - \hat{t}\right)\left(m^2 - \hat{u}\right)}{\hat{s}^2} \mathcal{H}_{gg}^{(2)}\left(x, q_\perp\right) - \frac{1}{N_c^2} \mathcal{H}_{gg}^{(3)}\left(x, q_\perp\right) \right) \right\}. \tag{14.2}$$

In the massless limit, the angular dependence is lost, and the cross section is reduced to the following expression:

$$\frac{\mathrm{d}\sigma^{pA \to q\bar{q}X}}{\mathrm{d}\mathcal{P}.\mathcal{S}.}\bigg|_{m=0} = \frac{\alpha_s^2}{2C_F} \frac{1}{\hat{s}^2} x_p \mathcal{G}\left(x_p, \mu^2\right) \frac{\hat{t}^2 + \hat{u}^2}{2\hat{u}\hat{t}}$$

$$\times \left\{ \frac{\hat{t}^2 + \hat{u}^2}{\hat{s}^2} \mathcal{F}_{gg}^{(1)}\left(x, q_\perp\right) + \frac{2\hat{u}\hat{t}}{\hat{s}^2} \mathcal{F}_{gg}^{(2)}\left(x, q_\perp\right) - \frac{1}{N_c^2} \mathcal{F}_{gg}^{(3)}\left(x, q_\perp\right) \right\}. \tag{14.3}$$

which is the same as the one obtained within the TMD framework (Eq. (65) of [76] in the large-N_c limit, Eq. (4.14) in [127] at finite-N_c).

Likewise, we find for the polarized part of the cross section (at leading order in $m^2/\tilde{P}_\perp^2$):

$$\frac{\mathrm{d}\sigma^{pA \to q\bar{q}X}}{\mathrm{d}\mathcal{P}.\mathcal{S}.}\bigg|_{\phi} = \frac{\alpha_s^2}{2C_F} \frac{1}{\hat{s}^2} x_p \mathcal{G}\left(x_p, \mu^2\right) \frac{2m^2}{\tilde{P}_\perp^2} \cos\left(2\phi\right)$$

$$\times \left\{ \frac{\hat{t}^2 + \hat{u}^2}{\hat{s}^2} \mathcal{H}_{gg}^{(1)}\left(x, q_\perp\right) + \frac{2\hat{u}\hat{t}}{\hat{s}^2} \mathcal{H}_{gg}^{(2)}\left(x, q_\perp\right) - \frac{1}{N_c^2} \mathcal{H}_{gg}^{(3)}\left(x, q_\perp\right) \right\}, \tag{14.4}$$

Using the sum rules of Eqs. (13.67) and (13.69), $\mathcal{F}_{gg}^{(2)}(x, q_\perp)$ and $\mathcal{H}_{gg}^{(2)}(x, q_\perp)$ can be eliminated in favor of the better-known adjoint dipole TMD, yielding, again in leading order of $m^2/\tilde{P}_\perp^2$:

$$\left.\frac{\mathrm{d}\sigma^{pA \to q\bar{q}X}}{\mathrm{d}\mathcal{P}.\mathcal{S}.}\right|_{m=0} = \frac{\alpha_s^2}{2C_F}\frac{1}{\hat{s}^2}x_p\mathcal{G}\left(x_p, \mu^2\right)\frac{\hat{t}^2 + \hat{u}^2}{2\hat{u}\hat{t}}$$
$$\times \left\{\mathcal{F}_{gg}^{(1)}(x, q_\perp) - \frac{2\hat{u}\hat{t}}{\hat{s}^2}xG_A^{(2)}(x, q_\perp) - \frac{1}{N_c^2}\mathcal{F}_{gg}^{(3)}(x, q_\perp)\right\}, \tag{14.5}$$

and:

$$\left.\frac{\mathrm{d}\sigma^{pA \to q\bar{q}X}}{\mathrm{d}\mathcal{P}.\mathcal{S}.}\right|_{\phi} = \frac{\alpha_s^2}{2C_F}\frac{1}{\hat{s}^2}x_p\mathcal{G}\left(x_p, \mu^2\right)\frac{2m^2}{\tilde{P}_\perp^2}\cos(2\phi)$$
$$\times \left\{\mathcal{H}_{gg}^{(1)}(x, q_\perp) - \frac{2\hat{u}\hat{t}}{\hat{s}^2}xG_A^{(2)}(x, q_\perp) - \frac{1}{N_c^2}\mathcal{H}_{gg}^{(3)}(x, q_\perp)\right\}. \tag{14.6}$$

Expressions (14.4) and (14.6) for the polarized cross section are the main analytical results of this work. In an independent study, Ref. [137], the authors follow a similar approach, but limit themselves to the GBW model for the gluon TMDs. While being equally simple as the one found in Ref. [137], our result is more general, since it is model-independent. We will demonstrate that, when explicitly evaluating the TMDs in the GBW model, Eq. (14.6) indeed coincides with the findings of our colleagues.

$\mathcal{F}_{gg}^{(1,2,3)}$ and $\mathcal{H}_{gg}^{(1,2,3)}$ can be evaluated analytically in the McLerran-Venugopalan model, at finite-N_c. The results are:

$$\mathcal{F}_{gg}^{(1)}(x, q_\perp) = \frac{S_\perp}{\alpha_s}\frac{C_F}{N_c^2}\frac{1}{32\pi^3}\int \mathrm{d}r\frac{J_0(q_\perp r)}{r}e^{-\frac{N_c}{2}\Gamma(r)}\left[64\left(e^{\frac{N_c}{2}\Gamma(r)} - 1\right)\right.$$
$$\left. - \alpha_s^2 N_c^4\mu_A^2 r^4\left(1 - 2\gamma_E + \ln 4 + \ln\frac{1}{r^2\Lambda^2}\right)^2 + 8\alpha_s N_c\left(N_c^2 - 2\right)\mu_A r^2\ln\frac{1}{r^2\Lambda^2}\right)\right] \tag{14.7}$$

$$\mathcal{H}_{gg}^{(1)}(x, q_\perp) = \frac{S_\perp}{\alpha_s}\frac{C_F}{N_c^2}\frac{1}{32\pi^3}\int \mathrm{d}r\frac{J_2(q_\perp r)}{r}e^{-\frac{N_c}{2}\Gamma(r)}\left[64\frac{1}{\ln\frac{1}{r^2\Lambda^2}}\left(e^{\frac{N_c}{2}\Gamma(r)} - 1\right)\right.$$
$$\left. + \alpha_s^2 N_c^4\mu_A^2 r^4\left(1 - 2\gamma_E + \ln 4 + \ln\frac{1}{r^2\Lambda^2}\right)^2 + 8\alpha_s\mu_A N_c\left(N_c^2 - 2\right)r^2\right] \tag{14.8}$$

$$\mathcal{F}_{gg}^{(2)}(x, q_\perp) = \frac{S_\perp}{\alpha_s}\frac{C_F}{N_c^2}\frac{1}{32\pi^3}\int \mathrm{d}r\frac{J_0(q_\perp r)}{r}e^{-\frac{N_c}{2}\Gamma(r)}\left[64\left(e^{\frac{N_c}{2}\Gamma(r)} - 1\right)\right.$$
$$\left. + N_c^4\mu_A^2\alpha_s^2 r^4\left(1 - 2\gamma_E + \ln 4 + \ln\frac{1}{r^2\Lambda^2}\right)^2 - 16\alpha_s N_c\mu_A r^2\ln\frac{1}{r^2\Lambda^2}\right] \tag{14.9}$$

$$\mathcal{H}_{gg}^{(2)}(x, q_\perp) = \frac{S_\perp}{\alpha_s}\frac{C_F}{N_c^2}\frac{1}{32\pi^3}\int \mathrm{d}r\frac{J_2(q_\perp r)}{r}e^{-\frac{N_c}{2}\Gamma(r)}$$
$$\left[64\left(e^{\frac{N_c}{2}\Gamma(r)} - 1\right)\frac{1}{\ln\frac{1}{r^2\Lambda^2}} - \alpha_s^2 N_c^4\mu_A^2 r^4\left(1 - 2\gamma_E + \ln 4 + \ln\frac{1}{r^2\Lambda^2}\right)^2 - 16\alpha_s N_c\mu_A r^2\right] \tag{14.10}$$

78

The expressions for the Weizsäcker-Williams gluon TMD, $\mathcal{F}_{gg}^{(3)}(x, q_\perp)$, and its polarized partner $\mathcal{H}_{gg}^{(3)}(x, q_\perp)$ in the MV model (see Eqs. (F.9) and (F.13)) were already established in the literature, see for instance [143–145].

We are now ready to turn to the numerical part of this work, in which we implement our gluon TMDs on the lattice and evolve them with JIMWLK. The following section is devoted to casting expressions (13.49) and (13.50) in a more appropriate form.

15   Implementation on the lattice

In this short chapter we derive, for completeness, the particular forms in which we cast the gluon TMDs in order to implement them numerically. Our starting points are the definitions Eqs. (13.49), (13.50). For example, $\mathcal{F}_{gg}^{(1)}(x, q_\perp)$ can be written as:

$$
\begin{aligned}
\mathcal{F}_{gg}^{(1)}(x, q_\perp) &= \frac{4}{g_s^2} \frac{1}{N_c} \int \frac{\mathrm{d}^2\mathbf{v}\,\mathrm{d}^2\mathbf{v}'}{(2\pi)^3} e^{-i\mathbf{q}_\perp \cdot (\mathbf{v}-\mathbf{v}')} \Big\langle \mathrm{Tr}\left([\partial_i U(\mathbf{v})]\left[\partial_i U^\dagger(\mathbf{v}')\right]\right) \mathrm{Tr}\left(U(\mathbf{v}') U^\dagger(\mathbf{v})\right) \Big\rangle_x, \\
&= \frac{4}{g_s^2} \frac{1}{N_c} \int \frac{\mathrm{d}^2\mathbf{v}\,\mathrm{d}^2\mathbf{v}'}{(2\pi)^3} e^{-i\mathbf{q}_\perp \cdot (\mathbf{v}-\mathbf{v}')} \Big\langle [\partial_i U(\mathbf{v})]_{ij}\left[\partial_i U^\dagger(\mathbf{v}')\right]_{ji} U(\mathbf{v}')_{kl} U^\dagger(\mathbf{v})_{lk} \Big\rangle_x, \\
&= \frac{4}{g_s^2} \frac{1}{N_c} \int \frac{\mathrm{d}^2\mathbf{v}\,\mathrm{d}^2\mathbf{v}'}{(2\pi)^3} e^{-i\mathbf{q}_\perp \cdot (\mathbf{v}-\mathbf{v}')} \Big\langle [\partial_i U(\mathbf{v})]_{ij} U^\dagger(\mathbf{v})_{lk}\left[\partial_i U^\dagger(\mathbf{v}')\right]_{ji} U(\mathbf{v}')_{kl} \Big\rangle_x, \\
&= \frac{4}{g_s^2} \frac{1}{N_c} \int \frac{\mathrm{d}^2\mathbf{v}\,\mathrm{d}^2\mathbf{v}'}{(2\pi)^3} e^{-i\mathbf{q}_\perp \cdot (\mathbf{v}-\mathbf{v}')} \Big\langle [\partial_i U(\mathbf{v})] U^\dagger(\mathbf{v})_{lk}\left([\partial_i U(\mathbf{v}')]_{ij} U^\dagger(\mathbf{v}')_{lk}\right)^* \Big\rangle_x, \\
&= \frac{8\pi}{g_s^2} \frac{1}{N_c} \sum_{i=1}^{2} \sum_{ij=1}^{N_c^2} \sum_{lk=1}^{N_c^2} \Big\langle \Big| \int \frac{\mathrm{d}^2\mathbf{v}}{(2\pi)^2} e^{-i\mathbf{q}_\perp \cdot \mathbf{v}} [\partial_i U(\mathbf{v})]_{ij} U^\dagger(\mathbf{v})_{lk} \Big|^2 \Big\rangle_x.
\end{aligned}
\tag{15.1}
$$

where we used the fact that:

$$
\begin{aligned}
\left[\partial_i U^\dagger(\mathbf{x})\right]_{ij} &= \left[\partial_i \mathcal{P} \exp\left(ig \int_{+\infty}^{-\infty} \mathrm{d}x^+ A_c^-(x^+, \mathbf{x}) t^c\right)\right]_{ij}, \\
&= ig \int_{+\infty}^{-\infty} \mathrm{d}z^+ U_{ik}(+\infty, z^+; \mathbf{x})\left[\partial_i A_c^-(z^+, \mathbf{x}) t_{kl}^c\right] U_{lj}(z^+, -\infty; \mathbf{x}), \\
&= \left(-ig \int_{+\infty}^{-\infty} \mathrm{d}z^+ U_{ki}(z^+, +\infty; \mathbf{x})\left[\partial_i A_c^-(z^+, \mathbf{x}) t_{lk}^c\right] U_{jl}(-\infty, z^+; \mathbf{x})\right)^*, \\
&= [\partial_i U(\mathbf{x})]_{ji}^*.
\end{aligned}
\tag{15.2}
$$

In a similar calculation, we can show that:

$$
\mathcal{F}_{gg}^{(2)}\left(x, q_\perp\right) = -\frac{8\pi}{g_s^2}\frac{1}{N_c}\sum_{ij=1}^{N_c^2}\sum_{lk=1}^{N_c^2}\mathrm{Re}\Big\langle\left(\int\frac{\mathrm{d}^2\mathbf{v}}{(2\pi)^2}e^{-i\mathbf{q}_\perp\cdot\mathbf{v}}\left[\partial_i U\left(\mathbf{v}\right)\right]_{ij}U^\dagger\left(\mathbf{v}\right)_{lk}\right)
$$
$$
\times\left(\int\frac{\mathrm{d}^2\mathbf{v}'}{(2\pi)^2}e^{-i\mathbf{q}_\perp\cdot\mathbf{v}'}U\left(\mathbf{v}'\right)_{ij}\left[\partial_i U\left(\mathbf{v}'\right)\right]_{kl}^*\right)^*\Big\rangle_x, \tag{15.3}
$$
$$
\mathcal{F}_{gg}^{(3)}\left(x, q_\perp\right) = \frac{8\pi}{g_s^2}\sum_{i=1}^{2}\sum_{ij=1}^{N_c^2}\Big\langle\Big|\int\frac{\mathrm{d}^2\mathbf{v}}{(2\pi)^2}e^{-i\mathbf{q}_\perp\cdot\mathbf{v}}U^\dagger\left(\mathbf{v}\right)\partial_i U\left(\mathbf{v}\right)\Big|_{ij}^2\Big\rangle_x.
$$

For $\mathcal{H}_{gg}^{(1)}\left(x, q_\perp\right)$, $\mathcal{H}_{gg}^{(2)}\left(x, q_\perp\right)$ and $\mathcal{H}_{gg}^{(3)}\left(x, q_\perp\right)$, we find the following formulas:

$$
\mathcal{H}_{gg}^{(1)}\left(x, q_\perp\right) = \frac{16\pi}{g_s^2}\frac{1}{N_c}\sum_{ij=1}^{N_c^2}\sum_{lk=1}^{N_c^2}\Big\langle\Big|\frac{q_\perp^i}{q_\perp}\int\frac{\mathrm{d}^2\mathbf{v}}{(2\pi)^2}e^{-i\mathbf{q}_\perp\cdot\mathbf{v}}\left[\partial_i U\left(\mathbf{v}\right)\right]_{ij}U^\dagger\left(\mathbf{v}\right)_{lk}\Big|^2\Big\rangle_x - \mathcal{F}_{gg}^{(1)}\left(x, q_\perp\right).
$$

$$
\mathcal{H}_{gg}^{(2)}\left(x, q_\perp\right) = -\frac{16\pi}{g_s^2}\frac{1}{N_c}\sum_{ij=1}^{N_c^2}\sum_{lk=1}^{N_c^2}\mathrm{Re}\Big\langle\left(\frac{q_\perp^i}{|q_\perp|}\int\frac{\mathrm{d}^2\mathbf{v}}{(2\pi)^2}e^{-i\mathbf{q}_\perp\cdot\mathbf{v}}\left[\partial_i U\left(\mathbf{v}\right)\right]_{ij}U^\dagger\left(\mathbf{v}\right)_{lk}\right)
$$
$$
\times\left(\frac{q_\perp^j}{|q_\perp|}\int\frac{\mathrm{d}^2\mathbf{v}'}{(2\pi)^2}e^{-i\mathbf{q}_\perp\cdot\mathbf{v}'}U\left(\mathbf{v}'\right)_{ij}\left[\partial_j U\left(\mathbf{v}'\right)\right]_{kl}^*\right)^*\Big\rangle_x - \mathcal{F}_{gg}^{(2)}\left(x, q_\perp\right), \tag{15.4}
$$

$$
\mathcal{H}_{gg}^{(3)}\left(x, q_\perp\right) = \frac{16\pi}{g_s^2}\sum_{ij=1}^{N_c^2}\Big\langle\Big|\frac{q_\perp^i}{|q_\perp|}\int\frac{\mathrm{d}^2\mathbf{v}}{(2\pi)^2}e^{-i\mathbf{q}_\perp\cdot\mathbf{v}}U^\dagger\left(\mathbf{v}\right)\partial_i U\left(\mathbf{v}\right)\Big|_{ij}^2\Big\rangle_x - \mathcal{F}_{gg}^{(3)}\left(x, q_\perp\right).
$$

16   Results from QCD lattice JIMWLK evolution

The JIMWLK evolution equation can be simulated on a two dimensional transverse QCD lattice. The numerical code with which we perform the evolution has been written by Claude Roiesnel, and was used previously in Ref. [1]. It is primarily based on the algorithms described in Refs. [149, 150]. The plots we show here are the results of 50 independent simulations with a lattice size $L = 1024$.

For the sake of comparison, let us assign an approximate scale to the results presented here. The saturation scale on the lattice is defined via the correlation length:

$$
R_s \equiv \frac{\sqrt{2}}{Q_s}, \tag{16.1}
$$

which in turn is determined from the numerical values of the dipole correlator, requiring:

$$
D\left(R_s\right) = e^{-1/2}. \tag{16.2}
$$

From the numerical analysis, the optimal value of the correlation length was determined to be:

$$
R_s \simeq 66\, a. \tag{16.3}
$$

If we assume a starting Bjorken-x of $x_0 = 10^{-2}$, with associated saturation scale $Q_s^2(x_0) = 0.2\,\mathrm{GeV}^2$, we can restore the lattice spacing a in the above formula and find:

$$a = \frac{\sqrt{2}}{66 \times \sqrt{0.2}}\,\mathrm{GeV}^{-1} \simeq 0.05\,\mathrm{GeV}^{-1}. \tag{16.4}$$

It is worth keeping in mind that, due to lattice and discretization effects, the lattice results are only dependable up to:

$$q_\perp a \lesssim \frac{\pi}{4}, \tag{16.5}$$

which corresponds to $q_\perp \simeq 16\,\mathrm{GeV}$. The rapidity evolution is expressed in terms of

$$\frac{\alpha_s}{\pi^2} y = \frac{\alpha_s}{\pi^2} \ln \frac{x_0}{x}, \tag{16.6}$$

where the numerical code evolves the TMDs in steps of $\left(\alpha_s/\pi^2\right)\delta y = 10^{-4}$. Choosing $\alpha_s = 0.15$, a value of $\left(\alpha_s/\pi^2\right)y = 0.1$ corresponds to $x = 10^{-5}$. The different values of $\left(\alpha_s/\pi^2\right)y$, for which we plot the numerical results, are listed in Table 1, along with the corresponding value of Bjorken-x as well as the approximate value of the saturation scale.

Our results for $\mathcal{F}_{gg}^{(1)}(x, q_\perp)$, $\mathcal{F}_{gg}^{(2)}(x, q_\perp)$ and $\mathcal{F}_{gg}^{(3)}(x, q_\perp)$ match indeed with the earlier work in Ref. [1]. Furthermore, we reproduce, at least quantitatively, the numerical results for $\mathcal{F}_{gg}^{(3)}(x, q_\perp)$ and $\mathcal{H}_{gg}^{(3)}(x, q_\perp)$ in Ref. [151].

A first important observation to be made is that the data confirms the claims we made earlier in the introduction, namely, the property that in the limit of large $q_\perp$ the HEF or $k_\perp$-factorization regime is recovered, in which the TMDs, set apart by their intricate gauge link structure, converge to a common unintegrated PDF. The sole exceptions are $\mathcal{F}_{gg}^{(2)}(x, q_\perp)$ and $\mathcal{H}_{gg}^{(2)}(x, q_\perp)$, which disappear (Fig. 20).

Furthermore, the TMDs shift towards larger values of $q_\perp$ if we evolve towards smaller values of x. This is of course to be expected from the fact that the distributions follow the saturation scale $Q_s^2(x)$, which grows when Bjorken-x becomes smaller.

The information on the gluon polarization is washed out by the evolution fairly fast: $\mathcal{H}_{gg}^{(1)}$ and $\mathcal{H}_{gg}^{(2)}$ are small to begin with, and $\mathcal{H}_{gg}^{(3)}$ is strongly suppressed after the first steps in the evolution (cf. (18)).

Finally, for very small values of $q_\perp$, $\mathcal{F}_{gg}^{(1)}(x, q_\perp)$ is equal to $\mathcal{F}_{gg}^{(2)}(x, q_\perp)$ and $\mathcal{H}_{gg}^{(1)}(x, q_\perp)$ is equal to $\mathcal{H}_{gg}^{(2)}(x, q_\perp)$. This is a consequence of the identities Eqs. (13.67) and (13.69), in combination with the fact that the adjoint dipole TMD $xG_A^{(2)}(x, q_\perp)$ disappears for $q_\perp = 0$, which follows directly from Eq. (13.68).
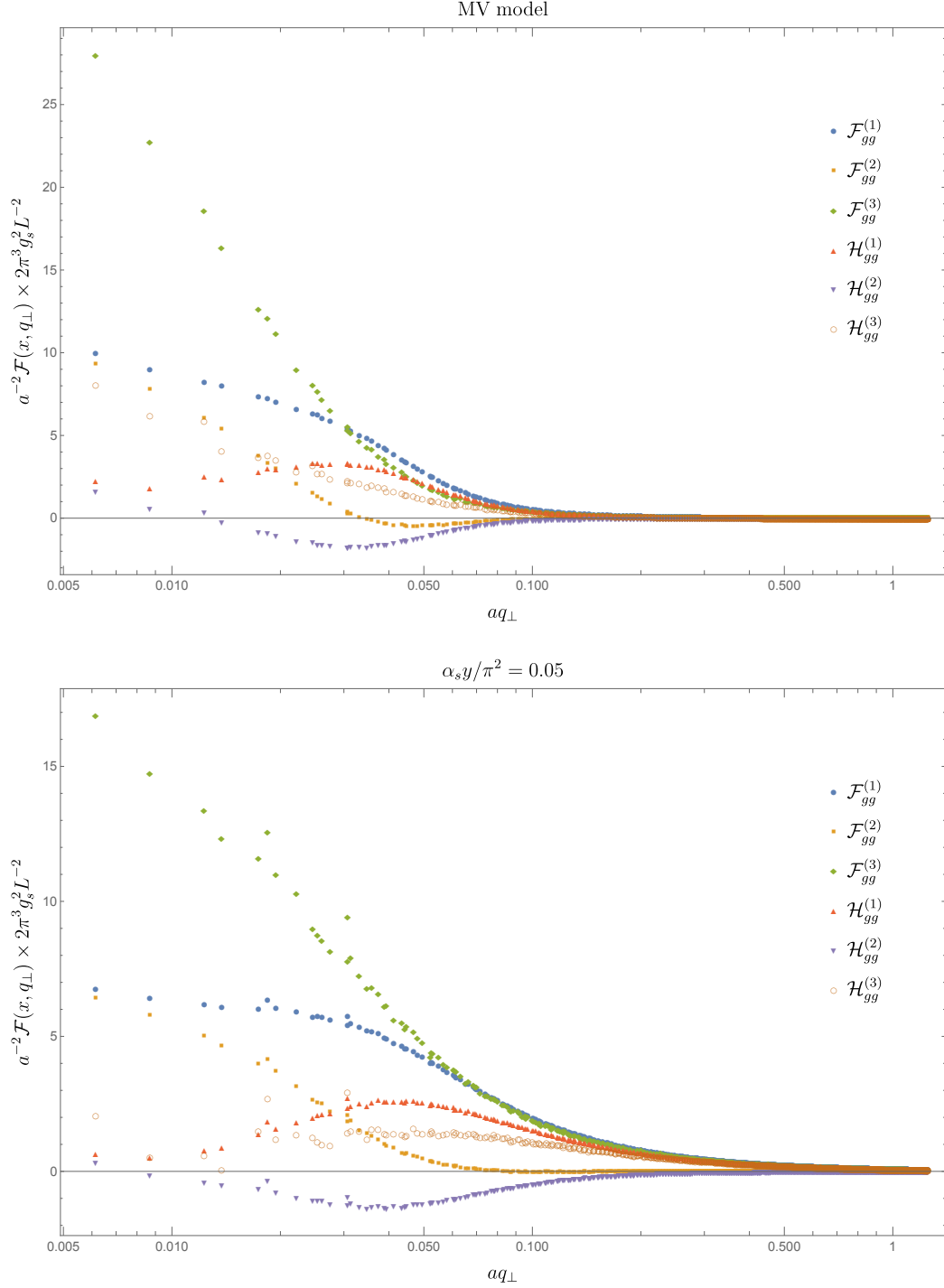
Figure 18: Above: the initial conditions (MV model) for all six gluon TMDs on the QCD lattice. Below: the gluon TMDs after 500 steps in the rapidity evolution.
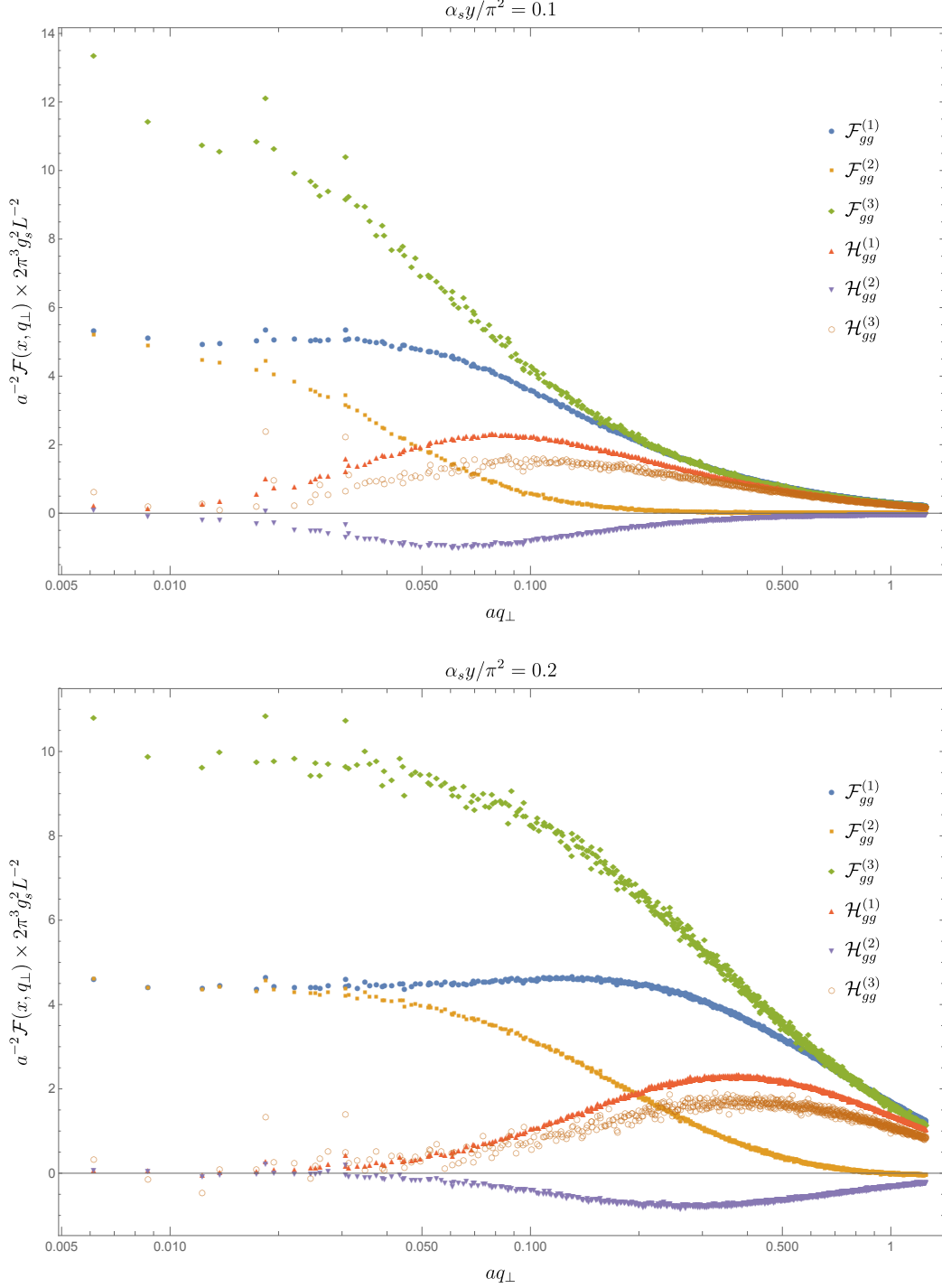
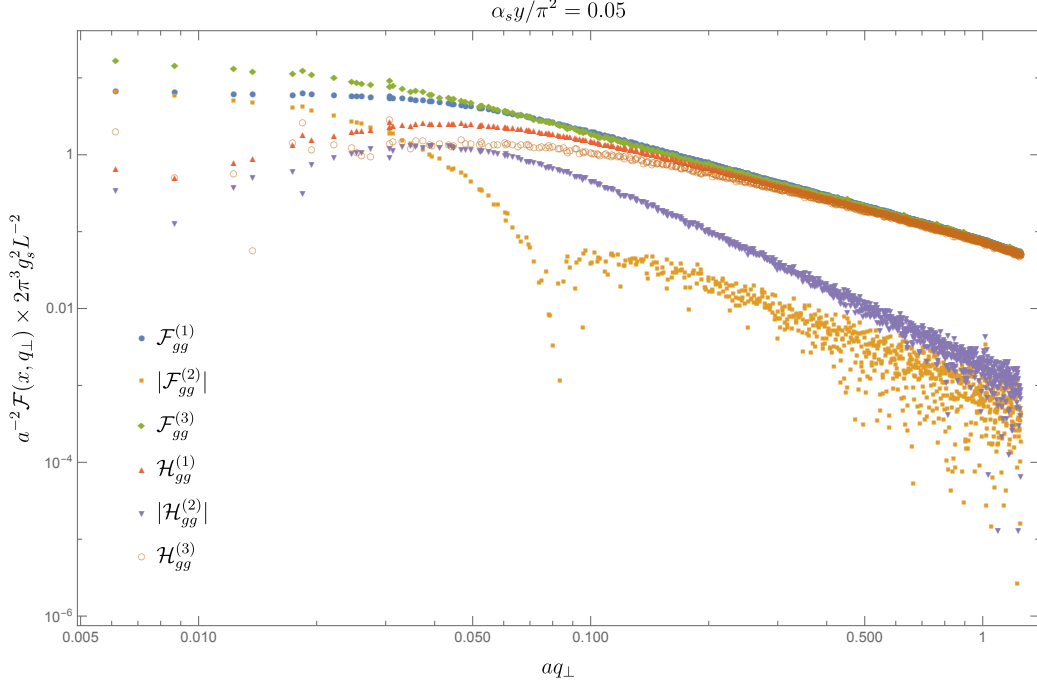Figure 19: The gluon TMDs after 1000 (above) and 2000 (below) steps in the rapidity evolution.

Figure 20: The gluon TMDs after 500 steps in the rapidity evolution with a logarithmic y-axis. The convergence of $\mathcal{F}_{gg}^{(2)}$ and $\mathcal{H}_{gg}^{(2)}$ to zero (their absolute value is depicted), for large values of $q_\perp$, is now apparent, while the other gluon TMDs exhibit the same power tail.

$\left(\alpha_s/\pi^2\right) y$	x	Q_s
0	$x_0 = 10^{-2}$	$0.4\,\mathrm{GeV}$
0.05	$4 \cdot 10^{-4}$	$0.7\,\mathrm{GeV}$
0.1	10^{-5}	$1\,\mathrm{GeV}$
0.2	$2 \cdot 10^{-8}$	$6\,\mathrm{GeV}$

Table 1: The values of $\left(\alpha_s/\pi^2\right) y$ versus Bjorken-x, and the corresponding value of the saturation scale, calculated from the dipole using Eqs. (16.2), (16.1).

17 $\quad \gamma A \to q\bar{q}X$

Before turning to the conclusions, we should remark that from our present study of dijet production in proton-nucleus collisions, the results for the photoproduction case $\gamma A \to q\bar{q}X$ appear as a simple corollary.

Indeed, when computing the $\gamma^* A \to q\bar{q}X$ cross section within the CGC, Sec. 13.1, the only difference with the case in which a photon interacts with the nucleus (for example in DIS) is the different coupling constant and the lack of color charge. Therefore, the equivalent of the term Eq. (13.13),

which encodes the interaction of the projectile with the CGC, is given by:

$$\Phi^\lambda_{ss',ij}\left(p^+, k_1^+, \mathbf{x} - \mathbf{b}\right) \equiv \left(U^\dagger_{il}(\mathbf{b})\, U_{lj}(\mathbf{x}) - 1_{ij}\right)\phi^\lambda_{s's}\left(p, k_1^+, \mathbf{x} - \mathbf{b}\right). \tag{17.1}$$

When taking the absolute value squared, Eq. (13.21), we now obtain the much simpler expression:

$$\begin{aligned}
&\int \mathcal{D}\left[\mathcal{A}\right]\left|\Phi\left(\mathcal{A}\right)\right|^2 \; _\mathcal{A}\langle 0|\left(U^\dagger_{il}(\mathbf{u})\,U_{lj}(\mathbf{v}) - 1_{ij}\right)^* \phi^{\lambda*}_{ss'}\left(p, k_1^+, \mathbf{u} - \mathbf{v}\right) \\
&\times \left(U^\dagger_{il}(\mathbf{u}')\,U_{lj}(\mathbf{v}') - 1_{ij}\right)\phi^\lambda_{ss'}\left(p, k_1^+, \mathbf{u}' - \mathbf{v}'\right)|0\rangle_\mathcal{A} \\
&= \phi^{\lambda*}_{ss'}\left(p, k_1^+, \mathbf{u} - \mathbf{v}\right)\phi^\lambda_{ss'}\left(p, k_1^+, \mathbf{u}' - \mathbf{v}'\right)\left(\text{Tr}\Big\langle U(\mathbf{u})\,U^\dagger(\mathbf{u}')\,U(\mathbf{v}')\,U^\dagger(\mathbf{v})\Big\rangle_x \right. \\
&\left. - \text{Tr}\Big\langle U(\mathbf{v})\,U^\dagger(\mathbf{u})\Big\rangle_x - \text{Tr}\Big\langle U(\mathbf{v}')\,U^\dagger(\mathbf{u}')\Big\rangle_x + N_c\right).
\end{aligned} \tag{17.2}$$

The cross section for the $\gamma A \to q\bar{q}X$ finally becomes, changing $\alpha_s \to \alpha_{em}e_q^2$:

$$\begin{aligned}
\frac{\mathrm{d}\sigma^{\gamma A \to q\bar{q}X}}{\mathrm{d}^3 k_1 \mathrm{d}^3 k_2} &= \alpha_{em}e_q^2 N_c \delta\left(k_1^+ + k_2^+ - p^+\right)\int \frac{\mathrm{d}^2\mathbf{x}}{(2\pi)^2}\frac{\mathrm{d}^2\mathbf{y}}{(2\pi)^2}\frac{\mathrm{d}^2\mathbf{x}'}{(2\pi)^2}\frac{\mathrm{d}^2\mathbf{y}'}{(2\pi)^2}e^{i\mathbf{k}_{1\perp}\cdot(\mathbf{y}-\mathbf{y}')}e^{i(\mathbf{k}_{2\perp}-\mathbf{p}_\perp)\cdot(\mathbf{x}-\mathbf{x}')} \\
&\times \sum_{\lambda ss'}\phi^{\lambda*}_{s's}\left(p^+, k_1^+, \mathbf{x} - \mathbf{y}\right)\phi^\lambda_{s's}\left(p^+, k_1^+, \mathbf{x}' - \mathbf{y}'\right) \\
&\times \left(S^{(4)}\left(\mathbf{x}, \mathbf{y}, \mathbf{y}', \mathbf{x}'\right) - D(\mathbf{y}, \mathbf{x}) - D(\mathbf{y}', \mathbf{x}') + 1\right),
\end{aligned} \tag{17.3}$$

in accordance with the result quoted in Ref. [76]. In the above expression, the familiar dipole appears, along with the gauge link structure:

$$S^{(4)}\left(\mathbf{x}, \mathbf{y}, \mathbf{y}', \mathbf{x}'\right) \equiv \frac{1}{N_c}\text{Tr}\Big\langle U(\mathbf{x})\,U^\dagger(\mathbf{x}')\,U(\mathbf{y}')\,U^\dagger(\mathbf{y})\Big\rangle_x. \tag{17.4}$$

Taking the correlation limit, we obtain:

$$\begin{aligned}
\frac{\mathrm{d}\sigma^{\gamma A \to q\bar{q}X}}{\mathrm{d}\mathcal{P}.\mathcal{S}.} &= \alpha_s\alpha_{em}e_q^2\delta\left(\frac{k_1^+ + k_2^+}{p^+} - 1\right)z(1-z)\frac{1}{(\tilde{P}_\perp^2 + m^2)^4} \\
&\times \left\{\left((\tilde{P}_\perp^4 + m^4)(z^2 + (1-z)^2) + 2m^2\tilde{P}_\perp^2\right)\mathcal{F}^{(3)}_{gg}(x, q_\perp)\right. \\
&\left. + z(1-z)\,4m^2\tilde{P}_\perp^2\cos(2\phi)\,\mathcal{H}^{(3)}_{gg}(x, q_\perp)\right\}.
\end{aligned} \tag{17.5}$$

In terms of the Mandelstam variables, we find, keeping only the leading terms in $m^2/\tilde{P}_\perp^2$:

$$\left.\frac{\mathrm{d}\sigma^{\gamma A \to q\bar{q}X}}{\mathrm{d}\mathcal{P}.\mathcal{S}.}\right|_{m=0} = \alpha_s\alpha_{em}e_q^2\delta\left(\frac{k_1^+ + k_2^+}{p^+} - 1\right)\frac{\hat{t}^2 + \hat{u}^2}{\hat{s}^3}\mathcal{F}^{(3)}_{gg}(x, q_\perp), \tag{17.6}$$

and

$$\frac{\mathrm{d}\sigma^{\gamma A \to q\bar{q}X}}{\mathrm{d}\mathcal{P}.\mathcal{S}.}\bigg|_{\phi} = 2\alpha_s \alpha_{em} e_q^2 \delta\left(\frac{k_1^+ + k_2^+}{p^+} - 1\right) \frac{\hat{u}\hat{t}}{\hat{s}^3} \frac{2m^2}{\tilde{P}_\perp^2} \cos\left(2\phi\right) \mathcal{H}_{gg}^{(3)}\left(x, q_\perp\right). \tag{17.7}$$

Since the incoming photon doesn't produce initial state radiation, as compared to the gluon in the process $pA \to q\bar{q}X$, the corresponding cross section is much simpler, and only the Weizsäcker-Williams gluon TMD $\mathcal{F}_{gg}^{(3)}\left(x, q_\perp\right)$ and its polarized partner, $\mathcal{H}_{gg}^{(3)}\left(x, q_\perp\right)$, play a role.

Incidentally, from Eq. (17.3), restoring the virtuality of the photon (hence we have to take both the longitudinal and the transverse $\gamma \to q\bar{q}$ wave function into account) and integrating over k_1 and k_2, one recovers the dipole DIS cross section, given by Eqs. (4.7) and (5.6).

18 Conclusion and outlook

In this part of the thesis, we used the Color Glass Condensate to compute the cross section for the forward production of two heavy quarks in dilute-dense, i.e. proton-nucleon collisions. In the result, given by Eqs. (13.52) or (14.2), we could discern six different Wilson line correlators, which, by comparing with TMD calculation, could be identified as the small-x limits of six gluon TMDs: three unpolarized ones, and their three partners which describe the linearly polarized gluons in the unpolarized nucleus. We obtained analytical expressions (14.7), (14.9), (14.8), (14.10), (F.9) and (F.13) for the TMDs in the McLerran-Venugopalan model at finite-N_c, and showed that, when limiting ourself to the simple Golec-Biernat and Wüsthoff model, the result of Ref. [137] is recovered. Furthermore, the gluon TMDs were implemented on the QCD lattice, and the nonlinear JIMWLK evolution in rapidity was carried out numerically, as shown in Figs. 18 and 19. As expected, the distributions we obtained are centered around the saturation momentum $Q_s\left(x\right)$, and either disappear or coincide in the limit $k_\perp \gg Q_s$.

At least in principle, our predictions could be measured at the LHC. Moreover, we showed that in the simpler process $\gamma A \to q\bar{q}X$, only two of the gluon TMDs appear: $\mathcal{F}_{gg}^{(3)}\left(x, q_\perp\right)$ and $\mathcal{H}_{gg}^{(3)}\left(x, q_\perp\right)$. These could be extracted from measurements in a future electron-ion collider (Ref. [147]), or in ultraperipheral collisions at RHIC (Ref. [152]), and be then used to constrain the four other TMDs that play a role in the $pA \to q\bar{q}X$. In addition, it should be possible to apply our calculation to proton-proton collisions at very high energies, taking care of the proton's smaller transverse area as compared to a nucleus by taking the impact-parameter dependence into account.

Finally, for completeness we should note that there are other possible sources for the azimuthal asymmetry of the heavy quarks, which are not included in our CGC analysis, see e.g. Refs. [144, 147, 153, 154].

Part IV

Renormalization of the jet quenching parameter

19 Introduction

In high-energy collisions of two heavy nuclei, an extremely dense and hot state of QCD matter is produced known as the quark-gluon plasma (QGP), see for instance Ref. [155] and references therein. Hard jets that were produced during the scattering, are attenuated by this plasma when traveling through on their way to the detector. This phenomenon and the resulting set of observables, such as dijet asymmetries, angular broadening or a suppression of the hadron yield, are collectively known as 'jet quenching' (see, e.g. Refs. [15, 156]), first theorized by J. Bjorken (Ref. [157]). Jet quenching is one of the principal probes to resolve the properties of the QGP.

In this part of the thesis, we concentrate on one aspect of jet quenching: the transverse momentum broadening of a hard parton traveling through the medium, caused by the –in general multiple– scatterings off the plasma's constituents (Refs. [158, 159]). The aim is to employ small-x techniques to study the radiative corrections, due to the emission of soft gluons, to this broadening. Since the hard parton interacts with the nuclear medium during its whole lifetime, rather than during a very short time interval, the problem differs significantly from what we encountered earlier in proton-nucleus collisions, for which the CGC approach was applicable. In particular, the medium cannot be regarded as a shockwave anymore, and as a result, to be applicable, the JIMWLK evolution equation needs to be extended beyond the eikonal approximation.

Interestingly, theoretical studies indicate that transverse momentum broadening is intimately related to jet energy loss through induced gluon radiation (Refs. [158, 160–170], or Refs. [2–4, 159, 171–180] for some recent developments). Both only depend on the medium via the so-called jet quenching parameter $\hat{q}$ (see [181] for a recent extraction), which can be regarded as a transport coefficient of the medium (Refs. [182, 183]). As it was first pointed out in [3], it turns out that the radiative corrections to the transverse momentum broadening can be absorbed into a renormalization of $\hat{q}$.

We start this part by introducing the non-eikonal (in the sense that the transverse coordinates of the soft gluon are allowed to vary during the multiple scatterings off the medium) generalization of the JIMWLK Hamiltonian, constructed in Ref. [4], and demonstrate its reduction to the regular JIMWLK evolution in the limit in which the medium is a shockwave. We then carefully analyze its structure, in particular the cancellation of divergences through the interplay of real and virtual contributions.

We then turn to the problem of transverse momentum broadening, and show how our generalized high-energy evolution equation can be applied to resum the large logarithms, associated with soft gluon radiation, which appear when calculating the radiative corrections to the broadening. To double leading logarithmic accuracy, the evolution equation can be solved analytically, resulting in a renormalization of the jet quenching parameter. Interestingly, the problem of gluon radiation in an extended medium is drastically different from the one in a shockwave, in particular, the medium introduces a mutual dependence between the longitudinal and transverse phase space of the gluon

fluctuation. As a result, the double logarithmic evolution is not the same as the one in the vacuum, which we encountered in Sec. 2.

Finally, we give an outline of the calculation in Ref. [2], in which the authors were able to compute a single iteration of the evolution to single logarithmic accuracy. During my internship with Dr. Iancu, it was the aim to try to solve evolution equation Eq. (22.12), derived in Ref. [4], which in principle contains all the leading logarithmic contributions. Solving this equation would therefore be tantamount to a full resummation of the single leading logarithms. At the present moment, however, it is not clear whether such a resummation is possible, or even meaningful, beyond DLA accuracy. Rather, we closely follow Ref. [4] and set up the approach to the problem, elucidating on the small-x physics we encountered earlier by studying the more difficult example of in-medium radiation. As such, this chapter should be seen as a case-study of a theoretical problem which is interesting in its own right, even if, ultimately, we didn't reach our original goal.

20 A general high-energy evolution equation

The Hamiltonian H for the high-energy evolution of a right-moving projectile through a dense medium is given by (see Fig. 21).

$$H = \frac{\omega}{2\pi} \int \mathrm{d}t_2 \int^{t_2} \mathrm{d}t_1 \int \mathrm{d}^2\mathbf{r}_2 \int \mathrm{d}^2\mathbf{r}_1 G_{ab}^{--}\left(t_2, \mathbf{r}_2, t_1, \mathbf{r}_1; \omega\right) J^a\left(t_2, \mathbf{r}_2\right) J^b\left(t_1, \mathbf{r}_1\right), \qquad (20.1)$$

corresponding to the following evolution equation for the S-matrix $\mathcal{O}$ of the projectile–medium interaction:

$$\frac{\partial \mathcal{O}}{\partial Y} = H\mathcal{O}. \qquad (20.2)$$

As usual, we assume that the gluon fluctuation, like its parent quark or gluon, has a longitudinal momentum component $p^+ = \omega$ that is much larger than its transverse momentum. It therefore only couples to the 'minus' field $\alpha_a \equiv A_a^-$ of the (left-moving) medium. The operator $J^a\left(t, \mathbf{r}\right)$, defined as:

$$J^a\left(t, \mathbf{r}\right) \equiv \frac{\delta}{\delta\alpha_a\left(t, \mathbf{r}\right)}, \qquad (20.3)$$

generates the emission or absorption of a soft gluon from the projectile, which is required to be built from Wilson lines:

$$U\left(\mathbf{x}\right) = \mathcal{P}e^{ig_s \int \mathrm{d}z^+ \alpha_a\left(z^+, \mathbf{r}\right)t^a}. \qquad (20.4)$$

The propagation of the soft gluon, with energy ω, through the medium, is described by the in-medium propagator G_{ab}^{--}, given by (see e.g. Refs. [4, 89]):

$$G_{ab}^{--}\left(t_2, \mathbf{r}_2, t_1, \mathbf{r}_1; \omega\right) = \frac{1}{\omega^2}\partial_{\mathbf{r}_1}^i\partial_{\mathbf{r}_2}^i G_{ab}\left(t_2, \mathbf{r}_2, t_1, \mathbf{r}_1; \omega\right) + \frac{i}{\omega^2}\delta_{ab}\delta\left(t_2 - t_1\right)\delta^{(2)}\left(\mathbf{r}_2 - \mathbf{r}_1\right). \qquad (20.5)$$

The first term in the above expression is referred to as the radiation part of the propagator, while the second term, which is instantaneous and local, is called the Coulomb part. The object $G_{ab}\left(t_2, \mathbf{r}_2, t_1, \mathbf{r}_1; \omega\right)$ is known as the scalar propagator, and is given by the non-relativistic path
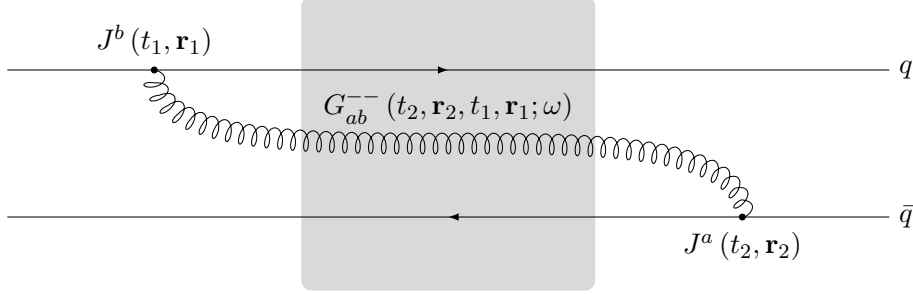
Figure 21: One step in the non-eikonal high-energy evolution of a dipole.

integral for a particle with an effective mass ω in two spatial dimensions, in a color background field:

$$G_{ab}\left(t_2, \mathbf{r}_2, t_1, \mathbf{r}_1; \omega\right) = \frac{1}{2\omega} \int \left[\mathcal{D}\mathbf{r}\left(t\right)\right] \exp\left\{i\frac{\omega}{2} \int_{t_1}^{t_2} \mathrm{d}t\, \dot{\mathbf{r}}^2\left(t\right)\right\} W_{ab}^\dagger\left(t_2, t_1, \mathbf{r}\left(t\right)\right). \tag{20.6}$$

The non-eikonal, in the sense that the transverse coordinates are allowed to vary, interaction of the soft gluon with the color fields in the medium is encoded in $W_{ab}^\dagger$, which is the generalization of a Wilson line to a functional of the gluon's transverse trajectory $\mathbf{r}\left(t\right)$:

$$W_{ab}^\dagger\left(t_2, t_1, \mathbf{r}\left(t\right)\right) \equiv \bar{\mathcal{P}} \exp\left(ig_s \int_{t_1}^{t_2} \mathrm{d}t\, \alpha_a\left(t, \mathbf{r}\left(t\right)\right) T^a\right), \tag{20.7}$$

20.1 Recovering the JIMWLK equation

To motivate the expression (20.1) for the evolution Hamiltonian, let us show that it is reduced to the JIMWLK Hamiltonian, Eq. (10.6), in the limit in which the medium is a shockwave.

Indeed, taking the shockwave to be centered around $z^+ = t = 0$, the action of the operators $J^a\left(t, \mathbf{r}\right)$ on the Wilson lines inside the S-matrix $\mathcal{O}$ yields:

$$J^a\left(t, \mathbf{r}\right) W_{\mathbf{z}}^\dagger = -ig_s \delta^{(2)}\left(\mathbf{r} - \mathbf{z}\right) W_{\mathbf{z}}^\dagger\left(\infty, t\right) T^a W_{\mathbf{z}}^\dagger\left(t, -\infty\right). \tag{20.8}$$

In the vacuum, i.e. when their path doesn't cross the shockwave, the Wilson lines become equal to one, as there is no background field for the gluon to interact with. We can then make use of the transitivity rule Eq. (A.8) to write:

$$\begin{aligned} t < 0: \quad & W_{\mathbf{z}}^\dagger = W_{\mathbf{z}}^\dagger\left(\infty, t\right) W_{\mathbf{z}}^\dagger\left(t, -\infty\right) = W_{\mathbf{z}}^\dagger\left(\infty, t\right), \\ t > 0: \quad & W_{\mathbf{z}}^\dagger = W_{\mathbf{z}}^\dagger\left(\infty, t\right) W_{\mathbf{z}}^\dagger\left(t, -\infty\right) = W_{\mathbf{z}}^\dagger\left(t, -\infty\right), \end{aligned} \tag{20.9}$$

using which Eq. (20.8) can be simplified as follows:

$$\begin{aligned} t < 0: \quad & J^a\left(t, \mathbf{r}\right) W_{\mathbf{z}}^\dagger = R_{\mathbf{r}}^a W_{\mathbf{z}}^\dagger, \\ t > 0: \quad & J^a\left(t, \mathbf{r}\right) W_{\mathbf{z}}^\dagger = L_{\mathbf{r}}^a W_{\mathbf{z}}^\dagger. \end{aligned} \tag{20.10}$$

In the above formula, we introduce the 'right' and 'left' operators $R_{\mathbf{r}}^a$ and $L_{\mathbf{r}}^a$, defined by their action on a Wilson line:

$$
\begin{aligned}
R_{\mathbf{r}}^a W_{\mathbf{z}}^\dagger &\equiv -ig_s \delta^{(2)}\left(\mathbf{r}-\mathbf{z}\right) W_{\mathbf{z}}^\dagger T^a, \\
L_{\mathbf{r}}^a W_{\mathbf{z}}^\dagger &\equiv -ig_s \delta^{(2)}\left(\mathbf{r}-\mathbf{z}\right) T^a W_{\mathbf{z}}^\dagger,
\end{aligned}
\tag{20.11}
$$

and:

$$
\begin{aligned}
R_{\mathbf{r}}^a W_{\mathbf{z}} &\equiv ig_s \delta^{(2)}\left(\mathbf{r}-\mathbf{z}\right) T^a W_{\mathbf{z}}, \\
L_{\mathbf{r}}^a W_{\mathbf{z}} &\equiv ig_s \delta^{(2)}\left(\mathbf{r}-\mathbf{z}\right) W_{\mathbf{z}} T^a.
\end{aligned}
\tag{20.12}
$$

The operators $J^a(t,\mathbf{r})$ thus generate a gluon vertex either before or after the shockwave. An important feature of Eq. (20.10) is that it is independent of time. Therefore, assuming that the S-matrix $\mathcal{O}$ is built from Wilson lines and is time-independent as well, so is the action of $J(t,\mathbf{r})$ on $\mathcal{O}$. As a consequence, the problem of the full time integration in Eq. (20.1) is reduced to the much simpler problem of evaluating the integrals over t_1 and t_2 over the in-medium propagator Eq. (20.5) in the shockwave limit:

$$
\int \mathrm{d}t_2 \int^{t_2} \mathrm{d}t_1 G_{ab}^{--}\left(t_2,\mathbf{r}_2,t_1,\mathbf{r}_1;\omega\right).
\tag{20.13}
$$

One distinguishes three different cases, corresponding to three different regions for the time integrations in Eq. (20.1). In the first two cases:

$$
-\infty < t_1 \leq t_2 < 0 \quad \text{or} \quad 0 < t_1 \leq t_2 < \infty,
\tag{20.14}
$$

the gluon is emitted and reabsorbed prior to, or after, the interaction with the shockwave (similar to diagrams (a) and (c) in the dipole-shockwave scattering in Fig. 11). The gluon fluctuation thus takes place in the vacuum, and the Wilson line functional Eq. (20.7), encoding the gluon's interaction with the color background, becomes simply:

$$
W_{ab}^\dagger\left(t_2,t_1,\mathbf{r}\left(t\right)\right) \overset{\text{vacuum}}{\to} \delta_{ab}.
\tag{20.15}
$$

Correspondingly, the scalar propagator, Eq. (20.6), reduces to the non-relativistic two-dimensional propagator, familiar from quantum mechanics:

$$
\begin{aligned}
G_{ab}\left(t_2,\mathbf{r}_2,t_1,\mathbf{r}_1;\omega\right) &\overset{\text{vacuum}}{\to} \frac{\delta_{ab}}{2\omega} G_0\left(t_2,\mathbf{r}_2,t_1,\mathbf{r}_1;\omega\right), \\
&\equiv \frac{\delta_{ab}}{2\omega} \int \left[\mathcal{D}\mathbf{r}\left(t\right)\right] \exp\left\{i\frac{\omega}{2}\int_{t_1}^{t_2}\mathrm{d}t\,\dot{\mathbf{r}}^2\left(t\right)\right\}, \\
&= \frac{\delta_{ab}}{2\omega}\int \frac{\mathrm{d}^2\mathbf{k}_\perp}{(2\pi)^2} e^{i\mathbf{k}_\perp\left(\mathbf{r}_2-\mathbf{r}_1\right)} e^{-i\frac{k_\perp^2}{2\omega}\left(t_2-t_1\right)}.
\end{aligned}
\tag{20.16}
$$

To proceed, let us focus on the case in which the gluon fluctuation takes place before the collision: $-\infty < t_1 \leq t_2 < 0$. The time integrations over the radiation piece of the in-medium propagator can

be performed as follows:

$$\int_{-\infty}^{0} dt_2 \int_{-\infty}^{t_2} dt_1 G_{ab,0,\mathrm{rad}}^{--} \left(t_2, \mathbf{r}_2, t_1, \mathbf{r}_1; \omega\right),$$

$$= \frac{\delta_{ab}}{2\omega^3} \int_{-\infty}^{0} dt_2 \int_{-\infty}^{t_2} dt_1 \partial_{\mathbf{r}_1}^{i} \partial_{\mathbf{r}_2}^{i} \int \frac{d^2 \mathbf{k}_\perp}{(2\pi)^2} e^{i\mathbf{k}_\perp (\mathbf{r}_2 - \mathbf{r}_1)} e^{-i\frac{k_\perp^2}{2\omega}(t_2 - t_1)} e^{\epsilon(t_2 + t_1)},$$

$$= \frac{\delta_{ab}}{2\omega^3} \int_{-\infty}^{0} dt_2 \int \frac{d^2 \mathbf{k}_\perp}{(2\pi)^2} k_\perp^2 e^{i\mathbf{k}_\perp (\mathbf{r}_2 - \mathbf{r}_1)} \frac{e^{2\epsilon t_2}}{ik^- + \epsilon}, \tag{20.17}$$

$$= \frac{\delta_{ab}}{2\omega^3} \int \frac{d^2 \mathbf{k}_\perp}{(2\pi)^2} k_\perp^2 e^{i\mathbf{k}_\perp (\mathbf{r}_2 - \mathbf{r}_1)} \left(\frac{1}{2\epsilon} \frac{1}{ik^-} + \frac{1}{2} \frac{1}{(k^-)^2} + \mathcal{O}(\epsilon) \right),$$

where we wrote $k^- = k_\perp^2/2\omega$. In the calculation above, we introduced an infinitesimal constant $\epsilon > 0$ to parametrize the divergences stemming from gluon fluctuations in the far past. The finite (in ϵ) part of Eq. (20.17) yields (using Eq. (B.2)):

$$\frac{\delta_{ab}}{\omega} \int \frac{d^2 \mathbf{k}_\perp}{(2\pi)^2} \frac{1}{k_\perp^2} e^{i\mathbf{k}_\perp (\mathbf{r}_2 - \mathbf{r}_1)} = \frac{\delta_{ab}}{\omega} \frac{1}{(2\pi)^2} \int d^2 \mathbf{z} \, \mathcal{K}_{\mathbf{r}_1 \mathbf{r}_2 \mathbf{z}}, \tag{20.18}$$

while we obtain for the singular part:

$$-\frac{i}{2\epsilon} \frac{\delta_{ab}}{\omega^2} \int \frac{d^2 \mathbf{k}_\perp}{(2\pi)^2} e^{i\mathbf{k}_\perp (\mathbf{r}_2 - \mathbf{r}_1)} = -\frac{i}{2\epsilon} \frac{\delta_{ab}}{\omega^2} \delta^{(2)} \left(\mathbf{r}_2 - \mathbf{r}_1\right). \tag{20.19}$$

The 'large-time' divergency when $\epsilon \to 0$ (see Fig. 22) is not physical, and has to cancel with the similar large-time divergency coming from the Coulomb part of the propagator. Indeed, we have:

$$\int_{-\infty}^{0} dt_2 \int_{-\infty}^{t_2} dt_1 G_{ab,0,\mathrm{Coul}}^{--} \left(t_2, \mathbf{r}_2, t_1, \mathbf{r}_1; \omega\right)$$

$$= \frac{1}{2} \int_{-\infty}^{0} dt_2 \int_{-\infty}^{0} dt_1 \frac{i}{\omega^2} \delta_{ab} \delta\left(t_2 - t_1\right) \delta^{(2)} \left(\mathbf{r}_2 - \mathbf{r}_1\right) e^{\epsilon(t_2 + t_1)}, \tag{20.20}$$

$$= \frac{i}{2\epsilon} \frac{1}{\omega^2} \delta_{ab} \delta^{(2)} \left(\mathbf{r}_2 - \mathbf{r}_1\right),$$

which is exactly the opposite of Eq. (20.19).

In conclusion, performing the time integrations over the in-medium propagator, corresponding to a gluon fluctuation before the shockwave, yields:

$$\int_{-\infty}^{0} dt_2 \int_{-\infty}^{t_2} dt_1 G_{ab}^{--} \left(t_2, \mathbf{r}_2, t_1, \mathbf{r}_1; \omega\right) = \frac{\delta_{ab}}{\omega} \frac{1}{(2\pi)^2} \int_{\mathbf{z}} \mathcal{K}_{\mathbf{r}_1 \mathbf{r}_2 \mathbf{z}}. \tag{20.21}$$

When the gluon fluctuation takes place after the scattering: $0 < t_1 \leq t_2 < \infty$, exactly the same result is found. This time, the large-time divergences correspond to fluctuations in the far future (see Fig. 22), and are once again cancelled between the radiative and the Coulomb part of the propagator.

Let us now study the case where the soft gluon crosses the shockwave:

$$-\infty < t_1 < 0 < t_2 < \infty. \tag{20.22}$$

The Coulomb part of the propagator (20.1) disappears, since it is local in time, hence we only have to compute the radiative term. Because the medium is a shockwave, we can make the usual assumption that the transverse position of the gluon doesn't change during the scattering. As a result, the Wilson line functional $W_{ab}^{\dagger}(t_2, t_1, \mathbf{r}(t))$ reduces to the familiar, eikonal, Wilson line $W_{ab}^{\dagger}(t_2, t_1, \mathbf{r}(0))$, and the scalar propagator, Eq. (20.6), can be simplified as follows:

$$
\begin{aligned}
G_{ab}(t_2, \mathbf{r}_2, t_1, \mathbf{r}_1; \omega) &= \frac{1}{2\omega} \int [\mathcal{D}\mathbf{r}(t)] \exp\left\{i\frac{\omega}{2} \int_{t_1}^{t_2} \mathrm{d}t\, \dot{\mathbf{r}}^2(t)\right\} W_{ab}^{\dagger}(t_2, t_1, \mathbf{r}(t)), \\
&= \frac{1}{2\omega} \int [\mathcal{D}\mathbf{r}(t)] \exp\left\{i\frac{\omega}{2} \int_{t_1}^{t_2} \mathrm{d}t\, \dot{\mathbf{r}}^2(t)\right\} \int \mathrm{d}^2\mathbf{z}\, \delta^{(2)}(\mathbf{z} - \mathbf{r}(0)) W_{ab}^{\dagger}(t_2, t_1, \mathbf{z}), \\
&= \frac{1}{2\omega} \int \mathrm{d}^2\mathbf{z}\, G_0(t_2, \mathbf{r}_2 - \mathbf{z}; \omega) G_0(-t_1, \mathbf{z} - \mathbf{r}_1; \omega) W_{ab}^{\dagger}(\mathbf{z}),
\end{aligned} \tag{20.23}
$$

where, in the last line, we used that:

$$W_{ab}^{\dagger}(t_1 < 0 < t_2, \mathbf{z}) = W_{ab}^{\dagger}(\infty, -\infty, \mathbf{z}) = W_{ab}^{\dagger}(\mathbf{z}). \tag{20.24}$$

The time integrations in Eq. (20.13) can now be performed separately:

$$
\begin{aligned}
&\frac{1}{2\omega} \int_{-\infty}^{0} \mathrm{d}t_1 \partial_{\mathbf{r}_1}^i G_0(-t_1, \mathbf{z} - \mathbf{r}_1; \omega) \\
&= \frac{1}{2\omega} \int_{-\infty}^{0} \mathrm{d}t_1 \partial_{\mathbf{r}_1}^i \int \frac{\mathrm{d}^2\mathbf{k}_{\perp}}{(2\pi)^2} e^{i\mathbf{k}_{\perp}(\mathbf{z} - \mathbf{r}_1)} e^{i\frac{k_{\perp}^2}{2\omega}t_1} e^{\epsilon t_1}, \\
&= -\frac{i}{2\omega} \int \frac{\mathrm{d}^2\mathbf{k}_{\perp}}{(2\pi)^2} k_{\perp}^i e^{i\mathbf{k}_{\perp}(\mathbf{z} - \mathbf{r}_1)} \frac{1}{ik^- + \epsilon}, \\
&= -\int \frac{\mathrm{d}^2\mathbf{k}_{\perp}}{(2\pi)^2} \frac{k_{\perp}^i}{k_{\perp}^2} e^{i\mathbf{k}_{\perp}(\mathbf{z} - \mathbf{r}_1)} = \frac{i}{2\pi} \frac{\mathbf{r}_1^i - \mathbf{z}^i}{(\mathbf{r}_1 - \mathbf{z})^2},
\end{aligned} \tag{20.25}
$$

and analogously

$$\frac{1}{2\omega} \int_0^{\infty} \mathrm{d}t_2 \partial_{\mathbf{r}_2}^i G_0(t_2, \mathbf{r}_2 - \mathbf{z}; p^+) = \frac{i}{2\pi} \frac{\mathbf{r}_2^i - \mathbf{z}^i}{(\mathbf{r}_2^i - \mathbf{z}^i)^2}. \tag{20.26}$$

Combining these two results, we find:

$$\int_{-\infty}^{0} \mathrm{d}t_1 \int_0^{\infty} \mathrm{d}t_2 G_{ab}^{--}(t_2, \mathbf{r}_2, t_1, \mathbf{r}_1; \omega) = -\frac{1}{(2\pi)^2} \frac{2}{\omega} \int_{\mathbf{z}} \mathcal{K}_{\mathbf{r}_1 \mathbf{r}_2 \mathbf{z}} W_{ab}^{\dagger}(\mathbf{z}). \tag{20.27}$$

We evaluated the time integrals over the in-medium propagator for three different configurations, corresponding to a gluon fluctuation before and after the interaction of the dipole with the shockwave, and to a fluctuation that participates in the scattering. Combining the results (20.21) and

(20.27) with the action Eq. (20.10) of the functional derivatives $J(t, \mathbf{r})$ on the operator $\mathcal{O}$, we can finally calculate the r.h.s. of the generalized high-energy evolution equation (20.2):

$$H\mathcal{O} \stackrel{\text{shockwave}}{\to} \frac{1}{(2\pi)^3} \int_{\mathbf{xyz}} \mathcal{K}_{\mathbf{xyz}} \left(R_{\mathbf{x}}^a R_{\mathbf{y}}^a + L_{\mathbf{x}}^a L_{\mathbf{y}}^a - 2L_{\mathbf{x}}^a W_{\mathbf{z}}^{\dagger ab} R_{\mathbf{y}}^b \right) \mathcal{O}$$
$$= -H_{\text{JIMWLK}}. \tag{20.28}$$

This is indeed another formulation of the JIMWLK Hamiltonian, Eq. (10.6):

$$H_{\text{JIMWLK}} \equiv -\frac{1}{(2\pi)^3} \int_{\mathbf{xyz}} \mathcal{K}_{\mathbf{xyz}} \frac{\delta}{\delta \alpha_Y^a(\mathbf{x})} \left(1 + W_{\mathbf{x}}^\dagger W_{\mathbf{y}} - W_{\mathbf{x}}^\dagger W_{\mathbf{z}} - W_{\mathbf{z}}^\dagger W_{\mathbf{y}} \right)^{ab} \frac{\delta}{\delta \alpha_Y^b(\mathbf{y})}, \tag{20.29}$$

which can be proven with the help of definitions (20.11) and (20.12). To do so, let us observe that, for a generic operator $\mathcal{O}$ that is built from Wilson lines, the action of $L_{\mathbf{x}}^a$ and $R_{\mathbf{x}}^a$ is equivalent to:

$$L_{\mathbf{x}}^a \mathcal{O} = \frac{\delta}{\delta \alpha_Y^a(\mathbf{x})} \mathcal{O},$$
$$R_{\mathbf{x}}^a \mathcal{O} = \frac{\delta}{\delta \alpha_Y^b(\mathbf{x})} W_{\mathbf{x}}^{\dagger bc} \mathcal{O}, \tag{20.30}$$

from which it follows immediately that:

$$\left(L_{\mathbf{x}}^c L_{\mathbf{y}}^c + R_{\mathbf{x}}^c R_{\mathbf{y}}^c \right) \mathcal{O} = \frac{\delta}{\delta \alpha_Y^a(\mathbf{x})} \left(1 + W_{\mathbf{x}}^\dagger W_{\mathbf{y}} \right)^{ab} \frac{\delta}{\delta \alpha_Y^b(\mathbf{y})} \mathcal{O}. \tag{20.31}$$

Furthermore, to prove the equality:

$$2L_{\mathbf{x}}^a W_{\mathbf{z}}^{\dagger ab} R_{\mathbf{y}}^b \mathcal{O} = \frac{\delta}{\delta \alpha_Y^a(\mathbf{x})} \left(W_{\mathbf{z}}^\dagger W_{\mathbf{y}} W_{\mathbf{x}}^\dagger W_{\mathbf{z}} \right)^{ab} \frac{\delta}{\delta \alpha_Y^b(\mathbf{y})} \mathcal{O}, \tag{20.32}$$

we should show that:

$$L_{\mathbf{x}}^a W_{\mathbf{z}}^{\dagger ab} R_{\mathbf{y}}^b \mathcal{O} = L_{\mathbf{x}}^a W_{\mathbf{x}}^{\dagger ab} R_{\mathbf{z}}^b \mathcal{O}. \tag{20.33}$$

Choosing an auxiliary Wilson line $W_{\mathbf{u}}^\dagger$, we find that the l.h.s. of the above equation is equal to (using the short-hand notation $\delta_{\mathbf{xy}} = \delta^{(2)}(\mathbf{x} - \mathbf{y})$):

$$L_{\mathbf{x}}^a W_{\mathbf{z}}^{\dagger ac} W_{\mathbf{y}}^{cb} L_{\mathbf{y}}^b W_{\mathbf{u}}^\dagger = -ig_s \delta_{\mathbf{yu}} L_{\mathbf{x}}^a W_{\mathbf{z}}^{\dagger ac} W_{\mathbf{y}}^{cb} T^b W_{\mathbf{u}}^\dagger,$$
$$= g_s^2 \delta_{\mathbf{yu}} \delta_{\mathbf{xy}} W_{\mathbf{z}}^{\dagger ac} W_{\mathbf{y}}^{cd} T_{db}^a T^b W_{\mathbf{u}}^\dagger - g_s^2 \delta_{\mathbf{yu}} \delta_{\mathbf{xu}} W_{\mathbf{z}}^{\dagger ac} W_{\mathbf{y}}^{cb} T^b T^a W_{\mathbf{u}}^\dagger, \tag{20.34}$$
$$= -g_s^2 \delta_{\mathbf{yu}} \delta_{\mathbf{xy}} W_{\mathbf{z}}^{\dagger ac} W_{\mathbf{y}}^{cb} T^a T^b W_{\mathbf{u}}^\dagger,$$

where we used that $L_{\mathbf{x}}^a W_{\mathbf{z}}^{\dagger ac} \propto T_{ac}^a = 0$, as well as:

$$\left[T^a, T^b \right] = -T_{bc}^a T^c. \tag{20.35}$$

The r.h.s. of Eq. (20.33) gives:

$$
\begin{aligned}
L_\mathbf{x}^a W_\mathbf{x}^{\dagger ac} W_\mathbf{z}^{cb} L_\mathbf{y}^b W_\mathbf{u}^\dagger &= -ig_s \delta_\mathbf{yu} L_\mathbf{x}^a W_\mathbf{x}^{\dagger ac} W_\mathbf{z}^{cb} T^b W_\mathbf{u}^\dagger, \\
&= g_s^2 \delta_\mathbf{yu} \delta_\mathbf{xz} W_\mathbf{x}^{\dagger ac} W_\mathbf{z}^{cd} T_{db}^a T^b W_\mathbf{u}^\dagger - g_s^2 \delta_\mathbf{yu} \delta_\mathbf{xu} W_\mathbf{x}^{\dagger ac} W_\mathbf{z}^{cb} T^b T^a W_\mathbf{u}^\dagger, \qquad (20.36) \\
&= -g_s^2 \delta_\mathbf{yu} \delta_\mathbf{xu} W_\mathbf{z}^{\dagger bc} W_\mathbf{x}^{ca} T^b T^a W_\mathbf{u}^\dagger,
\end{aligned}
$$

which is equal to Eq. (20.34), thus proving relation (20.33). It is then easy to check that Eq. (20.32) follows from Eq. (20.33), concluding our proof of the equivalence of the Hamiltonians (20.29) and (20.28).

20.2   Local form of the evolution Hamiltonian

We showed that, in the limit where the medium is a shockwave, the high-energy evolution Hamiltonian, Eq. (20.1) is reduced to the familiar JIMWLK Hamiltonian. The next step in our analysis is to study our Hamiltonian in the general case of an extended medium, scrutinizing the possible divergences, and explicitly verifying their cancellation.

First, notice that when deriving the JIMWLK equation (cf. Sec. 9), we were never bothered by large-time divergences, such as the ones we encountered in the previous paragraph. The reason for this is that in the case of JIMWLK, the gluon fluctuation was always confined to the rapidity bin $Y + \mathrm{d}Y \simeq \ln x^+ + \mathrm{d}x^+/x^+$ under consideration, and hence to a fixed interval of the longitudinal position, centered around the position of the shockwave. In the present case, however, time is a variable over which we integrate. Therefore, the operators $J^a(t, \mathbf{r})$ need to be supplemented with an exponential cutoff, which parametrizes the spurious large-time divergences:

$$
J^a(t, \mathbf{r}) \rightarrow J^a(t, \mathbf{r}) e^{-\epsilon|t|}, \qquad (20.37)
$$

just like we did in the calculations in the previous paragraph.

With this adjustment, let us study the evolution Hamiltonian (20.1) in the vacuum, which we can do by setting the gluon fields in the target equal to zero: $\alpha_a = 0$. Since, in this case, the action of the functional derivatives $J^a(t, \mathbf{x})$ becomes time-independent, we can once again explicitly perform the time integrations over the in-medium propagator Eq. (20.5):

$$
G_{0,ab}^{--}(t_2, \mathbf{r}_2, t_1, \mathbf{r}_1; \omega) = \frac{\delta_{ab}}{2\omega^3} \partial_{\mathbf{r}_1}^i \partial_{\mathbf{r}_2}^i G_0(t_2, \mathbf{r}_2, t_1, \mathbf{r}_1; \omega) + \frac{i}{\omega^2} \delta_{ab} \delta(t_2 - t_1) \delta^{(2)}(\mathbf{r}_2 - \mathbf{r}_1). \qquad (20.38)
$$

The integrations over the radiation part yield, plugging in Eq. (20.16) for the scalar propagator in

Fourier space and in the vacuum:

$$
\int \mathrm{d}t_2 \int \mathrm{d}t_1 G_{0,\mathrm{rad}}^{--} \left(t_2, t_1, \mathbf{k}_\perp; \omega\right) e^{-\epsilon|t_2|} e^{-\epsilon|t_1|}
$$

$$
= \frac{k_\perp^2}{2\omega^3} \int_{-\infty}^{+\infty} \mathrm{d}t_2 \int_{-\infty}^{t_2} \mathrm{d}t_1 e^{-ik^-(t_2-t_1)} e^{-\epsilon|t_2|} e^{-\epsilon|t_1|},
$$

$$
= \frac{k_\perp^2}{2\omega^3} \int_0^{+\infty} \mathrm{d}t_2 \left(\left. \frac{e^{-ik^-(t_2-t_1)} e^{-\epsilon t_1}}{ik^- - \epsilon} \right|_0^{t_2} + \left. \frac{e^{-ik^-(t_2-t_1)} e^{\epsilon t_1}}{ik^- + \epsilon} \right|_{-\infty}^0 \right) e^{-\epsilon t_2} \tag{20.39}
$$

$$
+ \frac{k_\perp^2}{2\omega^3} \int_{-\infty}^0 \mathrm{d}t_2 \left. \frac{e^{-ik^-(t_2-t_1)} e^{\epsilon t_1}}{ik^- + \epsilon} \right|_{-\infty}^{t_2} e^{\epsilon t_2} = -\frac{i}{\omega^2} \frac{1}{\epsilon},
$$

which cancels precisely with the time integrations over the Coulomb part of the propagator:

$$
\int \mathrm{d}t_2 \int \mathrm{d}t_1 G_{0,\mathrm{Coul}}^{--} \left(t_2, t_1, \mathbf{k}_\perp; \omega\right) e^{-\epsilon|t_2|} e^{-\epsilon|t_1|}
$$

$$
= \frac{i}{\omega^2} \int_{-\infty}^{+\infty} \mathrm{d}t_2 \int_{-\infty}^{t_2} \mathrm{d}t_1 \delta\left(t_2 - t_1\right) e^{-\epsilon|t_2|} e^{-\epsilon|t_1|}, \tag{20.40}
$$

$$
= \frac{i}{\omega^2} \int_{-\infty}^{+\infty} \mathrm{d}t_2 e^{-2\epsilon|t_2|} = \frac{i}{\omega^2} \frac{1}{\epsilon}.
$$

As a result, integrating the in-medium propagator over time, in the absence of interactions with the medium, yields zero:

$$
\int \mathrm{d}t_2 \int \mathrm{d}t_1 G_{0,ab}^{--} \left(t_2, t_1, \mathbf{k}_\perp; \omega\right) e^{-\epsilon|t_2|} e^{-\epsilon|t_1|} = 0, \tag{20.41}
$$

or equivalently:

$$
H\mathcal{O}|_{\alpha=0} = 0. \tag{20.42}
$$

Rather than being a mathematical coincidence, the above equality is required to be fulfilled on physical grounds. Indeed, in the absence of scattering, whatever fluctuations take place in the projectile, they cannot influence the evolution of the S-matrix. In the vacuum, the action of the evolution Hamiltonian on an S-matrix therefore has to disappear.

Remarkably, property (20.42) can be exploited to rewrite the action of the Hamiltonian on an observable in an alternative way, in which the various cancellations of infinities take place locally in time. Returning to the case of an extended medium, that is $\alpha_a \neq 0$, the action of the two functional

derivatives on a dipole $D_Y (\mathbf{x} - \mathbf{y}) \equiv \langle S_{\mathbf{xy}} \rangle_Y$ is:

$$
\begin{aligned}
& J^b (t_2, \mathbf{r}_2) \, J^a (t_1, \mathbf{r}_1) \, D_Y (\mathbf{x} - \mathbf{y}) \\
& = -g_s^2 \delta_{\mathbf{xr}_1} \delta_{\mathbf{xr}_2} \frac{1}{N_c} \mathrm{Tr} \Big\langle U_{\mathbf{x}}^\dagger (\infty, t_2) \, t^b U_{\mathbf{x}}^\dagger (t_2, t_1) \, t^a U_{\mathbf{x}}^\dagger (t_1, -\infty) \, U_{\mathbf{y}} \Big\rangle_Y \\
& \quad + g_s^2 \delta_{\mathbf{xr}_1} \delta_{\mathbf{yr}_2} \frac{1}{N_c} \mathrm{Tr} \Big\langle U_{\mathbf{x}}^\dagger (\infty, t_1) \, t^a U_{\mathbf{x}}^\dagger (t_1, -\infty) \, U_{\mathbf{y}} (-\infty, t_2) \, t^b U_{\mathbf{y}} (t_2, \infty) \Big\rangle_Y \\
& \quad + g_s^2 \delta_{\mathbf{yr}_1} \delta_{\mathbf{xr}_2} \frac{1}{N_c} \mathrm{Tr} \Big\langle U_{\mathbf{x}}^\dagger (\infty, t_2) \, t^b U_{\mathbf{x}}^\dagger (t_2, -\infty) \, U_{\mathbf{y}} (-\infty, t_1) \, t^a U_{\mathbf{y}} (t_1, \infty) \Big\rangle_Y \\
& \quad - g_s^2 \delta_{\mathbf{yr}_1} \delta_{\mathbf{yr}_2} \frac{1}{N_c} \mathrm{Tr} \Big\langle U_{\mathbf{x}}^\dagger U_{\mathbf{y}} (-\infty, t_1) \, t^a U_{\mathbf{y}} (t_1, t_2) \, t^b U_{\mathbf{y}} (t_2, \infty) \Big\rangle_Y .
\end{aligned}
\tag{20.43}
$$

Assuming that the medium averages are local in time, in the spirit of the CGC (see Eq. (8.32)), they can be factorized, like we did when computing the dipole in the MV model, cf. Eq. (8.36). This yields:

$$
\begin{aligned}
& J^b (t_2, \mathbf{r}_2) \, J^a (t_1, \mathbf{r}_1) \, D_Y (\mathbf{x} - \mathbf{y}) \\
& = g_s^2 \left(\delta_{\mathbf{xr}_1} \delta_{\mathbf{yr}_2} + \delta_{\mathbf{yr}_1} \delta_{\mathbf{xr}_2} - \delta_{\mathbf{xr}_1} \delta_{\mathbf{xr}_2} - \delta_{\mathbf{yr}_1} \delta_{\mathbf{yr}_2} \right) \\
& \quad \times \Big\langle S_{\mathbf{xy}} (t_2, \infty) \Big\rangle_Y \Big\langle S_{\mathbf{xy}} (-\infty, t_1) \Big\rangle_Y \frac{1}{N_c} \mathrm{Tr} \Big\langle t^b U_{\mathbf{x}}^\dagger (t_2, t_1) \, t^a U_{\mathbf{y}} (t_1, t_2) \Big\rangle_Y .
\end{aligned}
\tag{20.44}
$$

The action of the Coulomb part of the Hamiltonian on the dipole then gives:

$$
\begin{aligned}
H_{\mathrm{Coul}} D_Y (\mathbf{x} - \mathbf{y}) &= \frac{i}{4\pi} \frac{\delta_{ab}}{\omega} \int_{t_2 t_1} \int_{\mathbf{r}_2 \mathbf{r}_1} \delta (t_2 - t_1) \, \delta^{(2)} (\mathbf{r}_2 - \mathbf{r}_1) \, J^b (t_2, \mathbf{r}_2) \, J^a (t_1, \mathbf{r}_1) \, D_Y (\mathbf{x} - \mathbf{y}) , \\
&= i \alpha_s \frac{C_F}{\omega} D_Y (\mathbf{x} - \mathbf{y}) \int_t e^{-2\epsilon |t|} \int_{\mathbf{r}_2 \mathbf{r}_1} \delta^{(2)} (\mathbf{r}_2 - \mathbf{r}_1) \left(\delta_{\mathbf{xr}_1} \delta_{\mathbf{yr}_2} + \delta_{\mathbf{yr}_1} \delta_{\mathbf{xr}_2} - \delta_{\mathbf{xr}_1} \delta_{\mathbf{xr}_2} - \delta_{\mathbf{yr}_1} \delta_{\mathbf{yr}_2} \right) , \\
&= -\delta_{\mathbf{xx}} i \alpha_s \frac{C_F}{\omega} \frac{1}{\epsilon} D_Y (\mathbf{x} - \mathbf{y}) .
\end{aligned}
\tag{20.45}
$$

Clearly, the above result is plagued by several divergences, which are illustrated in Fig. 22. As we already explained, ϵ parametrizes the large-time singularities $\epsilon \to 0$. Furthermore, there is a soft divergence when $\omega \to 0$, and finally, due to the local nature of H_{Coul}, there are transverse tadpole divergences $\delta^{(2)} (\mathbf{0})$. Since the divergent eigenvalue of the dipole in Eq. (20.45) is independent of the gluon fields in the target, we have that:

$$
\begin{aligned}
H_{\mathrm{Coul}} D_Y (\mathbf{x} - \mathbf{y}) &= -\delta_{\mathbf{xx}} i \alpha_s \frac{C_F}{\omega} \frac{1}{\epsilon} D_Y (\mathbf{x} - \mathbf{y}) , \\
&= H_{\mathrm{Coul}} D_Y (\mathbf{x} - \mathbf{y}) \big|_{\alpha = 0} \, D_Y (\mathbf{x} - \mathbf{y}) .
\end{aligned}
\tag{20.46}
$$

Therefore, by virtue of Eq. (20.42), the large-time and tadpole divergences will be cancelled by the action of H_{rad} on the dipole, like we checked explicitly in the case of a shockwave (cf. Eqs. (20.17), (20.19), and (20.20)). Using Eq. (20.42), the above identity allows us to write the action of the Hamiltonian as follows:

$$
H D_Y (\mathbf{x} - \mathbf{y}) = \left(H_{\mathrm{rad}} - H_{\mathrm{rad}} D_\tau (\mathbf{x} - \mathbf{y}) \big|_{\alpha = 0} \right) D_Y (\mathbf{x} - \mathbf{y}) ,
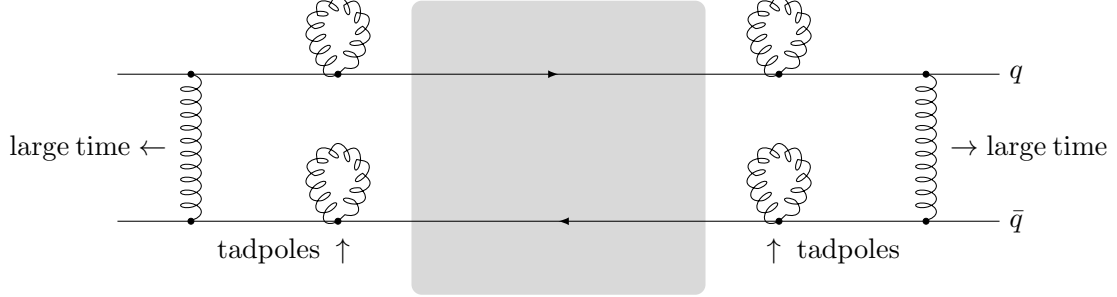\tag{20.47}
$$

Figure 22: The divergences appearing in the high-energy evolution of a dipole using the Hamiltonian Eq. (20.1).

which is now formulated only in terms of the radiation part of the Hamiltonian. Although we took the example of a dipole operator to prove the above identity, the arguments we used were generic, and therefore we expect it to hold for any gauge-invariant observable $\mathcal{O}$ built from Wilson lines:

$$H\mathcal{O} = \Big(H_{\rm rad} - H_{\rm rad}\mathcal{O}|_{\alpha=0}\Big)\mathcal{O}, \tag{20.48}$$

or, more explicitly:

$$H\mathcal{O} = \frac{\omega}{2\pi} \int_{-\infty}^{+\infty} {\rm d}t_2 \int_{-\infty}^{t_2} {\rm d}t_1 \int {\rm d}^2\mathbf{r}_2 \int {\rm d}^2\mathbf{r}_1 \Big(\mathcal{H}_{\rm rad} - \mathcal{H}_{\rm rad}\mathcal{O}|_{\alpha=0}\Big)\mathcal{O}, \tag{20.49}$$

where we defined:

$$\mathcal{H}_{\rm rad} \equiv G_{ab,{\rm rad}}^{--}\left(t_2, \mathbf{r}_2, t_1, \mathbf{r}_1; \omega\right) J^a\left(t_2, \mathbf{r}_2\right) J^b\left(t_1, \mathbf{r}_1\right). \tag{20.50}$$

Evaluating equation (20.49) in the vacuum, using $\mathcal{O}|_{\alpha=0} = 1$, we see that the property (20.42) is now satisfied locally in time and space:

$$\Big(\mathcal{H}_{\rm rad} - \mathcal{H}_{\rm rad}\mathcal{O}|_{\alpha=0}\Big)\mathcal{O}\Big|_{\alpha=0} = 0, \tag{20.51}$$

implying that the tadpole and large-time divergences are cancelled locally, before the evaluation of the integrals. When they are harmless enough, i.e. when they are logarithmic, the soft divergences $\omega \to 0$ will of course be resummed by solving the evolution equation. Moreover, since the contributions of the terms in which the gluon fluctuation doesn't cross the medium, are always independent of the background fields α, we have that:

$$\mathcal{H}_{\rm rad}^{\rm non-cross}\mathcal{O} = \mathcal{H}_{\rm rad}^{\rm non-cross}\mathcal{O}\big|_{\alpha=0}\,\mathcal{O}, \tag{20.52}$$

and therefore

$$H^{\rm non-cross}\mathcal{O} = 0. \tag{20.53}$$

Not only does this imply that only the time orderings in which the gluon fluctuation crosses the medium play a role in Eq. (20.49), the above property also assures that the evolution equation in

this form is free from large-time divergences, since these are precisely generated by the non-crossing terms.

In conclusion, Eq. (20.49) is a more robust form of the action of the Hamiltonian, in particular in cases where it is difficult to perform the time integrations explicitly. Furthermore, cast in this form, the Hamiltonian allows a probabilistic interpretation, in which the 'real term' $\mathcal{H}_{\mathrm{rad}}\mathcal{O}$ describes the change in the S-matrix due to a real emission, while the 'virtual term' $\mathcal{H}_{\mathrm{rad}}\mathcal{O}|_{\alpha=0}\mathcal{O}$ takes care of the conservation of probability.

As an example, let us calculate the action of Eq. (20.49) on the dipole S-matrix. From Eq. (20.44), in the case in which the gluon fluctuation doesn't cross the medium, the functional derivatives yield:

$$
\begin{aligned}
&J^b\left(t_2, \mathbf{r}_2\right) J^a\left(t_1, \mathbf{r}_1\right) D_Y\left(\mathbf{x}-\mathbf{y}\right) \\
&\stackrel{\text{non-cross.}}{=} g_s^2 C_F\left(\delta_{\mathbf{x}\mathbf{r}_1}\delta_{\mathbf{y}\mathbf{r}_2}+\delta_{\mathbf{y}\mathbf{r}_1}\delta_{\mathbf{x}\mathbf{r}_2}-\delta_{\mathbf{x}\mathbf{r}_1}\delta_{\mathbf{x}\mathbf{r}_2}-\delta_{\mathbf{y}\mathbf{r}_1}\delta_{\mathbf{y}\mathbf{r}_2}\right) D_Y\left(\mathbf{x}-\mathbf{y}\right), \\
&= J^b\left(t_2, \mathbf{r}_2\right) J^a\left(t_1, \mathbf{r}_1\right) D_Y\left(\mathbf{x}-\mathbf{y}\right)\Big|_{\alpha=0} D_Y\left(\mathbf{x}-\mathbf{y}\right),
\end{aligned}
\tag{20.54}
$$

confirming our assertion (20.53) that only the crossing terms play a role. For these terms, we have:

$$
\begin{aligned}
&H_{\mathrm{rad}}^{\mathrm{cross}} D_Y\left(\mathbf{x}-\mathbf{y}\right) \\
&= \frac{1}{4\pi}\frac{1}{\omega}\int_{t_2 t_1}^{\mathrm{cross}}\int_{\mathbf{r}_2\mathbf{r}_1}\partial_{\mathbf{r}_1}^i\partial_{\mathbf{r}_2}^i\frac{1}{2\omega}\int[\mathcal{D}\mathbf{r}(t)]\exp\left\{i\frac{\omega}{2}\int_{t_1}^{t_2}\mathrm{d}t\dot{\mathbf{r}}^2(t)\right\} \\
&\quad\times W_{ab}^\dagger\left(t_2, t_1, \mathbf{r}(t)\right) J^b\left(t_2, \mathbf{r}_2\right) J^a\left(t_1, \mathbf{r}_1\right) D_Y\left(\mathbf{x}-\mathbf{y}\right), \\
&= -\frac{\alpha_s}{\omega}\int_{t_2 t_1}^{\mathrm{cross}}\partial_{\mathbf{r}_1}^i\partial_{\mathbf{r}_2}^i\frac{1}{2\omega}\int[\mathcal{D}\mathbf{r}(t)]\exp\left\{i\frac{\omega}{2}\int_{t_1}^{t_2}\mathrm{d}t\dot{\mathbf{r}}^2(t)\right\} \\
&\quad\times\left\langle S_{\mathbf{x}\mathbf{y}}\left(t_2, \infty\right)\right\rangle_Y\left\langle S_{\mathbf{x}\mathbf{y}}\left(-\infty, t_1\right)\right\rangle_Y \\
&\quad\times\left(\frac{N_c}{2}\left\langle S_{\mathbf{y}\mathbf{r}(t)}\left(t_1, t_2\right) S_{\mathbf{r}(t)\mathbf{x}}\left(t_1, t_2\right)\right\rangle_Y-\frac{1}{2N_c}\left\langle S_{\mathbf{x}\mathbf{y}}\left(t_1, t_2\right)\right\rangle_Y\right)\Bigg|_{\mathbf{r}_1=\mathbf{y}}^{\mathbf{r}_1=\mathbf{x}}\Bigg|_{\mathbf{r}_2=\mathbf{y}}^{\mathbf{r}_2=\mathbf{x}}.
\end{aligned}
\tag{20.55}
$$

To obtain the last equality in the calculation above, we plugged the Wilson functional $W_{ab}^\dagger\left(t_2, t_1, \mathbf{r}(t)\right)$ into the medium average in Eq. (20.44), after which we made use of Eq. (A.10). In the vacuum limit $\alpha_a = 0$, the above result becomes:

$$
\begin{aligned}
H_{\mathrm{rad}}^{\mathrm{cross}} D_Y\left(\mathbf{x}-\mathbf{y}\right)\big|_{\alpha=0} = &-\frac{\alpha_s C_F}{\omega}\int_{t_2 t_1}^{\mathrm{cross}}\partial_{\mathbf{r}_1}^i\partial_{\mathbf{r}_2}^i \\
&\times\frac{1}{2\omega}\int[\mathcal{D}\mathbf{r}(t)]\exp\left\{i\frac{\omega}{2}\int_{t_1}^{t_2}\mathrm{d}t\dot{\mathbf{r}}^2(t)\right\}\Bigg|_{\mathbf{r}_1=\mathbf{y}}^{\mathbf{r}_1=\mathbf{x}}\Bigg|_{\mathbf{r}_2=\mathbf{y}}^{\mathbf{r}_2=\mathbf{x}},
\end{aligned}
\tag{20.56}
$$

and therefore, the r.h.s. of evolution equation (20.49) gives:

$$
\begin{aligned}
H D_Y\left(\mathbf{x}-\mathbf{y}\right) = &\frac{\alpha_s}{\omega}\frac{N_c}{2}\int_{t_2 t_1}^{\mathrm{cross}}\partial_{\mathbf{r}_1}^i\partial_{\mathbf{r}_2}^i\frac{1}{2\omega}\int[\mathcal{D}\mathbf{r}(t)]\exp\left\{i\frac{\omega}{2}\int_{t_1}^{t_2}\mathrm{d}t\dot{\mathbf{r}}^2(t)\right\} \\
&\times\left\langle S_{\mathbf{x}\mathbf{y}}\left(t_2, \infty\right)\right\rangle_Y\left\langle S_{\mathbf{x}\mathbf{y}}\left(-\infty, t_1\right)\right\rangle_Y \\
&\times\left(\left\langle S_{\mathbf{x}\mathbf{y}}\left(t_1, t_2\right)\right\rangle_Y-\left\langle S_{\mathbf{y}\mathbf{r}(t)}\left(t_1, t_2\right) S_{\mathbf{r}(t)\mathbf{x}}\left(t_1, t_2\right)\right\rangle_Y\right)\Bigg|_{\mathbf{r}_1=\mathbf{y}}^{\mathbf{r}_1=\mathbf{x}}\Bigg|_{\mathbf{r}_2=\mathbf{y}}^{\mathbf{r}_2=\mathbf{x}}.
\end{aligned}
\tag{20.57}
$$

The above formula, in combination with Eq. (20.2), is our 'master equation' for the non-eikonal high-energy evolution of a dipole through a medium. It will play a major role in the next section, where we will use it to calculate the evolution of the jet quenching parameter.

To conclude this section, let us once again consider the limit in which the medium is a shockwave, which allows us to explicitly evaluate the integrals over time:

$$
\int_{t_2 t_1}^{\text{cross}} \overset{\text{sw.}}{\to} 2 \int_{-\infty}^{0} \mathrm{d}t_1 \int_{0}^{\infty} \mathrm{d}t_2. \tag{20.58}
$$

Using the intermediate results from Eqs. (20.25) and (20.26), Eq. (20.57) becomes:

$$
\begin{aligned}
\frac{\partial}{\partial Y} D_Y (\mathbf{x} - \mathbf{y}) &= -\frac{\alpha_s C_F}{\pi^2} \int_{\mathbf{z}} \mathcal{K}_{\mathbf{r}_1 \mathbf{r}_2 \mathbf{z}} \left(\left\langle S_{\mathbf{xy}} \right\rangle_Y - \left\langle S_{\mathbf{yz}} S_{\mathbf{zx}} \right\rangle_Y \right) \Big|_{\mathbf{r}_1 = \mathbf{y}}^{\mathbf{r}_1 = \mathbf{x}} \Big|_{\mathbf{r}_2 = \mathbf{y}}^{\mathbf{r}_2 = \mathbf{x}}. \\
&= \frac{\alpha_s C_F}{\pi^2} \int_{\mathbf{z}} \mathcal{M}_{\mathbf{xyz}} \left(\left\langle S_{\mathbf{yz}} S_{\mathbf{zx}} \right\rangle_Y - \left\langle S_{\mathbf{xy}} \right\rangle_Y \right),
\end{aligned} \tag{20.59}
$$

which is of course the first equation in the Balitsky hierarchy, as expected. We should make the remark that, for a shockwave, the virtual crossing term Eq. (20.56) is:

$$
-H_{\text{rad}}^{\text{cross}} D_Y (\mathbf{x} - \mathbf{y})\big|_{\alpha=0} D_Y (\mathbf{x} - \mathbf{y}) = -\frac{\alpha_s C_F}{\pi^2} \int_{\mathbf{z}} \mathcal{M}_{\mathbf{xyz}} D_Y (\mathbf{x} - \mathbf{y}). \tag{20.60}
$$

Since this term measures the decrease in the probability to find the original dipole at the time of the interaction, we expect it to be equal to the contributions from the non-crossing gluon fluctuations, which take place before or after the interaction. That this is indeed the case, is apparent from the following calculation:

$$
\begin{aligned}
H_{\text{rad}}^{\text{non}-\text{cross}} D_Y (\mathbf{x} - \mathbf{y}) &= \frac{1}{4\pi} \frac{1}{\omega} \int_{t_2 t_1}^{\text{non}-\text{cross}} \int_{\mathbf{r}_2 \mathbf{r}_1} \partial_{\mathbf{r}_1}^i \partial_{\mathbf{r}_2}^i \frac{1}{2\omega} \int [\mathcal{D} \mathbf{r}(t)] \exp \left\{ i \frac{\omega}{2} \int_{t_1}^{t_2} \mathrm{d}t \dot{\mathbf{r}}^2(t) \right\} \\
&\times W_{ab}^\dagger (t_2, t_1, \mathbf{r}(t)) J^b (t_2, \mathbf{r}_2) J^a (t_1, \mathbf{r}_1) D_Y (\mathbf{x} - \mathbf{y}), \\
&= -\frac{\alpha_s C_F}{\omega} \int_{t_2 t_1}^{\text{non}-\text{cross}} \int_{\mathbf{r}_2 \mathbf{r}_1} \partial_{\mathbf{r}_1}^i \partial_{\mathbf{r}_2}^i \frac{1}{2\omega} \int [\mathcal{D} \mathbf{r}(t)] \exp \left\{ i \frac{\omega}{2} \int_{t_1}^{t_2} \mathrm{d}t \dot{\mathbf{r}}^2(t) \right\} \\
&\times D_Y (\mathbf{x} - \mathbf{y}) \Big|_{\mathbf{r}_1 = \mathbf{y}}^{\mathbf{r}_1 = \mathbf{x}} \Big|_{\mathbf{r}_2 = \mathbf{y}}^{\mathbf{r}_2 = \mathbf{x}} \overset{\text{sw.}}{=} -\frac{\alpha_s C_F}{\pi^2} \int_{\mathbf{z}} \mathcal{M}_{\mathbf{xyz}} D_Y (\mathbf{x} - \mathbf{y}).
\end{aligned} \tag{20.61}
$$

This further supports our assertion that the evolution process can be given a probabilistic interpretation, where $(\bar{\alpha}/2\pi) \mathcal{M}_{\mathbf{xyz}} \mathrm{d}Y \mathrm{d}^2 \mathbf{z}$ is the differential probability for a dipole, with legs at the positions $(\mathbf{x}, \mathbf{y})$, to emit a gluon with energy ω at a transverse coordinate $\mathbf{z}$.

21 Transverse momentum broadening

We are now ready to introduce (one aspect of) the problem of jet quenching, to which we aim to apply the machinery of non-eikonal high-energy evolution, on which we elaborated in the previous section.
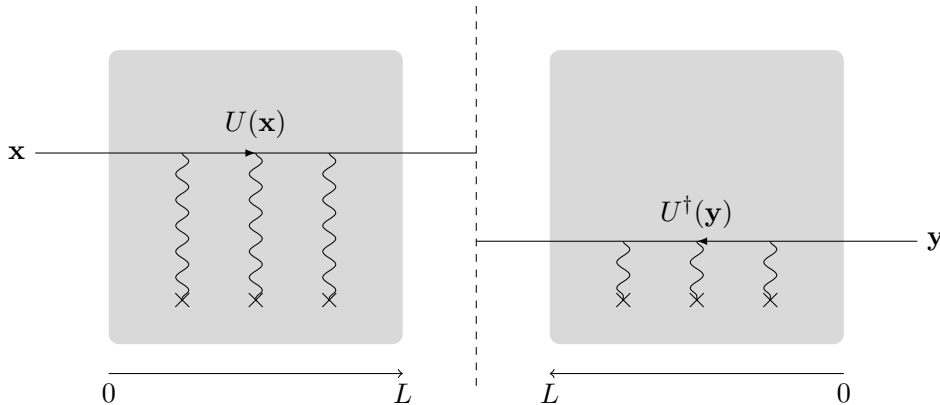
Figure 23: The leading-order cross section for the transverse momentum broadening of a parton traversing the medium.

The transverse momentum distribution of a highly energetic parton, obtained after traveling through, and interacting with, a nuclear medium (see Refs. [15, 158, 184, 185]), is easily calculated at tree level by multiplying the Wilson line in the amplitude with the one in the complex conjugate amplitude, which both resum the multiple soft scatterings of the parton with the background field in the eikonal approximation, see Fig. 23. The result is:

$$\frac{\mathrm{d}N}{\mathrm{d}^2\mathbf{k}_\perp} = \frac{1}{(2\pi)^2} \int \mathrm{d}^2\mathbf{r} e^{-i\mathbf{k}_\perp \cdot \mathbf{r}} D(\mathbf{r}), \tag{21.1}$$

where $\mathbf{r} = \mathbf{x} - \mathbf{y}$, and where $D(\mathbf{r})$ is the usual dipole, see Eq. (5.5), limited to the longitudinal extent L of the medium:

$$D(\mathbf{r}) = \exp\left(-\frac{g_s^2}{\mu_A} \frac{C_F}{2} \int_0^L \mathrm{d}x^+ \lambda_A(x^+) \Gamma(\mathbf{r})\right). \tag{21.2}$$

It should be stressed that, in contrast to e.g. DIS, the dipole in the present formalism is not a physical one, but rather a mathematical construction corresponding to the quark in the amplitude times its complex conjugate.

The second moment of the distribution Eq. (21.1) gives the transverse momentum broadening (TMB) of the parton:

$$\begin{aligned} \langle k_\perp^2 \rangle &= \int \mathrm{d}^2\mathbf{k}_\perp k_\perp^2 \frac{\mathrm{d}N}{\mathrm{d}^2\mathbf{k}_\perp}, \\ &= -\partial_\mathbf{r}^2 D(\mathbf{r})\big|_{\mathbf{r}=\mathbf{0}}. \end{aligned} \tag{21.3}$$

The above definitions are only useful if they come with a set of assumptions about the nuclear medium. First, since the parton is very fast: $p^+ = \omega \gg p_\perp$, it only interacts with the 'minus' medium gluon fields $\alpha_a(x^+, \mathbf{x}) \equiv A_a^-(x^+, \mathbf{x})$. For a weakly-coupled quark-gluon plasma, which is the medium in which we are interested, we can presume –in the spirit of the Color Glass Condensate–

that the only non-trivial gluon correlator is the two-point function:

$$\langle \alpha_a \left(x^+, \mathbf{x} \right) \alpha_b \left(y^+, \mathbf{y} \right) \rangle = \frac{1}{g_s^2} \delta_{ab} \delta \left(x^+ - y^+ \right) \lambda_A \left(x^+ \right) L \left(\mathbf{x} - \mathbf{y} \right). \tag{21.4}$$

Note that the roles of the $+$ and $-$ coordinate are reversed with respect to the corresponding expression in the MV model (see Eq. (8.32)), since in our case the nuclear medium is a left-mover. In addition, the plasma comes with a natural infrared cutoff, provided by the Debye mass m_D, which corresponds to the screening of the color interactions over a transverse distance $\sim 1/m_D$. Parametrically, we have that $m_D^2 \sim \alpha_s N_c T^2$ and $Q_s^2 \sim \alpha_s^2 N_c^2 T^3 L$ (see e.g. Ref. [173]), and therefore, for a large medium that is very hot, the Debye mass is much smaller than the saturation scale Q_s:

$$m_D \ll Q_s. \tag{21.5}$$

Finally, the medium is assumed to be uniform both in the longitudinal direction and in the transverse plane.

When $r \ll 1/m_D$, which, as we shall argue later, is always the case in the regime of our interest, the dipole can be evaluated to logarithmic accuracy in what we will call the 'MV approximation' (cf. Eqs. (8.38), (8.42) and (8.41)), yielding:

$$D \left(\mathbf{r} \right) \simeq \exp \left(-\frac{1}{4} Q_s^2 \left(r^2 \right) \mathbf{r}^2 \right),$$
$$Q_s^2 \left(r^2 \right) \equiv \alpha_s C_F \mu_A \ln \frac{1}{r^2 m_D^2}. \tag{21.6}$$

In the above formula, the transverse color charge density μ_A appears, which in the CGC was given by Eq. (8.29):

$$\mu_A \equiv g_s^2 \int \mathrm{d}z^+ \lambda_A \left(z^+ \right) = \frac{g_s^2 A}{2\pi R_A^2}. \tag{21.7}$$

In the present case, it is more appropriate to work with the number density n_0 of the color charges in the medium, related to μ_A as follows:

$$\mu_A = g_s^2 \int_0^L \mathrm{d}z^+ \lambda_A \left(z^+ \right) = g_s^2 n_0 L, \tag{21.8}$$

where we used the fact that the medium is homogeneous. Eq. (21.6) can now be rewritten as:

$$D \left(\mathbf{r} \right) \simeq \exp \left(-\frac{1}{4} \hat{q} \left(r^2 \right) L \mathbf{r}^2 \right),$$
$$\hat{q} \left(r^2 \right) \equiv \frac{Q_s^2 \left(r^2 \right)}{L} = 4\pi \alpha_s^2 C_F n_0 \ln \frac{1}{r^2 m_D^2}, \tag{21.9}$$

where we introduced the jet quenching parameter $\hat{q}$: an intrinsic scale of the nuclear medium whose significance will become more clear in what follows. Parametrically, we have that $n_0 \sim N_c T^3$ (see Ref. [173]) and hence $\hat{q} \sim \alpha_s^2 N_c^2 T^3$.

With the above expression for the dipole, we are now ready to evaluate the transverse momentum distribution, Eq. (21.1). For momenta $m_D^2 \ll k_\perp^2 \lesssim Q_s^2$, the integral over $\mathbf{r}$ is dominated by small dipole sizes $r \sim 1/Q_s$ and can be evaluated by neglecting the logarithmic dependence $\sim \ln r^2 m_D^2$ in $\hat{q}$:

$$
\begin{aligned}
\frac{\mathrm{d}N}{\mathrm{d}^2\mathbf{k}_\perp} &= \frac{1}{(2\pi)^2} \int_{1/Q_s} \mathrm{d}^2\mathbf{r}\, e^{-i\mathbf{k}_\perp \cdot \mathbf{r}} \exp\left(-\frac{1}{4}\hat{q}L\mathbf{r}^2\right), \\
&\simeq \frac{1}{\pi Q_s^2} e^{-k_\perp^2/Q_s^2}.
\end{aligned}
\tag{21.10}
$$

From Eq. (21.3), we then obtain the following result for the transverse momentum broadening:

$$
\left\langle k_\perp^2 \right\rangle = \hat{q}L = Q_s^2.
\tag{21.11}
$$

The above results imply that, within approximations of interest, the transverse momentum broadening of a parton traveling through the medium can be regarded as a diffusive process. Due to multiple soft scatterings of the parton with the medium, the system performs a random walk in transverse momentum space, corresponding to a Gaussian distribution of the parton momenta. The jet quenching parameter $\hat{q}$, introduced in Eq. (21.9), is found to be equal to the average transverse momentum broadening of the parton per unit distance. A gluon with lifetime τ thus picks up a transverse momentum:

$$
k_{\mathrm{br}}^2 (\tau) = \hat{q}\tau.
\tag{21.12}
$$

In the case where the whole transverse momentum of the gluon fluctuation is obtained through the interaction with the medium, the above formula implies:

$$
k_{\mathrm{br}}^2 (\omega) = \sqrt{\hat{q}\omega} \quad \text{and} \quad \tau_{\mathrm{br}} (\omega) = \sqrt{\frac{\omega}{\hat{q}}}.
\tag{21.13}
$$

After traversing the whole length L of the plasma, the TMB turns out to be equal to the medium saturation scale Q_s^2.

Note that, in the above approximation, Eq. (21.10), the probability distribution is already normalized:

$$
\int_{k_\perp \sim Q_s} \mathrm{d}^2\mathbf{k} \frac{\mathrm{d}N}{\mathrm{d}^2\mathbf{k}_\perp} = 1.
\tag{21.14}
$$

However, the diffusion approximation we just described ignores the fact that the 'true' transverse momentum distribution has a tail $\sim 1/k_\perp^4$, which is caused by single hard collisions with $k_\perp \gg Q_s$. Indeed, in such a case, the integral in Eq. (21.1) over the dipole size is cut off at a value $r \sim 1/k_\perp \ll 1/Q_s$. It is therefore more appropriate to expand the exponential, but to keep the

logarithmic r-dependence of $\hat{q}$:

$$
\begin{aligned}
\frac{\mathrm{d}N}{\mathrm{d}^2\mathbf{k}_\perp} &= \frac{1}{(2\pi)^2} \int \mathrm{d}^2\mathbf{r}\, e^{-i\mathbf{k}_\perp \cdot \mathbf{r}} \exp\left(-\frac{1}{4}\hat{q}\left(r^2\right) L\mathbf{r}^2\right), \\
&\simeq -\frac{\alpha_s^2}{4\pi} C_F n_0 L \int \mathrm{d}^2\mathbf{r}\, \mathbf{r}^2 e^{-i\mathbf{k}_\perp \cdot \mathbf{r}} \ln \frac{1}{r^2 m_D^2}, \\
&= -\frac{\alpha_s^2}{4\pi} C_F n_0 L \times \left(-\frac{16\pi}{k_\perp^4} + \mathcal{O}\left(Q_s\right)\right), \\
&= \frac{1}{\pi Q_s^2 \ln\left(Q_s^2/m_D^2\right)} \frac{Q_s^4}{k_\perp^4}.
\end{aligned}
\tag{21.15}
$$

The above single hard collisions are rare events, suppressed by a large logarithm $\ln\left(Q_s^2/m_D^2\right)$, which explains why the multiple soft scatterings already approximately exhaust the integral over the probability Eq. (21.14). However, these hard collisions render the definition (21.3) of TMB as the second moment of $\mathrm{d}N/\mathrm{d}^2\mathbf{k}$ divergent (see also the discussions in Refs. [2, 158, 174]). In what follows, we will therefore always focus on the typical events, encoded in Eq. (21.10), in which the transverse momentum broadening is a diffusive process caused by multiple soft scatterings. Accordingly, we assume throughout this work that the fictitious dipole has a size $r \sim 1/Q_s$.

22 Resummation of the soft radiative corrections to the TMB

Equipped with the machinery that we developed in section 20, we are ready to study the high-energy QCD corrections to the transverse momentum broadening of a parton in a medium. Indeed, the TMB can be written as the Fourier transform of a fictitious dipole, Eq. (21.3). The soft gluon fluctuations, associated with this dipole, will be resummed with the help of the BK equation (20.57), generalized beyond the eikonal approximation.

Before delving into the equations, we should stress a couple of remarkable differences between the present problem and the calculations that we performed in the context of the Color Glass Condensate.

First, in the CGC, the energy E of the incoming probe was always assumed to be much larger than the characteristic energy ω_c of the target. Therefore, a large phase space was available for gluon fluctuations from the dipole, with energy $\omega_c \ll \omega \ll E$ and accordingly very large lifetimes $\tau \gg L$. As a result, the target could be treated as a shockwave, and the large logarithms $\alpha_s \ln E/\omega_c \simeq \alpha_s \ln 1/x$ were resummed in the JIMWLK/BK equation. In the present context of jet quenching, however, the energy phase space looks completely different. Now, both the probe and the target have an energy scale of the same order ($\sim 10^2\,\mathrm{GeV}$ at the LHC), hence the soft gluon fluctuations that we are interested in have an energy ω much smaller than the medium energy scale ω_c, and correspondingly a short lifetime τ as compared to the medium length:

$$
\omega \ll \omega_c \quad \text{and} \quad \tau \ll L.
\tag{22.1}
$$

Thus, the large logarithms that will be resummed in the problem at hand stem from the following region of phase space:

$$\omega_0 \ll \omega \ll \omega_c, \tag{22.2}$$

where ω_0 is a lower cutoff which will be specified in a moment.

Related to this, there is a second, more dramatic difference with the shockwave case: the fact that in the phase space for the gluon fluctuation, in the approximation of our interest, the medium introduces a strong correlation between the limits for the energy ω and for the transverse momentum $k_\perp^2$ of the gluon. We will come back to this in detail later, but let us already present one consequence of this correlation, namely the precise expression for the maximum ω_c of the gluon's energy. Indeed, from Eq. (22.1), we have that lifetime of the gluon fluctuation is limited by the medium size, hence:

$$\tau_{\mathrm{max}} = L. \tag{22.3}$$

Since $\tau = 2\omega/p_\perp^2$, this means that:

$$\frac{2\omega_c}{p_{\perp,\mathrm{min}}^2} = L. \tag{22.4}$$

The minimal transverse momentum $p_{\perp,\mathrm{min}}^2$ of the gluon is now obtained from the argument that, for small transverse momenta, the derivation of the momentum broadening of an eikonal parton, in the previous chapter, equally applies to the gluon fluctuation under consideration. Hence, during its lifetime the gluon obtains at least a momentum $p_{\perp,\mathrm{min}}^2 (\tau) = \hat{q}\tau$ due to multiple soft scattering, and after traveling through the medium $p_{\perp,\mathrm{min}}^2 (L) = \hat{q}L$ (cf. Eqs. (21.11), (21.12)), from which we obtain the following value for the maximal gluon energy ω_c:

$$\omega_c = Q_s^2 L = \hat{q}L^2. \tag{22.5}$$

Likewise, a lower cutoff l_0 on the lifetime, whose physical origin we will explain later, yields a value $\omega_0 = \hat{q}l_0^2$ for the lower limit on the energy. Thus, the presence of the medium imposes restrictions on the lifetime of the gluon fluctuations, resulting in the phase space (see Fig. 24):

$$l_0 \ll \tau \ll L \quad \leftrightarrow \quad \omega_0 = \hat{q}l_0^2 \ll \omega \ll \omega_c = \hat{q}L^2. \tag{22.6}$$

As we will see, a second consequence of the mutual dependency of the transverse and longitudinal phase space is the existence of double large logarithms in the same large ratio $\omega_c/\omega_0 = L/l_0$. This is in contrast to the DLA in the shockwave, in which the logarithms $\ln Q^2/\Lambda_{\mathrm{QCD}}^2$ and $\ln 1/x$ are large separately (cf. (3.31)). We will analytically perform the resummation of the double large logarithms associated with soft gluon fluctuations, and demonstrate that they can be absorbed into a renormalization of the jet quenching parameter.

22.1 Evolution equation for the dipole

In order to apply the generalized high-energy evolution equation for a dipole, Eqs. (20.2) and (20.57), to the problem of transverse momentum broadening, let us perform a couple of manipulations to cast the equation into a more useful form. First, using

$$\frac{\partial D_\omega (\mathbf{x} - \mathbf{y})}{\partial \omega} = D_\omega (\mathbf{x} - \mathbf{y}) \, \frac{\partial \ln D_\omega (\mathbf{x} - \mathbf{y})}{\partial \omega}, \tag{22.7}$$
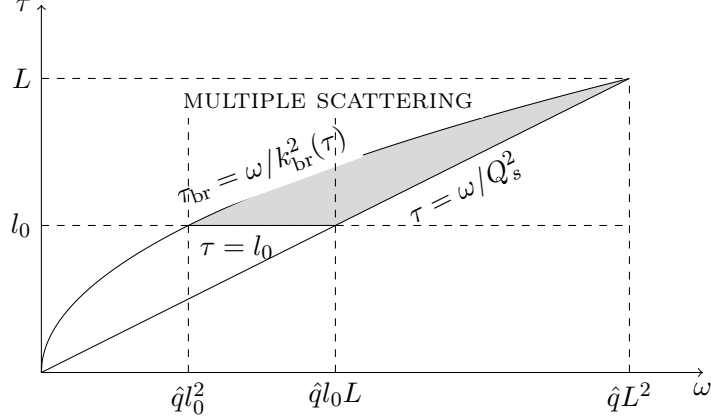
Figure 24: The phase space for the virtual gluon in the high-energy evolution of the jet quenching parameter. The shaded region, bounded by the limits $k_{\mathrm{br}}^2 \leq k_\perp^2 \leq Q_s^2$ and $l_0 \leq \tau \leq L$, corresponds to the kinematic region of single scattering.

the evolution equation becomes:

$$
\omega \frac{\partial \ln D_\omega \left(\mathbf{x} - \mathbf{y} \right)}{\partial \omega} = \frac{\alpha_s}{\omega} \frac{N_c}{2} \int_{t_2 t_1}^{\mathrm{cross}} \partial_{\mathbf{r}_1}^i \partial_{\mathbf{r}_2}^i \frac{1}{2\omega} \int \left[\mathcal{D} \mathbf{r} \left(t \right) \right] \exp \left\{ i \frac{\omega}{2} \int_{t_1}^{t_2} \mathrm{d}t \dot{\mathbf{r}}^2 \left(t \right) \right\}
$$
$$
\times \left. \left(1 - \left\langle S_{\mathbf{yr}(t)} \left(t_1, t_2 \right) S_{\mathbf{r}(t)\mathbf{x}} \left(t_1, t_2 \right) \right\rangle_\omega \left\langle S_{\mathbf{xy}} \left(t_1, t_2 \right) \right\rangle_\omega^{-1} \right) \right|_{\mathbf{r}_1 = \mathbf{y}}^{\mathbf{r}_1 = \mathbf{x}} \Big|_{\mathbf{r}_2 = \mathbf{y}}^{\mathbf{r}_2 = \mathbf{x}}. \tag{22.8}
$$

Note that we write the evolution in function of the energy ω, rather than the rapidity $\tau = \ln P/\omega$, in order to prevent confusion with the gluon's lifetime, also denoted τ. We are interested in soft gluon fluctuations whose probability is enhanced by a large logarithm in the energy $\sim \ln \omega_c/\omega$. Correspondingly, we expect the lifetime $\tau \simeq \omega/k_\perp^2$ of the gluon to be small as well, hence it is a good approximation to assume that the fluctuation takes place deeply inside the medium, i.e. $0 \ll t_1 < t_2 \ll L$. The time integrations in Eq. (22.8) thus reduce to:

$$
\int_{t_2 t_1}^{\mathrm{cross}} \rightarrow \int_0^L \mathrm{d}t_2 \int_0^{t_2} \mathrm{d}t_1. \tag{22.9}
$$

Furthermore, introducing the notation:

$$
\bar{\Gamma}_\omega \left(\mathbf{r} \right) \equiv \frac{n_0}{2\mu_A} \Gamma_\omega \left(\mathbf{r} \right), \tag{22.10}
$$

the (anti)quark-gluon dipole in the medium can be written as:

$$
D_\omega \left(t_2, t_1, \mathbf{r} \right) = \exp \left(-g_s^2 C_F \tau \bar{\Gamma}_\omega \left(\mathbf{r} \right) \right), \tag{22.11}
$$

where we identified $\tau = t_2 - t_1$. Lastly, in the large-N_c limit, the medium average over the two dipoles factorizes, and we can finally write:

$$
L\omega \frac{\partial \bar{\Gamma}_\omega (\mathbf{x}, \mathbf{y})}{\partial \omega} = \frac{1}{4\pi\omega^2} \int_0^L \mathrm{d}t_2 \int_0^{t_2} \mathrm{d}t_1 \partial_{\mathbf{r}_1}^i \partial_{\mathbf{r}_2}^i \int [\mathcal{D}\mathbf{r}(t)] \exp\left\{ i\frac{\omega}{2} \int_{t_1}^{t_2} \mathrm{d}t \dot{\mathbf{r}}^2 (t) \right\}
$$
$$
\times \left[\exp\left\{ -g_s^2 \frac{N_c}{2} \int_{t_1}^{t_2} \mathrm{d}t \left(\bar{\Gamma}_\omega (\mathbf{x}, \mathbf{r}(t)) + \bar{\Gamma}_\omega (\mathbf{y}, \mathbf{r}(t)) - \bar{\Gamma}_\omega (\mathbf{x}, \mathbf{y}) \right) \right\} - 1 \right] \Bigg|_{\mathbf{r}_1=\mathbf{y}}^{\mathbf{r}_1=\mathbf{x}} \Bigg|_{\mathbf{r}_2=\mathbf{y}}^{\mathbf{r}_2=\mathbf{x}}.
\tag{22.12}
$$

In what follows, we further study the above equation, scrutinize its regions of validity, and solve it in the double leading logarithmic approximation.

22.2 Single scattering approximation

It is apparent from formula (22.11) that the dipole S-matrix resums the amplitudes $g_s^2 C_F \bar{\Gamma}_\omega (\mathbf{r})$ for a single scattering per unit time, for which we established the evolution equation (22.12). When the exponent of Eq. (22.11) is small enough, i.e. when:

$$
g_s^2 C_F \tau \bar{\Gamma}_\omega (\mathbf{r}) \ll 1,
\tag{22.13}
$$

the dipole can be expanded to leading order:

$$
D_\omega (t_2, t_1, \mathbf{r}) \simeq 1 - g_s^2 C_F \tau \bar{\Gamma}_\omega (\mathbf{r}),
\tag{22.14}
$$

approximating the full dipole-medium interaction with one single scattering off the medium constituents.

In the previous paragraph we argued that, since we are interested in the contributions that are amplified by large logarithms, we can focus on gluon fluctuations in the soft limit $\omega \to 0$, in which the gluon's lifetime $\tau \simeq \omega/k_\perp^2$ is very short. At first sight, this leading logarithmic approximation complies with the requirement for single scattering Eq. (22.13). However, in the denominator of τ, there is the transverse momentum $k_\perp^2$ of the gluon, which, when very small, can still invalidate Eq. (22.13). This implies that the single scattering regime is naturally associated with the double, rather than the single, leading logarithmic approximation of evolution equation Eq. (22.12). In this regime, ω is small enough and $k_\perp$ is large enough for requirement (22.13) to be satisfied.

To show more precisely how the DLA solution to Eq. (22.12) comes into play, let us simplify the evolution equation (22.12) within the single scattering approximation by linearizing the exponential in the r.h.s.:

$$
L\omega \frac{\partial \bar{\Gamma}_\omega (\mathbf{r})}{\partial \omega} = -\frac{\alpha_s}{\omega^2} \frac{N_c}{2} \int_0^L \mathrm{d}t_2 \int_0^{t_2} \mathrm{d}t_1 \int_{t_1}^{t_2} \mathrm{d}t \partial_{\mathbf{r}_1}^i \partial_{\mathbf{r}_2}^i \int [\mathcal{D}\mathbf{r}(t)] \exp\left\{ i\frac{\omega}{2} \int_{t_1}^{t_2} \mathrm{d}t \dot{\mathbf{r}}^2 (t) \right\}
$$
$$
\times \left(\bar{\Gamma}_\omega (\mathbf{x}, \mathbf{r}(t)) + \bar{\Gamma}_\omega (\mathbf{y}, \mathbf{r}(t)) - \bar{\Gamma}_\omega (\mathbf{x}, \mathbf{y}) \right) \Bigg|_{\mathbf{r}_1=\mathbf{y}}^{\mathbf{r}_1=\mathbf{x}} \Bigg|_{\mathbf{r}_2=\mathbf{y}}^{\mathbf{r}_2=\mathbf{x}}.
\tag{22.15}
$$

Rewriting the time integrations as follows:

$$
\int_0^L \mathrm{d}t_2 \int_0^{t_2} \mathrm{d}t_1 \int_{t_1}^{t_2} \mathrm{d}t = \int_0^L \mathrm{d}t \int_0^t \mathrm{d}t_1 \int_t^L \mathrm{d}t_2,
\tag{22.16}
$$

and introducing $1 = \int_{\mathbf{z}} \delta^{(2)} (\mathbf{z} - \mathbf{r}(t))$, Eq. (22.15) becomes:

$$L\omega \frac{\partial \bar{\Gamma}_\omega (\mathbf{r})}{\partial \omega} = -\frac{\alpha_s}{\omega^2} \frac{N_c}{2} \int_0^L \mathrm{d}t \int_0^t \mathrm{d}t_1 \int_t^L \mathrm{d}t_2 \partial_{\mathbf{r}_1}^i \partial_{\mathbf{r}_2}^i$$

$$\times \int \mathrm{d}^2 \mathbf{z}\, G_0 (t_2, \mathbf{r}_2, t, \mathbf{z}; \omega) G_0 (t, \mathbf{z}, t_1, \mathbf{r}_1; \omega) \left(\bar{\Gamma}_\omega (\mathbf{x}, \mathbf{z}) + \bar{\Gamma}_\omega (\mathbf{y}, \mathbf{z}) - \bar{\Gamma}_\omega (\mathbf{x}, \mathbf{y}) \right) \Big|_{\mathbf{r}_1 = \mathbf{y}}^{\mathbf{r}_1 = \mathbf{x}} \Big|_{\mathbf{r}_2 = \mathbf{y}}^{\mathbf{r}_2 = \mathbf{x}} . \qquad (22.17)$$

The time integrals can now be calculated explicitly, similar to what we did in Eqs. (20.25) and (20.26):

$$\frac{1}{2\omega} \int_t^L \mathrm{d}t_2 \partial_{\mathbf{r}_2}^i G_0 (t_2 - t, \mathbf{r}_2 - \mathbf{z}; \omega)$$

$$= -\frac{i}{2\omega} \int \frac{\mathrm{d}^2 \mathbf{k}_\perp}{(2\pi)^2} k_\perp^i e^{i\mathbf{k}_\perp (\mathbf{r}_2 - \mathbf{z})} \frac{1}{ik^-} \left(e^{-ik^- (L-t)} - 1 \right), \qquad (22.18)$$

$$\simeq \frac{i}{2\pi} \frac{\mathbf{r}_2^i - \mathbf{z}^i}{(\mathbf{r}_2 - \mathbf{z})^2},$$

and

$$\frac{1}{2\omega} \int_0^t \mathrm{d}t_1 \partial_{\mathbf{r}_1}^i G_0 (t - t_1, \mathbf{z} - \mathbf{r}_1; \omega)$$

$$= -\frac{i}{2\omega} \int \frac{\mathrm{d}^2 \mathbf{k}_\perp}{(2\pi)^2} k_\perp^i e^{i\mathbf{k}_\perp (\mathbf{z} - \mathbf{r}_1)} \frac{1}{ik^-} \left(1 - e^{-ik^- t} \right), \qquad (22.19)$$

$$\simeq \frac{i}{2\pi} \frac{\mathbf{r}_1^i - \mathbf{z}^i}{(\mathbf{r}_1 - \mathbf{z})^2}.$$

In the above calculations, we neglected the exponentials $e^{-ik^- (L-t)} \approx e^{-ik^- t} \approx 0$ in order to obtain the familiar Weizsäcker-Williams wave functions $\sim x^i/x^2$. These approximations are well-justified within our LLA approach, since we both assume that the scattering takes place deeply inside the medium $0 \ll t \ll L$, and require that the gluon lifetime τ is small, hence $t + \tau \ll L$ and $\tau \ll t$.

From the above intermediate results, we easily obtain the following equation:

$$\omega \frac{\partial \bar{\Gamma}_\omega (\mathbf{x}, \mathbf{y})}{\partial \omega} = \frac{\bar{\alpha}}{2\pi} \int \mathrm{d}^2 \mathbf{z} \mathcal{M}_{\mathbf{xyz}} \left(\bar{\Gamma}_\omega (\mathbf{x}, \mathbf{z}) + \bar{\Gamma}_\omega (\mathbf{y}, \mathbf{z}) - \bar{\Gamma}_\omega (\mathbf{x}, \mathbf{y}) \right), \qquad (22.20)$$

in which finally the logarithmic enhancement $\mathrm{d}\omega/\omega$ is explicit. Although this evolution equation closely resembles the BFKL equation for a dipole in a shockwave (see Eq. (5.24)), it differs on some crucial points. Indeed, the regular BFKL equation is an evolution equation for dipole amplitudes $\langle T(\mathbf{r}) \rangle_\omega$ in the dilute regime, valid in the limit in which these amplitudes, and therefore the corresponding dipole sizes, are small: $\langle T(\mathbf{r}) \rangle_\omega \sim r^2 \ll 1/Q_s^2$ (cf. (5.27)). Eq. (22.20), however, is formulated in function of the amplitudes per unit time $\bar{\Gamma}_\omega (\mathbf{r})$, for which the condition (22.13) has to hold. Since, from the requirement $\tau \ll L$, the (anti)quark-gluon dipoles are very short-living in comparison with their parents, they can become very large and still satisfy Eq. (22.13):

$$\bar{\Gamma}_\omega (\mathbf{x}, \mathbf{z}), \bar{\Gamma}_\omega (\mathbf{y}, \mathbf{z}) \gg \bar{\Gamma}_\omega (\mathbf{x}, \mathbf{y}). \qquad (22.21)$$

107

In the MV approximation,

$$g_s^2 C_F \bar{\Gamma}_\omega (r) \simeq \frac{1}{4} \hat{q} \left(r^2 \right) r^2, \tag{22.22}$$

which follows from Eqs. (21.9) and (22.11), formula (22.21) becomes:

$$(\mathbf{x} - \mathbf{z})^2, (\mathbf{y} - \mathbf{z})^2 \gg (\mathbf{x} - \mathbf{y})^2 \sim 1/Q_s^2. \tag{22.23}$$

This observation motivates us to write an approximation to Eq. (22.20) which –as will become clear shortly– is tantamount to the double logarithmic approximation. Assuming that the daughter dipoles are indeed much larger than their parent, as in Eq. (22.21), the latter can be omitted from the r.h.s. of Eq. (22.20). The difference between both daughter dipoles then becomes negligible, hence we write $\bar{\Gamma}_\omega (\mathbf{x}, \mathbf{z}) \simeq \bar{\Gamma}_\omega (\mathbf{y}, \mathbf{z})$ and $\mathbf{B}^2 \equiv (\mathbf{x} - \mathbf{z})^2 \simeq (\mathbf{y} - \mathbf{z})^2$, thus obtaining:

$$\omega \, \frac{\partial \bar{\Gamma}_\omega (r)}{\partial \omega} = \bar{\alpha} r^2 \int_{1/Q_s^2}^{2/k_{\mathrm{br}}^2(\omega)} \frac{\mathrm{d}B^2}{B^4} \bar{\Gamma}_\omega (B), \tag{22.24}$$

where $\mathbf{r} \equiv \mathbf{x} - \mathbf{y}$ is the size of the parent dipole. The integration limits in the above equation are crucial, and are obtained as follows: first, in order for the assumption (22.21), which asserts that the daughter dipoles are clearly distinguishable from their parent, to be valid, we require that:

$$B^2 \gg r^2 \sim 1/Q_s^2. \tag{22.25}$$

again making use of the MV approximation Eq. (22.22). Second, the upper limit in Eq. (22.24) comes from the single scattering requirement, Eq. (22.13):

$$2 g_s^2 C_F \tau \bar{\Gamma}_\omega (\mathbf{B}) \ll 1, \tag{22.26}$$

where the factor two accounts for the two daughter dipoles. Using the MV approximation to write $g_s^2 C_F \bar{\Gamma}_\omega (\mathbf{B}) = \frac{1}{4} \hat{q} B^2$, the above expression yields the following upper limit on the daughter dipole size:

$$B^2 \ll \frac{2}{\hat{q}\tau} = \frac{2}{k_{\mathrm{br}}^2(\omega)}, \tag{22.27}$$

where we identified $\hat{q}\tau$ with the average transverse momentum acquired by the gluon due to multiple soft scatterings off the medium constituents: $k_{\mathrm{br}}^2(\omega) = \hat{q}\tau \simeq \sqrt{\omega \hat{q}}$ (see Eq. (21.12)). The onset of the multiple soft scattering regime therefore acts as the infrared cutoff (instead of Λ_{QCD}^2 in the vacuum) for the DLA.

Interestingly, there is yet another requirement, that we overlooked. Indeed, we argued already (see Eq. (22.6)) that the gluon fluctuations should take place deeply inside the medium, which led to the requirement:

$$l_0 \ll \tau \ll L. \tag{22.28}$$

The upper limit is automatically satisfied Eq. (22.27):

$$\tau_{\mathrm{max}} \simeq \frac{\omega_c}{k_{\perp,\mathrm{min}}^2} = \frac{\omega_c}{k_{\mathrm{br}}^2(\omega)} = \frac{\hat{q} L^2}{\hat{q}\tau} = L. \tag{22.29}$$
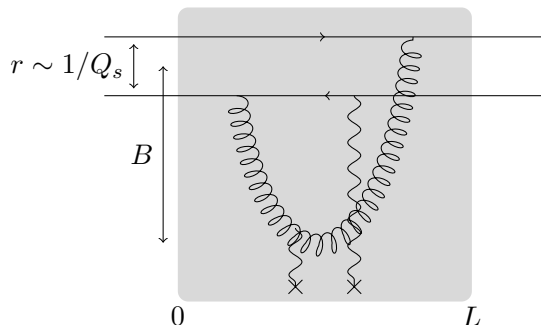
Figure 25: One step in the evolution of a dipole through the nuclear medium in the DLA approximation, as encoded in Eq. (22.24). The size B of the qg and $\bar{q}g$ daughter dipoles is much larger than the size r of the parent dipole.

However, this is not the case for the lower limit $l_0 \ll \tau$, hence we have to enforce it explicitly, modifying the upper limit $k_\perp^2 \ll Q_s^2$ for the gluon's momentum (from Eq. (22.25)) to $k_\perp^2 \ll \min\left(Q_s^2, 2\omega/l_0\right)$.

In summary, the phase space of the double-logarithmic regime is the one restricted by the following limits on the energy and on the transverse extent of the gluon fluctuation:

$$\omega_0 = \hat{q} l_0^2 \ll \omega \ll \omega_c = \hat{q} L^2,$$
$$\max\left(r^2 \sim \frac{1}{Q_s^2}, \frac{l_0}{2\omega}\right) \ll B^2 \ll \frac{2}{k_{\mathrm{br}}^2(\omega)}. \tag{22.30}$$

One step in the evolution is illustrated in Fig. 25, and the DLA phase space is depicted in Fig. 24 (in terms of (τ, ω)).

23 Renormalization of the jet quenching parameter

We will now solve evolution equation (22.24) explicitly in the double logarithmic approximation. Interestingly, the evolution preserves the MV approximation Eq. (22.22). This implies that the double-logarithmic high-energy corrections can be absorbed into a renormalization of the jet quenching parameter $\hat{q}_\omega$. Indeed, combining Eqs. (22.22) and (22.24), one obtains the following evolution equation for $\hat{q}_\omega(r)$:

$$\omega \frac{\partial \hat{q}_\omega(r)}{\partial \omega} = \bar{\alpha} \int \frac{\mathrm{d}B^2}{B^2} \hat{q}_\omega(B), \tag{23.1}$$

or, in integral form with the correct limits, Eq. (22.30):

$$\hat{q}_\omega(r) = \bar{\alpha} \int_{\omega_0}^{\omega_c} \frac{\mathrm{d}\omega}{\omega} \int_{\max(r^2, l_0/2\omega)}^{2/k_{\mathrm{br}}^2(\omega)} \frac{\mathrm{d}B^2}{B^2} \hat{q}_\omega(B). \tag{23.2}$$

This equation can be solved iteratively as follows: denoting the zeroth-order solution, which we assume to be scale-independent, as $\hat{q}^{(0)}$, we have that:

$$
\begin{aligned}
\delta\hat{q}_\omega^{(1)}\left(r\right) &= \bar{\alpha}\hat{q}^{(0)} \int_{l_0/2r^2}^{\omega_c} \frac{\mathrm{d}\omega}{\omega} \int_{r^2}^{2/k_{\mathrm{br}}^2(\omega)} \frac{\mathrm{d}B^2}{B^2} + \bar{\alpha}\hat{q}^{(0)} \int_{\omega_0}^{l_0/2r^2} \frac{\mathrm{d}\omega}{\omega} \int_{l_0/2\omega}^{2/k_{\mathrm{br}}^2(\omega)} \frac{\mathrm{d}B^2}{B^2}, \\
&= \bar{\alpha}\hat{q}^{(0)} \int_{l_0/2r^2}^{\omega_c} \frac{\mathrm{d}\omega}{\omega} \ln \frac{2}{k_{\mathrm{br}}^2(\omega)\,r^2} + \bar{\alpha}\hat{q}^{(0)} \int_{\omega_0}^{l_0/2r^2} \frac{\mathrm{d}\omega}{\omega} \ln \frac{4\omega}{k_{\mathrm{br}}^2(\omega)\,l_0}, \\
&\simeq \bar{\alpha}\hat{q}^{(0)} \int_{l_0/2r^2}^{\omega_c} \frac{\mathrm{d}\omega}{\omega} \ln \frac{Q_s^2}{k_{\mathrm{br}}^2(\omega)} + \bar{\alpha}\hat{q}^{(0)} \int_{\omega_0}^{l_0/2r^2} \frac{\mathrm{d}\omega}{\omega} \ln \frac{4\omega}{k_{\mathrm{br}}^2(\omega)\,l_0}.
\end{aligned}
\tag{23.3}
$$

From Eqs. (22.6), (21.11) and (21.13), the logarithms of the transverse momentum scales can be written in function of the energies:

$$
\begin{aligned}
\ln \frac{Q_s^2}{k_{\mathrm{br}}^2(\omega)} &= \ln \sqrt{\frac{\omega_c}{\omega}}, \\
\ln \frac{\omega}{k_{\mathrm{br}}^2(\omega)\,l_0} &= \ln \sqrt{\frac{\omega}{\omega_0}},
\end{aligned}
\tag{23.4}
$$

hence we obtain:

$$
\begin{aligned}
\delta\hat{q}_\omega^{(1)}\left(r\right) &\simeq \frac{\bar{\alpha}}{2}\hat{q}^{(0)} \int_{l_0/2r^2}^{\omega_c} \frac{\mathrm{d}\omega}{\omega} \ln \frac{\omega_c}{\omega} + \frac{\bar{\alpha}}{2}\hat{q}^{(0)} \int_{\omega_0}^{l_0/2r^2} \frac{\mathrm{d}\omega}{\omega} \ln \frac{\omega}{\omega_0}, \\
&= \frac{\bar{\alpha}}{4}\hat{q}^{(0)} \left(\ln^2 \frac{r^2\omega_c}{l_0} + \ln^2 \frac{l_0}{r^2\omega_0} \right).
\end{aligned}
\tag{23.5}
$$

The 'physical' jet quenching parameter is then the one evaluated on the point $\tau = L$ and $p_\perp^2 = Q_s^2$, and is equal to:

$$
\hat{q}_{\omega_c}\left(1/Q_s^2\right) = \hat{q}^{(0)} \left(1 + \frac{\bar{\alpha}}{2} \ln^2 \frac{L}{l_0} + \mathcal{O}\left(\bar{\alpha}^2\right) \right).
\tag{23.6}
$$

In order to calculate the next-to-leading order correction, and eventually resum all DLA contributions, it is more convenient to work in the phase space $\left(\tau, k_\perp^2\right)$, with τ the lifetime of the gluon. We then do not have to make use of the –somewhat awkward to handle– condition $B_{\min} = \max\left(r^2 \sim \frac{1}{Q_s^2}, \frac{l_0}{2\omega}\right)$ anymore, but instead, the DLA regime is simply defined by (writing $k_\perp^2 \sim 1/B^2$):

$$
l_0 \ll \tau \ll L, \quad \text{and} \quad k_{\mathrm{br}}^2 = \hat{q}\tau \ll k_\perp^2 \ll Q_s^2.
\tag{23.7}
$$

The integral form of the DLA evolution equation (23.2) then becomes:

$$
\hat{q}_\tau\left(p_\perp^2\right) = \bar{\alpha} \int_{l_0}^{\tau} \frac{\mathrm{d}\tau'}{\tau'} \int_{\hat{q}\tau'}^{p_\perp^2} \frac{\mathrm{d}k_\perp^2}{k_\perp^2} \hat{q}_{\tau'}\left(k_\perp^2\right).
\tag{23.8}
$$

It is easy to check that the first iteration of the solution to the above equation is the same as Eq. (23.5), as it should. In order to obtain the next iteration, one should observe that the contributions

that generate a large logarithm are the ones in which each subsequent emission has a shorter lifetime than the one of its parent, resulting in a gluon density that keeps growing (cf. the discussion on BFKL, Sec. 5):

$$L \gg \tau_1 \gg \tau_2 \gg ... \gg l_0. \tag{23.9}$$

Interestingly, however, in our case the strong ordering of the virtualities is opposite to the one in DGLAP. Indeed, remember that when building the DGLAP ladders, each emission is treated as if coming from an on-shell parton: an approximation which can only be valid when the virtuality of each radiated parton is much larger than the previous one. In our case of in-medium radiation, due to the requirement (22.21), it is precisely the other way around: each gluon that is emitted results in a daughter dipole with a larger transverse size B, and hence a smaller transverse momentum $k_\perp \sim 1/B$, than its parent:

$$Q_s^2 \gg k_{1\perp}^2 \gg k_{2\perp}^2 \gg ... \gg k_{\mathrm{br}}^2 (\tau). \tag{23.10}$$

Implementing the orderings (23.9) and (23.10), the second iteration of Eq. (23.8) is:

$$\begin{aligned}
\delta \hat{q}_\tau^{(2)} \left(p_\perp^2\right) &= \bar{\alpha}^2 \hat{q}^{(0)} \int_{l_0}^\tau \frac{\mathrm{d}\tau_1}{\tau_1} \int_{\hat{q}\tau_1}^{p_\perp^2} \frac{\mathrm{d}k_{1\perp}^2}{k_{1\perp}^2} \int_{l_0}^{\tau_1} \frac{\mathrm{d}\tau_2}{\tau_2} \int_{\hat{q}\tau_2}^{k_{1\perp}^2} \frac{\mathrm{d}k_{2\perp}^2}{k_{2\perp}^2}, \\
&= \frac{\bar{\alpha}^2}{2} \hat{q}^{(0)} \int_{l_0}^\tau \frac{\mathrm{d}\tau_1}{\tau_1} \int_{\hat{q}\tau_1}^{p_\perp^2} \frac{\mathrm{d}k_{1\perp}^2}{k_{1\perp}^2} \ln \frac{\tau_1}{l_0} \ln \frac{k_{1\perp}^4}{\hat{q}^2 \tau_1 l_0}, \\
&= \frac{\bar{\alpha}^2}{2} \hat{q}^{(0)} \int_{l_0}^\tau \frac{\mathrm{d}\tau_1}{\tau_1} \ln \frac{\tau_1}{l_0} \ln \frac{p_\perp^2}{l_0 \hat{q}} \ln \frac{p_\perp^2}{\hat{q}\tau_1}, \\
&= \frac{\bar{\alpha}^2}{12} \hat{q}^{(0)} \ln^2 \frac{\tau}{l_0} \ln \frac{p_\perp^2}{l_0 \hat{q}} \ln \frac{p_\perp^6}{\hat{q}^3 \tau^2 l_0},
\end{aligned} \tag{23.11}$$

which, on the physical point $\tau = L$ and $p_\perp^2 = Q_s^2$ yields:

$$\delta \hat{q}_L^{(2)} \left(Q_s^2\right) = \hat{q}^{(0)} \frac{\bar{\alpha}^2}{12} \ln^4 \frac{L}{l_0}. \tag{23.12}$$

As it turns out (see Refs. [2–4]), the full solution to Eq. (23.8) is found to be:

$$\hat{q}_L \left(Q_s^2\right) = \hat{q}^{(0)} \frac{1}{\sqrt{\bar{\alpha}} \ln \frac{L}{l_0}} I_1 \left(2\sqrt{\bar{\alpha}} \ln \frac{L}{l_0}\right), \tag{23.13}$$

of which $\delta \hat{q}_L^{(1)} \left(Q_s^2\right)$, Eq. (23.6) and $\delta \hat{q}_L^{(2)} \left(Q_s^2\right)$ are indeed the first terms in the expansion in $\bar{\alpha}$. This is our final result for the radiative corrections to the jet quenching parameter in the double leading approximation. For a small coupling constant $\bar{\alpha} \sim 0.3$, a lower bound $l_0 \sim 1/T$ with the temperature $T \sim 300\,\mathrm{MeV}$, and a plasma with longitudinal extent $L \sim 5\,\mathrm{fermi}$, the enhancement seems to be rather sizable, of the order:

$$\hat{q}_L \left(Q_s^2\right) \sim 1.8 \, \hat{q}^{(0)}. \tag{23.14}$$

111

24   Multiple soft scattering and gluon saturation

In the previous sections, we constructed a high-energy evolution equation for a probe in an extended nuclear medium, and applied this equation to the fictitious dipole that describes the transverse momentum broadening of a parton in this medium. Since the MV approximation for a dipole turned out to be conserved by the evolution, at least to DLA accuracy, the double large logarithms associated with soft gluon fluctuations could be absorbed into a renormalization of the jet quenching parameter $\hat{q}$.

In order to gain further insight into the physics of transverse momentum broadening, and to elucidate on the similarities and differences with the Color Glass Condensate, let us have a closer look on the above analysis from the point of view of the target.

First however, we should explain the physical basis for the lower bound l_0 on the gluon's lifetime (see Ref. [2]). Since the gluon fluctuation has $k_\perp^2 \ll Q_s^2$, we can treat it as being nearly on shell and write:

$$k^\mu = \left(\omega, k^- \simeq \frac{k_\perp^2}{2\omega}, \mathbf{k}_\perp \right). \tag{24.1}$$

The gluon is emitted from a right-moving parent $P \simeq (P^+, 0^-, \mathbf{0})$, from which it cannot inherit a momentum component k^-. Hence, this component is obtained from the interactions with the medium constituents. Since the lifetime of the gluon is $\tau \sim 1/k^-$, this confirms our earlier assertions that the medium imposes strong conditions on the gluon lifetime. A typical thermal parton of the medium has, in the medium rest frame, a momentum component $p^- \sim T$. Upon interacting with the gluon fluctuation, a fraction $x = k^-/p^- \leq 1$ of this momentum is absorbed by the gluon, and we find:

$$\tau \simeq \frac{1}{k^-} = \frac{1}{xp^-}. \tag{24.2}$$

In the single scattering approximation, the maximal momentum component k^- that the gluon can obtain from the interaction with the medium is therefore given by $x = 1$, corresponding to a lower limit $\tau_{\min} = l_0 \equiv 1/T$ on the gluon's lifetime.

Let us now perform a Lorentz boost to an infinite momentum frame for the left-moving medium, in which all the soft gluons emitted by the fictitious dipole can be regarded as partons of the medium. In the rest frame of the plasma, gluons with energy ω and transverse momentum $k_\perp$ correspond to a Lorentz factor $\gamma \simeq \omega/k_\perp$ (cf. (1.8)). Therefore, since the gluon fluctuations that we are interested in have $k_\perp \gtrsim k_{\mathrm{br}}$, the medium should be boosted with a factor

$$\gamma \simeq \frac{\omega_{\max}}{k_{\perp,\min}} \simeq \frac{\omega_c}{k_{\mathrm{br}}(\omega_c)} = \frac{\omega_c}{Q_s} = \sqrt{\hat{q}L^3}, \tag{24.3}$$

for all the relevant fluctuations to be naturally associated with the medium, instead of with the dipole. Accordingly, the high-energy evolution of the fictitious dipole can be viewed as the evolution of the gluon distribution in the medium.

Interestingly, this evolution differs from the one we encountered previously in the case of a shockwave. This is a consequence of the fact that, on the –for the left-moving medium– longitudinal axis x^+, the gluon fluctuations do not necessarily overlap with each other. This is in sharp contrast with

the CGC, where it was always assumed that for each step in the evolution, the semi-fast gluons were well located from the point of view of the soft gluons, and hence could be integrated out and absorbed into the color sources for the latter.

To quantify this better, let us revisit the gluon occupation number, Eq. (4.11), for a shockwave, but now in unintegrated form:

$$
\begin{aligned}
\varphi\left(x, k_{\perp}\right) & \equiv \frac{4 \pi^{3}}{N_{c}^{2}-1} \frac{1}{\pi R^{2}} x \frac{\mathrm{d} N}{\mathrm{d} x \mathrm{d}^{2} \mathbf{k}_{\perp}}, \\
& =\frac{4 \pi^{3}}{N_{c}^{2}-1} \frac{1}{\pi R^{2}} \mathcal{F}_{g g}^{(3)}\left(x, k_{\perp}\right) .
\end{aligned}
\tag{24.4}
$$

In the dilute approximation and at lowest order, the Weizsäcker-Williams gluon distribution is equal to the amount of valence quarks in the medium: $A N_{c}$, times the corresponding tree-level Bremsstrahlung spectrum $\alpha_{s} C_{F} / \pi^{2} k_{\perp}^{2}$ (see Eqs. (8.53), (8.55)):

$$
\begin{aligned}
\varphi\left(x, k_{\perp}\right) & \simeq \frac{4 \pi^{3}}{N_{c}^{2}-1} \frac{1}{\pi R^{2}} A N_{c} \frac{\alpha_{s} C_{F}}{\pi^{2} k_{\perp}^{2}}, \\
& \simeq \frac{1}{\alpha_{s} N_{c}} \frac{Q_{s g}^{2}}{k_{\perp}^{2}} .
\end{aligned}
\tag{24.5}
$$

Indeed, approaching the saturation scale from the dilute regime, the gluon occupation number reaches its maximal allowed value $\varphi \sim 1 / \alpha_{s} N_{c}$ when $k_{\perp}^{2}=Q_{s g}^{2} \simeq \alpha_{s} N_{c} \mu_{A}$. To extend the validity of definition (24.4) to an extended medium, we should observe that the distribution $\varphi\left(x, k_{\perp}\right)$ is integrated in the k^{-}-direction, since

$$
\varphi\left(x, k_{\perp}\right) \propto x \frac{\mathrm{d} N}{\mathrm{d} x \mathrm{d}^{2} \mathbf{k}_{\perp}}=k^{-} \frac{\mathrm{d} N}{\mathrm{d} k^{-} \mathrm{d}^{2} \mathbf{k}_{\perp}} .
\tag{24.6}
$$

A truly three-dimensional gluon occupation number $\varphi_{\text {med }}\left(k^{-}, k_{\perp}\right)$, appropriate for an extended medium, is therefore obtained by writing:

$$
\begin{aligned}
\varphi_{\text {med }}\left(k^{-}, k_{\perp}\right) & \equiv \frac{4 \pi^{3}}{N_{c}^{2}-1} \frac{1}{\pi R^{2} L} \frac{\mathrm{d} N}{\mathrm{d} k^{-} \mathrm{d}^{2} \mathbf{k}_{\perp}}, \\
& =\frac{4 \pi^{3}}{N_{c}^{2}-1} \frac{1}{\pi R^{2} L} \frac{\mathcal{F}_{g g}^{(3)}\left(k^{-}, k_{\perp}\right)}{k^{-}} .
\end{aligned}
\tag{24.7}
$$

Again in the dilute limit and at lowest order, this yields:

$$
\varphi_{\text {med }}\left(k^{-}, k_{\perp}\right) \simeq 4 \pi \alpha_{s} n_{0} \frac{1}{k^{-} k_{\perp}^{2}},
\tag{24.8}
$$

where now the three-dimensional density n_{0}, Eq. (21.8), comes into play, instead of the transverse one (μ_{A} / g_{s}^{2}, see Eq. (21.7), which is encoded in $Q_{s g}^{2}$ in Eq. (24.5)). If we now use the above quantity to estimate the saturation scale, requiring

$$
\varphi_{\text {med }}\left(k^{-}, Q_{s g}^{2}\right) \sim \frac{1}{\alpha_{s} N_{c}},
\tag{24.9}
$$

we obtain:

$$Q_{sg,\text{med}}^2 = 4\pi\alpha_s^2 N_c n_0 \frac{1}{k^-} = Q_{sg}^2 \times \frac{1}{Lk^-}. \tag{24.10}$$

Since the lifetime of a right-mover is given by $\tau \sim 1/k^-$, and using Eq. (21.9) as well as the relation $N_c Q_s^2 = C_F Q_{sg}^2$, we find that:

$$Q_{s,\text{med}}^2(\tau) = Q_s^2 \frac{\tau}{L} = \hat{q}\tau \simeq \hat{q}\frac{T}{x}. \tag{24.11}$$

The average transverse momentum obtained by a gluon after multiple soft scatterings with the medium: $k_{\text{br}}^2(\tau) = \hat{q}\tau$, is therefore equal to the saturation line $Q_{s,\text{med}}^2(\tau)$ in a frame in which the target is highly relativistic. In contrast to a shockwave, in which the x-dependence of the saturation scale comes into play after considering evolution (see Sec. 4 and Refs. [33, 34, 53]), in the present case this dependence is already strongly present at tree-level.

In the double logarithmic approximation, we found out that the evolution led to a renormalization of $\hat{q}$. Hence, to DLA-accuracy, Eq. (24.8) becomes:

$$\varphi_{\text{med}}\left(k^-, k_\perp\right) \simeq \frac{1}{\alpha_s N_c} \frac{\hat{q}_\tau\left(k_\perp\right)}{k^- k_\perp^2}. \tag{24.12}$$

The fact that the momentum broadening k_{br}^2 due to multiple soft scattering can be interpreted as the medium saturation scale $Q_{s,\text{med}}^2$ is not a coincidence. Rather, it can be seen from the 'complete', i.e., valid beyond the single scattering approximation, evolution equation (22.12) that the multiple scattering effects become sizable when the exponent is of order one. However, in the MV approximation, this is equal to the requirement that:

$$1 \sim g_s^2 \frac{N_c}{2}\tau\bar{\Gamma}_\omega\left(\mathbf{r}\left(t\right)\right) \simeq \frac{1}{4}\tau\hat{q}_\tau r^2 \sim \hat{q}_\tau \frac{1}{k^- k_\perp^2}$$

$$\iff \quad \varphi_{\text{med}}\left(Q_{s,\text{med}}^2\left(\tau\right)\right) \sim \frac{1}{\alpha_s N_c}. \tag{24.13}$$

The saturation line is thus given to DLA-accuracy by:

$$Q_{s,\text{med}}^2\left(\tau\right) = \hat{q}_\tau\left(Q_{s,\text{med}}^2\left(\tau\right)\right)\tau. \tag{24.14}$$

Revisiting the steps leading to our result (23.13), it is easy to see that we have:

$$\hat{q}\left(x\right) = \hat{q}^{(0)}\frac{1}{\sqrt{\bar{\alpha}}\ln\frac{1}{x}}I_1\left(2\sqrt{\bar{\alpha}}\ln\frac{1}{x}\right). \tag{24.15}$$

In the limit $2\sqrt{\bar{\alpha}}\ln(1/x) \gg 1$, this can be used to solve Eq. (24.14), for which we find:

$$Q_{s,\text{med}}^2\left(x\right) \simeq \frac{Q_{s,0}^2}{x^{1+\gamma_s}} \tag{24.16}$$

with $\gamma_s = 2\sqrt{\bar{\alpha}}$. Hence, the double logarithmic contributions of the high-energy evolution add a small-x anomalous dimension γ_s to the x-dependence of the saturation line in a medium, which is already strong at tree-level (cf. Eq. (24.11)).

25 Beyond the single scattering approximation

In this section, we have a closer look at the full evolution equation (22.12) beyond the single scattering approximation. In particular, we argue that the limits for the gluon phase space, which we introduced using semi-quantitative arguments, are indeed encoded in the formalism.

To do so, let us rewrite Eq. (22.12) in the harmonic approximation (writing Eq. (22.22) and furthermore neglecting the logarithmic r-dependence of $\hat{q}$):

$$
\begin{aligned}
L\omega\frac{\partial\bar{\Gamma}_\omega\left(\mathbf{x},\mathbf{y}\right)}{\partial\omega} &= \frac{1}{4\pi\omega^2}\int_0^L \mathrm{d}t_2\int_0^{t_2}\mathrm{d}t_1\partial_{\mathbf{r}_1}^i\partial_{\mathbf{r}_2}^i\int[\mathcal{D}\mathbf{r}\left(t\right)]\exp\left\{i\frac{\omega}{2}\int_{t_1}^{t_2}\mathrm{d}t\dot{\mathbf{r}}^2\left(t\right)\right\} \\
&\times\left[\exp\left\{-\frac{1}{4}\hat{q}\int_{t_1}^{t_2}\mathrm{d}t\left((\mathbf{x}-\mathbf{r}\left(t\right))^2+(\mathbf{y}-\mathbf{r}\left(t\right))^2-(\mathbf{x}-\mathbf{y})^2\right)\right\}-1\right]\Bigg|_{\mathbf{r}_1=\mathbf{y}}^{\mathbf{r}_1=\mathbf{x}}\Bigg|_{\mathbf{r}_2=\mathbf{y}}^{\mathbf{r}_2=\mathbf{x}}.
\end{aligned}
\tag{25.1}
$$

In the above equation, we can discern both the vacuum propagator of the gluon:

$$
G_0\left(\mathbf{r}_2,\mathbf{r}_1,\tau\right)=\int[\mathcal{D}\mathbf{r}\left(t\right)]\exp\left\{i\frac{\omega}{2}\int_{t_1}^{t_2}\mathrm{d}t\dot{\mathbf{r}}^2\left(t\right)\right\},
\tag{25.2}
$$

as well as the Green function that describes the motion of the gluon in an imaginary harmonic potential, which describes the multiple soft scatterings with the background:

$$
\begin{aligned}
G\left(\mathbf{r}_2,\mathbf{r}_1,\tau\right)\equiv\int[\mathcal{D}\mathbf{r}\left(t\right)]\exp\left\{i\frac{\omega}{2}\int_{t_1}^{t_2}\mathrm{d}t\dot{\mathbf{r}}^2\left(t\right)\right\} \\
\times\exp\left\{-\frac{1}{4}\hat{q}\int_{t_1}^{t_2}\mathrm{d}t\left((\mathbf{x}-\mathbf{r}\left(t\right))^2+(\mathbf{y}-\mathbf{r}\left(t\right))^2\right)\right\}.
\end{aligned}
\tag{25.3}
$$

For both, we can write down an explicit expression, provided by a standard calculation (see e.g. [186]):

$$
G_0\left(\mathbf{r}_2,\mathbf{r}_1,\tau\right)=-i\frac{\omega}{2\pi\tau}e^{i\frac{\omega}{2\tau}(\mathbf{r}_2-\mathbf{r}_1)^2},
\tag{25.4}
$$

$$
\begin{aligned}
G\left(\mathbf{r}_2,\mathbf{r}_1,\tau\right)=&-\frac{i}{2\pi}\frac{\omega\Omega}{\sinh\Omega\tau} \\
\times\exp&\left\{\frac{i}{2}\frac{\omega\Omega}{\sinh\Omega\tau}\left[\left((\mathbf{r}_2-\mathbf{R})^2+(\mathbf{r}_1-\mathbf{R})^2\right)\cosh\Omega\tau-2\left(\mathbf{r}_2-\mathbf{R}\right)\cdot\left(\mathbf{r}_1-\mathbf{R}\right)\right]\right\},
\end{aligned}
\tag{25.5}
$$

where

$$
\mathbf{R}\equiv\frac{\mathbf{x}+\mathbf{y}}{2},\quad\text{and}\quad\Omega\equiv\frac{1+i}{\sqrt{2}}\sqrt{\frac{\hat{q}}{\omega}}.
\tag{25.6}
$$

In the notation:

$$
N_\omega\left(\mathbf{x}\right)\equiv\frac{\partial S}{\partial\ln\omega}=\omega S\frac{\partial\ln S}{\partial\omega}\quad=-g^2C_FLS\omega\frac{\partial\bar{\Gamma}_\omega\left(\mathbf{x}\right)}{\partial\omega},
\tag{25.7}
$$

$$e^{-\frac{1}{4}\hat{q}\mathbf{x}^2 t_1} \; G(\mathbf{r}_2, \mathbf{r}_1, \tau) \, e^{-\frac{1}{4}\hat{q}\mathbf{x}^2(L-t_2)}$$
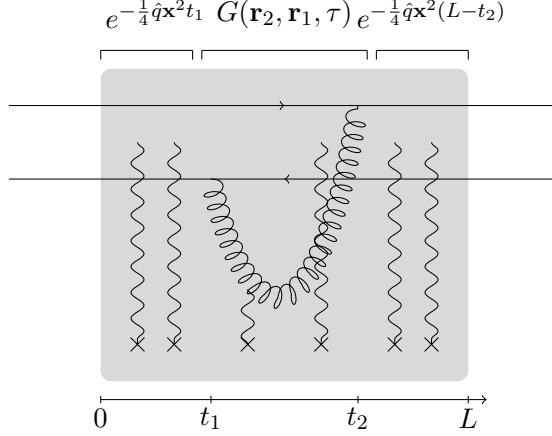

Figure 26: One step in the evolution of a dipole through the nuclear medium, as encoded in Eq. (25.8).

and, without loss of generality, setting $\mathbf{y} = \mathbf{0}$, Eq. (25.1) becomes:

$$N_\omega(\mathbf{x}) = \frac{-\alpha_s N_c}{2\omega^2} \int_0^L \mathrm{d}t_2 \int_0^{t_2} \mathrm{d}t_1 \partial^i_{\mathbf{r}_1} \partial^i_{\mathbf{r}_2}$$

$$\left(e^{-\frac{\hat{q}}{4}(L-t_2)\mathbf{x}^2} G(\mathbf{r}_2, \mathbf{r}_1, \tau) e^{-\frac{\hat{q}}{4}t_1\mathbf{x}^2} - e^{-\frac{\hat{q}}{4}L\mathbf{x}^2} G_0(\mathbf{r}_2, \mathbf{r}_1, \tau) \right) \Bigg|_{\mathbf{r}_2=\mathbf{0}}^{\mathbf{r}_2=\mathbf{x}} \Bigg|_{\mathbf{r}_1=\mathbf{0}}^{\mathbf{r}_1=\mathbf{x}}. \tag{25.8}$$

A nice feature of the above equation (we cast it in such a form to match the notations in Ref. [2]) is that it paints a very transparent picture of the physics at work (see Fig. 26): one step in the evolution corresponds to a gluon emission, whose motion in the transverse plane, as well as its multiple scattering (and the one of the parent dipole) off the medium, is encoded in the Green function $G(\mathbf{r}_2, \mathbf{r}_1, \tau = t_2 - t_1)$. Before and after the gluon fluctuation, the parent dipole undergoes multiple soft scattering, described by $\exp\left(-\frac{\hat{q}}{4}\mathbf{x}^2 t_1\right)$ and $\exp\left(-\frac{\hat{q}}{4}\mathbf{x}^2(L-t_2)\right)$, respectively. From this, the virtual contributions are subtracted, which correspond to the free gluon propagator times the multiple scattering factor of the parent dipole. Note that in Ref. [2], the factor $\exp\left(-\frac{\hat{q}}{4}\mathbf{x}^2 L\right)$ isn't included, since the authors obtain their evolution equation in the spirit of the BDMPS-Z formalism, in which they simply subtract a medium independent contribution $G_0(\mathbf{r}_2, \mathbf{r}_1, \tau)$. In this sense, the work of Iancu (Ref. [4]), to which this part of the thesis is devoted, can be regarded as a more formal, and ultimately more correct, approach to the same problem. By carefully constructing the in-medium evolution equation, we do obtain the correct virtual term which however, as we have seen, doesn't play a role in the double logarithmic approximation. Rather, the virtual contribution will become important when performing the calculation to single-logarithmic accuracy, for which the authors of Ref. [2] inserted the correct virtual corrections by hand.

Let us now show, as we already announced, that the limits to the phase space of the gluon fluctuation are encoded in Eq. (25.8). For this, we should first make the observation that the factor $\sqrt{\omega/\hat{q}}$, which appears in the definition of Ω, Eq. (25.6), is equal to the lifetime τ_{br} of a gluon whose

transverse momentum is solely obtained from multiple soft scatterings off the medium. Indeed, we have:

$$k_{\rm br}^2 = \hat{q}\tau, \quad \text{and} \quad \tau \simeq \frac{2\omega}{k_{\rm br}^2},$$

$$\iff \quad \tau_{\rm br}(\omega) \simeq \sqrt{\frac{\omega}{\hat{q}}}. \tag{25.9}$$

The region of multiple scattering is therefore the one above the $\tau_{\rm br}(\omega)$-line in the (τ, ω)-plane (see Fig. 24). Accordingly, this regime corresponds to values:

$$\Omega\tau = \frac{1+i}{\sqrt{2}}\frac{\tau}{\tau_{\rm br}} \gg 1 \tag{25.10}$$

for which:

$$G(\mathbf{r}_2, \mathbf{r}_1, \tau \gg \tau_{\rm br}) \simeq -\frac{i}{\pi}\omega\Omega e^{-\Omega\tau} \exp\left\{i\frac{\omega\Omega}{2}\left((\mathbf{r}_2-\mathbf{R})^2 + (\mathbf{r}_1-\mathbf{R})^2\right)\right\}. \tag{25.11}$$

Gluon fluctuations with a lifetime that surpasses the characteristic lifetime $\tau_{\rm br}(\omega)$ are thus exponentially suppressed. The emergence of the characteristic lifetime, during which the gluon undergoes coherent scattering with the medium, is recognized as an aspect of the Landau-Pomeranchuk-Migdal (LPM) effect (Refs. [187, 188]) in QCD (BDMPS-Z, see Refs. [158, 162–169]).

Furthermore, for values $\tau \sim \tau_{\rm br}$:

$$G(\mathbf{r}_2, \mathbf{r}_1, \tau \sim \tau_{\rm br}) \propto \exp\left\{\frac{i}{2}\omega\Omega\left((\mathbf{r}_2-\mathbf{R})^2 + (\mathbf{r}_1-\mathbf{R})^2\right)\right\},$$

$$\propto \exp\left\{-\frac{1}{\sqrt{2}}\frac{\omega}{\tau_{\rm br}}B^2\right\}, \tag{25.12}$$

hence the growth of the gluon fluctuation is restricted to $B^2 \lesssim 2/k_{\rm br}^2(\omega)$, as we anticipated in Eqs. (22.27), (22.30).

Finally, for small lifetimes $\tau \ll \tau_{\rm br}$ (but still $\tau \gg \omega/Q_s^2$), one can recover the double logarithmic approximation by expanding the r.h.s. of Eq. (25.8) around small sizes $\mathbf{x}$ of the parent dipole:

$$e^{-\frac{\hat{q}}{4}L\mathbf{x}^2}\partial_{\mathbf{r}_1} \cdot \partial_{\mathbf{r}_2} G_0(\mathbf{r}_2, \mathbf{r}_1, \tau)\Big|_{\mathbf{0}}^{\mathbf{x}}\Big|_{\mathbf{0}}^{\mathbf{x}} \simeq \frac{2i\omega^3}{\pi\tau^3}x^2,$$

$$e^{-\frac{\hat{q}}{4}(L-\tau)\mathbf{x}^2}\partial_{\mathbf{r}_1} \cdot \partial_{\mathbf{r}_2} G(\mathbf{r}_2, \mathbf{r}_1, \tau)\Big|_{\mathbf{0}}^{\mathbf{x}}\Big|_{\mathbf{0}}^{\mathbf{x}} \simeq \frac{i\omega^3\Omega^3}{2\pi\sinh^3\Omega\tau}x^2\left(\sinh^2\Omega\tau + 4\right), \tag{25.13}$$

such that:

$$N_\omega(\mathbf{x}) \simeq \frac{-i\alpha_s N_c}{4\pi\omega^2}x^2 \int_0^L \mathrm{d}t_2 \int_0^{t_2} \mathrm{d}t_1 \left(\frac{\omega}{\tau}\right)^3 \left(\frac{(\Omega\tau)^3}{\sinh^3\Omega\tau}\left(\sinh^2\Omega\tau + 4\right) - 4\right). \tag{25.14}$$

In Eq. (25.13) we see that, as expected, the virtual corrections do not play a role at the present DLA accuracy. Rewriting the time integrations as follows:

$$\int_0^L dt_2 \int_0^{t_2} dt_1 f\left(\tau = t_2 - t_1\right) = \int_0^L dt_2 \int_0^{t_2} d\tau f\left(\tau\right),$$
$$= \int_0^L dt_2 \int_0^L d\tau \Theta\left(t_2 - \tau\right) f\left(\tau\right), \qquad (25.15)$$
$$= \int_0^L d\tau \left(L - \tau\right) f\left(\tau\right),$$

the equation becomes:

$$N_\omega\left(\mathbf{x}\right) = \frac{-i\alpha_s N_c \omega}{4\pi} x^2 \int_{l_0}^L d\tau \frac{L-\tau}{\tau^3} \left(\frac{(\Omega\tau)^3}{\sinh^3 \Omega\tau} \left(\sinh^2 \Omega\tau + 4\right) - 4\right). \qquad (25.16)$$

Finally, taking the single scattering limit, i.e. $\Omega\tau$ small:

$$N_\omega\left(\mathbf{x}\right) \simeq \frac{i\alpha_s N_c}{4\pi\omega^2} x^2 \int_{l_0}^L d\tau \left(L - \tau\right) \left(\frac{\omega}{\tau}\right)^3 (\Omega\tau)^2,$$
$$= \frac{-\alpha_s N_c}{4\pi} \hat{q} x^2 \int_{l_0}^L dt \frac{L-\tau}{\tau}. \qquad (25.17)$$

Combining this result with Eq. (25.7) and with the definition (21.3) of transverse momentum broadening, we obtain:

$$\langle k_\perp^2 \rangle = \frac{\alpha_s N_c}{\pi} \hat{q} \int_{l_0}^L d\tau \frac{L-\tau}{\tau} \int_{\hat{q}\tau^2}^{\hat{q}L\tau} \frac{d\omega}{\omega},$$
$$\simeq \frac{\bar{\alpha}}{2} \hat{q} L \ln^2 \frac{L}{l_0}. \qquad (25.18)$$

in agreement with our result (23.5).

The authors of Ref. [2] push the calculation even further, to single logarithmic accuracy, that is: they manage to calculate all logarithmic contributions deeply inside the region $l_0 \ll \tau \ll L$ and $\omega_0 \ll \omega \ll \omega_c$ (see Fig. 24). Let us quickly sketch their approach: first, one chooses a point $\tau_{\mathrm{br}} \ll \tau_0 \ll \omega/Q_s^2$, hence within the single scattering region. The integration from this point onwards to the maximal lifetime $\tau = L$, crossing the multiple scattering boundary $\tau = \tau_{\mathrm{br}}\left(\omega\right)$, is then governed by Eq. (25.14):

$$N_\omega^{\tau_0 \to L}\left(\mathbf{x}\right) \simeq \frac{-i\alpha_s N_c}{4\pi\omega^2} x^2 \int_{\tau_0}^L d\tau \left(L - \tau\right) \left(\frac{\omega}{\tau}\right)^3 \left(\frac{(\Omega\tau)^3}{\sinh^3 \Omega\tau} \left(\sinh^2 \Omega\tau + 4\right) - 4\right). \qquad (25.19)$$

That is, the original dipole size is still assumed to be small enough for the harmonic approximation to hold ($N_\omega\left(\mathbf{x}\right) \propto x^2$), yet one doesn't enforce single scattering: there is no expansion in $\Omega\tau$.

This result is then matched with the integration that crosses the boundary $\tau = \omega/Q_s^2$, which is the regime in which the gluon's transverse size is of the same order as the parent dipole. The appropriate

equation is now the single-scattering 'BFKL' equation (22.20), in which the virtual term is crucial to guarantee ultraviolet convergence. Note that the time integrations, that we evaluated in Eqs. (22.18), (22.19), need to be restored in order to extract an integral over τ that can be matched with the one in Eq. (25.19). We have, approximately:

$$
\int_0^L \mathrm{d}t \int_0^t \mathrm{d}t_1 \int_t^L \mathrm{d}t_2 G_0\left(t_2, \mathbf{r}_2, t, \mathbf{z}; \omega\right) G_0\left(t, \mathbf{z}, t_1, \mathbf{r}_1; \omega\right)
$$
$$
\simeq L \int_{l_0}^{\tau_0} \mathrm{d}\tau \int_{-\tau}^0 \mathrm{d}t_1 G_0\left(\tau + t_1, \mathbf{r}_2, 0, \mathbf{z}; \omega\right) G_0\left(0, \mathbf{z}, t_1, \mathbf{r}_1; \omega\right),
\tag{25.20}
$$

which is in accordance with the manipulations in Eqs. (22.18), (22.19), in which we neglected the exponentials in L and t. The result is:

$$
N_\omega^{l_0 \to \tau_0}(\mathbf{x}) = \frac{\alpha_s}{\omega^2} \frac{N_c}{8} \hat{q} e^{-\frac{1}{4}\hat{q}Lx^2} L \int_{l_0}^{\tau_0} \mathrm{d}\tau \int_{-\tau}^0 \mathrm{d}t_1 \partial_{\mathbf{r}_1}^i \partial_{\mathbf{r}_2}^i
$$
$$
\times \int \mathrm{d}^2\mathbf{z}\, G_0\left(\tau + t_1, \mathbf{r}_2, 0, \mathbf{z}; \omega\right) G_0\left(0, \mathbf{z}, t_1, \mathbf{r}_1; \omega\right) \left((\mathbf{x} - \mathbf{z})^2 + z^2 - x^2\right)\Big|_{\mathbf{r}_1=\mathbf{0}}^{\mathbf{r}_1=\mathbf{x}}\Big|_{\mathbf{r}_2=\mathbf{0}}^{\mathbf{r}_2=\mathbf{x}}.
\tag{25.21}
$$

Finally, near the boundary $\tau = l_0$, the gluon distribution of the nucleon at large values of x is probed, since $\tau \simeq l_0/x$ (see the discussion in the previous section). The approximation that $\hat{q}$ is a constant is only valid in small-x, and therefore breaks down. In Ref. [2] this problem is circumvented by calculating directly the induced gluon radiation of a highly-energetic quark and setting $\langle k_\perp^2 \rangle \simeq k_\perp^2$, where $k_\perp$ is the transverse momentum of the radiated gluon. The result is:

$$
\langle k_\perp^2 \rangle \simeq \bar{\alpha} \int \frac{\mathrm{d}\omega}{\omega} \hat{q}L \left(\ln \frac{t_0}{L} + \gamma_E\right).
\tag{25.22}
$$

Matching results (25.19) with (25.22) for $\omega < \hat{q}l_0 L$, and (25.19) with (25.21) for $\omega > \hat{q}l_0 L$, one obtains the final result for the leading-order correction to the transverse momentum broadening to single leading logarithmic accuracy:

$$
\langle k_\perp^2 \rangle \simeq \bar{\alpha}\hat{q}L \left[\left(\ln 2 - \frac{1}{3}\right) \ln \frac{L}{l_0} + \frac{1}{2} \ln^2 \frac{L}{l_0}\right] + C,
\tag{25.23}
$$

where C is constant that cannot be calculated in the present formalism.

26 Conclusion

After constructing a non-eikonal generalization of the JIMWLK equation, we were well-equipped to attack the problem of the radiative corrections to the transverse momentum broadening of a hard parton that travels through a nuclear medium. To double leading logarithmic accuracy, these corrections could be absorbed into a renormalization of the jet quenching parameter, recovering the results in Refs. [2, 3]. Moreover, from our more formal evolution point of view, we derived the

complete in-medium evolution equation for a dipole, Eq. (22.12), which contains all the virtual terms necessary to guarantee ultraviolet convergence. In principle, solving the equation would be tantamount to the resummation of all the leading logarithmic corrections to $\hat{q}$, the single large logarithms included. In practice, however, we do not know how to solve such a functional integro-differential equation, which is complicated by the mixing of the longitudinal and transverse phase space due to the influence of the medium. Furthermore, most probably the LLA corrections cannot be associated with a renormalization of $\hat{q}$ anymore, but one rather has to renormalize the transverse momentum broadening $\langle k_{\perp}^2 \rangle$ itself.

Part V

Appendices

A   Lie algebra and Wilson line relations

The representations of $SU(3)$ are always Hermitian: $t^a = t^{a\dagger}$, hence:

$$t^a_{ij} = t^{a*}_{ji}. \tag{A.1}$$

The adjoint representation of $SU(3)$ is generated by the matrices:

$$T^a_{bc} = -if^{abc}, \tag{A.2}$$

where f^{abc} are the structure constants, given by:

$$\left[l^a, l^b\right] = if^{abc}l^c, \tag{A.3}$$

and where l^a are the generators of any $SU(3)$ representation. The structure constants f^{abc} are real and antisymmetric, hence:

$$T^a_{bc} = -T^{a*}_{bc}. \tag{A.4}$$

In our conventions, we define a Wilson line in the fundamental and adjoint representation, respectively, as follows:

$$U(\mathbf{x}) \equiv \mathcal{P} \exp\left(ig_s \int dx^+ A^-_c(\mathbf{x}) t^c\right),$$
$$W(\mathbf{x}) \equiv \mathcal{P} \exp\left(ig_s \int dx^+ A^-_c(\mathbf{x}) T^c\right), \tag{A.5}$$

where the path ordering operator $\mathcal{P}$ orders the color matrices from left to right, such that the rightmost matrix is the one that appears last along the integration path. The Hermitian conjugate of a Wilson line is then equal to:

$$U^\dagger(\mathbf{x}) = \left(\mathcal{P}\exp\left(ig_s \int dx^+ A^-_c(\mathbf{x}) t^c\right)\right)^\dagger = \bar{\mathcal{P}} \exp\left(\left(ig_s \int dx^+ A^-_c(\mathbf{x}) t^c\right)^\dagger\right),$$
$$= \bar{\mathcal{P}}\exp\left(-ig_s \int dx^+ A^-_c(\mathbf{x}) t^c\right) = U_\leftrightarrow(\mathbf{x}), \tag{A.6}$$

where $\bar{\mathcal{P}}$ is the anti-path ordering operator, ordering the color matrices from right to left according to their appearance along the path. Hermitian conjugation is therefore tantamount to inverting the direction along the integration path of the Wilson line.

Using the notation $U_\mathbf{x}(a, b)$ for a Wilson line over a finite length:

$$U_\mathbf{x}(a, b) \equiv \mathcal{P} \exp\left(ig_s \int_a^b dx^+ A^-_c(\mathbf{x}) t^c\right), \tag{A.7}$$

it is clear that the following rule holds:

$$U_{\mathbf{x}}\left(a,b\right)=U_{\mathbf{x}}\left(a,c\right)U_{\mathbf{x}}\left(c,b\right). \tag{A.8}$$

From Eq. (A.4), one has that:

$$\begin{aligned} W_{ab}^{*}\left(\mathbf{x}\right)&=\left(\mathcal{P}\exp\left(ig_{s}\int \mathrm{d}x^{+}A_{c}^{-}T^{c}\right)^{*}\right)_{ab},\\ &=\left(\mathcal{P}\exp\left(-ig_{s}\int \mathrm{d}x^{+}A_{c}^{-}T^{c*}\right)\right)_{ab},\\ &=W_{ab}\left(\mathbf{x}\right), \end{aligned} \tag{A.9}$$

and hence a Wilson line in the adjoint representation is real.

Using the expansion of the Wilson lines around unity, we find the following important identity:

$$U^{\dagger}t^{a}U=W_{ac}t^{c}. \tag{A.10}$$

The same identity holds for Wilson lines in the adjoint representation:

$$W^{\dagger}t^{a}W=W_{ac}t^{c}. \tag{A.11}$$

We will frequently take the traces over the representation matrices

$$\begin{aligned} \mathrm{Tr}\left(t^{a}t^{b}\right)&=\frac{1}{2}\delta_{ab},\\ \mathrm{Tr}\left(T^{a}T^{b}\right)&=N_{c}\delta_{ab}, \end{aligned} \tag{A.12}$$

and use the very important Fierz identity:

$$t_{ij}^{a}t_{kl}^{a}=\frac{1}{2}\delta_{il}\delta_{jk}-\frac{1}{2N_{c}}\delta_{ij}\delta_{kl}. \tag{A.13}$$

The Casimir operators of the fundamental and adjoint representation are:

$$t_{ik}^{a}t_{kj}^{a}=C_{F}\delta_{ij},\quad\text{with}\quad C_{F}\equiv\frac{N_{c}^{2}-1}{2N_{c}}, \tag{A.14}$$

and

$$T_{ac}^{d}T_{cb}^{d}=N_{c}\delta_{ab}. \tag{A.15}$$

B Some useful integrals

The following integral, which is the Green function of the two-dimensional Laplace equation, will often play a role in our calculations:

$$\begin{aligned} \int \mathrm{d}^{2}\mathbf{k}_{\perp}\frac{e^{i\mathbf{k}_{\perp}\mathbf{r}}}{k_{\perp}^{2}}&=2\pi\int_{\Lambda}^{\infty}\frac{\mathrm{d}k_{\perp}}{k_{\perp}}J_{0}\left(k_{\perp}r\right),\\ &=2\pi\ln\frac{1}{r\Lambda}. \end{aligned} \tag{B.1}$$

Moreover, one can show that:

$$\int d^2\mathbf{k}_\perp \frac{e^{i\mathbf{k}_\perp \mathbf{r}}}{k_\perp^2} = \int d^2\mathbf{z} \frac{z^i (r+z)^i}{z^2 (\mathbf{r}+\mathbf{z})^2}, \tag{B.2}$$

and

$$\int d^2\mathbf{k}_\perp \frac{k_\perp^i}{k_\perp^2} e^{i\mathbf{k}_\perp \mathbf{x}} = 2\pi i \frac{x^i}{x^2}. \tag{B.3}$$

C Light-cone perturbation theory conventions

We follow the so-called 'Kogut-Soper' conventions [17], in which the transverse polarization vectors of the gluon are written as follows:

$$\epsilon_\lambda^\mu (k) = \left(0, \frac{k_\perp \cdot \epsilon_\perp^\lambda}{k^+}, \epsilon_\perp^\lambda\right), \tag{C.1}$$

and the longitudinal polarization vector (with $Q^2 = k^2$):

$$\epsilon_L^\mu (k) = \left(0, \frac{Q}{k^+}, 0\right). \tag{C.2}$$

One chooses circular polarization, in which

$$\boldsymbol{\epsilon}_\perp^1 = \frac{1}{\sqrt{2}} \begin{pmatrix} 1 \\ i \end{pmatrix}, \qquad \boldsymbol{\epsilon}_\perp^2 = \frac{1}{\sqrt{2}} \begin{pmatrix} 1 \\ -i \end{pmatrix}, \tag{C.3}$$

with $\boldsymbol{\epsilon}_\perp^{\lambda\dagger} \cdot \boldsymbol{\epsilon}_\perp^{\lambda'} = \delta^{\lambda\lambda'}$. We work in the chiral representation of the gamma matrices:

$$\gamma^0 = \begin{pmatrix} 0 & I \\ I & 0 \end{pmatrix}, \quad \gamma^i = \begin{pmatrix} 0 & -\sigma^i \\ \sigma^i & 0 \end{pmatrix}, \tag{C.4}$$

$$\gamma^+ = \begin{pmatrix} 0 & 0 & 0 & 0 \\ 0 & 0 & 0 & \sqrt{2} \\ \sqrt{2} & 0 & 0 & 0 \\ 0 & 0 & 0 & 0 \end{pmatrix}, \quad \gamma^1 = \begin{pmatrix} 0 & 0 & 0 & -1 \\ 0 & 0 & -1 & 0 \\ 0 & 1 & 0 & 0 \\ 1 & 0 & 0 & 0 \end{pmatrix}, \quad \gamma^2 = \begin{pmatrix} 0 & 0 & 0 & i \\ 0 & 0 & -i & 0 \\ 0 & -i & 0 & 0 \\ i & 0 & 0 & 0 \end{pmatrix}, \tag{C.5}$$

with the usual Pauli matrices:

$$\sigma^1 = \begin{pmatrix} 0 & 1 \\ 1 & 0 \end{pmatrix}, \quad \sigma^2 = \begin{pmatrix} 0 & -i \\ i & 0 \end{pmatrix}, \quad \sigma^3 = \begin{pmatrix} 1 & 0 \\ 0 & -1 \end{pmatrix}. \tag{C.6}$$
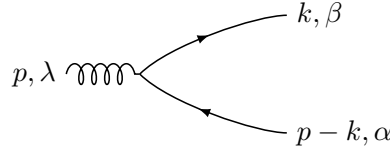
With these conventions, the Dirac spinors are given by:

$$u_+ (k) = \frac{1}{2^{1/4}\sqrt{k^+}} \begin{pmatrix} \sqrt{2}k^+ \\ k_1 + ik_2 \\ m \\ 0 \end{pmatrix}, \qquad u_- (k) = \frac{1}{2^{1/4}\sqrt{k^+}} \begin{pmatrix} 0 \\ m \\ -k_1 + ik_2 \\ \sqrt{2}k^+ \end{pmatrix}, \tag{C.7}$$

and

$$v_+ (k) = \frac{1}{2^{1/4}\sqrt{k^+}} \begin{pmatrix} 0 \\ -m \\ -k_1 + ik_2 \\ \sqrt{2}k^+ \end{pmatrix}, \qquad v_- (k) = \frac{1}{2^{1/4}\sqrt{k^+}} \begin{pmatrix} \sqrt{2}k^+ \\ k_1 + ik_2 \\ -m \\ 0 \end{pmatrix}. \tag{C.8}$$

D   The $g \to q\bar{q}$ wave function

Choosing $p^\mu = \left(p^+, \left(p_\perp^2 - Q^2\right)/2p^+, \mathbf{p}_\perp\right)$ to be the momentum of the gluon, and k and $q \equiv p - k$ the momenta of the quark and antiquark, respectively, the wave function will have the form:

$$\psi_{\alpha\beta}^{\lambda,L} (p, k) = \frac{1}{\sqrt{8 (p - k)^+ p^+ k^+}} \frac{\bar{u}_\beta (k) \gamma_\mu \epsilon_{\lambda,L}^\mu (p) v_\alpha (p - k)}{(p - k)^- + k^- - p^-}, \tag{D.1}$$

where:

$$\gamma_\mu \epsilon_\lambda^\mu (k) = \gamma^+ \frac{\mathbf{k}_\perp \cdot \boldsymbol{\epsilon}_\perp^\lambda}{k^+} - \gamma_\perp \cdot \epsilon_\perp^\lambda, \tag{D.2}$$

$$= \begin{pmatrix} 0 & 0 & 0 & \epsilon_1^\lambda - i\epsilon_2^\lambda \\ 0 & 0 & \epsilon_1^\lambda + i\epsilon_2^\lambda & \sqrt{2}\frac{\mathbf{k}_\perp \cdot \boldsymbol{\epsilon}_\perp^\lambda}{k^+} \\ \sqrt{2}\frac{\mathbf{k}_\perp \cdot \boldsymbol{\epsilon}_\perp^\lambda}{k^+} & -\epsilon_1^\lambda + i\epsilon_2^\lambda & 0 & 0 \\ -\epsilon_1^\lambda - i\epsilon_2^\lambda & 0 & 0 & 0 \end{pmatrix}, \tag{D.3}$$

and

$$\gamma_\mu \epsilon_L^\mu (k) = \gamma^+ \epsilon_L^- (k) = \frac{Q}{p^+} \begin{pmatrix} 0 & 0 & 0 & 0 \\ 0 & 0 & 0 & \sqrt{2} \\ \sqrt{2} & 0 & 0 & 0 \\ 0 & 0 & 0 & 0 \end{pmatrix}. \tag{D.4}$$

The energy denominator is the same for each spin configuration, and can be calculated as follows:

$$\begin{aligned}
(p - k)^- + k^- - p^- &= \frac{m^2 + (\mathbf{p}_\perp - \mathbf{k}_\perp)^2}{2 (p^+ - k^+)} + \frac{k_\perp^2 + m^2}{2k^+} - \frac{p_\perp^2 - Q^2}{2p^+}, \\
&= \frac{(\mathbf{k}_\perp - z\mathbf{p}_\perp)^2 + m^2 + (1 - z) zQ^2}{2 (p^+ - k^+) z}.
\end{aligned} \tag{D.5}$$

Helicity minus - minus

In the case of a longitudinal polarized gluon, the numerator reads:

$$\bar{u}_- (k) \gamma_\mu \epsilon_L^\mu (p) v_+ (q) = \frac{1}{\sqrt{2k^+ (p-k)^+}} \frac{Q}{p^+} \left(\begin{array}{cccc} -k_1 - ik_2, & \sqrt{2}k^+, & 0, & m \end{array} \right)$$

$$\times \begin{pmatrix} 0 & 0 & 0 & 0 \\ 0 & 0 & 0 & \sqrt{2} \\ \sqrt{2} & 0 & 0 & 0 \\ 0 & 0 & 0 & 0 \end{pmatrix} \begin{pmatrix} 0 \\ -m \\ -q_1 + iq_2 \\ \sqrt{2}q^+ \end{pmatrix} = \frac{2zQq^+}{\sqrt{k^+ (p-k)^+}}, \tag{D.6}$$

while we have for the transverse case:

$$\bar{u}_- (k) \gamma_\mu \epsilon_\lambda^\mu (p) v_+ (q)$$

$$= \frac{1}{\sqrt{2k^+ (p-k)^+}} \left(\sqrt{2}q^+ \left(\epsilon_1^\lambda - i\epsilon_2^\lambda \right) (-k_1 - ik_2) \right.$$

$$+ \sqrt{2}k^+ \left((-q_1 + iq_2) \left(\epsilon_1^\lambda + i\epsilon_2^\lambda \right) + 2q^+ \frac{\mathbf{p}_\perp \cdot \boldsymbol{\epsilon}_\perp^\lambda}{p^+} \right) \right),$$

$$= \frac{1}{\sqrt{k^+ (p-k)^+}} \left(2q^+ \delta_{\lambda 1} (-k_1 - ik_2) + 2k^+ (-q_1 + iq_2) \delta_{\lambda 2} + 2zq^+ \mathbf{p}_\perp \cdot \boldsymbol{\epsilon}_\perp^\lambda \right), \tag{D.7}$$

$$= \frac{1}{\sqrt{k^+ (p-k)^+}} \left(-2q^+ \delta_{\lambda 1} \mathbf{k}_\perp \cdot \boldsymbol{\epsilon}_\perp^1 - 2k^+ \delta_{\lambda 2} \mathbf{q}_\perp \cdot \boldsymbol{\epsilon}_\perp^2 + 2zq^+ \mathbf{p}_\perp \cdot \boldsymbol{\epsilon}_\perp^\lambda \right),$$

$$= \frac{1}{\sqrt{k^+ (p-k)^+}} \left(-2q^+ \delta_{\lambda 1} (\mathbf{k}_\perp - z\mathbf{p}_\perp) \cdot \boldsymbol{\epsilon}_\perp^1 + 2k^+ \delta_{\lambda 2} (\mathbf{k}_\perp - z\mathbf{p}_\perp) \cdot \boldsymbol{\epsilon}_\perp^2 \right),$$

where in the last line we used the definition $\mathbf{q}_\perp = \mathbf{p}_\perp - \mathbf{k}_\perp$. Finally, one obtains the following expressions for the wave functions:

$$\psi_{--}^L (p, k) = \frac{1}{\sqrt{8 (p-k)^+ p^+ k^+}} \frac{2 (p^+ - k^+) z}{(\mathbf{k}_\perp - z\mathbf{p}_\perp)^2 + m^2 + (1-z) zQ^2} \frac{2zQq^+}{\sqrt{k^+ (p-k)^+}},$$

$$= \sqrt{\frac{2}{p^+}} \frac{Qz (1-z)}{(\mathbf{k}_\perp - z\mathbf{p}_\perp)^2 + m^2 + (1-z) zQ^2}, \tag{D.8}$$

$$\psi_{--}^{T\lambda} (p, k) = \frac{1}{\sqrt{8 (p-k)^+ p^+ k^+}} \frac{2 (p^+ - k^+) z}{(\mathbf{k}_\perp - z\mathbf{p}_\perp)^2 + m^2 + (1-z) zQ^2}$$

$$\times \frac{1}{\sqrt{k^+ (p-k)^+}} \left(-2q^+ \delta_{\lambda 1} (\mathbf{k}_\perp - z\mathbf{p}_\perp) \cdot \boldsymbol{\epsilon}_\perp^1 + 2k^+ \delta_{\lambda 2} (\mathbf{k}_\perp - z\mathbf{p}_\perp) \cdot \boldsymbol{\epsilon}_\perp^2 \right), \tag{D.9}$$

$$= \sqrt{\frac{2}{p^+}} \frac{- (1-z) \delta_{\lambda 1} (\mathbf{k}_\perp - z\mathbf{p}_\perp) \cdot \boldsymbol{\epsilon}_\perp^1 + z\delta_{\lambda 2} (\mathbf{k}_\perp - z\mathbf{p}_\perp) \cdot \boldsymbol{\epsilon}_\perp^2}{(\mathbf{k}_\perp - z\mathbf{p}_\perp)^2 + m^2 + (1-z) zQ^2}.$$

Helicity plus - plus

For the longitudinal polarized gluon, the numerator reads:

$$\bar{u}_+ (k) \gamma_\mu \epsilon_L^\mu (p) v_- (q) = \frac{2zQq^+}{\sqrt{k^+ (p-k)^+}}, \tag{D.10}$$

and in the transverse case, we have:

$$\bar{u}_+ (k) \gamma_\mu \epsilon_\lambda^\mu (p) v_- (q)$$
$$= \frac{1}{\sqrt{k^+ (p-k)^+}} \left(2k^+ (\mathbf{k}_\perp - z\mathbf{p}_\perp) \cdot \boldsymbol{\epsilon}_\perp^1 \delta_{\lambda 1} - 2q^+ \delta_{\lambda 2} (\mathbf{k}_\perp - z\mathbf{p}_\perp) \cdot \boldsymbol{\epsilon}_\perp^2 \right). \tag{D.11}$$

The wave functions finally read:

$$\psi_{++}^L (p, k) = \frac{1}{\sqrt{8(p-k)^+ p^+ k^+}} \frac{2(p^+ - k^+) z}{(\mathbf{k}_\perp - z\mathbf{p}_\perp)^2 + m^2 + (1-z) zQ^2} \frac{2zQq^+}{\sqrt{k^+ (p-k)^+}},$$
$$= \sqrt{\frac{2}{p^+}} \frac{Q(1-z) z}{(\mathbf{k}_\perp - z\mathbf{p}_\perp)^2 + m^2 + (1-z) zQ^2}, \tag{D.12}$$

and

$$\psi_{++}^\lambda (p, k) = \frac{1}{\sqrt{8(p-k)^+ p^+ k^+}} \frac{2(p^+ - k^+) z}{(\mathbf{k}_\perp - z\mathbf{p}_\perp)^2 + m^2 + (1-z) zQ^2}$$
$$\times \frac{1}{\sqrt{k^+ (p-k)^+}} \left(2k^+ (\mathbf{k}_\perp - z\mathbf{p}_\perp) \cdot \boldsymbol{\epsilon}_\perp^1 \delta_{\lambda 1} - 2q^+ \delta_{\lambda 2} (\mathbf{k}_\perp - z\mathbf{p}_\perp) \cdot \boldsymbol{\epsilon}_\perp^2 \right), \tag{D.13}$$
$$= \sqrt{\frac{2}{p^+}} \frac{z \delta_{\lambda 1} (\mathbf{k}_\perp - z\mathbf{p}_\perp) \cdot \boldsymbol{\epsilon}_\perp^1 - (1-z) \delta_{\lambda 2} (\mathbf{k}_\perp - z\mathbf{p}_\perp) \cdot \boldsymbol{\epsilon}_\perp^2}{(\mathbf{k}_\perp - z\mathbf{p}_\perp)^2 + m^2 + (1-z) zQ^2}.$$

Helicity-flip cases

For the longitudinal polarization, we have:

$$\bar{u}_+ (k) \gamma_\mu \epsilon_L^\mu (p) v_+ (q) = 0,$$
$$\bar{u}_- (k) \gamma_\mu \epsilon_L^\mu (p) v_- (q) = 0. \tag{D.14}$$

The numerators for the transversely polarized gluon are given by:

$$\bar{u}_+ (k) \gamma_\mu \epsilon_\lambda^\mu (p) v_+ (q) = \frac{\sqrt{2} m p^+}{\sqrt{k^+ (p-k)^+}} \delta_{\lambda 1},$$

$$\bar{u}_- (k) \gamma_\mu \epsilon_\lambda^\mu (p) v_- (q) = \frac{-\sqrt{2} m p^+}{\sqrt{k^+ (p-k)^+}} \delta_{\lambda 2}. \tag{D.15}$$

The wave functions read:

$$\psi_{+-}^{L}(p,k) = \psi_{-+}^{L}(p,k) = 0, \tag{D.16}$$

$$\psi_{+-}^{\lambda}(p,k) = \frac{1}{\sqrt{8(p-k)^{+}p^{+}k^{+}}} \frac{2(p^{+}-k^{+})z}{(\mathbf{k}_{\perp}-z\mathbf{p}_{\perp})^{2}+m^{2}+(1-z)zQ^{2}} \frac{mp^{+}}{\sqrt{k^{+}(p-k)^{+}}}\sqrt{2}\delta_{\lambda 1},$$
$$= \sqrt{\frac{2}{p^{+}}} \frac{1}{(\mathbf{k}_{\perp}-z\mathbf{p}_{\perp})^{2}+m^{2}+(1-z)zQ^{2}} \frac{m}{\sqrt{2}}\delta_{\lambda 1}, \tag{D.17}$$

$$\psi_{-+}^{\lambda}(p,k) = \frac{1}{\sqrt{8(p-k)^{+}p^{+}k^{+}}} \frac{2(p^{+}-k^{+})z}{(\mathbf{k}_{\perp}-z\mathbf{p}_{\perp})^{2}+m^{2}+(1-z)zQ^{2}} \frac{-p^{+}m}{\sqrt{k^{+}(p-k)^{+}}}\sqrt{2}\delta_{\lambda 2}$$
$$= \sqrt{\frac{2}{p^{+}}} \frac{1}{(\mathbf{k}_{\perp}-z\mathbf{p}_{\perp})^{2}+m^{2}+(1-z)zQ^{2}} \frac{-m}{\sqrt{2}}\delta_{\lambda 2}. \tag{D.18}$$

A general expression for the wave function

The wave functions for the specific helicity cases can be written in full generality as follows:

$$\psi_{\alpha\beta}^{T\lambda}(p,k) = \sqrt{\frac{2}{p^{+}}} \frac{1}{(\mathbf{k}_{\perp}-z\mathbf{p}_{\perp})^{2}+\epsilon_{f}^{2}}$$
$$\times \begin{cases} (z\delta_{\alpha+}\delta_{\beta+}-(1-z)\delta_{\alpha-}\delta_{\beta-})(\mathbf{k}_{\perp}-z\mathbf{p}_{\perp})\cdot\boldsymbol{\epsilon}_{\perp}^{1}+\frac{m}{\sqrt{2}}\delta_{\alpha+}\delta_{\beta-} & \lambda=1 \\ (z\delta_{\alpha-}\delta_{\beta-}-(1-z)\delta_{\alpha+}\delta_{\beta+})(\mathbf{k}_{\perp}-z\mathbf{p}_{\perp})\cdot\boldsymbol{\epsilon}_{\perp}^{2}-\frac{m}{\sqrt{2}}\delta_{\alpha-}\delta_{\beta+} & \lambda=2 \end{cases}, \tag{D.19}$$

and

$$\psi_{\alpha\beta}^{L}(p,k) = \sqrt{\frac{2}{p^{+}}} \frac{Qz(1-z)}{(\mathbf{k}_{\perp}-z\mathbf{p}_{\perp})^{2}+\epsilon_{f}^{2}}\delta_{\alpha\beta}, \tag{D.20}$$

where we defined:

$$\epsilon_{f}^{2} \equiv m^{2}+(1-z)zQ^{2}. \tag{D.21}$$

In the mixed Fourier-coordinate representation, the wave functions become:

$$\phi_{\alpha\beta}^{T\lambda}(p,z,\mathbf{r}) \equiv \int d^{2}\mathbf{k}_{\perp}e^{i\mathbf{k}_{\perp}\cdot\mathbf{r}}\psi_{\alpha\beta}^{T\lambda}(p,k), \tag{D.22}$$

$$\phi_{\alpha\beta}^{T\lambda}(p,z,\mathbf{r}) = 2\pi\sqrt{\frac{2}{p^{+}}}e^{iz\mathbf{p}_{\perp}\cdot\mathbf{r}}$$
$$\times \begin{cases} i\epsilon_{f}K_{1}(\epsilon_{f}r)\frac{\mathbf{r}\cdot\boldsymbol{\epsilon}_{\perp}^{1}}{r}(z\delta_{\alpha-}\delta_{\beta-}-(1-z)\delta_{\alpha+}\delta_{\beta+})+\frac{m}{\sqrt{2}}K_{0}(\epsilon_{f}r)\delta_{\alpha+}\delta_{\beta-} & \lambda=1 \\ i\epsilon_{f}K_{1}(\epsilon_{f}r)\frac{\mathbf{r}\cdot\boldsymbol{\epsilon}_{\perp}^{2}}{r}(z\delta_{\alpha+}\delta_{\beta+}-(1-z)\delta_{\alpha-}\delta_{\beta-})-\frac{m}{\sqrt{2}}K_{0}(\epsilon_{f}r)\delta_{\alpha-}\delta_{\beta+} & \lambda=2 \end{cases}, \tag{D.23}$$

127

and

$$\phi_{\alpha\beta}^{L}\left(p,z,\mathbf{r}\right) \equiv \int \mathrm{d}^2\mathbf{k}_{\perp} e^{i\mathbf{k}_{\perp}\cdot\mathbf{r}} \psi_{\alpha\beta}^{L}\left(p,k\right),$$

$$= \sqrt{\frac{2}{p^+}} \int \frac{\mathrm{d}^2\mathbf{k}_{\perp}}{(2\pi)^2} e^{i\mathbf{k}_{\perp}\cdot\mathbf{r}} \frac{Qz\left(1-z\right)}{\left(\mathbf{k}_{\perp} - z\mathbf{p}_{\perp}\right)^2 + \epsilon_f^2} \delta_{\alpha\beta}, \tag{D.24}$$

$$= 2\pi\sqrt{\frac{2}{p^+}} e^{iz\mathbf{p}_{\perp}\cdot\mathbf{r}} Qz\left(1-z\right) K_0\left(\epsilon_f r\right) \delta_{\alpha\beta},$$

where we made use of the following identities:

$$\int \mathrm{d}^2\mathbf{k}_{\perp} \frac{e^{i\mathbf{k}_{\perp}\cdot\mathbf{r}}}{k_{\perp}^2 + m^2} = 2\pi K_0\left(mr\right),$$

$$\int \mathrm{d}^2\mathbf{k}_{\perp} \frac{k_{\perp}^i e^{i\mathbf{k}_{\perp}\cdot\mathbf{r}}}{k_{\perp}^2 + m^2} = 2\pi i m \frac{r^i}{r} K_1\left(mr\right). \tag{D.25}$$

The wave function squared

Neglecting the phase $e^{iz\mathbf{p}_{\perp}\cdot\mathbf{r}}$, the square of the absolute value of the wave function squared, summed over all outgoing quantum numbers, and averaged over the polarization and color charge of the incoming gluon is:

$$\left|\phi_T^{g\to q\bar{q}}\left(p^+,z,\mathbf{r},\mathbf{r}'\right)\right|^2 = \frac{1}{2} \frac{1}{N_c^2-1} \sum_{ab} \mathrm{Tr}\left(t^a t^b\right) \sum_{\lambda\alpha\beta} \phi_{\alpha\beta}^{T\lambda}\left(p^+,z,\mathbf{r}\right) \phi_{\alpha\beta}^{T\lambda*}\left(p^+,z,\mathbf{r}'\right),$$

$$= \frac{2\pi^2}{p^+} \left(\epsilon_f^2 K_1\left(\epsilon_f r\right) K_1\left(\epsilon_f r'\right) \frac{\mathbf{r}\cdot\mathbf{r}'}{rr'} \left(z^2 + (1-z)^2\right) \right. \tag{D.26}$$

$$\left. + m^2 K_0\left(\epsilon_f r'\right) K_0\left(\epsilon_f r\right) \right),$$

where we used the easy to prove identity:

$$\frac{\mathbf{r}\cdot\boldsymbol{\epsilon}_{\perp}^1}{r} \frac{\mathbf{r}'\cdot\boldsymbol{\epsilon}_{\perp}^{1*}}{r'} + \frac{\mathbf{r}\cdot\boldsymbol{\epsilon}_{\perp}^2}{r} \frac{\mathbf{r}'\cdot\boldsymbol{\epsilon}_{\perp}^{2*}}{r'} = \frac{\mathbf{r}\cdot\mathbf{r}'}{rr'}, \tag{D.27}$$

and where we added the color matrices t^a. In the limit $m \to 0$ and $Q^2 \to 0$, and therefore $\epsilon_f \to 0$, we have that:

$$\lim_{\epsilon_f\to 0} \epsilon_f^2 K_1\left(\epsilon_f r\right) K_1\left(\epsilon_f r'\right) = \frac{1}{rr'},$$

$$\lim_{\epsilon_f\to 0} \epsilon_f^2 K_0\left(\epsilon_f r\right) K_0\left(\epsilon_f r'\right) = 0, \tag{D.28}$$

and as a result Eq. (D.26) simplifies to:

$$\lim_{\epsilon_f\to 0} \left|\phi_T^{g\to q\bar{q}}\left(p^+,z,\mathbf{r},\mathbf{r}'\right)\right|^2 = \frac{(2\pi)^2}{p^+} \frac{\mathbf{r}\cdot\mathbf{r}'}{r^2 r'^2} \left(z^2 + (1-z)^2\right). \tag{D.29}$$

128

Likewise, for the longitudinal polarized gluon, again neglecting the phase factor $e^{iz\mathbf{p}_\perp \cdot \mathbf{r}}$, we obtain:

$$\left|\phi_L^{g\to q\bar{q}}\left(p^+, z, \mathbf{r}, \mathbf{r}'\right)\right|^2 = \frac{1}{N_c^2 - 1} \sum_{ab} \mathrm{Tr}\left(t^a t^b\right) \sum_{\alpha\beta} \phi_{\alpha\beta}^L\left(p^+, z, \mathbf{r}\right) \phi_{\alpha\beta}^{L*}\left(p^+, z, \mathbf{r}'\right),$$

$$= \frac{2\pi^2}{p^+} 4Q^2 z^2 \left(1 - z\right)^2 K_0\left(\epsilon_f r\right) K_0\left(\epsilon_f r'\right), \tag{D.30}$$

which obviously vanishes in the limit $Q^2 \to 0$.

The absolute value of the wave function squared in momentum space, and in the limits $Q^2 \to 0$ and $m^2 \to 0$ (hence the longitudinally polarized gluon disappears) yields:

$$\left|\psi_T^{g\to q\bar{q}}\left(p, k\right)\right|^2 = \frac{1}{2} \sum_{\lambda\alpha\beta} \psi_{\alpha\beta}^{\lambda\dagger}\left(p, k\right) \psi_{\alpha\beta}^{\lambda}\left(p, k\right) = \frac{1}{p^+} \frac{z^2 + \left(1 - z\right)^2}{k_\perp^2}, \tag{D.31}$$

where we used that:

$$\left(\mathbf{k}_\perp \cdot \boldsymbol{\epsilon}_\perp^1\right)\left(\mathbf{k}_\perp \cdot \boldsymbol{\epsilon}_\perp^{1*}\right) = \left(\mathbf{k}_\perp \cdot \boldsymbol{\epsilon}_\perp^2\right)\left(\mathbf{k}_\perp \cdot \boldsymbol{\epsilon}_\perp^{2*}\right) = \frac{k_\perp^2}{2}. \tag{D.32}$$

Note that we chose our definitions in such a way that the wavefunctions for $g \to q\bar{q}$ and $\gamma \to q\bar{q}$ are the same, which is why we had to add the trace over color matrices and the average over gluon color explicitly when computing the wavefunction squared in the $g \to q\bar{q}$ case. The wavefunction squared for $\gamma \to q\bar{q}$ is now simply obtained from Eq. (D.26) by the substitution:

$$\frac{1}{N_c^2 - 1} \sum_{ab} \mathrm{Tr}\left(t^a t^b\right) \to \delta^{ij}\delta^{ji}, \tag{D.33}$$

or equivalently:

$$\frac{1}{2} \to N_c. \tag{D.34}$$

E The $q \to gq$ wave function
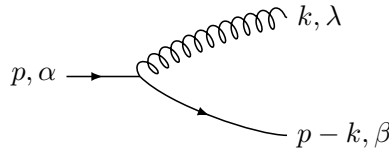
The wave function of the dressed quark is given by:

$$\psi_{\alpha\beta}^{\lambda}\left(p, k\right) = \frac{1}{\sqrt{8\left(p - k\right)^+ p^+ k^+}} \frac{\bar{u}_\beta\left(p - k\right) \gamma_\mu \epsilon_\lambda^\mu\left(k\right) u_\alpha\left(p\right)}{\left(p - k\right)^- + k^- - p^-}, \tag{E.1}$$

where, using the notation $z = k^+/p^+$, the energy denominator reads:

$$\frac{1}{\left(p - k\right)^- + k^- - p^-} = \frac{2z\left(p^+ - k^+\right)}{\left(\mathbf{k}_\perp - z\mathbf{p}_\perp\right)^2 + z^2 m^2}. \tag{E.2}$$

Spin up - spin up

The numerator is given by:

$$
\bar{u}_+ (p-k)\, \gamma_\mu \epsilon_\lambda^\mu (k)\, u_+ (p)
$$
$$
= \frac{2p^+}{z\sqrt{p^+ (p-k)^+}} \left((1-z)\, \delta_{\lambda 1} \left(\mathbf{k}_\perp - z\mathbf{p}_\perp \right) \cdot \boldsymbol{\epsilon}_\perp^{(1)} + \delta_{\lambda 2} \left(\mathbf{k}_\perp - z\mathbf{p}_\perp \right) \cdot \boldsymbol{\epsilon}_\perp^{(2)} \right),
\tag{E.3}
$$

and the wave function for the spin up - spin up case yields:

$$
\psi_{++}^\lambda (p,k) = \sqrt{\frac{2}{k^+}} \frac{\left((1-z)\, \delta_{\lambda 1} + \delta_{\lambda 2} \right) \left(\mathbf{k}_\perp - z\mathbf{p}_\perp \right) \cdot \boldsymbol{\epsilon}_\perp^\lambda}{\left(\mathbf{k}_\perp - z\mathbf{p}_\perp \right)^2 + z^2 m^2}.
\tag{E.4}
$$

Spin down - spin down

The numerator gives:

$$
\bar{u}_- (q)\, \gamma_\mu \epsilon_\lambda^\mu (k)\, u_- (p)
$$
$$
= \frac{2p^+}{z\sqrt{p^+ (p-k)^+}} \left(\delta_{\lambda 1} \left(\mathbf{k}_\perp - z\mathbf{p}_\perp \right) \cdot \boldsymbol{\epsilon}_\perp^{(1)} + (1-z)\, \delta_{\lambda 2} \left(\mathbf{k}_\perp - z\mathbf{p}_\perp \right) \cdot \boldsymbol{\epsilon}_\perp^{(2)} \right),
\tag{E.5}
$$

and we obtain the following wave function:

$$
\psi_{--}^\lambda (p,k) = \sqrt{\frac{2}{k^+}} \frac{\left(\delta_{\lambda 1} + (1-z)\, \delta_{\lambda 2} \right) \left(\mathbf{k}_\perp - z\mathbf{p}_\perp \right) \cdot \boldsymbol{\epsilon}_\perp^\lambda}{\left(\mathbf{k}_\perp - z\mathbf{p}_\perp \right)^2 + z^2 m^2}.
\tag{E.6}
$$

The spin-flip cases

The wave function for the spin-flip cases is much simpler, as is apparent from the expressions we find for the numerators:

$$
\bar{u}_+ (q)\, \gamma_\mu \epsilon_\lambda^\mu (k)\, u_- (p) = \frac{\sqrt{2} k^+ m \delta_{\lambda 1}}{\sqrt{p^+ (p-k)^+}},
$$
$$
\bar{u}_- (q)\, \gamma_\mu \epsilon_\lambda^\mu (k)\, u_+ (p) = -\frac{\sqrt{2} k^+ m \delta_{\lambda 2}}{\sqrt{p^+ (p-k)^+}}.
\tag{E.7}
$$

From this, we find the following results for the wave functions:

$$
\psi_{+-}^\lambda (p,k) = \frac{1}{\sqrt{k^+}} \frac{z^2 m \delta_{\lambda 1}}{\left(\mathbf{k}_\perp - z\mathbf{p}_\perp \right)^2 + z^2 m^2},
$$
$$
\psi_{-+}^\lambda (p,k) = \frac{1}{\sqrt{k^+}} \frac{-z^2 m \delta_{\lambda 2}}{\left(\mathbf{k}_\perp - z\mathbf{p}_\perp \right)^2 + z^2 m^2}.
\tag{E.8}
$$

Total result for the wave function

Taking all these pieces together, we finally arrive at:

$$
\begin{aligned}
\psi^\lambda_{\alpha\beta}(p,k) = {} & \frac{1}{\sqrt{k^+}} \frac{1}{(\mathbf{k}_\perp - z\mathbf{p}_\perp)^2 + z^2 m^2} \\
& \times \begin{cases}
\sqrt{2}\,(\mathbf{k}_\perp - z\mathbf{p}_\perp)\cdot\boldsymbol{\epsilon}^1_\perp \left[\delta_{\alpha-}\delta_{\beta-} + (1-z)\,\delta_{\alpha+}\delta_{\beta+}\right] + mz^2\delta_{\alpha+}\delta_{\beta-} & \lambda = 1 \\
\sqrt{2}\,(\mathbf{k}_\perp - z\mathbf{p}_\perp)\cdot\boldsymbol{\epsilon}^2_\perp \left[\delta_{\alpha+}\delta_{\beta+} + (1-z)\,\delta_{\alpha-}\delta_{\beta-}\right] - mz^2\delta_{\alpha-}\delta_{\beta+} & \lambda = 2
\end{cases}.
\end{aligned}
\tag{E.9}
$$

Averaging over the incoming spin, and summing over the outgoing spin and polarization, we obtain in the massless limit:

$$
\left|\psi^{q\to qg}_T(p,k)\right|^2 = \frac{1}{2}\sum_{\alpha\beta\lambda}\psi^\lambda_{\alpha\beta}(p,k)\,\psi^{\lambda*}_{\alpha\beta}(p,k) = \frac{1}{k^+}\frac{1+(1-z)^2}{k_\perp^2}.
\tag{E.10}
$$

In mixed Fourier-coordinate representation, again making use of the identities in Eq. (D.25), one obtains the expression for the wave function encountered in Refs. [143, 148]:

$$
\phi^\lambda_{\alpha\beta}(p,z,\mathbf{r}) \equiv \int \mathrm{d}^2\mathbf{k}_\perp\, e^{i\mathbf{k}_\perp\cdot\mathbf{r}}\psi^\lambda_{\alpha\beta}(p,k),
\tag{E.11}
$$

$$
\begin{aligned}
\phi^\lambda_{\alpha\beta}(p,z,\mathbf{r}) = {} & \frac{2\pi m}{\sqrt{k^+}}e^{iz\mathbf{p}_\perp\cdot\mathbf{r}} \\
& \times \begin{cases}
iz\sqrt{2}K_1(mz|\mathbf{r}|)\frac{\mathbf{r}\cdot\boldsymbol{\epsilon}^1_\perp}{|\mathbf{r}|}\left[\delta_{\alpha-}\delta_{\beta-} + (1-z)\,\delta_{\alpha+}\delta_{\beta+}\right] + z^2 K_0(mz|\mathbf{r}|)\delta_{\alpha+}\delta_{\beta-} & \lambda = 1 \\
iz\sqrt{2}K_1(mz|\mathbf{r}|)\frac{\mathbf{r}\cdot\boldsymbol{\epsilon}^2_\perp}{|\mathbf{r}|}\left[\delta_{\alpha+}\delta_{\beta+} + (1-z)\,\delta_{\alpha-}\delta_{\beta-}\right] - z^2 K_0(mz|\mathbf{r}|)\delta_{\alpha-}\delta_{\beta+} & \lambda = 2
\end{cases}.
\end{aligned}
\tag{E.12}
$$

F Analytical calculation of the gluon TMDs in the MV model

F.1 Weizsäcker-Williams gluon TMDs $\mathcal{F}^{(3)}_{gg}$ and $\mathcal{H}^{(3)}_{gg}$

Let us start with the calculation of the Weizsäcker-Williams gluon TMD $\mathcal{F}^{(3)}_{gg}$, as well as its partner $\mathcal{H}^{(3)}_{gg}$ which corresponds to the linearly polarized gluons in the target. From their definition in Eq. (13.49), we see that the central object is the quadrupole operator:

$$
\frac{\partial}{\partial x^i}\frac{\partial}{\partial y^j}\frac{1}{N_c}\mathrm{Tr}\left\langle U(\mathbf{x})\,U^\dagger(\mathbf{v}')\,U(\mathbf{y})\,U^\dagger(\mathbf{v})\right\rangle_x\bigg|_{\mathbf{x}=\mathbf{v},\,\mathbf{y}=\mathbf{v}'}.
\tag{F.1}
$$

This operator was already calculated in McLerran-Venugopalan model in Ref. [143]:

$$
\frac{1}{N_c}\mathrm{Tr}\Big\langle U\left(\mathbf{x}\right)U^\dagger\left(\mathbf{v}'\right)U\left(\mathbf{y}\right)U^\dagger\left(\mathbf{v}\right)\Big\rangle_x
$$

$$
= e^{-\frac{C_F}{2}\left(\Gamma(\mathbf{x}-\mathbf{v})+\Gamma(\mathbf{y}-\mathbf{v}')\right)}e^{-\frac{N_c}{4}\mu^2 F(\mathbf{x},\mathbf{y};\mathbf{v},\mathbf{v}')+\frac{1}{2N_c}\mu^2 F(\mathbf{x},\mathbf{v};\mathbf{y},\mathbf{v}')}
$$

$$
\times \left[\left(\frac{\sqrt{\Delta}+F\left(\mathbf{x},\mathbf{y};\mathbf{v},\mathbf{v}'\right)}{2\sqrt{\Delta}}-\frac{F\left(\mathbf{x},\mathbf{v};\mathbf{y},\mathbf{v}'\right)}{\sqrt{\Delta}}\right)e^{\frac{N_c}{4}\mu^2\sqrt{\Delta}}\right.
$$

$$
\left.+\left(\frac{\sqrt{\Delta}-F\left(\mathbf{x},\mathbf{y};\mathbf{v},\mathbf{v}'\right)}{2\sqrt{\Delta}}+\frac{F\left(\mathbf{x},\mathbf{v};\mathbf{y},\mathbf{v}'\right)}{\sqrt{\Delta}}\right)e^{-\frac{N_c}{4}\mu^2\sqrt{\Delta}}\right], \tag{F.2}
$$

where

$$
F\left(\mathbf{x},\mathbf{y},\mathbf{v},\mathbf{w}\right)\equiv L_{\mathbf{xv}}-L_{\mathbf{xw}}+L_{\mathbf{yw}}-L_{\mathbf{yv}}, \tag{F.3}
$$

and

$$
\Delta\equiv F^2\left(\mathbf{x},\mathbf{y};\mathbf{v},\mathbf{v}'\right)+\frac{4}{N_c^2}F\left(\mathbf{x},\mathbf{v};\mathbf{y},\mathbf{v}'\right)F\left(\mathbf{x},\mathbf{v}';\mathbf{y},\mathbf{v}\right). \tag{F.4}
$$

Eq. (F.1) becomes after a lot of tedious algebra:

$$
\frac{\partial}{\partial x^i}\frac{\partial}{\partial y^j}\frac{1}{N_c}\mathrm{Tr}\Big\langle U\left(\mathbf{x}\right)U^\dagger\left(\mathbf{v}'\right)U\left(\mathbf{y}\right)U^\dagger\left(\mathbf{v}\right)\Big\rangle_x\Big|_{\mathbf{x}=\mathbf{v},\,\mathbf{y}=\mathbf{v}'}
$$

$$
=\frac{C_F}{N_c}\frac{1-e^{-\frac{N_c}{2}\Gamma(\mathbf{v}-\mathbf{v}')}}{\Gamma\left(\mathbf{v}-\mathbf{v}'\right)}\frac{\partial}{\partial v^i}\frac{\partial}{\partial v'^j}\Gamma\left(\mathbf{v}-\mathbf{v}'\right), \tag{F.5}
$$

and therefore $\mathcal{F}_{gg}^{(3)}\left(x,q_\perp\right)$ can be written as:

$$
\mathcal{F}_{gg}^{(3)}\left(x,q_\perp\right)=-\frac{4}{g_s^2}C_F\delta_{ij}\int\frac{\mathrm{d}^2\mathbf{v}\mathrm{d}^2\mathbf{v}'}{(2\pi)^3}e^{-i\mathbf{q}_\perp\cdot(\mathbf{v}-\mathbf{v}')}\frac{1-e^{-\frac{N_c}{2}\Gamma(\mathbf{v}-\mathbf{v}')}}{\Gamma\left(\mathbf{v}-\mathbf{v}'\right)}\frac{\partial}{\partial v^i}\frac{\partial}{\partial v'^j}\Gamma\left(\mathbf{v}-\mathbf{v}'\right). \tag{F.6}
$$

Using the identity:

$$
\frac{\partial}{\partial v^i}\frac{\partial}{\partial v'^j}\Gamma\left(\mathbf{v}-\mathbf{v}'\right)=-2g_s^2\mu_A\int\frac{\mathrm{d}^2\mathbf{k}_\perp}{(2\pi)^2}\frac{k_\perp^i k_\perp^j}{k_\perp^4}e^{i\mathbf{k}_\perp\cdot(\mathbf{v}-\mathbf{v}')}, \tag{F.7}
$$

as well as the expression for the saturation scale in the MV model, Eq. (8.42), we obtain:

$$
\frac{\partial}{\partial x^i}\frac{\partial}{\partial y^j}\frac{1}{N_c}\mathrm{Tr}\Big\langle U\left(\mathbf{x}\right)U^\dagger\left(\mathbf{v}'\right)U\left(\mathbf{y}\right)U^\dagger\left(\mathbf{v}\right)\Big\rangle_x\Big|_{\mathbf{x}=\mathbf{v},\,\mathbf{y}=\mathbf{v}'}
$$

$$
=g_s^2\mu_A\frac{2C_F}{(\mathbf{v}-\mathbf{v}')^2 Q_{sg}^2\left(\mathbf{v}-\mathbf{v}'\right)}\left(e^{-\frac{(\mathbf{v}-\mathbf{v}')^2}{4}Q_{sg}^2(\mathbf{v}-\mathbf{v}')}-1\right)\int\frac{\mathrm{d}^2\mathbf{k}_\perp}{(2\pi)^2}\frac{k_\perp^i k_\perp^j}{k_\perp^4}e^{i\mathbf{k}_\perp\cdot(\mathbf{v}-\mathbf{v}')}. \tag{F.8}
$$

Combining Eqs. (13.49), (F.1), and (F.8), as well as using Eq. (B.1), we obtain the following expression for the Weizsäcker-Williams distribution:

$$
\begin{aligned}
\mathcal{F}_{gg}^{(3)}\left(x, q_{\perp}\right) &= 16\mu_A C_F N_c S_{\perp} \int \frac{\mathrm{d}^2\mathbf{r}}{(2\pi)^3} e^{-i\mathbf{q}_{\perp}\cdot r} \frac{1 - e^{-\frac{r^2}{4}Q_{sg}^2(r)}}{\mathbf{r}^2 Q_{sg}^2(r)} \int \frac{\mathrm{d}^2\mathbf{k}_{\perp}}{(2\pi)^2} \frac{e^{i\mathbf{k}_{\perp}\cdot r}}{k_{\perp}^2}, \\
&= \frac{2C_F S_{\perp}}{\alpha_s \pi^2} \int \frac{\mathrm{d}^2\mathbf{r}}{(2\pi)^2} e^{-i\mathbf{q}_{\perp}\cdot r} \frac{1}{r^2}\left(1 - e^{-\frac{r^2}{4}Q_g^2(r)}\right),
\end{aligned}
\tag{F.9}
$$

in accordance with what we found in Eq. (8.51) using a slightly different approach.

The linearly polarized partner of $\mathcal{F}_{gg}^{(3)}$: $\mathcal{H}_{gg}^{(3)}$ (see Eq. (13.50)), can also be calculated, combining Eq. (13.50) with Eqs. (F.1) and (F.8):

$$
\begin{aligned}
&\mathcal{H}_{gg}^{(3)}\left(x, q_{\perp}\right) \\
&= \frac{4C_F}{g_s^2} \int \frac{\mathrm{d}^2\mathbf{v}\mathrm{d}^2\mathbf{v}'}{(2\pi)^3} e^{-i\mathbf{q}_{\perp}\cdot(\mathbf{v}-\mathbf{v}')} \frac{e^{-\frac{N_c}{2}\Gamma(\mathbf{v}-\mathbf{v}')} - 1}{\Gamma(\mathbf{v}-\mathbf{v}')}\left(\frac{2q_{\perp}^i q_{\perp}^j}{q_{\perp}^2} - \delta^{ij}\right) \frac{\partial}{\partial v^i} \frac{\partial}{\partial v'^j}\Gamma(\mathbf{v}-\mathbf{v}'), \\
&= -2g_s^2 \mu_A \frac{8C_F}{g_s^2} S_{\perp} N_c \int \frac{\mathrm{d}^2\mathbf{v}\mathrm{d}^2\mathbf{v}'}{(2\pi)^3} e^{-i\mathbf{q}_{\perp}\cdot r} \\
&\frac{e^{-\frac{r^2}{4}Q_{sg}^2(r^2)} - 1}{r^2 Q_g^2(r^2)}\left(\frac{2q_{\perp}^i q_{\perp}^j}{q_{\perp}^2} - \delta^{ij}\right)\int \frac{\mathrm{d}^2\mathbf{k}_{\perp}}{(2\pi)^2} \frac{k_{\perp}^i k_{\perp}^j}{k_{\perp}^4} e^{i\mathbf{k}_{\perp}\cdot(\mathbf{v}-\mathbf{v}')}, \\
&= \frac{2N_c C_F}{\pi^3}\mu_A S_{\perp} \int \mathrm{d}r \frac{1}{rQ_{sg}^2(r)}\left(1 - e^{-\frac{r^2}{4}Q_{sg}^2(r)}\right) \\
&\times \int \mathrm{d}\phi e^{-iq_{\perp}\cdot r\cos\alpha} \int \frac{\mathrm{d}^2\mathbf{k}_{\perp}}{(2\pi)^2} \frac{1}{k_{\perp}^4} e^{i\mathbf{k}_{\perp}\cdot r}\left(\frac{2\left(\mathbf{k}_{\perp}\cdot\mathbf{q}_{\perp}\right)^2}{q_{\perp}^2} - k_{\perp}^2\right).
\end{aligned}
\tag{F.10}
$$

Using the intermediate result:

$$
\begin{aligned}
\int \frac{\mathrm{d}^2\mathbf{k}_{\perp}}{(2\pi)^2}\frac{1}{k_{\perp}^4}e^{i\mathbf{k}_{\perp}\cdot r}\left(\frac{2\left(\mathbf{k}_{\perp}\cdot\mathbf{q}_{\perp}\right)^2}{q_{\perp}^2} - k_{\perp}^2\right) &= \int \frac{\mathrm{d}k_{\perp}\mathrm{d}\theta}{(2\pi)^2}\frac{1}{k_{\perp}}e^{i\mathbf{k}_{\perp}\cdot r\cos\theta}\left(2\cos^2(\theta+\alpha) - 1\right), \\
&= -\frac{1}{2\pi}\cos(2\alpha)\int_0^\infty \frac{\mathrm{d}k_{\perp}}{k_{\perp}}J_2\left(k_{\perp}r\right), \\
&= -\frac{\cos(2\alpha)}{4\pi},
\end{aligned}
\tag{F.11}
$$

where $\alpha = \widehat{\mathbf{q}_{\perp}\mathbf{r}}$, as well as employing the integral representation of the Bessel function of the first kind:

$$
\int_0^{2\pi} \mathrm{d}\phi\, e^{-iq_{\perp}r\cos\phi}\cos 2\phi = -2\pi J_2\left(q_{\perp}r\right),
\tag{F.12}
$$

we obtain:

$$
\mathcal{H}_{gg}^{(3)}\left(x, q_{\perp}\right) = \frac{C_F S_{\perp}}{\alpha_s \pi^3}\int \mathrm{d}r \frac{J_2\left(q_{\perp}r\right)}{r\ln\frac{1}{r^2\Lambda^2}}\left(1 - e^{-\frac{r^2}{4}Q_{sg}^2(r)}\right).
\tag{F.13}
$$

F.2 Distributions built from dipoles: $\mathcal{F}_{gg}^{(1)}$, $\mathcal{H}_{gg}^{(1)}$, $\mathcal{F}_{gg}^{(2)}$ and $\mathcal{H}_{gg}^{(2)}$

Just like the correlator of four Wilson lines in the previous section, the correlator of the product of two dipoles is also known in the MV model (see Ref. [142]):

$$
\frac{1}{N_c^2}\Big\langle \text{Tr}\left(U\left(\mathbf{x}\right)U^\dagger\left(\mathbf{y}\right)\right)\text{Tr}\left(U\left(\mathbf{v}'\right)U^\dagger\left(\mathbf{v}\right)\right)\Big\rangle_x
$$
$$
= e^{-\frac{C_F}{2}\left(\Gamma(\mathbf{x}-\mathbf{y})+\Gamma(\mathbf{v}'-\mathbf{v})\right)}e^{-\frac{N_c}{4}\mu^2 F(\mathbf{x},\mathbf{v}';\mathbf{y},\mathbf{v})+\frac{1}{2N_c}\mu^2 F(\mathbf{x},\mathbf{y};\mathbf{v}',\mathbf{v})}
$$
$$
\times\left[\left(\frac{F\left(\mathbf{x},\mathbf{v}';\mathbf{y},\mathbf{v}\right)+\sqrt{D}}{2\sqrt{D}}-\frac{F\left(\mathbf{x},\mathbf{y};\mathbf{v}',\mathbf{v}\right)}{N_c^2\sqrt{D}}\right)e^{\frac{N_c}{4}\mu^2\sqrt{D}}\right.
$$
$$
\left.-\left(\frac{F\left(\mathbf{x},\mathbf{v}';\mathbf{y},\mathbf{v}\right)-\sqrt{D}}{2\sqrt{D}}-\frac{F\left(\mathbf{x},\mathbf{y};\mathbf{v}',\mathbf{v}\right)}{N_c^2\sqrt{D}}\right)e^{-\frac{N_c}{4}\mu^2\sqrt{D}}\right], \tag{F.14}
$$

where

$$
D \equiv F^2\left(\mathbf{x},\mathbf{v}';\mathbf{y},\mathbf{v}\right)+\frac{4}{N_c^2}F\left(\mathbf{x},\mathbf{y};\mathbf{v}',\mathbf{v}\right)F\left(\mathbf{x},\mathbf{v};\mathbf{v}',\mathbf{y}\right), \tag{F.15}
$$

and where F is defined as in Eq. (F.3). We have that:

$$
\frac{1}{N_c^2}\frac{\partial}{\partial x^i}\frac{\partial}{\partial y^j}\Big\langle \text{Tr}\left(U\left(\mathbf{x}\right)U^\dagger\left(\mathbf{y}\right)\right)\text{Tr}\left(U\left(\mathbf{v}'\right)U^\dagger\left(\mathbf{v}\right)\right)\Big\rangle_x\Big|_{\mathbf{x}=\mathbf{v},\,\mathbf{y}=\mathbf{v}'}
$$
$$
= \frac{C_F}{8N_c^3}\frac{e^{-\frac{N_c}{2}\Gamma(\mathbf{v}-\mathbf{v}')}}{\Gamma\left(\mathbf{v}-\mathbf{v}'\right)}\left[16\left(1-e^{\frac{N_c}{2}\Gamma(\mathbf{v}-\mathbf{v}')}\right)\frac{\partial}{\partial x^i}\frac{\partial}{\partial y^j}\Gamma\left(\mathbf{x}-\mathbf{y}\right)\right.
$$
$$
\left.+\Gamma\left(\mathbf{v}-\mathbf{v}'\right)\left(N_c^4\frac{\partial}{\partial x^i}\Gamma\left(\mathbf{x}-\mathbf{v}'\right)\frac{\partial}{\partial y^j}\Gamma\left(\mathbf{v}-\mathbf{y}\right)-4N_c\left(N_c^2-2\right)\frac{\partial}{\partial x^i}\frac{\partial}{\partial y^j}\Gamma\left(\mathbf{x}-\mathbf{y}\right)\right)\right]. \tag{F.16}
$$

The gluon TMD $\mathcal{F}_{gg}^{(1)}\left(x,q_\perp\right)$ (see Eq. (13.49)) then becomes:

$$
\mathcal{F}_{gg}^{(1)}\left(x,q_\perp\right) = \frac{S_\perp}{\alpha_s}\frac{C_F}{N_c^2}\frac{1}{16\pi^2}\int\frac{\mathrm{d}^2\mathbf{r}}{\left(2\pi\right)^2}e^{-i\mathbf{q}_\perp\cdot\mathbf{r}}\frac{e^{-\frac{N_c}{2}\Gamma(\mathbf{r})}}{\Gamma\left(\mathbf{r}\right)}
$$
$$
\left[-32\mu_A\alpha_s\left(1-e^{\frac{N_c}{2}\Gamma(\mathbf{r})}\right)\frac{1}{\pi}\int\mathrm{d}^2\mathbf{k}_\perp\frac{e^{i\mathbf{k}_\perp\cdot\mathbf{r}}}{k_\perp^2}\right.
$$
$$
+\Gamma\left(\mathbf{r}\right)\left(4\alpha_s^2 N_c^4\mu_A^2\frac{1}{\pi^2}\int\mathrm{d}^2\mathbf{k}_\perp\int\mathrm{d}^2\mathbf{l}_\perp\frac{\mathbf{k}_\perp\cdot\mathbf{l}_\perp}{l_\perp^4 k_\perp^4}e^{i(\mathbf{k}_\perp+\mathbf{l}_\perp)\cdot\mathbf{r}}\right.
$$
$$
\left.\left.+8\alpha_s N_c\left(N_c^2-2\right)\mu_A\frac{1}{\pi}\int\mathrm{d}^2\mathbf{k}_\perp\frac{e^{i\mathbf{k}_\perp\cdot\mathbf{r}}}{k_\perp^2}\right)\right], \tag{F.17}
$$

where we used the following intermediate results for the derivatives of $\Gamma\left(\mathbf{x}-\mathbf{y}\right)$:

$$\frac{\partial}{\partial x^i}\frac{\partial}{\partial y^i}\Gamma\left(\mathbf{x}-\mathbf{y}\right)\Big|_{\mathbf{x}=\mathbf{v},\mathbf{y}=\mathbf{v}'} = -2\mu_A g_s^2 \int \frac{\mathrm{d}^2\mathbf{k}_\perp}{(2\pi)^2}\frac{e^{i\mathbf{k}_\perp\cdot(\mathbf{v}-\mathbf{v}')}}{k_\perp^2},$$

$$\frac{\partial}{\partial x^i}\Gamma\left(\mathbf{x}-\mathbf{v}'\right)\frac{\partial}{\partial y^i}\Gamma\left(\mathbf{v}-\mathbf{y}\right)\Big|_{\mathbf{x}=\mathbf{v},\mathbf{y}=\mathbf{v}'} = \left(2\mu_A g_s^2\right)^2 \int \frac{\mathrm{d}^2\mathbf{k}_\perp}{(2\pi)^2}\int\frac{\mathrm{d}^2\mathbf{l}_\perp}{(2\pi)^2}\frac{\mathbf{k}_\perp\cdot\mathbf{l}_\perp}{l_\perp^4 k_\perp^4}e^{i(\mathbf{k}_\perp+\mathbf{l}_\perp)(\mathbf{v}-\mathbf{v}')}. \tag{F.18}$$

Finally, using Eq. (B.1), as well as:

$$\int \mathrm{d}^2\mathbf{k}_\perp \int \mathrm{d}^2\mathbf{l}_\perp \frac{\mathbf{k}_\perp\cdot\mathbf{l}_\perp}{l_\perp^4 k_\perp^4}e^{i(\mathbf{k}_\perp+\mathbf{l}_\perp)\cdot\mathbf{r}} = \int\frac{\mathrm{d}k_\perp \mathrm{d}\theta}{k_\perp^2}\int\frac{\mathrm{d}l_\perp \mathrm{d}\phi}{l_\perp^2}\cos\left(\phi-\theta\right)e^{ik_\perp r\cos(\theta)}e^{il_\perp r\cos(\phi)},$$

$$= -4\pi^2 \int_\Lambda^\infty \frac{\mathrm{d}k_\perp}{k_\perp^2}\int_\Lambda^\infty\frac{\mathrm{d}l_\perp}{l_\perp^2}J_1\left(k_\perp r\right)J_1\left(l_\perp r\right), \tag{F.19}$$

$$= -\frac{1}{4}\pi^2 r^2\left(1-2\gamma_E+\ln 4+\ln\frac{1}{r^2\Lambda^2}\right)^2,$$

Eq. (F.17) becomes:

$$\mathcal{F}_{gg}^{(1)}\left(x,q_\perp\right) = \frac{S_\perp}{\alpha_s}\frac{C_F}{N_c^2}\frac{1}{32\pi^3}\int \mathrm{d}r\frac{J_0\left(q_\perp r\right)}{r}e^{-\frac{N_c}{2}\Gamma(r)}\left[64\left(e^{\frac{N_c}{2}\Gamma(r)}-1\right)\right.$$

$$\left. -\alpha_s^2 N_c^4\mu_A^2 r^4\left(1-2\gamma_E+\ln 4+\ln\frac{1}{r^2\Lambda^2}\right)^2+8\alpha_s N_c\left(N_c^2-2\right)\mu_A r^2\ln\frac{1}{r^2\Lambda^2}\right)\right]. \tag{F.20}$$

As usual, the computation of $\mathcal{H}_{gg}^{(1)}\left(x,q_\perp\right)$ requires a bit more effort. Combining Eq. (13.50) with Eq. (F.16), we find:

$$\mathcal{H}_{gg}^{(1)}\left(x,q_\perp\right) = \left(\frac{2q_\perp^i q_\perp^j}{q_\perp^2}-\delta^{ij}\right)\frac{4N_c}{g_s^2}\int\frac{\mathrm{d}^2\mathbf{v}\mathrm{d}^2\mathbf{v}'}{(2\pi)^3}e^{-i\mathbf{q}_\perp\cdot(\mathbf{v}-\mathbf{v}')}$$

$$\frac{C_F}{8N_c^3}\frac{e^{-\frac{N_c}{2}\Gamma(\mathbf{v}-\mathbf{v}')}}{\Gamma\left(\mathbf{v}-\mathbf{v}'\right)}\left[16\left(1-e^{\frac{N_c}{2}\Gamma(\mathbf{v}-\mathbf{v}')}\right)\frac{\partial}{\partial x^i}\frac{\partial}{\partial y^j}\Gamma\left(\mathbf{x}-\mathbf{y}\right)\right. \tag{F.21}$$

$$\left. +\Gamma\left(\mathbf{v}-\mathbf{v}'\right)\left(N_c^4\frac{\partial}{\partial x^i}\Gamma\left(\mathbf{x}-\mathbf{v}'\right)\frac{\partial}{\partial y^j}\Gamma\left(\mathbf{v}-\mathbf{y}\right)-4N_c\left(N_c^2-2\right)\frac{\partial}{\partial x^i}\frac{\partial}{\partial y^j}\Gamma\left(\mathbf{x}-\mathbf{y}\right)\right)\right].$$

With the help of the following results:

$$
\left(\frac{2q_\perp^i q_\perp^j}{q_\perp^2} - \delta^{ij}\right)\frac{\partial}{\partial x^i}\frac{\partial}{\partial y^j}\Gamma\left(\mathbf{x}-\mathbf{y}\right)
$$

$$
= -2\mu_A g_s^2 \int \frac{\mathrm{d}^2\mathbf{k}_\perp}{(2\pi)^2}\frac{1}{k_\perp^2}\left(\frac{2\left(\mathbf{q}_\perp\cdot\mathbf{k}_\perp\right)^2}{q_\perp^2 k_\perp^2}-1\right)e^{i\mathbf{k}_\perp(\mathbf{v}-\mathbf{v}')} \tag{F.22}
$$

$$
\times\left(\frac{2q_\perp^i q_\perp^j}{q_\perp^2}-\delta^{ij}\right)\frac{\partial}{\partial x^i}\Gamma\left(\mathbf{x}-\mathbf{v}'\right)\frac{\partial}{\partial y^j}\Gamma\left(\mathbf{v}-\mathbf{y}\right),
$$

$$
= \left(2\mu_A g_s^2\right)^2\int\frac{\mathrm{d}^2\mathbf{k}_\perp}{(2\pi)^2}\int\frac{\mathrm{d}^2\mathbf{l}_\perp}{(2\pi)^2}\frac{1}{k_\perp^4 l_\perp^4}\left(\frac{2\left(\mathbf{q}_\perp\cdot\mathbf{k}_\perp\right)\left(\mathbf{q}_\perp\cdot\mathbf{l}_\perp\right)}{q_\perp^2}-\mathbf{k}_\perp\cdot\mathbf{l}_\perp\right)e^{i(\mathbf{k}_\perp+\mathbf{l}_\perp)(\mathbf{v}-\mathbf{v}')},
$$

which can be evaluated further with the help of Eq. (F.11), and with:

$$
\int\mathrm{d}^2\mathbf{k}_\perp\int\mathrm{d}^2\mathbf{l}_\perp\frac{1}{k_\perp^4 l_\perp^4}\left(\frac{2\left(\mathbf{q}_\perp\cdot\mathbf{k}_\perp\right)\left(\mathbf{q}_\perp\cdot\mathbf{l}_\perp\right)}{q_\perp^2}-\mathbf{k}_\perp\cdot\mathbf{l}_\perp\right)e^{i(\mathbf{k}_\perp+\mathbf{l}_\perp)\cdot\mathbf{r}}
$$

$$
= \int\frac{\mathrm{d}k_\perp\mathrm{d}\theta}{k_\perp^2}\int\frac{\mathrm{d}l_\perp\mathrm{d}\phi}{l_\perp^2}\left(2\cos\left(\theta+\alpha\right)\cos\left(\phi+\alpha\right)-\cos\left(\theta-\phi\right)\right)e^{ik_\perp r\cos(\theta)}e^{il_\perp r\cos(\phi)}, \tag{F.23}
$$

$$
= -4\pi^2\int_\Lambda^\infty\frac{\mathrm{d}k_\perp}{k_\perp^2}\int_\Lambda^\infty\frac{\mathrm{d}l_\perp}{l_\perp^2}J_1\left(k_\perp r\right)J_1\left(l_\perp r\right)\cos\left(2\alpha\right),
$$

$$
= -\frac{1}{4}\pi^2 r^2\cos\left(2\alpha\right)\left(1-2\gamma_E+\ln 4+\ln\frac{1}{r^2\Lambda^2}\right)^2,
$$

we finally obtain:

$$
\mathcal{H}_{gg}^{(1)}\left(x,q_\perp\right) = \frac{S_\perp}{\alpha_s}\frac{C_F}{N_c^2}\frac{1}{32\pi^3}\int\mathrm{d}r\frac{J_2\left(q_\perp r\right)}{r}e^{-\frac{N_c}{2}\Gamma(r)}\left[64\frac{1}{\ln\frac{1}{r^2\Lambda^2}}\left(e^{\frac{N_c}{2}\Gamma(r)}-1\right)\right.
$$

$$
\left.+\alpha_s^2 N_c^4\mu_A^2 r^4\left(1-2\gamma_E+\ln 4+\ln\frac{1}{r^2\Lambda^2}\right)^2+8\alpha_s\mu_A N_c\left(N_c^2-2\right)r^2\right]. \tag{F.24}
$$

We can follow the same procedure to calculate $\mathcal{F}_{gg}^{(2)}$ and $\mathcal{H}_{gg}^{(2)}$. Indeed, from Eq. (F.14) we obtain:

$$
\frac{1}{N_c^2}\frac{\partial^2}{\partial x^i\partial y^j}\mathrm{Re}\left\langle\mathrm{Tr}\left(U\left(\mathbf{x}\right)U^\dagger\left(\mathbf{v}'\right)\right)\mathrm{Tr}\left(U\left(\mathbf{y}\right)U^\dagger\left(\mathbf{v}\right)\right)\right\rangle_x\Big|_{\mathbf{x}=\mathbf{v},\mathbf{y}=\mathbf{v}'}
$$

$$
= \frac{C_F}{8N_c^3}\frac{e^{-\frac{N_c}{2}\Gamma(\mathbf{v}-\mathbf{v}')}}{\Gamma\left(\mathbf{v}-\mathbf{v}'\right)}\left[16\left(e^{\frac{N_c}{2}\Gamma(\mathbf{v}-\mathbf{v}')}-1\right)\frac{\partial^2}{\partial v^i\partial v'^j}\Gamma\left(\mathbf{v}-\mathbf{v}'\right)\right. \tag{F.25}
$$

$$
\left.+\Gamma\left(\mathbf{v}-\mathbf{v}'\right)\left(N_c^4\frac{\partial}{\partial x^i}\Gamma\left(\mathbf{x}-\mathbf{v}'\right)\frac{\partial}{\partial y^j}\Gamma\left(\mathbf{v}-\mathbf{y}\right)\Big|_{\mathbf{x}=\mathbf{v},\mathbf{y}=\mathbf{v}'}-8N_c\frac{\partial^2}{\partial v^i\partial v'^j}\Gamma\left(\mathbf{v}-\mathbf{v}'\right)\right)\right].
$$

Plugging this into the definition of $\mathcal{F}_{gg}^{(2)}$, Eq. (13.49), and using the intermediate results Eqs. (F.18), (F.19) and (B.1), we end up with:

$$
\mathcal{F}_{gg}^{(2)}\left(x,q_{\perp}\right) = \frac{S_{\perp}}{\alpha_s}\frac{C_F}{N_c^2}\frac{1}{32\pi^3}\int \mathrm{d}r \frac{J_0\left(q_{\perp}r\right)}{r}e^{-\frac{N_c}{2}\Gamma(r)}\left[64\left(e^{\frac{N_c}{2}\Gamma(r)}-1\right)\right.
$$
$$
\left.+ N_c^4\mu_A^2\alpha_s^2 r^4\left(1-2\gamma_E+\ln 4 +\ln\frac{1}{r^2\Lambda^2}\right)^2 - 16\alpha_s N_c\mu_A r^2\ln\frac{1}{r^2\Lambda^2}\right].
$$

(F.26)

Likewise, combining Eq. (13.50) with Eqs. (F.25), (F.22), (F.23), (F.11) and (F.12), we obtain the following expression for $\mathcal{H}_{gg}^{(2)}$:

$$
\mathcal{H}_{gg}^{(2)}\left(x,q_{\perp}\right) = \frac{S_{\perp}}{\alpha_s}\frac{C_F}{N_c^2}\frac{1}{32\pi^3}\int \mathrm{d}r \frac{J_2\left(q_{\perp}r\right)}{r}e^{-\frac{N_c}{2}\Gamma(r)}
$$
$$
\left[64\left(e^{\frac{N_c}{2}\Gamma(r)}-1\right)\frac{1}{\ln\frac{1}{r^2\Lambda^2}}-\alpha_s^2 N_c^4\mu_A^2 r^4\left(1-2\gamma_E+\ln 4+\ln\frac{1}{r^2\Lambda^2}\right)^2-16\alpha_s N_c\mu_A r^2\right].
$$

(F.27)

F.3 Relations between the gluon TMDs

Let us first calculate the adjoint dipole gluon TMD $xG_A^{(2)}\left(x,q_{\perp}\right)$, defined earlier in Eq. (13.63). Taking the derivatives of the correlator of two dipoles, Eq. (F.14), we obtain:

$$
\frac{\partial^2}{\partial x^i \partial y^j}\left\langle \mathrm{Tr}\left(U\left(\mathbf{x}\right)U^{\dagger}\left(\mathbf{y}\right)\right)\mathrm{Tr}\left(U\left(\mathbf{y}\right)U^{\dagger}\left(\mathbf{x}\right)\right)\right\rangle_x\bigg|_{\mathbf{x}=\mathbf{v},\mathbf{y}=\mathbf{v}'}
$$
$$
= \frac{C_F}{2}N_c^2 e^{-\frac{N_c}{2}\Gamma(\mathbf{v}-\mathbf{v}')}\left(N_c\frac{\partial}{\partial x^i}\Gamma\left(\mathbf{x}-\mathbf{v}'\right)\frac{\partial}{\partial y^i}\Gamma\left(\mathbf{v}-\mathbf{y}\right)-2\frac{\partial}{\partial v^i}\frac{\partial}{\partial v'^i}\Gamma\left(\mathbf{v}-\mathbf{v}'\right)\right),
$$
$$
= 2C_F N_c\frac{\partial}{\partial v^i}\frac{\partial}{\partial v'^i}e^{-\frac{N_c}{2}\Gamma(\mathbf{v}-\mathbf{v}')},
$$

(F.28)

from which we find the following expression for $xG_A^{(2)}\left(x,q_{\perp}\right)$:

$$
xG_A^{(2)}\left(x,q_{\perp}\right) = 4\frac{C_F}{g_s^2}\frac{1}{N_c^2-1}2C_F N_c\int\frac{\mathrm{d}^2\mathbf{v}\,\mathrm{d}^2\mathbf{v}'}{(2\pi)^3}e^{-i\mathbf{q}_{\perp}\cdot(\mathbf{v}-\mathbf{v}')}\frac{\partial}{\partial v^i}\frac{\partial}{\partial v'^i}e^{-\frac{N_c}{2}\Gamma(\mathbf{v}-\mathbf{v}')},
$$
$$
= 4\frac{C_F}{g_s^2}\int\frac{\mathrm{d}^2\mathbf{v}\,\mathrm{d}^2\mathbf{v}'}{(2\pi)^3}q_{\perp}^2 e^{-i\mathbf{q}_{\perp}\cdot(\mathbf{v}-\mathbf{v}')}e^{-\frac{N_c}{2}\Gamma(\mathbf{v}-\mathbf{v}')},
$$
$$
= \frac{S_{\perp}C_F}{2\alpha_s\pi^2}\int\frac{\mathrm{d}^2\mathbf{r}}{(2\pi)^2}q_{\perp}^2 e^{-i\mathbf{q}_{\perp}\cdot\mathbf{r}}e^{-\frac{N_c}{2}\Gamma(\mathbf{r})}.
$$

(F.29)

From the other derivatives of the correlator of two dipoles, Eqs. (F.16) and (F.25), together with the definitions of $\mathcal{F}_{gg}^{(1)}$ and $\mathcal{F}_{gg}^{(2)}$, Eq. (13.49), we easily find:

$$
\mathcal{F}_{gg}^{(1)}\left(x,q_{\perp}\right) - \mathcal{F}_{gg}^{(2)}\left(x,q_{\perp}\right) = xG_A^{(2)}\left(x,q_{\perp}\right),
$$

(F.30)

and hence the rule Eq. (13.67) still holds in the MV model. Using Eq. (13.68), it is easy to show that the same is true for the difference between $\mathcal{H}_{gg}^{(1)}(x, q_\perp)$ and $\mathcal{H}_{gg}^{(2)}(x, q_\perp)$:

$$\mathcal{H}_{gg}^{(1)}(x, q_\perp) - \mathcal{H}_{gg}^{(2)}(x, q_\perp) = xG_A^{(2)}(x, q_\perp). \tag{F.31}$$

For the sum of $\mathcal{F}_{gg}^{(1)}(x, q_\perp)$ and $\mathcal{F}_{gg}^{(1)}(x, q_\perp)$, we find:

$$\begin{aligned}
&\mathcal{F}_{gg}^{(1)}(x, q_\perp) + \mathcal{F}_{gg}^{(2)}(x, q_\perp) \\
&= -\frac{16}{g_s^2}\frac{C_F}{N_c^2}\int\frac{\mathrm{d}^2\mathbf{v}\mathrm{d}^2\mathbf{v}'}{(2\pi)^3}e^{-i\mathbf{q}_\perp\cdot(\mathbf{v}-\mathbf{v}')}\frac{1-e^{-\frac{N_c}{2}\Gamma(\mathbf{v}-\mathbf{v}')}}{\Gamma(\mathbf{v}-\mathbf{v}')}\frac{\partial}{\partial v^i}\frac{\partial}{\partial v'^i}\Gamma(\mathbf{v}-\mathbf{v}'), \\
&-\frac{2}{g_s^2}\frac{C_F}{N_c}\left(N_c^2-4\right)\int\frac{\mathrm{d}^2\mathbf{v}\mathrm{d}^2\mathbf{v}'}{(2\pi)^3}e^{-i\mathbf{q}_\perp\cdot(\mathbf{v}-\mathbf{v}')}e^{-\frac{N_c}{2}\Gamma(\mathbf{v}-\mathbf{v}')}\frac{\partial}{\partial v^i}\frac{\partial}{\partial v'^i}\Gamma(\mathbf{v}-\mathbf{v}').
\end{aligned} \tag{F.32}$$

In the first term of the above formula, we recognize the Weizsäcker-Williams gluon TMD $\mathcal{F}_{gg}^{(3)}(x, q_\perp)$, with the help of its expression in terms of $\Gamma(\mathbf{v}-\mathbf{v}')$, Eq. (F.6). Furthermore, using the formula for the double derivative of $\Gamma(\mathbf{v}-\mathbf{v}')$, Eq. (F.18) in combination with Eq. (B.1), as well as the definition of the saturation scale Eq. (8.43), we can easily show that

$$\mathcal{F}_{gg}^{(1)}(x, q_\perp) + \mathcal{F}_{gg}^{(2)}(x, q_\perp) = \frac{4}{N_c^2}\mathcal{F}_{gg}^{(3)}(x, q_\perp) + \left(1-\frac{4}{N_c^2}\right)xG_{q\bar{q}}(x, q), \tag{F.33}$$

where we defined the following auxiliary TMD:

$$xG_{q\bar{q}}(x, q) \equiv \frac{S_\perp N_c}{2\pi^2\alpha_s}\int\frac{\mathrm{d}^2\mathbf{r}}{(2\pi)^2}Q_s^2\left(r^2\right)e^{-i\mathbf{q}_\perp\cdot\mathbf{r}}e^{-\frac{N_c}{2}\Gamma(\mathbf{r})}. \tag{F.34}$$

Likewise, we have for $\mathcal{H}_{gg}^{(1)}(x, q_\perp)$ and $\mathcal{H}_{gg}^{(2)}(x, q_\perp)$:

$$\mathcal{H}_{gg}^{(1)}(x, q_\perp) + \mathcal{H}_{gg}^{(2)}(x, q_\perp) = \frac{4}{N_c^2}\mathcal{H}_{gg}^{(3)}(x, q_\perp) + \left(1-\frac{4}{N_c^2}\right)xH_{q\bar{q}}(x, q), \tag{F.35}$$

where $xH_{q\bar{q}}(x, q)$ is defined as follows:

$$xH_{q\bar{q}}(x, q) = \frac{N_c^2-1}{8\pi^3}S_\perp\mu_A\int\mathrm{d}r\,rJ_2\left(q_\perp r\right)e^{-\frac{N_c}{2}\Gamma(\mathbf{r})}. \tag{F.36}$$

F.4 Large-N_c limit

In the large-N_c limit, the computation of $\mathcal{F}_{gg}^{(1)}(x, q_\perp)$, $\mathcal{F}_{gg}^{(2)}(x, q_\perp)$, $\mathcal{H}_{gg}^{(1)}(x, q_\perp)$ and $\mathcal{H}_{gg}^{(2)}(x, q_\perp)$ is considerably easier, since the correlator of two dipoles factorizes, as we already saw in the context of the BK equation (see Eq. (5.20)).

In addition, the large-N_c limit allows us to derive some simple expressions for $\mathcal{F}_{gg}^{(1)}$, $\mathcal{F}_{gg}^{(2)}$, $\mathcal{H}_{gg}^{(1)}$ and $\mathcal{H}_{gg}^{(2)}$, which are useful to compare with the literature. To this end, we introduce the dipole gluon distribution $xG^{(2)}(x, q_\perp)$, this time in the fundamental representation:

$$xG^{(2)}(x, q_\perp) \equiv \frac{4N_c}{g_s^2} \int \frac{\mathrm{d}^2\mathbf{v}\mathrm{d}^2\mathbf{v}'}{(2\pi)^3} e^{-i\mathbf{q}_\perp(\mathbf{v}-\mathbf{v}')} \left.\frac{\partial^2}{\partial x^i \partial y^i} D(\mathbf{x}-\mathbf{y})\right|_{\mathbf{x}=\mathbf{v},\,\mathbf{y}=\mathbf{v}'}, \tag{F.37}$$

which will take over the role of $xG_A^{(2)}(x, q_\perp)$ in the finite-N_c calculations. Just like in the case of $xG_A^{(2)}(x, q_\perp)$, Eq. (F.29), instead of computing the derivatives of $\Gamma(\mathbf{v}-\mathbf{v}')$ directly, it is more elegant to perform a partial integration, which yields the compact formula:

$$xG^{(2)}(x, q_\perp) = \frac{S_\perp q_\perp^2 N_c}{2\pi^2 \alpha_s} F(x, q_\perp), \tag{F.38}$$

where we introduced the following auxiliary Gaussian function:

$$F(x, q_\perp) \equiv \int \frac{\mathrm{d}^2\mathbf{x}}{(2\pi)^2} e^{i\mathbf{q}_\perp\mathbf{x}} D(\mathbf{x}). \tag{F.39}$$

We can use this to rewrite $\mathcal{F}_{gg}^{(1)}$ and $\mathcal{F}_{gg}^{(2)}$ as convolutions of $xG^{(2)}$ and F. Indeed, using the large-N_c factorization of a correlator of two dipoles, Eq. (5.20), we write for $\mathcal{F}_{gg}^{(1)}$:

$$\begin{aligned}
&\mathcal{F}_{gg}^{(1)}(x, q_\perp) \\
&= \frac{4N_c}{g_s^2} \int \frac{\mathrm{d}^2\mathbf{v}\mathrm{d}^2\mathbf{v}'}{(2\pi)^3} e^{-i\mathbf{q}_\perp(\mathbf{v}-\mathbf{v}')} \left(\frac{\partial}{\partial v^i}\frac{\partial}{\partial v'^j} D(\mathbf{v}-\mathbf{v}')\right) \int \mathrm{d}^2\mathbf{x}\, \delta^{(2)}(\mathbf{x}-\mathbf{v}'+\mathbf{v}) D(\mathbf{x}), \\
&= \frac{4N_c}{g_s^2} \int \frac{\mathrm{d}^2\mathbf{v}\mathrm{d}^2\mathbf{v}'}{(2\pi)^3} e^{-i\mathbf{q}_\perp(\mathbf{v}-\mathbf{v}')} \left(\frac{\partial}{\partial v^i}\frac{\partial}{\partial v'^j} D(\mathbf{v}-\mathbf{v}')\right) \int \mathrm{d}^2\mathbf{x} \int \frac{\mathrm{d}^2\mathbf{k}_\perp}{(2\pi)^2} e^{i\mathbf{k}_\perp(\mathbf{x}-\mathbf{v}'+\mathbf{v})} D(\mathbf{x}), \\
&= \frac{4N_c}{g_s^2} \int \mathrm{d}^2\mathbf{k}_\perp \int \frac{\mathrm{d}^2\mathbf{v}\mathrm{d}^2\mathbf{v}'}{(2\pi)^3} e^{-i(\mathbf{q}_\perp-\mathbf{k}_\perp)(\mathbf{v}-\mathbf{v}')} \left(\frac{\partial}{\partial v^i}\frac{\partial}{\partial v'^j} D(\mathbf{v}-\mathbf{v}')\right) F(x, k_\perp), \\
&= \int \mathrm{d}^2\mathbf{k}_\perp\, xG^{(2)}(x, q_\perp - k_\perp) F(x, k_\perp) = \int \mathrm{d}^2\mathbf{k}_\perp\, xG^{(2)}(x, k_\perp) F(x, q_\perp - k_\perp).
\end{aligned} \tag{F.40}$$

In the same fashion, it is straightforward to obtain the following relations between $\mathcal{F}_{gg}^{(1)}$, $\mathcal{H}_{gg}^{(1)}$, $\mathcal{F}_{gg}^{(2)}$, $\mathcal{H}_{gg}^{(2)}$, $xG^{(2)}$ and F:

$$\begin{aligned}
\mathcal{H}_{gg}^{(1)}(x, q_\perp) &= 2\int \mathrm{d}^2\mathbf{k}_\perp \frac{(\mathbf{q}_\perp \cdot \mathbf{k}_\perp)^2}{k_\perp^2 q_\perp^2} xG^{(2)}(x, k_\perp) F(x, q_\perp - k_\perp) - \mathcal{F}_{gg}^{(1)}(x, q_\perp), \\
\mathcal{F}_{gg}^{(2)}(x, q_\perp) &= -\int \mathrm{d}^2\mathbf{k}_\perp \frac{\mathbf{q}_\perp \cdot \mathbf{k}_\perp}{k_\perp^2} xG^{(2)}(x, k_\perp) F(x, q_\perp - k_\perp) + \mathcal{F}_{gg}^{(1)}(x, q_\perp),
\end{aligned} \tag{F.41}$$

$$\mathcal{F}_{gg}^{(1)}(x, q_\perp) - \mathcal{F}_{gg}^{(2)}(x, q_\perp) = \mathcal{H}_{gg}^{(1)}(x, q_\perp) - \mathcal{H}_{gg}^{(2)}(x, q_\perp). \tag{F.42}$$

G The gluon TMDs in the GBW model

The GBW model differs from the MV model in that there is no logarithmic r-dependence in the saturation scale:

$$Q_s^2 = \alpha_s C_F \mu_A, \quad \text{and} \quad Q_{sg}^2 \equiv \frac{N_c}{C_F} Q_s^2 = \alpha_s \mu_A N_c, \tag{G.1}$$

which greatly simplifies calculations.

Just like in the MV model, starting from the double derivative of the correlator of two dipoles, Eqs. (F.16) and (F.25), and making the identification: $\Gamma(r) = r^2 Q_{sg}^2 / 2N_c$, we obtain the following expressions for the gluon TMDs, only valid in the GBW model:

$$\mathcal{F}_{gg}^{(1)}(x, q_\perp) = \frac{1}{16\pi^2 \alpha_s} \frac{C_F}{N_c^2} S_\perp \int \frac{\mathrm{d}^2 \mathbf{r}}{(2\pi)^2} e^{-i\mathbf{q}_\perp \cdot \mathbf{r}} e^{-\frac{r^2 Q_{sg}^2}{4}}$$

$$\left[\frac{64}{r^2} \left(e^{\frac{r^2 Q_{sg}^2}{4}} - 1 \right) - N_c^2 r^2 Q_g^4 + 8 \left(N_c^2 - 2 \right) Q_{sg}^2 \right],$$

$$\mathcal{H}_{gg}^{(1)}(x, q_\perp) = \frac{S_\perp}{\alpha_s} \frac{1}{32\pi^3} C_F Q_{sg}^4 \int \mathrm{d}r\, r^3 J_2(q_\perp r) e^{-\frac{r^2 Q_{sg}^2}{4}}, \tag{G.2}$$

$$\mathcal{F}_{gg}^{(2)}(x, q_\perp) = \frac{1}{16\pi^2 \alpha_s} \frac{C_F}{N_c^2} S_\perp \int \frac{\mathrm{d}^2 \mathbf{r}}{(2\pi)^2} e^{-i\mathbf{q}_\perp \cdot \mathbf{r}} e^{-\frac{r^2 Q_{sg}^2}{4}}$$

$$\left[\frac{64}{r^2} \left(e^{\frac{r^2 Q_{sg}^2}{4}} - 1 \right) + N_c^2 r^2 Q_{sg}^4 - 16 Q_{sg}^2 \right],$$

$$\mathcal{H}_{gg}^{(2)}(x, q_\perp) = -\mathcal{H}_{gg}^{(1)}(x, q_\perp).$$

Moreover, from the formulas we found for $\mathcal{F}_{gg}^{(3)}(x, q_\perp)$ and $\mathcal{H}_{gg}^{(3)}(x, q_\perp)$ in the MV model, Eqs. (F.9) and (F.13), we immediately obtain the corresponding expression in the GBW model by simply neglecting the logarithm in the saturation scale.

In addition, it is easy to derive the following relations, useful when comparing with the literature:

$$\mathcal{F}_{gg}^{(1)}(x, q_\perp) + \mathcal{F}_{gg}^{(2)}(x, q_\perp) = \frac{4}{N_c^2} \mathcal{F}_{gg}^{(3)}(x, q_\perp) + \left(1 - \frac{4}{N_c^2} \right) x G_{q\bar{q}}(x, q_\perp),$$

$$\mathcal{F}_{gg}^{(1)}(x, q_\perp) - \mathcal{F}_{gg}^{(2)}(x, q_\perp) = x G_A^{(2)}(x, q_\perp), \tag{G.3}$$

$$\mathcal{H}_{gg}^{(1)}(x, q_\perp) + \mathcal{H}_{gg}^{(2)}(x, q_\perp) = 0,$$

$$\mathcal{H}_{gg}^{(1)}(x, q_\perp) - \mathcal{H}_{gg}^{(2)}(x, q_\perp) = x G_A^{(2)}(x, q_\perp),$$

where we introduced the TMD $x G_{q\bar{q}}(x, q_\perp)$, defined earlier in Eq. (F.34).

Using the above identities, the unpolarized part, Eq. (14.3), of the $pA \to q\bar{q}X$ cross section becomes:

$$\left. \frac{\mathrm{d}\sigma^{pA \to q\bar{q}X}}{\mathrm{d}\mathcal{P}.\mathcal{S}.} \right|_{GBW} = \frac{\alpha_s^2}{2C_F} \frac{1}{\hat{s}^2} x_p \mathcal{G}(x_p, \mu^2) \frac{\hat{t}^2 + \hat{u}^2}{4\hat{u}\hat{t}}$$

$$\times \left\{ \frac{(\hat{t} - \hat{u})^2}{\hat{s}^2} x G_A(x, q_\perp) + \left(1 - \frac{4}{N_c^2} \right) x G_{q\bar{q}}(x, q_\perp) + \frac{2}{N_c^2} \mathcal{F}_{gg}^{(3)}(x, q_\perp) \right\}, \tag{G.4}$$

confirming the result found in Eq. (54) of Ref. [137]. Whether we agree with the result for the polarization-dependent part, Eq. (55) in the same reference, depends on the order of operations. Starting from the GBW model, as we do in the present subsection, the polarized part, Eq. (14.4) of our CGC cross section gives:

$$
\begin{aligned}
\left. \frac{\mathrm{d}\sigma^{pA\to q\bar{q}X}}{\mathrm{d}\mathcal{P}.\mathcal{S}.} \right|_{\phi,GBW} &= \frac{\alpha_s^2}{2C_F} \frac{1}{\hat{s}^2} x_p \mathcal{G}\left(x_p, \mu^2\right) \frac{m^2}{\widetilde{P}_\perp^2} \cos\left(2\phi\right) \\
&\times \left\{ \frac{\left(\hat{t}-\hat{u}\right)^2}{\hat{s}^2} xG_A\left(x, q_\perp\right) - \frac{2}{N_c^2}\mathcal{H}_{gg}^{(3)}\left(x, q_\perp\right) \right\},
\end{aligned}
\tag{G.5}
$$

in contradiction with the result quoted in [137]:

$$
\begin{aligned}
\left. \frac{\mathrm{d}\sigma^{pA\to q\bar{q}X}}{\mathrm{d}\mathcal{P}.\mathcal{S}.} \right|_{\phi} &= \frac{\alpha_s^2}{2C_F} \frac{1}{\hat{s}^2} x_p \mathcal{G}\left(x_p, \mu^2\right) \frac{m^2}{\widetilde{P}_\perp^2} \cos\left(2\phi\right) \\
&\times \left\{ \frac{\left(\hat{t}-\hat{u}\right)^2}{\hat{s}^2} xG_A^{(2)}\left(x, q_\perp\right) + \left(1 - \frac{4}{N_c^2}\right) xH_{q\bar{q}}\left(x, q_\perp\right) + \frac{2}{N_c^2}\mathcal{H}_{gg}^{(3)}\left(x, q_\perp\right) \right\}.
\end{aligned}
\tag{G.6}
$$

However, if we evaluate the cross section (14.4) first in the MV model, and afterwards make the transition to the GBW model by simply neglecting the logarithms $\ln 1/r^2\Lambda^2$ in the expressions for the gluon TMDs, we recover precisely the above expression.

References

[1] C. Marquet, E. Petreska, and C. Roiesnel, JHEP **1610** (2016) 065.

[2] T. Liou, A. H. Mueller, and B. Wu, Nucl. Phys. **A916** (2013) 102.

[3] J. P. Blaizot and Y. Mehtar-Tani, Nucl. Phys. **A929** (2014) 202.

[4] E. Iancu, JHEP **1410** (2014) 95.

[5] E. Iancu, *Physics of the Color Glass Condensate* (Saclay, INSPIRE-1494642, 2005).

[6] Y. V. Kovchegov and E. Levin, *Quantum Chromodynamics at High Energy* (Cambridge University Press, 2012).

[7] F. Gelis, Int. J. Mod. Phys. **A28** (2013) 1330001.

[8] F. Halzen and A. D. Martin, *Quarks and Leptons: an Introductory Course in Modern Particle Physics* (John Wiley and Sons, 1984).

[9] A. H. Mueller, *Parton Saturation - An Overview* (arXiv:hep-ph/0111244v1, 2001).

[10] M. Peskin and D. Schroeder, *An Introduction to Quantum Field Theory* (Addison-Wesley Publishing Company, 1995).

[11] C. Ewerz, A. von Manteuffel, and O. Nachtmann, Phys. Rev. **D77** (2008) 074022.

[12] J. D. Bjorken, Phys. Rev. **179** (1969).

[13] R. P. Feynman, *Photon Hadron Interactions* (W. A. Benjamin, New York, 1971).

[14] Particle Data Group, Chin. Phys. **C** (2016) 100001.

[15] J. Casalderrey-Solana and C. A. Salgado, Acta Phys. Polon. **B38** (2007) 3731.

[16] H. Jung, *QCD and Monte Carlo* (course taught in Antwerp, 2013).

[17] S. Brodsky, H. Pauli, and S. Pinsky, Phys. Rep. **301** (1998) 229.

[18] G. F. Sterman, *An Introduction to Quantum Field Theory* (Cambridge University Press, 1993).

[19] S. Munier, *Contributions à l'étude de la chromodynamique quantique perturbative appliquée à la diffusion profondément inélastique à petit $x\_ Bj$*, Ph.D. thesis (2000).

[20] V. N. Gribov and L. N. Lipatov, Sov. J. Nucl. Phys. **15** (1972) 438.

[21] G. Altarelli and G. Parisi, Nucl. Phys. **B126** (1977) 298.

[22] Y. L. Dokshitzer, Sov. Phys. JETP **46** (1977) 641.

References

[23] R. K. Ellis, W. J. Stirling, and B. R. Webber, *QCD and Collider Physics* (Cambridge University Press, 1996).

[24] H1 and ZEUS Collab., H. Abramovicz et al., Eur. Phys. J. **C75** (2015) 580.

[25] A. H. Mueller, *Small-x Physics, High Parton Densities and Parton Saturation in QCD* (arXiv:hep-ph/9911289v1, 1999).

[26] V. Barone and E. Predazzi, *High-Energy Particle Diffraction* (Springer-Verlag, 2002).

[27] N. N. Nikolaev and B. G. Zakharov, Z. Phys. C. **49** (1991) 607.

[28] A. H. Mueller, Nucl. Phys. **B558** (1999) 285.

[29] K. Golec-Biernat and M. Wüsthoff, Phys. Rev. **59** (1998) 24.

[30] A. M. Stasto, K. Golec-Biernat, and J. Kwiecinski, Phys. Rev. Lett. **86** (2001) 596.

[31] A. Prokudin, Int. J. Mod. Phys. Conf. Ser. **20** (2012).

[32] L. V. Gribov, E. M. Levin, and M. G. Ryskin, Phys. Rep. **100** (1983).

[33] E. Iancu, K. Itakura, and L. McLerran, Nucl. Phys. **A708** (2002) 327.

[34] A. H. Mueller and D. N. Triantafyllopoulos, Nucl. Phys. **B640** (2002) 331.

[35] J. Bartels, K. Golec-Biernat, and H. Kowalski, Phys. Rev. **D66** (2002) 014001.

[36] H. Kowalski and D. Teaney, Phys. Rev. **D68** (2003) 114005.

[37] E. Iancu, K. Itakura, and S. Munier, Phys. Lett. **B590** (2004) 199.

[38] A. H. Rezaeian, M. Siddikov, M. Van de Klundert et al., Phys. Rev. **D87** (2013) 034002.

[39] J. L. Albacete and Y. V. Kovchegov, Phys. Rev. **D75** (2007) 125021.

[40] Y. V. Kovchegov and H. Weigert, Nucl. Phys. **A789** (2007) 260.

[41] Y. V. Kovchegov and H. Weigert, Nucl. Phys. **A784** (2007) 188.

[42] I. I. Balitsky, Phys. Rev. **D75** (2007) 014001.

[43] E. Iancu, J. D. Madrigal, A. H. Mueller et al., Nucl. Phys. **A956** (2016) 557.

[44] I. Balitsky and G. A. Chirilli, Phys. Rev. **D77** (2008) 014019.

[45] I. Balitsky and G. A. Chirilli, Phys. Rev. **D88** (2013) 111501.

[46] A. Kovner, M. Lublinksy, and Y. Mulian, Phys. Rev. **D89** (2014) 061704.

[47] J. L. Albacete, N. Armesto, J. G. Milhano et al., Phys. Rev. **D80** (2009).

[48] J. L. Albacete, N. Armesto, J. G. Milhano *et al.*, Eur. Phys. J. **C71** (2011) 1705.

[49] K. Kutak and S. Sapeta, Phys. Rev. **D86** (2012) 094043.

[50] J. Kuokkanen, K. Rummukainen, and H. Weigert, Nucl. Phys. **A875** (2012) 29.

[51] E. Iancu, J. D. Madrigal, A. H. Mueller *et al.*, Phys. Lett. **B750** (2015) 643.

[52] A. H. Mueller, Nucl. Phys. **B643** (2002) 501.

[53] D. N. Triantafyllopoulos, Nucl. Phys. **B648** (2003) 293.

[54] V. S. Fadin, E. A. Kuraev, and L. N. Lipatov, Phys. Lett. **60B** (1975) 50.

[55] E. A. Kuraev, L. N. Lipatov, and V. S. Fadin, Sov. Phys. JETP **44** (1976) 443.

[56] E. A. Kuraev, L. N. Lipatov, and V. S. Fadin, Sov. Phys. JETP **45** (1977) 199.

[57] I. I. Balitsky and L. N. Lipatov, Sov. J. Nucl. Phys. **28** (1978) 822.

[58] I. I. Balitsky, Nucl. Phys. **B463** (1996) 99.

[59] Y. V. Kovchegov, J. Kuokkanen, K. Rummukainen *et al.*, Nucl. Phys. **A823** (2009) 47.

[60] Y. V. Kovchegov, Phys. Rev. **D60** (1999) 034008.

[61] Y. V. Kovchegov, Phys. Rev. **D61** (2000) 074018.

[62] A. H. Mueller, Nucl. Phys. **B415** (1994) 373.

[63] A. H. Mueller, Nucl. Phys. **B437** (1995) 107.

[64] K. Kutak and A. M. Stasto, Eur. Phys. J. **C41** (2005) 343.

[65] J. R. Forshaw and D. A. Ross, *Quantum Chromodynamics and the Pomeron* (Cambridge University Press, 1997).

[66] A. Donnachie and P. V. Landshoff, Phys. Lett. **B296** (1992) 227.

[67] M. Froissart, Phys. Rev. **123** (1961) 1053.

[68] A. Martin, Lect. Notes Phys. **3** (1969).

[69] J. Bartels, J. Phys. **G19** (1993) 1611.

[70] J. Bartels, H. Lotter, and M. Vogt, Phys. Lett. **B373** (1996) 215.

[71] E. Iancu, K. Itakura, and L. McLerran, Nucl. Phys. **A724** (2003) 181.

[72] S. Catani, M. Ciafaloni, and F. Hautmann, Nucl. Phys. **B366** (1991) 135.

[73] J. C. Collins and R. K. Ellis, Nucl. Phys. **B360** (1991) 3.

[74] Y. V. Kovchegov and A. H. Mueller, Nucl. Phys. **B529** (1998) 451.

[75] L. McLerran and R. Venugopalan, Phys. Rev. **D59** (1999) 094002.

[76] F. Dominguez, C. Marquet, B.-W. Xiao *et al.*, Phys. Rev. **D83** (2011) 105005.

[77] J. C. Collins, *Foundations of Perturbative QCD* (Cambridge University Press, 2011).

[78] I. O. Cherednikov, T. Mertens, and F. F. Van der Veken, *Wilson Lines in Quantum Field Theory* (De Gruyter, 2014).

[79] D. Boer, P. Mulders, and F. Pijlman, Nucl. Phys. **B667** (2003) 201.

[80] F. Hautmann and H. Jung, Nucl. Phys. **B883** (2014) 1.

[81] F. Hautmann, H. Jung, and S. Taheri Monfared, Eur. Phys. J. **C74** (2014) 3082.

[82] F. Hautmann, H. Jung, M. Kraemer *et al.*, Eur. Phys. J. **C74** (2014) 3220.

[83] M. Ciafaloni, Nucl. Phys. **B296** (1988) 49.

[84] S. Catani, F. Fiorani, and G. Marchesini, Nucl. Phys. **B336** (1990) 18.

[85] G. Marchesini, Nucl. Phys. **B445** (1995) 49.

[86] L. McLerran and R. Venugopalan, Phys. Rev. **D49** (1994) 2233.

[87] L. McLerran and R. Venugopalan, Phys. Rev. **D49** (1994) 3352.

[88] L. McLerran and R. Venugopalan, Phys. Rev. **D50** (1994) 2225.

[89] E. Iancu, A. Leonidov, and L. McLerran, Nucl. Phys. **A692** (2001) 583.

[90] Y. V. Kovchegov, Phys. Rev. **D54** (1996) 9.

[91] E. Wessels, *Signatures of Gluon Saturation in High Energy Scattering*, Ph.D. thesis, Vrije Universiteit Amsterdam (2009).

[92] J. Jalilian-Marian, A. Kovner, A. Leonidov *et al.*, Nucl. Phys. **B504** (1997) 415.

[93] E. Iancu, A. Leonidov, and L. McLerran, Phys. Lett. **B510** (2001) 133.

[94] J. Jalilian-Marian, A. Kovner, A. Leonidov *et al.*, Phys. Rev. **D59** (1998) 014014.

[95] J. Jalilian-Marian, A. Kovner, and H. Weigert, Phys. Rev. **D59** (1998) 014015.

[96] E. Ferreiro, E. Iancu, A. Leonidov *et al.*, Nucl. Phys. **A703** (2002) 489.

[97] H. Weigert, Nucl. Phys. **A703** (2002) 823.

[98] E. Iancu and L. McLerran, Phys. Lett. **B510** (2001).

References

[99] Y. Hatta, E. Iancu, K. Itakura *et al.*, Nucl. Phys. **A760** (2005) 172.

[100] J. C. Collins, D. E. Soper, and G. F. Sterman, Adv. Ser. Direct. High Energy Phys. **5** (1989).

[101] CTEQ Collaboration, Rev. Mod. Phys. **67** (1995) 157.

[102] J. C. Collins, D. E. Soper, and G. F. Sterman, Nucl. Phys. **B308** (1988) 833.

[103] J. C. Collins, D. E. Soper, and G. F. Sterman, Phys. Lett. **134B** (1984) 263.

[104] J. W. Qiu, in *Santa Fe Polarized DY workshop* (2010).

[105] R. Angeles-Martinez, A. Bachetta, I. Balitsky *et al.*, Acta Phys. Pol. **B46** (2015) 12.

[106] T. C. Rogers, Eur. Phys. J. **A52** (2016) 153.

[107] A. Signori, *Flavor and Evolution Effects in TMD Phenomenology*, Ph.D. thesis, Vrije Universiteit Amsterdam (2016).

[108] D. Boer, Few-Body Syst. **58** (2017) 32.

[109] X. Ji, J. P. Ma, and F. Yuan, Phys. Lett. **B597** (2004) 299.

[110] M. G. Echevarria, A. Idilbi, and I. Scimemi, JHEP **1207** (2012) 002.

[111] X. Ji, J. P. Ma, and F. Yuan, Phys. Rev. **D71** (2005) 034005.

[112] J. C. Collins, D. E. Soper, and G. F. Sterman, Phys. Lett. **B126** (1983) 275.

[113] D. Boer and P. J. Mulders, Nucl. Phys. **B569** (2000) 505.

[114] P. J. Mulders and J. Rodrigues, Phys. Rev. **D63** (2001) 094021.

[115] S. J. Brodsky, D. S. Hwang, and I. Schmidt, Phys. Lett. **B530** (2002) 99.

[116] J. C. Collins, Phys. Lett. **B536** (2002) 43.

[117] A. V. Belitsky, X. Ji, and F. Yuan, Nucl. Phys. **B656** (2003) 165.

[118] D. W. Sivers, Phys. Rev. **D41** (1990) 83.

[119] M. Anselmino, M. Boglione, and F. Murgia, Phys. Lett. **B362** (1995) 164.

[120] U. D'Alesio and F. Murgia, Prog. Part. Nucl. Phys. **61** (2007) 394.

[121] S. J. Brodsky, D. S. Hwang, and I. Schmidt, Nucl. Phys. **B642** (2002) 344.

[122] Z.-B. Kang and J.-W. Qiu, Phys. Rev. Lett. **103** (2009) 172001.

[123] A. Bachetta, F. Delcarro, C. Pisano *et al.* (2017), JLAB-THY-17-2437, arXiv:1703.10157.

[124] S. Catani, M. Ciafaloni, and F. Hautmann, Phys. Lett. **B242** (1990) 97.

[125] S. Catani, M. Ciafaloni, and F. Hautmann, Phys. Lett. **B307** (1993) 147.

[126] S. Catani and F. Hautmann, Nucl. Phys. **B427** (1994) 475.

[127] P. Kotko, K. Kutak, C. Marquet *et al.*, JHEP **1509** (2015) 106.

[128] C. J. Bomhof, P. J. Mulders, and F. Pijlman, Eur. Phys. J. **C47** (2006) 147.

[129] J. C. Collins and J. W. Qiu, Phys. Rev. **D75** (2007) 114014.

[130] W. Vogelsang and F. Yuan, Phys. Rev. **D76** (2007) 094013.

[131] T. C. Rogers and P. J. Mulders, Phys. Rev. **D81** (2010) 094006.

[132] B. W. Xiao and F. Yuan, Phys. Rev. Lett. **105** (2010) 062001.

[133] M. Deak, F. Hautmann, H. Jung *et al.*, JHEP **0909** (2009) 121.

[134] A. van Hameren, P. Kotko, and K. Kutak, Phys. Rev. **D88** (2013) 094001.

[135] A. van Hameren, P. Kotko, K. Kutak *et al.*, Phys. Lett. **B737** (2014) 335.

[136] A. van Hameren, P. Kotko, K. Kutak *et al.*, Phys. Rev. **D89** (2014) 094014.

[137] E. Akcakaya, A. Schaefer, and J. Zhou, Phys. Rev. **D87** (2013) 054010.

[138] A. van Hameren, P. Kotko, K. Kutak *et al.*, JHEP **1612** (2016) 034.

[139] A. Dumitru, A. Hayashigaki, and J. Jalilian-Marian, Nucl. Phys. **765** (2006) 464.

[140] T. Altinoluk and A. Kovner, Phys. Rev. **D83** (2011) 105004.

[141] G. A. Chirilli, B. W. Xiao, and F. Yuan, Phys. Rev. Lett. **108** (2012) 122301.

[142] F. Dominguez, C. Marquet, and B. Wu, Nucl. Phys. **A823** (2009) 99.

[143] F. Dominguez, B.-W. Xiao, and F. Yuan, Phys. Rev. Lett. **106** (2011) 022301.

[144] A. Metz and J. Zhou, Phys. Rev. **D84** (2011) 051503.

[145] F. Dominguez, J.-W. Qiu, B.-W. Xiao *et al.*, Phys. Rev. **D85** (2012) 045003.

[146] E. Iancu and J. Laidet, Nucl. Phys. **A916** (2013) 48.

[147] D. Boer, S. J. Brodsky, P. J. Mulders *et al.*, Phys. Rev. Lett. **106** (2011) 132001.

[148] C. Marquet, Nucl. Phys. **A796** (2007) 41.

[149] K. Rummukainen and H. Weigert, Nucl. Phys. **A739** (2004) 183.

[150] T. Lappi and H. Mäntysaari, Eur. Phys. J. **C73** (2013) 2307.

References

[151] A. Dumitru, T. Lappi, and V. Skokov, Phys. Rev. Lett. **115** (2015) 252301.

[152] P. Kotko, K. Kutak, S. Sapeta *et al.*, Eur. Phys. J. **C77** (2017) 353.

[153] D. Boer, P. J. Mulders, and C. Pisano, Phys. Rev. **D80** (2009) 094017.

[154] C. Pisano, D. Boer, S. J. Brodsky *et al.*, JHEP **1310** (2013) 024.

[155] D. d'Enterria, J. Phys. G: Nucl. Part. Phys. **34** (2007) S53.

[156] D. d'Enterria, Landolt-Bornstein **23** (2010) 471.

[157] J. D. Bjorken, FERMILAB-PUB-82-059-THY (1982).

[158] R. Baier, Y. L. Dokshitzer, A. H. Mueller *et al.*, Nucl. Phys. **B484** (1997) 265.

[159] A. H. Mueller, B. Wu, B. W. Xiao *et al.*, Phys. Lett. **B763** (2016) 208.

[160] M. Gyulassy and X.-N. Wang, Nucl. Phys. **B420** (1994) 583.

[161] X.-N. Wang, M. Gyulassy, and M. Pluemer, Phys. Rev. **D51** (1995) 7.

[162] B. G. Zakharov, JETP Lett. **63** (1996) 952.

[163] B. G. Zakharov, JETP Lett. **65** (1997) 615.

[164] R. Baier, Y. L. Dokshitzer, S. Peigné *et al.*, Phys. Lett. **B345** (1995) 277.

[165] R. Baier, Y. L. Dokshitzer, A. H. Mueller *et al.*, Nucl. Phys. **B478** (1996) 577.

[166] R. Baier, Y. L. Dokshitzer, A. H. Mueller *et al.*, Nucl. Phys. **B483** (1997) 291.

[167] R. Baier, Y. L. Dokshitzer, A. H. Mueller *et al.*, Phys. Rev. **C58** (1998) 3.

[168] R. Baier, Y. L. Dokshitzer, A. H. Mueller *et al.*, Nucl. Phys. **B531** (1998) 403.

[169] R. Baier, D. Schiff, and B. G. Zakharov, Ann. Rev. Nucl. Part. Sci. **50** (2000) 37.

[170] U. A. Wiedemann, Nucl. Phys. **B588** (2000) 303.

[171] C. A. Salgado and U. A. Wiedemann, Phys. Rev. **D68** (2003) 014008.

[172] J. Casalderrey-Solana and X.-N. Wang, Phys. Rev. **C77** (2008) 024902.

[173] P. B. Arnold, Phys. Rev. **D79** (2009) 065025.

[174] P. B. Arnold, Phys. Rev. **D80** (2009) 025004.

[175] S. Caron-Huot, Phys. Rev. **D79** (2009) 065039.

[176] I. O. Cherednikov, J. Lauwers, and P. Taels, Eur. Phys. J. **C74** (2014) 2721.

References

[177] J. P. Blaizot, F. Dominguez, E. Iancu *et al.*, JHEP **1301** (2013) 143.

[178] Y. Mehtar-Tani, J. G. Milhano, and K. Tywoniuk, Int. J. Mod. Phys. **A28** (2013) 1340013.

[179] J. P. Blaizot, F. Dominguez, E. Iancu *et al.*, JHEP **1406** (2014) 075.

[180] B. Wu, JHEP **1412** (2014) 081.

[181] Jet Collaboration (K. M. Burke et al.), Phys. Rev. **C90** (2014) 014909.

[182] P. B. Arnold, G. D. Moore, and L. G. Yaffe, JHEP **0011** (2000) 001.

[183] P. B. Arnold, G. D. Moore, and L. G. Yaffe, JHEP **0305** (2003) 051.

[184] Y. V. Kovchegov and K. Tuchin, Phys. Rev. **D65** (2002) 074026.

[185] A. H. Mueller and S. Munier, Nucl. Phys. **A893** (2012) 43.

[186] R. P. Feynman and A. R. Hibbs, *Quantum Mechanics and Path Integrals* (Dover, New York, 2010).

[187] L. D. Landau and I. Y. Pomeranchuk, Dokl. Akad. Nauk. SSSR **92** (1953) 735.

[188] A. B. Migdal, Phys. Rev. **103** (1956) 1811.